Impaired and Enhanced Spatial Representations of the PSD-95 Knockout Mouse

by

Linus Da-Shih Sun

B.S. Molecular and Cellular Biology
University of California at Berkeley, 1994

SUBMITTED TO THE DEPARTMENT OF BIOLOGY IN PARTIAL FULFILMENT OF THE REQUIREMENTS FOR THE DEGREE OF

DOCTORATE OF PHILOSOPHY
AT THE
MASSACHUSETTS INSTITUTE OF TECHNOLOGY

SEPTEMBER 2003
[June 2004]

Signature of Author: _____
Linus Da-Shih Sun
Department of Biology
June 18, 2003

Certified by: _____
Matthew A. Wilson
Associate Professor of Biology and Brain & Cognitive Science
Thesis Supervisor

Accepted by: _____
Alan D. Grossman
Professor of Biology
Chairman, Department Committee for Graduate Studies

Impaired and Enhanced Spatial Representations of the
Post Synaptic Desnity-95 Knockout Mouse
by

Linus Da-Shih Sun

B.S. Molecular and Cellular Biology
University of California at Berkeley, 1994

Submitted to the Department of Biology on
June 18, 2003 in Partial Fulfillment of the
Requirements for the
Degree of Doctorate of Philosophy in Biology

ABSTRACT

Postsynaptic density protein-95 (PSD-95) is the second most abundantly expressed synaptic protein in the postnatal forebrain. It is an integral part of the postsynaptic scaffolding complex and helps recruit receptors, channels and associated factors involved with synaptic transmission. A mouse whose wildtype gene was replaced with truncation mutant of PSD-95 preserving two PDZ binding domains causes a spatial learning and memory deficit and a dramatic enhancement of synaptic strengthening. Long Term Potentiation is enhanced at all frequencies of stimulation (1-100Hz), while Long Term Depression is absent in the mutants. This study explores CA1 pyramidal cell spatial representations in the PSD-95 mutant mice. Mutants are not significantly different than controls in running velocity. Nor are its pyramidal cells or interneurons different than controls in: place cell firing rates, sparsity of run active cells, bursting behavior, or theta modulated activity. However, mutants do exhibit significantly larger place fields and wider spike waveforms. Mutants also expressed enhanced directionality of place fields and increased post-run sleep correlation of firing for overlapping place fields. Mutants also exhibited disruption of asymmetrical place fields and phase precession, the first such observation reported in mice. In conclusion, LTP alone is not enough for the active process of encoding experience. Instead, bi-directional synaptic plasticity is necessary for proper place field formation, correlation, directionality, asymmetry, phase precession, and the formation of spatial memories.

Thesis Supervisor: Matthew A. Wilson
Title: Associate Professor of Biology/Brain and Cognitive Science

Dedicated to the memory of my loving grandparents, Lusa Yu Sun,
Lok and Kit Ha Wong, whose dedication to the family
provided me with the unequalled opportunities
to study science and medicine.

To them I owe my inspiration to strive in my future endeavors.

Acknowledgements

These are the people I would like to thank: My advisor Matt, for being as generous as an advisor can be, who let me intellectually grow without arbitrary constraints on time or funding. The one truly invaluable thing that Matt provided to me more than anything else was his confidence that I would be capable to handle any number of projects that came my way. And also his sense of scientific integrity, which was a model to live by. I also want to thank Susumu Tonegawa, not only for the opportunities that were given to us, but for always being available and being truly enthusiastic in engaging in scientific discussion on issues of learning and memory. He is inspirational as a life long learner. I want to thank Andy Chess, who has been the quintessential committee advisor knowing no bounds in supporting his students and their scientific inquiries; also for providing me with support and truly critical advice on the next stage in my professional career. Kazu, who has truly been missed in the lab since he left, for providing entertainment, interesting conversation, critical technical help, truly remarkable collaborations, and limitless gossip. Al "Cajal" Lee, for teaching me how to think like and be a skeptical scientist, and for providing years of unlimited energy for political debate. Mayank for leading the way through the dark parts of the hippocampus. All the students who have worked with me in the years past, especially Bogdan, Cindy, Jeenah and Marg. Jie for her remarkable scientific and other support. Dave Gerber for tech help with the mouse colony. All current & former collaborators: Matt A., Hyejin, Brian, Pato, Josh. Very useful scientific discussions with Teru & the Brits (DJF&MJ). Material support: Jay. 6.00x support from Sujith & Eric. Late night dinner discussions with J,J,E. And all current and former Wilson/Tonegawa/Miller lab members!

I especially want to thank Eun-Joung for her time and understanding and patience. My father for his never-ending optimism and support. Mom & Bob for their steadfast advice and the extra check when I needed it. Jeff, Derek & Mike. Classmates Tien-yi & Esther. Anne, Jimmy, Brian, John R, Chizu, BC, Dani, Jasmine, Popi, Kenway, Mario, Albee, Jackie, Joe(s), Judilee, Cayce, Inge, & Jeremy. Greg, Chute, & Pavel. Max, Lee, Justin... Calvin, Ling, NiNi, Lin Family, Wong Family, Sun Family and many many more I haven't the space to list...

Table of Contents

CHAPTER 1 INTRODUCTION

Dementias and memory loss will be a major medical problem of this coming century.

Dementia has the potential to become a major public health concern during this century due to increasing life expectancy and growth of an ageing population. The most common type of dementia is memory loss and Alzheimer's disease (AD), which has been reported to occur in 50% of people over the age of 85. AD patients suffer from severe retrograde memory loss, including but not limited to the impaired learning of spatial information. Treatment for AD dementia is a terrible challenge that requires the understanding of the fundamental mechanisms on how memory is formed. Studies have shown that NMDA glutamate receptor subunits are significantly reduced in postmortem brain tissue (Bi & Sze, 2002), and recently AD is believed to be the result of synaptic failure (Selkoe, 2002). The understanding of the basic mechanism for hippocampal synaptic plasticity perhaps NMDA receptor function is of fundamental importance for the management one of the major medical problems of this coming century. The focus of this thesis will be to explain one possible mechanism for the formation of memories.

1.1 A Brief introduction to the hippocampus and LTP/LTD.

Ever since Scoville and Milner (1957) discovered that bilateral lesions in the hippocampus of patient H.M. lead to persistent impairment of his recent memories, an entire neuroscience community for memory research has focused on this "sea horse" structure. More than forty years have past and no less than 60,000 journal articles have been published on the hippocampus. It was shown that anterograde amnesia, the inability to form new memories, is specific to the CA1 region of the hippocampus in humans (Zola-Morgan, 1986). Monkey and rat

lesion models that have replicated the human phenomena all share a common thread claiming that the hippocampus is temporarily necessary for the binding of distributed representations in the neocortex in order to form a whole memory (Squire, 1992).

However, for the most part anatomical studies have shed little light on the basic mechanisms of how the hippocampus processes information and how it is responsible for the storage of memories. In the 1950's no one knew if memory was a gross anatomical phenomena nor did anyone have evidence that it was based a cellular representations. Hebb (1949) hypothesized of a synaptic associative timing model where the strengthening of relevant synapses between neurons is required for the formation of memories. However for the following 20 years, there was a significant lapse in knowledge at what was happening at the synaptic level because gross anatomical studies did not shed any light on the basic cellular mechanisms which allowed for individual neurons to form long-term changes. However, Bliss & Lomo (1970) discovered that a tetanus (a vigorous one second electrical stimulation at 100 Hz) of the perforant path, an upstream monosynaptic pathway in the hippocampus of a rabbit, caused coincident firing of target dentate granule cells resulting in a persistent change in synaptic strength as measured by size of the field Excitatory Post Synaptic Potentials (fEPSP). This persistent change was dubbed as Long Term Potentiation (LTP). Thus, LTP was borne as the putative synaptic mechanism for Hebbian associative learning and possibly the answer to the formation of memories. The mechanism of LTP was shown to bear many of the required mechanisms that computational models of associative memory would need: persistent but reversible synaptic strengthening, requirements of cooperativity and timing specificity (Markram, 1997). Though many questions still remain, the following 30 years after Bliss & Lomo's discovery, nearly 5000 papers have been published on the subject of LTP and we have learned much about the

fundamental molecular mechanisms which drive it (Malenka, 1999). The central dogma today of the mechanism of CA1 LTP begins with the requirement of the activation of the N-methyl-D-aspartate glutamate (NMDA) receptor on the postsynaptic cell, leading to upregulation of protein kinase activity, which subsequently activates cAMP-induced CREB transcription and subsequent long-lasting change of the synapse.

In the CA1 area of the hippocampus, LTP is commonly believed to be NMDA receptor mediated. NMDA receptor-channels are activated by simultaneous depolarization of the postsynaptic cell, releasing the magnesium block and the binding of glutamate. This allows the influx of calcium into the dendritic spine causing a cascade of second messenger interactions including protein kinase activity and activation of the cAMP-inducible CREB transcription factor resulting in gene expression, protein translation finally resulting in change in the postsynaptic dendrites and also via a retrograde messenger change in the presynaptic axon terminals (Nicoll, 1999). The requirement for simultaneous depolarization of the postsynaptic dendrite and binding of glutamate indicated that the NMDA receptor was a "coincidence" detector. Indeed the NMDA receptor was a great candidate of being the molecular switch mechanisms that define the Hebbian synapse. Thus the NMDA receptor was an excellent candidate for manipulating in order to test hypotheses ranging from synaptic strengthening to learning and memory. Morris and colleagues (1986) used pharmacological agents that blocked the activity of the NMDA receptor in vivo to show that both LTP is also blocked as well as spatial memory in the watermaze. This study was the first attempt to tie together: a molecular mechanism, a synaptic mechanism, the hippocampus, and memory consolidation. While this study determined a correlation between LTP and the formation of memories, it did not prove the corollary, that the formation of memories will necessarily cause LTP to be induced. This is an

important corollary to prove because while LTP represents the dominant theory that accounts for synaptic strengthening and learning and memory, there was the possibility that it could be erroneous, because LTP itself is artificially induced and perhaps itself and artifact. Moser et al. (1993) performed the corollary experiment and showed that LTP is indeed induced after learning in the rat has occurred. Knowing that LTP is a mechanism which strengthens synapses, if synapses were allowed to be strengthened limitlessly, the brain would saturate with super-strengthened connections. Thus a mechanism must exist to weaken them as well.

Thus the reversibility of LTP is as important a mechanism for maintaining a balanced neural network. A number of mechanisms have been identified that would account for this needed mechanism. *Heterosynaptic depression* was identified as the ability to tetanize and induce LTP in one CA3-CA1 pathway while causing a long-term depression (LTP) or synaptic weakening in the non-tetanized pathway (Lynch, 1977). Homosynaptic depression or *depotentiation* of a single pathway was discovered to occur if the pathway was stimulated at low frequency (Barrionuevo, 1980). More recently it was found that LTP or LTD can be markedly controlled by the relative spike-timing of pre and postsynaptic action potentials (Markram, 1997; Bi, 1998). Interestingly depotentiation and LTD are also dependent on the activation of NMDA receptors (Dudek, 1992; for review see Kemp, 2001). While the biological relevance of this artificial means of strengthening and weakening synaptic strengths have been hotly debated to this day, there is an undeniable increasing body of work which supports a conserved molecular and physiological mechanism that controls the bi-directional regulation of synaptic efficacy.

Although there are many forms of LTP that exist within the brain (Sanes, 1999), the central dogma for the core mechanism of memory formation in CA1 pyramidal cells today is based on the activation of the NMDA receptor on the postsynaptic subsequently activating

protein kinase activity which subsequently activates the cAMP-induced CREB transcription factor leading to long term changes of the affected synapses (Bailey, 1996). The long term changes that lead to increasing synaptic strength potentially include changes in dendritic spine morphology (Sorra, 2000) and more recently have been associated with increases in postsynaptic clustering and regulation of AMPA receptors (Hayashi, 2000; Malinow, 2002).

1.2 Second-order processes of the hippocampus as an alternative substrate for memories: place fields formed by the activity of CA1 pyramidal cells.

While numerous labs were studying the molecular and physiological processes involved in LTP activation, a small but dedicated group within the neuroscience community was avidly pursuing alternative techniques that might be able to quantify the neural substrate for memory. While LTP represented a first-order mechanism to explain synaptic strengthening, it likely that memory themselves are assembled from higher order process in the brain. O'Keefe (1972) made one of the great discoveries in the learning and memory field and proposed that the hippocampus was a potential site for the formation of a spatial map of the environment. CA1 pyramidal cells in the rat hippocampus formed "place fields" during active exploration where the firing rate (defined by total spikes/time) of a single pyramidal cell was significantly higher in specific locations of a spatial environment. Because CA1 was the putative site for memory formation, these "place fields" were an enticing possibility of being the neural substrate of spatial memories in the hippocampus.

There was a push to collect as much of this CA1 pyramidal cell data as possible in order to study the potential network properties of the hippocampus. Wilson (1993) pioneered the study of recording from multiple electrodes that made it possible to collect more than one hundred

cells simultaneously. This technique allowed for the unprecedented study of multiple cell-cell pair interactions during active behavior as well as during memory consolidations periods during sleep (Wilson, 2002).

1.3 Birth of molecular methods to address learning and memory: combining molecular neuroscience, physiology and behavior to address the memory consolidation question.

By the early 1990's the neuroscience community had the tools available to attempt to causally link a range of experimental techniques in order to produce one interdisciplinary field that can directly address the learning and memory problem. These groups would attempt the difficult task to link a genetic molecular manipulation with a physiological effect which would finally manifest itself into a behavioral phenotype. The explosion of molecular genetic techniques at this time also allowed research groups to produce numerous transgenic mouse models which primarily explored the molecules in the space inside of and around the synapse (Tonegawa, 2003). The field was dubbed "molecular and cellular cognition" and an increasing number of labs were joining the fray to study every possible postsynaptic molecule (Silva, 2003). The first mouse to be studied was the α-calcium calmodulin-dependent kinase II (αCaMKII) knockout mouse. Not only did this mouse exhibit reduced LTP but it also exhibited a spatial learning impairment (Silva, 1992). Later it was determined that in the post synaptic densities that αCamKII directly interacts with the NMDA receptor (for review see Sheng & Kim, 2002), providing further evidence of a conserved molecular mechanism to account for possible changes in LTP. The next target protein investigators aimed to knockout was the NMDA receptor itself. However the genetic ablation of the R1 subunit of the NMDA receptor from a mouse results in a homozygous lethal phenotype, thus making the genetic study of the NMDA receptor a challenge.

Additionally, modifications early in development may have altered the basic wiring structure of the hippocampus, thus making interpretation for adult function more difficult.

Tsien and colleagues solved the lethality and developmental problem by producing a knockout mouse whose NMDAR1 subunit was ablated only in the CA1 pyramidal cell layer of the hippocampus utilizing the phage P1 derived CRE-*loxP* recombination system (Tsien, 1996). In this system the CRE recombinase was under control of the CaMKII promoter and a critical portion of the NMDAR1 subunit was flanked by Lox recombination sites. Only in tissues expressing the CaMKII promoter (postnatal forebrain pyramidal cells) would produce CRE recombinase and thus excise the floxed NMDAR1 sequence knocking out the NMDA receptor in those cells. When tested in slice physiology preparations, it was discovered that this mouse was entirely absent of LTP and LTD, though standard synaptic transmission was unperturbed (Tsien, 1996). Additionally, this mouse also had a significant impairment in the acquisition of the Morris watermaze spatial memory task. Thus again, we see demonstration of a molecular manipulation that lead to a physiological change which translated into a functional change in memory performance. However, we still did not have any insight into the activity of hippocampal pyramidal cell *in vivo*. This piece of the puzzle was still missing.

The puzzle was solved when McHugh et al. (1996) employed muti-tetrode physiology analysis in CA1-NMDAR1 KO mice. They showed that overall firing rates of pyramidal cells and interneurons were not significantly different between mutants and controls. In other words, the mechanism that regulated overall synaptic transmission seemed to be normal. Additionally, the mutant mice exhibited normal theta activity in the hippocampus, suggesting normal rhythmic activity in the brain of the mouse. McHugh also showed that CA1 pyramidal cells in the hippocampus of the mouse do indeed form stable place fields. However mutant place fields were

significantly larger than controls. Instead of being a single gaussian shaped place field, the mutant fields were multi-peaked and disparate over space. It was noted that covariance of firing for place cells that overlapped in space was significantly reduced for the mutants. In other words, cells that fired in space together did NOT fire in time together, as opposed to control CA1 pyramidal cells that did fire in time together. McHugh and colleagues proposed that this lack of covariance of firing was to account for the mouse's inability to employ coactive CA1 pyramidal cells to form a spatial map because of a lack of coordinated activity as required by neural network models of learning. They also found a decrease in the relative directionality of a pyramidal cell, but not strongly significantly so. Interestingly they also discovered that peak to trough spike widths of pyramidal cells is narrower in the mutants than the controls, though there is no good explanation as to why this may be (perhaps there is altered potassium channel regulation in the mutants).

If we were to ask the basic question: what would happen to the spatial representations of space if we were to ablate LTP & LTD in a mouse's hippocampus? Studies conducted by Tsien, McHugh and colleagues provided a satisfactory answer to this question. They concluded that in NMDAR1 mutant mice: LTP & LTD are abolished in the CA3-CA1 network, learning is impaired, and spatial representations are degraded in CA1 pyramidal place cells. These conclusions are bolstered by the specific role that NMDAR1 plays in LTP and LTD, and also because of the region specificity of the knockout.

Since then, a number of similar studies, albeit suffering from an order of magnitude fewer cells analyzed compared with McHugh et al., have shown that a reduction in LTP in the hippocampus leads to place cell stability. Genetically modified mutations in CaMKII, PKA, and CREB activity also showed reduced place cell stability (Rotenberg, 1996; Rotenberg, 2000; Cho,

1998). Recently, in an elegant study, a reduction of LTP in the CA3 region of the hippocampus by selectively knocking out NMDA receptors caused mutant mice to lose the ability to complete patterns in cue degraded environments during the Morris watermaze task (Nakazawa, 2002, 2003). In a parallel study involving more than one hundred CA1 pyramidal cells in the CA3-NMDA KO mice, CA1 pyramidal cells had larger and more diffuse place fields during the cue degraded experiments. Recently, GluR2 null mutant mice which show an enhanced LTP phenotype have been reported to have unstable place fields and fewer active cells during run (Yan, 2002). However this study is marred by the fact that these mice are reported to suffer from a non-specific hyper-excitability that is reported to alter cognitive functions across multiple brain regions (Gerlai, 1998).

In summary there are a handful of genetically modified mice that have been utilized to address place field characteristics based on the mutant's abnormal LTP characteristics. All these mice suffered some sort of hippocampal memory impairments. With the exception of McHugh et al.'s co-variance, spike width, and directionality result and Nakazawa et al.'s degraded environment specific task, all these studies have reported larger or unstable place fields under various behavioral conditions. I propose one possible reason that this is the case is because of the lack of clean data that is collected. In all these studies, an open field apparatus was utilized because it is viewed as a natural environment that a mouse would forages for food. However, behavior in the open field is highly variable and non-repeatable due to variable paths that the mouse chooses to run, thus more subtle and specific effects may be lost in variability of behavioral noise. On a linear track, behavior is constrained, and repeated passes through the same environment ensures that the place field data collected will be comparable from traversal to traversal over time. Thus it was McHugh et al. and Nakazawa et al.'s utilization of the linear

track which was able to amplify a specific difference between mutants and controls that isn't possible in the open field. For example in Nakazawa et al (2003) the statistical significance of place field size differences was significantly stronger on the linear track than in the open field.

1.4 PSD-95 knockout mouse and enhanced LTP.

Thus far in the neuroscience community, genetically modified mice which have been produced to study the relationship between molecular events, physiological phenomena, and behavioral memory deficits have been limited in number. The number of mice without severe non-specific behavioral deficits is low. We have also only seen a few mice that are specifically deficient in their abilities to exhibit LTP. Thus when Migaud et al. (1998) produced a genetic variant of the post synaptic density-95 (PSD-95) gene in a C57BL/6 mouse strain background that exhibited enhanced LTP and deficient spatial learning in the watermaze, we thought this mouse would be ideal for the study of unidirectional synaptic plasticity and spatial representations in the hippocampus. I will explain the basic facets of this mutant animal and explain why it might be of interest to us.

Migaud and colleagues produced a truncation mutant of the PSD-95 protein (also known as SAP-97) by introducing a STOP codon within the 3rd PDZ domain of the gene (Figure 1.4.1). The first two PDZ domains, which direct protein-protein interactions with the GluR2A & GluR2B subunits of the NMDAR remain intact, however the 3rd PDZ domain is eliminated as well as the SH3 and GK homology domains. Data from Migaud et al. showed that this truncation mutant protein, PSD-95^{PDZ12} is not localized to the dendrites. This is consistent with the disruption of subcellular localization when the C-terminal regions are deleted in the drosophila homologous gene Dlg (Ruiz-Canada, 2002). However a different C-terminal

truncation of PSD-95 has shown to lack changes in its subcellular compartmentalization, synaptic structure as determined by electron microscopy, and GKAP postsynaptic density protein clustering (Klocker, 2002). Because a suitable antibody to PSD-95 was not available at the time to determine the exact localization of PSD-95^{PDZ12}, it is not known exactly where it is localized. However, gross morphological changes in anatomy were not observed and other groups have also reported that there are no morphological changes in synaptic structure. In summary, the PSD-95 KO mice have altered PSD-95^{PDZ12} clustering at the synapse, however show normal synaptic structure and GKAP protein clustering.

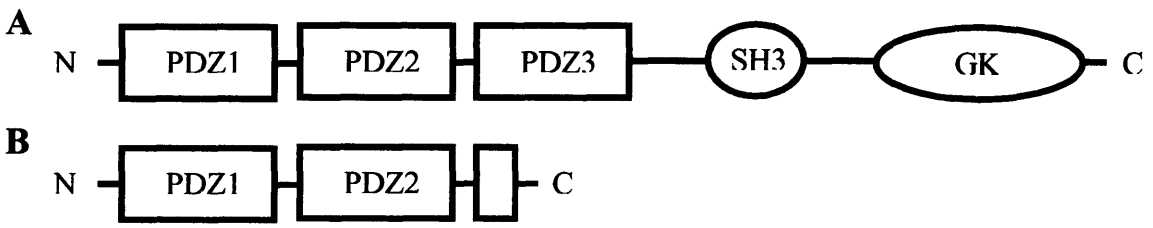

Figure 1.4.1 Schematic diagram of the wildtype PSD-95 protein and the truncation mutant designed by Migaud et al. (**A**) The full length PSD-95 consists of 3 PDZ domains, an SH3 domain, and a GK (guanylate kinase) domain. (**B**) The PSD-95^{PDZ12} mutation is truncated and includes the full PDZ1 and PDZ2 domains.

Slice electrophysiology of the PSD-95 KO mice was particularly interesting. Whole cell measurements showed that NMDA/glycine evoked currents are *not* significantly different and NMDA/AMPA ratios are normal. Thus, signifying that single cell NMDA/AMPA mediated spiking should be unchanged. Additionally, LTP was enhanced. From field potential experiments, Migaud et al. showed that AMPA evoked fEPSPs are normal. Secondly, paired

pulse facilitation is enhanced suggesting an enhanced presynaptic release mechanism of action, however the mechanism is unclear. Because PSD-95 is known to bind to potassium channels and possibly help cluster them, the mutant mouse potentially might have enhanced presynaptic release by longer lasting action potentials mediated by altered regulation of K+ channel clustering (Imamura, 2002). But again most interestingly, in field measurements, lower frequencies of tetanic stimulation (1 Hz) which usually induce LTD, actually induce LTP in the mutants. Higher frequencies of stimulation (10-100 Hz) still induce LTP, but are enhanced two fold compared to controls. Thus the mutant PSD-95 mouse has a shifted frequency of stimulation vs. LTP response curve (known as the BCM curve), such that the PSD-95 mutants only express LTP at all frequencies of stimulation. While the CA1-NMDAR1 KO mice entirely lacked any form of bidirectional synaptic plasticity, these mice actually exhibit enhanced unidirectional synaptic plasticity at all physiologically relevant frequencies. Is this mutation relevant for the mouse? Indeed it was, as the mutation caused a strong impairment of learning in a watermaze task. Although enhancing LTP might be naïvely thought to create a "smart" mouse because of the enhanced of synaptic plasticity, Migaud et al. concluded that bidirectional synaptic plasticity was necessary for the formation of spatial memories. As a subject for analysis for place cell electrophysiology, the properties of these mice were extremely interesting to us.

1.5 Review of PSD-95 structure and function.

The involvement of the postsynaptic density protein-95 in NMDA-receptors and in the impairment of learning and memory has been widely studied in the past five years. More than five hundred papers on various aspects of PSD-95 have been published but none dealing with the properties of PSD-95 reported in this study. Since the present study is particularly novel and

PSD-95 is so widely related to various electrophysiological functions, the implication of the present study must be considered from the point of view of existing knowledge of the gene. Although PSD-95 has been investigated from all angles, we focus our review only on a few of these studies that we consider most interesting and/or may be related to our study.

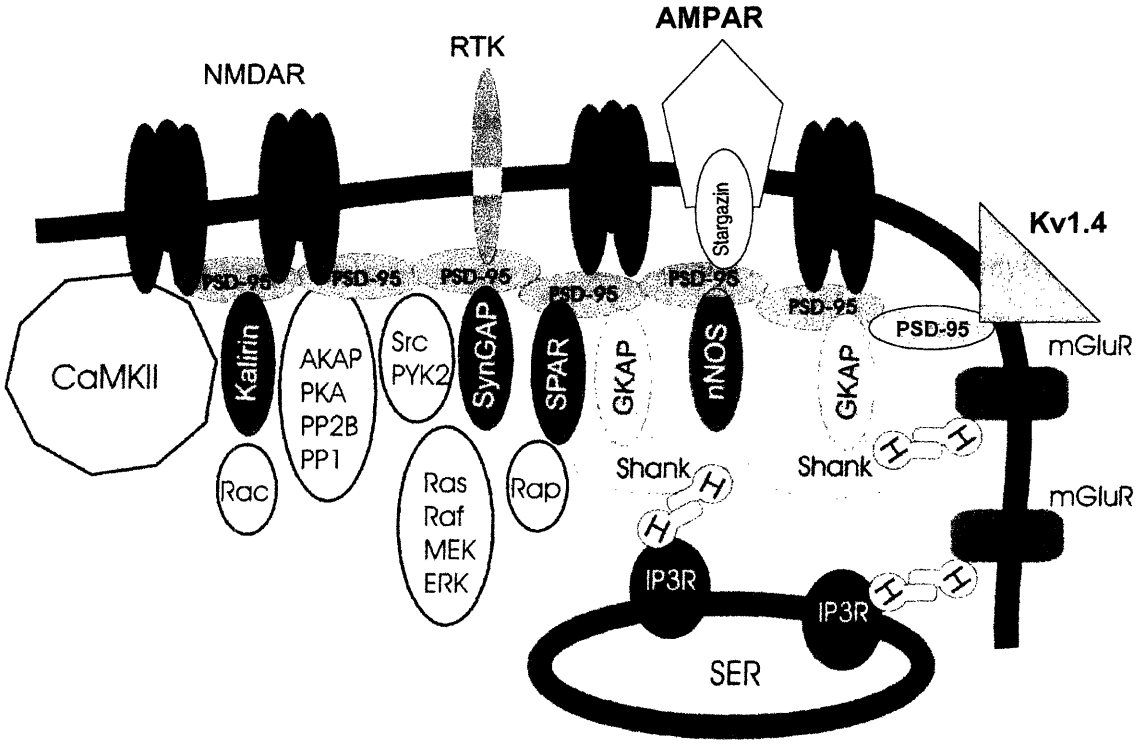

Figure 1.5.1 Hypothetical PSD adapted from Sheng and Kim, Science. 298, 776 (2002). PSD-95 represents an intermediate bridge between NMDAR receptors and other PSD proteins. The three major components of the PSD fraction are the NMDAR, PSD-95 and CaMKII proteins.

1.5.1 PSD-95 is an abundant postsynaptic scaffolding protein.

More background evidence to support the relevancy of PSD-95 at the synapse level will help bolster any causal claim we may make about its role in neural network function and behavior. PSD-95 is the second most abundant synaptic protein after CamKII. It is localized

mostly to postsynaptic densities and consists of 3 PDZ domains, an SH3 domain, and a GK (guanylate kinase) domain thus placing it in the membrane-associated guanylate kinase (MAGUKs) family as well as the PDZ domain containing family. PSD-95's true function is thought to be a structural. It helps recruit and clusters other postsynaptic factors by acting as a postsynaptic scaffolding protein (Kennedy, 1998; Sheng, 2002). The factors that PSD-95's interacts with include: NMDAR, Kalirin, AKAP, PKA, PP2B, PP1, SynGAP, GKAP, nNOS, RTK, and potassium channels (Kv1.4). By recruiting molecules to bear in close proximity with each other, PSD-95 assists in protein-protein interactions and possibly enhances the catalytic activity of these dynamic multi-subunit interactions.

1.5.2 PSD-95 binds directly to postsynaptic NMDAR and K+ channels, thus possibly affecting ionotropic receptor function.

The second PDZ domain of PSD-95 binds specifically to the NR2 subunit of the NMDAR, suggesting a possible regulatory role for PSD-95 in the clustering of NMDARs. This interaction may regulate NMDAR function, thus a mutant form of PSD-95 may affect synaptic strengthening by altering NMDAR function. Additionally, the PSD-95 PDZ1 and PDZ2 domains also bind to the Shaker-type potassium channel Kv1.4 via the PDZ1/2 domains (Imamura, 2002), also suggesting that K+ channels are clustered by PSD-95. The PSD-95 truncation mutant may also affect K+ channel clustering and thus function in pyramidal neurons. It is noteworthy to mention that K+ channel clustering has been studied in the same PSD-95 mutant mouse analyzed in this thesis.

The PSD-95 KO mouse shows evidence that the truncation mutation may not cluster K+ channels (Rasband, 2002) due to a lack of co-localization of PSD-95 and K+ channels at the

axonal regions immediately adjacent to the Nodes of Ranvier (juxtaparanodes). However this evidence was only examined at Nodes of Ranvier on myelinated axons and did not address possible K+ channel localization problems on CA1 pyramidal cells in the hippocampus. It is a relief to know that the primary result of the study concluded that PSD-95 KO mice have normal K+ clustering on myelinated axons of the optic nerve. This evidence suggests the existence of normal synaptic transmission in the visual pathway and thus normal visual function in the PSD-95 KO mouse. This data is a useful control that allows us to eliminate the possibility that the PSD-95 KO mouse suffers from a generalized visual system dysfunction.

1.5.3 PSD-95 involvement in maturation of excitatory synapses

El Husseini et al. (2000) found that exogenous expression of PSD-95 in hippocampal neurons drives maturation of glutamatergic synapses by enhancing postsynaptic clustering and activity. Postsynaptic expression of PSD-95 also enhanced maturation of the presynaptic terminal and increased the number and size of dendritic spines. The observed effects required synaptic clustering of PSD-95 but did not require its GK homology domain. These results demonstrated that PSD-95 is able to orchestrate synaptic development and implies its role in synapse stabilization and structural-based plasticity.

1.5.4 PSD-95 is involved in reciprocal interactions with the NMDA receptor subunit NR2A and α-CaMKII during LTP induction.

In previous literature, both α-CaMKII and PSD-95 have been shown to bind to the NR2 subunits of the NMDA receptor complex. Gardoni et al. (2001) showed that a C-terminal NR2A sequence was sufficient to bind both native and recombinant α-CaMKII and PSD-95 in an *in*

vitro GST-pulldown assay. They also showed that central portion of PSD-95 containing the PDZ domains (peptides 54-256) competed with the binding of both native and recombinant α-CaMKII to the NR2A C-terminal tail. A short sequence of α-CaMKII(1-325) competitively inhibited native PSD-95 and native α-CaMKII to bind NR2A. Thus, PSD-95 and α-CaMKII can compete with each other for binding to the NMDA receptor via the NR2A subunit. Interestingly, protein ratios of α-CaMKII to PSD-95 at the synapse increases after Glutamate/Glycine induction. This increase is inhibited by KN-93, a water-soluble CaMKII-specific inhibitor. LTP induction also increases the α-CaMKII/PSD-95 ratio at the synapse. These data suggest that a dynamic and reciprocal interaction of the NMDA receptor, α-CaMKII, and PSD-95 can exist during hippocampal synaptic plasticity.

1.5.5 PSD-95 plays a role in controlling synaptic strength by mediating AMPA receptor function at the synapse.

Using particle-mediated gene transfer, Beique and Andrade (2003) overexpressed PSD-95 in cortical pyramidal neurons in brain slices and assessed the consequences on synaptic transmission and plasticity. Evoked EPSCs caused greater AMPA receptor/NMDA receptor ratios in PSD-95 transfected pyramidal cells resulting in larger amplitude AMPAR-mediated evoked EPSCs compared to matched controls. Presynaptic release probability was determined not to be altered by paired pulsed facilitation analysis. Overexpression of PSD-95 was further accompanied by an increase in the frequency, but not amplitude, of AMPAR-mediated mEPSCs. Altogether these results indicate that overexpression of PSD-95 increased AMPAR-mediated synaptic transmission. They also found that PSD-95 overexpression greatly enhanced the probability of observing long-term depression. Beique et al. conclude PSD-95 plays a crucial

role in mediating synaptic strength via AMPAR regulation however this regulation is reflected by an increased number of synapses expressing AMPARs rather than an increased transmission function of AMPA receptors at individual synapses.

1.5.6 PSD-95 couples NMDARs to multiple downstream signaling pathways

At glutamatergic synapses, PSD-95 bridges NMDAR with the MAP Kinase ERK/Ras GTPase-activating protein SynGAP. The single molecular bridge between NMDAR and SynGAP, suggests that PSD-95 may play a role in NMDAR-dependent activation of Ras/MAP signaling pathways and in synaptic plasticity. Komiyama et al. (2002) examined MAPK (ERK2) signaling, LTP, and spatial learning in mice that were heterozygous nulls for the SynGAP gene. In SynGAP(+/-) mice, NMDAR stimulation induced an increase in ERK activation. In SynGAP(+/-) heterozygotes, CA1 LTP was significantly reduced but had normal basal synaptic transmission and NMDAR-mediated synaptic currents. Additionally, the double mutant SynGAP(+/-)/PSD-95(-/-) mouse showed enhanced LTP similar to the single mutant PSD-95(-/-), leading the authors to conclude that PSD-95 acts upstream of SynGAP.

1.5.7 AMPA-mediated Synaptic strength is regulated by palmitate cycling on PSD-95

The dynamic regulation of AMPA receptors is hotly debated at this moment and represents one probable mechanism for controlling synaptic strength via vesicle mediated insertion into the postsynaptic membrane (Hayashi, 2000). Palmitoylated PSD-95 associates with Stargazin, an AMPA receptor trafficking protein. El-Husseini et al. (2002) discovered that palmitate cycling of PSD-95 occurs at the synapse and is regulated by glutamate receptor activity. By acutely blocking palmitoylation of PSD-95, AMPA receptors fail to cluster at the

synapse. They also found that depalmitoylation of PSD-95 is required for rapid glutamate-mediated AMPA receptor internalization. El-Husseini and colleagues suggest that PSD-95, regulated by palmitoylation, regulates synaptic strength and thus activity-dependent plasticity.

1.5.8 PSD-95 promotes Fyn-mediated tyrosine phosphorylation of the N-methyl-D-aspartate receptor subunit NR2A

Fyn, a member of the Src-family protein-tyrosine kinase (PTK) which involves N-methyl-D-aspartate (NMDA) receptor function, was the second gene to be knocked out in a mouse which demonstrated a learning and memory impairment (Grant, 1992). Tezuka et al. (1999) showed that tyrosine phosphorylation of NR2A was reduced in fyn-mutant mice. They also showed that PSD-95 catalyzes Fyn-mediated tyrosine phosphorylation of NR2A by structurally clustering the two proteins together in space. Tezuka and colleagues suggest that PSD-95 is a recruiting catalyst for NMDA receptor activity by Fyn and other Src-family PTKs, by serving as a molecular scaffold for anchoring these PTKs to NR2A.

1.5.9 The C-terminal end of NMDA subunits NR2A,B and members of the PSD-95 family of membrane-associated guanylate kinases.

Niethammer and colleagues (1996) used the yeast two-hybrid system to screen a rat brain cDNA library. They identified an interaction between C-terminal end of NMDA receptor subunits 2A and 2B (NR2A and NR2B) with the first two PDZ domains of PSD-95. PSD-95 is also known to bind and cluster Shaker-type voltage-gated K+ channels (Kim, 1995). Thus the similarities between the C-terminal end of the NR2 subunits and K+ channels suggest a common

C-terminal binding motif for PDZ domains. This result predicted that PDZ domains function as modules for protein-protein interactions.

1.5.10 PSD-95 PDZ domains bind and regulate clustering of K+ potassium channels.

Kim et al. (1995) first showed that PSD-95 binds to Shaker-type K+ channel, Kv1.4, via the PDZ1 or PDZ2 domains. Imamura et al. (2002) introduced missense and deletion mutations into PDZ1 and/or PDZ2 of the full-length PSD-95 and demonstrated that mutants disrupt the association with target proteins. Transient transfection of COS-1 cells coexpressing the PDZ2 mutant and Kv1.4 showed significantly reduced clustering efficiency. Cells expressing the mutated PDZ1 domain exhibited clustering activity equivalent to the wild-type. Imamura et al. concluded that the PDZ2 domain of PSD-95, which has highest affinity for Kv1.4, is required for efficient ligand binding and subsequent channel clustering. Recently, Tanemoto and colleagues (2002) showed that PSD-95 clusters the abundantly expressed homomeric assembly of Kir5.1, an inward-rectifying K+ channel subunit which is believed to be nonfunctional.

1.5.11 PSD-95-associated RapGAP, SPAR, regulates the dendritic spine morphology

Pak and colleagues (2001) reported that SPAR, a Rap-specific GTPase-activating protein (RapGAP), interacts with the guanylate kinase-like (GK) domain of PSD-95 and forms a complex with PSD-95 and NMDA receptors in brain. In non-hippocampal cells, SPAR reorganized the actin cytoskeleton and recruited PSD-95 to F-actin. In hippocampal neurons, SPAR localized to dendritic spines and caused enlarged and irregular spine heads. Dominant negative SPAR constructs cause narrowing and elongation of spines. This result suggests that

thePSD-95 GK domain, which is absent in the PSD-95 KO mutant, is involved in the recruitment SPAR to the synapse and subsequent change in spine morphology.

1.5.12 PSD-95 three-dimensional structure and interaction with Kv1.4

Long et al. (2003) solved the three-dimensional structure of the first two PDZ domains of PSD-95. Increasing the spacing between PDZ1 and PDZ2 resulted in decreased binding between PDZ12 and its dimeric targets and also impaired the functional ability of PSD-95 to cluster Kv1.4 potassium channels in heterologous cells.

1.5.13 PSD-95 mediates nitric oxide synthase cellular trafficking and activity.

Recent evidence indicates that nitric oxide (NO) is a retrograde messenger that mediates hippocampal LTP in the stratum radiatum of the CA1 (Burette, 2002). Brenman et al. (1996) originally demonstrated that neuronal nitric oxide synthase (nNOS) binds selectively to the second PDZ domain of PSD-95. Watanabe et al. (2003) showed that dual palmitoylation of cysteine residues on PSD-95 and the requirement of its PDZ2 domain were necessary in order for PSD-95 to induce endogenous CaMKII to phosphorylate nNOS at Ser 847 in neuronal cells. Thus, PSD-95 is thought to regulate nNOS activity.

1.5.14 Schizophrenia, synaptic plasticity, and involvement of PSD-95.

A number of studies have suggested abnormal glutamatergic transmission in the cerebral cortex may underlie or perhaps contribute to the pathophysiology of schizophrenia. Dracheva et al. (2001) reported that NMDA receptor subunits are abnormally expressed in the dorsolateral

prefrontal cortex in elderly patients with schizophrenia. The disproportionate expression of the NR1 and NR2A subunits relative to NR2B expression may have implications for the pathophysiology of schizophrenia and the sensitivity of schizophrenic patients to glutamate and glutamatergic drugs. Ohnuma et al. (2000) examined expression of the PSD95 mRNA in the prefrontal cortex and hippocampus in postmortem material from neuroleptic-treated schizophrenics and normal controls. They showed that the expression of PSD95 was reduced in Brodmann area 9 of the prefrontal cortex but not in the hippocampus by in situ hybridization analysis. However Toyooka et al. (2002) examined the expression of many PDZ proteins: synapse-associated protein SAP-97, PSD-95, chapsyn-110, GRIP1 and SAP102, in post-mortem brains of schizophrenic patients and control subjects. They determined that SAP97 protein levels as well as its binding partner, GluR1, were decreased specifically in the prefrontal cortex of schizophrenic patients. There were no significant changes in the levels of the other PDZ proteins in any of the regions examined. Ohnuma and colleagues (2003) also showed that Fyn, a protein tyrosine phosphatase implicated in learning and memory (Grant, 1992), is significantly increased in expression in schizophrenia patients. These results further implicate the prefrontal cortex in the pathophysiology of schizophrenia and suggest dysfunction of NMDA receptors and other proteins involved in regulation of synaptic plasticity in the schizophrenic cortex.

1.5.15 PSD-95 and G protein-coupled receptors.

The 5-HT2A serotonin receptor is an important G protein-coupled receptor (GPCR) that mediates the effects of hallucinogens and is the target of a number of commonly prescribed medications, including atypical antipsychotics, antidepressants and anxiolytics. Xia et al. (2003) via co-immunoprecipitation assays determined that via its PDZ domain, the 5-HT2A receptor

interacted directly with PSD-95. Interestingly, the association with PSD-95 enhanced 5-HT2A receptor-mediated signal transduction. Additionally, 5-HT2A receptor and PSD-95 were co-localized in clusters on the cell surface of heterologous cells. Thus PSD-95 regulates the functional activity and intracellular trafficking of 5-HT2A receptors.

1.5.16 Additional evidence of the enhanced LTP phenotype in the PSD-95 KO mice.

There has been some speculation and skepticism of the enhanced LTP phenotype in the PSD-95 KO mice. Two independent labs have confirmed an enhanced LTP phenotype in the PSD-95 KO mutant mice. Early LTP in neonates is enhanced (M. Phillips and P. Goldman-Rakic, personal communication). Dentate LTP is also enhanced in these mutant mice (M. Jones, personal communication). However there is still some debate as to whether or not the PSD-95 KO mouse has an LTP phenotype or some sort of generalized non-specific deficit. There is evidence from other PSD-95 interactors that suggest a conserved mechanism. Protein Tyrosine Phosphatase alpha and delta contain D1 and D2 domains that both bind to the PDZ2 domain of PSD-95 (Lei, 2002). Two independent labs have determined that PTP-α & PTP-δ deficient mice both have enhanced LTP (Lei, 2002; Uetani, 2000). The combination of all these results suggests that an enhanced LTP phenotype is part of a conserved mechanism that is regulated by PSD-95 via its PDZ2 domain.

1.6 Purpose of thesis.

A priori, we did not know what to expect in the PSD-95 KO mouse. From this author's knowledge, spatial representations have never been studied in an animal that has a *specific* spatial memory impairments and enhanced LTP. Because neural-network models of learning,

which include bidirectional synaptic plasticity, predict that shifts in the frequency function of should be deleterious to cellular associative properties as well as learning and memory, the PSD-95 KO mouse would be predicted to have altered place field characteristics. The following electrophysiological parameters of pyramidal cell and interneurons in PSD-95 knockout mice are investigated in the present study: *place cell spike waveforms, place cell firing rate maps, place field cross correlation of overlapping fields, place cell directionality, theta modulated activity, place cell asymmetry and phase precession.* A few of these electrophysiological parameters have not been used previously in a similar mouse study. The implications of these parameters for the deficit in spatial learning and memory loss will be debated and a model will be presented in the discussion section.

CHAPTER 2 MATERIALS AND METHODS

2.1 Description of genetic variant of PSD-95 in knockout mouse.

In collaboration with Dr. Seth Grant, we have received a genetic variant of the PSD-95/SAP97 gene in a C57BL/6 background (Migaud, 1998 . Specifically this gene was "knocked out" by introducing a STOP codon within the 3rd PDZ domain of the gene (Figure 1.4.1). The first two PDZ domains, which direct protein-protein interactions with the GluR2A & GluR2B subunits of the NMDA receptor, remain intact however the 3rd PDZ domain is eliminated as well as the SH3 and GK homology domains. Data from Migaud et al. showed that this truncation mutant protein PSD-95^{PDZ12} is not localized to the dendrites. This is consistent with the disruption of subcellular localization when the C-terminal regions are deleted in the homologous gene Dlg (Ruiz-Canada, 2002). However a different C-terminal truncation of PSD-95/SAP97 has shown to lack changes in its subcellular compartmentalization, synaptic structure by EM, nor GKAP (see Figure post synaptic density protein clustering (Klocker, 2002). Because a suitable antibody to PSD-95 was not available at the time to determine the exact localization of PSD-95^{PDZ12}, it is not known exactly where it is localized. However, gross morphological changes in anatomy were not observed and other groups have also reported there are no morphological changes in synaptic structure nor GKAP protein clustering.

2.2 Rederivation of PSD-95 KO mice was required due to DCM housing infection.

The initial batch of mice that was sent to MIT was housed in the same room as a group of mice that was infected with the parasitic pinworm disease. Because of this, MIT's Department of Comparative Medicine (DCM) required us to rederive these mice through in-vitro fertilization

(IVF) in order to make sure that our study mice would not be infected with the parasites. The IVF was carried out by DCM and produced five mice, three of which were heterozygous for the PSD-95^{PDZ12} alleles. These heterozygous mice were crossed with wildtype C57BL/6 mice in order to increase the numbers of mutant animals for our studies.

2.3 The challenge of breeding the PSD-95 KO mouse was solved with multiple strategies.

Much of the difficulty of studying this mutant was due to issues of breeding. Breeding between heterozygote males and females produced very few homozygous offspring. Our low homozygous mutant yields were similar to the 16% yields that Migaud et al. reported. Thus, the only reliable way of producing homozygotes at high yield was to breed homozygous males and heterozygous females or vice verse. The breeding efficiency of these homozygote/heterozygote pairs was notably less efficient than breeding heterozygote/heterozygote pairs. Additionally, due to the proclivity of C57BL/6 mice to eat their own pups and reduce litter yields, we derived a protocol that would use white BALB/c mice as foster mothers (D.Gerber, personal communication). This protocol would entail breeding BALB/c wildtype pairs 2 days before we would breed an equivalent or greater number of the PSD-95 KO pairs. The males were removed from the cages of females after the mating plug was observed in the females. Seventeen days after the BALB/c mice were mated we would place cards on the BALB/c and PSD-95 KO mating cages to prevent the animal technicians from changing the cage bedding. Approximately 20 days after the mating of the PSD-95 pairs we would check for pups. All pups born to the PSD-95 KO pairs would be transferred to the BALB/c foster mothers. The BALB/c litters were reduced in size in order to accommodate additional PSD-95 pups. This procedure produced the most reliable number of homozygote males and females compared with all other procedures.

2.4 Updated genotyping protocol for PSD-95 KO.

Unfortunately in our hands the PCR genotyping protocol that we received was inadequate for our needs. On a regular basis we would not be able to genotype the genomic tail DNA of the mice due to poor of visualization of the PSD-95 mutant fragment in the PCR protocol. This caused a severe slowdown in the expansion of our mouse colony. Upon investigation of the primers that were provided in the original PCR genotyping protocol, two of the primers had complementary 3' overhangs. This is a cardinal sin for PCR protocols and thus one of the primers was redesigned. The resulting length of the new fragment was approximately 30 base pairs longer than the original fragment expected.

Primer Pair producing a 200 bp band:

	%GC	Melting temp
PSD#1 Sense 986-997	55%	70.3°C
5' AGG ACT CTC TTT GGT GGG CA 3'		
PSD#2 Anti-sense intron	54.5%	73.2°C
5' AAC CAA GGC GGA TCG TGA TCC A 3'		

Primer Pair producing a ~520 bp band:

PSD#3 neo Cassette-2	50%	71.3°C
5' GCC GCT TTT CTG GAT TCA TCG A 3'		
PSD#4 Anti-sense 1775-95 Coding region	52%	70.8°C
5' AAT CGC GGC CGT CTA TCT CAT 3'		

Primer PSD#3 was redesigned because the previous Neo-cassette primer was 73% GC rich, had relatively high melting temperature (76.2°C). It was also 3' complementary to the

PSD#2 primer for 3 base pairs, thus competitively blocking proper primer-template dimerization. The complementation would competitively decrease PCR efficiency for both primer pair reactions.

Additionally, a slightly altered PCR protocol was employed to increase signal to noise for the production of the desired PCR fragments. Specifically the temperature of the annealing steps was increased to 60 degrees and all times were changed to one-minute intervals.

With these improvements the present study was accelerated with increasing numbers of mutants. The full PCR protocol is outlined in Appendix H.

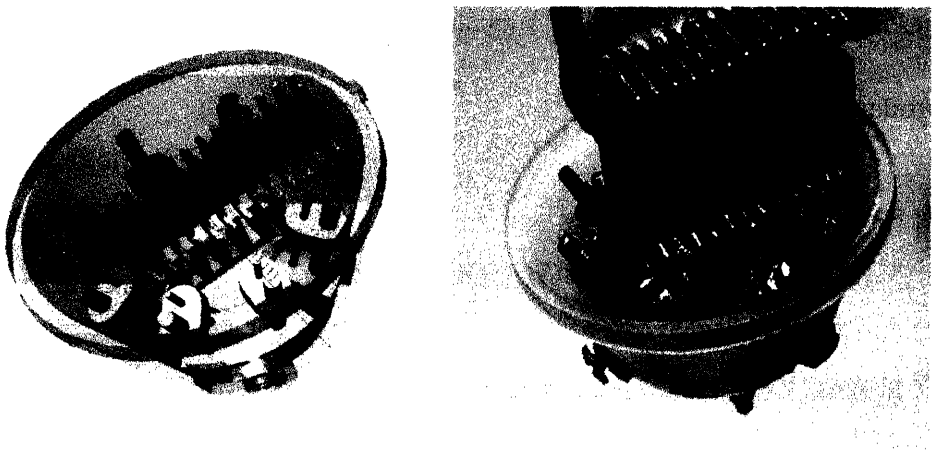

Figure 2.5.1. (a) Computer Aided Design (CAD) of mouse microdrive allowed for reproducible and easily manipulated designs. **(b)** Stereolithography (SLA) 3d printing was used to manufacture the SLAMdrive parts.

2.5 SLAMdrive: microdrive array building using CAD and 3d printing technology.

Producing reliable and accurate microdrive arrays for recording large numbers of channels from mice is a difficult endeavor. Previous microdrive array technology in the Wilson lab used entirely handmade components machined from steel cannuli and dental acrylic. While versatile and strong, these materials made it difficult to reproduce exactly the same drive for every experiment. It also made inter-drive variability manufactured by students highly variable (parts were not exchangeable as each drive was "unique"). Perhaps variations in weight and sizing might affect the datasets acquired from mouse behavioral electrophysiology. Thus, I wanted to develop a method of reliably producing a microdrive array that would not vary between different students involved in the manufacturing of these microdrive.

To improve accuracy and reproducibility, the choice was to choose computer-aided design (CAD). After a CAD designed microdrive part was produced there were a number of different technologies that could be employed to produce the part. 3d printing was selected because of the rapid prototyping capability and accuracy of the parts produced. Of the available 3d printing methods available I compared Objet™ and Stereolithography (SLA®) technology. Objet printing works by an inkjet style technology that prints layer by layer of a 3d object, each droplet of photosensitive epoxy is immediately cured by UV light. Objet offers the highest resolution in an softer amber-colored material. SLA employs a UV laser which solidifies a bath of photosensitive epoxy. SLA offers lower resolution (3mills/.003" in the XY axis and 1 mill in the Z axis; ViperSi system by 3dsystems.com) however offers a wider variety of materials. From experience the Objet material absorbed water over time and changed shape; the material was also much softer and crumbled more easily. While in the SLA system we used "Watershed" epoxy material which showed resilience and hydrophobic properties which did not change the

shape of the objects over time. Additionally, the PVC-like Watershed material was much tougher and easier to drill/manipulate than the Objet material. Hand tapped 0-80 threads which provided the grip for the manipulatable screws were easily created in the SLA material and were long lasting and resilient.

The microdrive parts that were produced by hand were the manipulatable and milled screws, 23 & 30-gauge cannula, and temporary 5.5/6 mill solid wire for reaming the cannula. The parts that were produced via 3d printing were the microdrive "base" array and the protective cone. (See Appendix I for a schematic design of the SLAMdrive)

All of the mice in the present study were fitted with microdrive arrays that were either produced on an SLA or Objet printer. With the watershed material SLA produced drives, CA1 pyramidal cells were stable for days to weeks as assessed by visual inspection of clusters in AD software.

While eight microdrives can possibly fit on this drive design, seven are actually used. Six microdrives are dedicated for 4-channel tetrodes while one microdrive is used for a single-channel reference electrode. On top of the microdrive is a Millmax™ connector to which each channel of the tetrodes is individually connected.

2.6 Tetrode manufacturing and loading on to the SLAMdrive array.

A single strand of nickel-chromium wire was looped twice and spun for 90 rotations in one direction followed by unwinding 45 rotations in the opposite direction. A hot air gun was used to lightly melt the external insulation and "bind" the wire strands together. Tetrodes were loaded into the microdrive and a final cut was made with a pair of sharp scissors, exposing 4 tips of the wire in a diamond shaped array. Tetrodes were splayed by hand at the top end of the

drive. The tips were cut to the appropriate length so as to allow optimal slack to the movement of each microdrive. Wires were lightly burned for a fraction of a second to expose conductive material. Subsequently, the burned tips of the tetrodes wire were glued to the pins of the Millmax™ connector at the top of the microdrive array with conductive silver paint and a small piece of shrink-wrap. The hot air gun was used to bind the tetrodes tips, paint, and Millmax pins together.

2.7 Signal amplification, reference potential selection, improving signal to noise.

The tetrodes will contain millivolt range field potentials that will be highly susceptible to noise. Thus signals are amplified at the level of the microdrive head stage via a custom made 24 channel Field Effect Transistor (FET) circuit board. Each FET output is connected to a thin copper wire which is extended to a custom made "patch box". We built a custom patch box which allowed us to determine which channel will be used as the common reference for all other tetrodes channels. A single dedicated tetrode on the microdrive was determined ahead of time to be the reference channel. However any channel of any tetrode could be suitably used as the reference. Additionally, a single skull screw attached to a wire was passed through the microdrive and pre-amplifier chip to the patch box's common ground in an effort to remove general noise from recordings.

2.8 Acquisition of spike and position data.

Tetrode channels were fed through to a Neuralynx Lynx-8 amplifier with a gain ranging up to a maximum of 40,000X. The amplified signal was fed to eight channel Keithly-Metrabyte ISA Analog to Digital acquisition cards in the PCs.

Spike data was acquired via "AD", a custom PC software program written by Matthew A. Wilson (1993) on 5 custom made Celeron PCs. The PCs contained clock counter cards that were cable synchronized in time with 1/10,000 second accuracy. One PC was dedicated as the MASTER computer which controlled the clock as well as control over data acquisition for the other PCs. Three PCs were dedicated for filtered spike waveform capturing and one PC was dedicated for continuously capturing EEG local field potentials.

For spike waveform filtering, the Analog to Digital (AD) cards were multiplexing 8 channels at 250 kHz which effectively samples each channel at 31,250 Hz. The spike waveform capturing PCs received from Lynx-8 amplifier output which was bandpassed between 300 Hz and 6 kHz (hardware 2-pole analog Butterworth filters). If the voltage difference between a tetrode channel and the reference was greater than a predefined threshold (approximately 80 mV), 6 pixels before the threshold crossing and 26 pixels after were saved as the spike "waveform". All four channels of a tetrode would be digitized if a single channel crossed threshold. Each waveform was time stamped and recorded in binary format to the hard drive. The time stamps were saved as 32-bit unsigned integers and the waveform amplitudes were saved as 16-bit signed integers (ranging from –2048 to +2048).

For continuous EEG field potential recordings, single channels from tetrodes were fed via the patch box to a separate Lynx-8 amplifier. This amplifier was set to bandpass the signal between 1 Hz and 3 kHz. Frequency of sampling was set to 50 kHz multiplexed to 8 channels, effectively sampling each channel at 6250 Hz (barely over the Nyquist frequency). Large EEG buffers were 32-bit unsigned integer time stamped and amplitude was saved as 16-bit signed integers. Needless to say EEG file sizes were much larger than filtered spike waveform files (~600MB for EEG files and ~100MB for spike files).

Position tracking of the mice was acquired via a black and white security camera sensitive to the infrared frequency. A set of front and back Infrared Light Emitting Diodes were attached to the fine wire cable far away from the tetrodes to avoid tracker noise. Front/Back lighting was driven by the Dragon Tracker System (San Diego Instruments) at 60 Hz and position was acquired via parallel port card acquisition at 60 Hz by the MASTER computer. Because one front and back diode was used to determine position, the effective frequency of position acquisition was 30 Hz. The pixel resolution of the tracker was 340x260 pixels. Effort was maintained in the subsequent analysis to eliminate "binning" and instead express pixel values in terms of "raw" tracker pixels. The pixel resolution was approximately 1.75 pixels/cm.

2.9 Surgical procedures.

Surgical procedures were similar to previous methods developed by Matthew A. Wilson (McHugh, 1996). The notable exception to the previous procedure includes the use of surgical grade silicone grease instead of bone wax. The full protocol is outlined in Appendix G.

2.10 Adjusting tetrodes to CA1 pyramidal cell layer.

There is much debate as to which is the best technique or protocol to acquire CA1 pyramidal cells in the mouse. The most successful protocol that I settled on was to "get there as soon as possible." The bottom of the microdrive 18-gauge thin-wall cannula was placed directly on the surface of the brain during surgery. All tetrodes were placed at the exit of the bottom cannula, and exit depths are measured in $1/8^{th}$ turns. As the tetrodes were lowered, we would monitor the amplified signal on an audio monitor. Dimpling of the brain occurred before the tetrodes would "burst" through the duramater. At approximately 20 $1/8^{ths}$, we would hear a

"rush" of noise and activity at which we would stop advancing the tetrode. Subsequent tetrodes would require a deeper depth before bursting through the duramater. After all tetrodes were in the brain we would pull back tetrodes by ½ a turn (or 4 1/8^{ths}) and wait overnight. Since the brain will be "dimpled" and pressed down upon it will eventually rise over time.

On day two of adjusting we would attempt to drive down through the noisy cortex and through the silent white matter through the corpus callosum to the superficial hippocampus. If sharp waves (SPWs)/ripple events were heard, we would immediately pull back our tetrodes back by 1-2 full turns to wait to the next day. We hypothesized that this would create empty "tracks" ahead of the tetrodes which would allow for the brain to rise to the surface skull level against the pressure of the tetrodes. It was too dangerous to leave a tetrodes fully extended because frequently we would come back the next day to find the tetrodes are actually in the CA1 pyramidal cell layer or worse, beyond it. Thus at the end of the day all tetrodes were pulled back by at least a full turn. Approximately over one week we would notice that the absolute depth of the superficial hippocampus would eventually rise and stay constant, allowing for stable place cell recordings.

In the next 7-14 days we would move the tetrodes ever so slightly forward until sharp waves (SPWs) were clearly audible and becoming visible on the EEG monitors. SPW's were seen equally in mutants and controls and were persistent when the mouse was in a immobile, consummatory, or slow-wave sleep state as is in rats supposedly generated by coordinated discharge of CA3 pyramidal cells (Buzsaki, 1983). Because SPW's above and below the CA1 pyramidal cell layers are distinctly different, we used SPW's as a general indication of the location of the CA1 pyramidal cell layer.

Once near the CA1 pyramidal cell layer, movements of the screws were limited to tenths of $1/8^{ths}$. Only when a visible separation or "bouquet" of clusters of units was apparent, was movement of tetrodes halted or limited to very fine adjustments of tenths of $1/8^{ths}$ (Figure 2.10.1). The time required for proper adjusting time ranged between 2½ to 4 weeks.

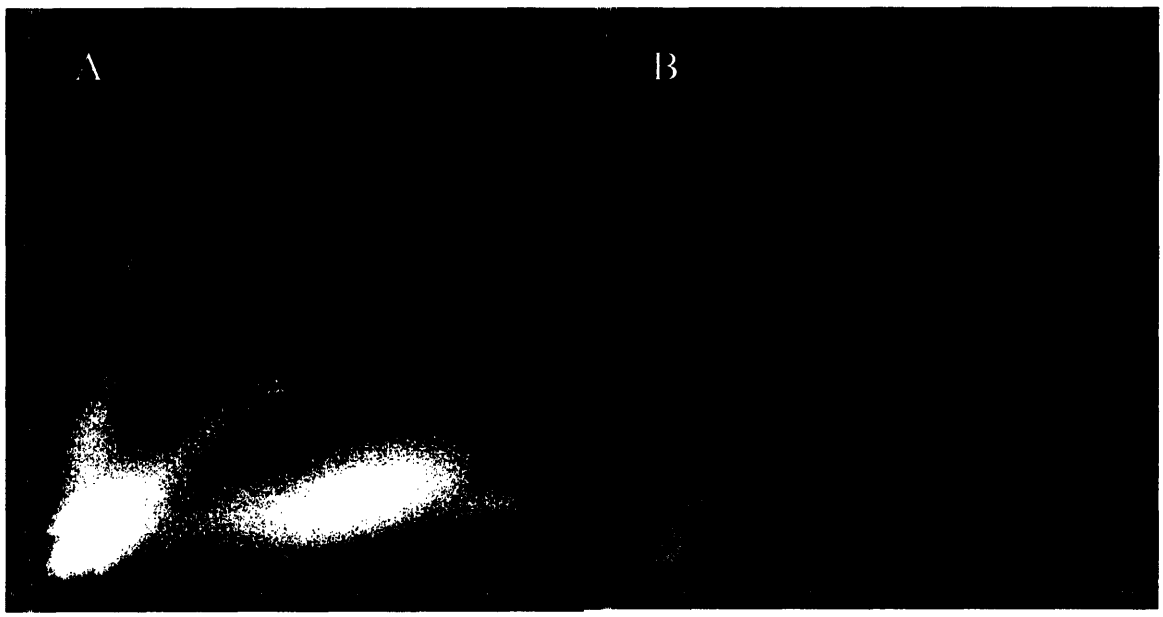

Figure 2.10.1. (A) Example of uncut bouquet of pyramidal units combining two sleep and one run session. **(B)** Example of manually clustered "units" using XCLUST software.

2.11 Methods for spike waveform sorting and pyramidal cell vs. interneuron identification.

Post processing of acquired data was entirely done on Linux workstations utilizing custom software. All spike waveforms were assigned timestamps and position and heading direction values. Utilizing XCLUST (Wilson, M.A.), spike waveforms were manually assigned to "units" based on semi-objective criteria. These criteria were based on visual inspection of pixel density in a two-dimensional projection of spike waveform amplitude values. I clustered together all

sleep and run sessions in a day's dataset. All units were primarily sorted in spike amplitude vs. spike amplitude space. If there were any ambiguities, timestamp vs. spike amplitude projections were used to identify spikes that might have been associated with a slightly wandering unit. Very unstable units were excluded from analysis. XCLUST exported all identified clustered "units" into individual text files. These text files were subsequently imported into MATLAB™ by custom scripts.

All further data analysis was done exclusively in MATLAB™. Following convention of McHugh et al. and Ranck et al. (1973), pyramidal cells were identified as having peak-to-trough widths that were greater than 320 μs. Interneurons were identified as having peak-to-trough widths between 95 μs and 255 μs. Those cells with intermediate peak-to-trough widths were excluded from the analysis. Complex Spike Index (CSI) was calculated in MATLAB and was not explicitly used to identify Interneurons. However, all narrow spike width units were almost always high firing rate cells with near zero CSI values typical of interneurons.

2.12 Categorization of pyramidal cells: elimination of low firing rate units helps improve data analysis and statistical inference.

Interneuronal units tend to be high firing rate cells which fire frequently in sleep and run epochs, thus they were never eliminated from analysis for firing too few spikes. However identified pyramidal cells were required to fire a minimum of 100 spikes in each sleep epoch otherwise, the entire cell was eliminated from analysis. Additionally if a cell fired fewer than 100 spikes during a run epoch, but greater than 100 spikes during each sleep epoch, that cell was categorized as a "Run Off" pyramidal cell. If a cell fired more than 100 spikes in all three epochs (two sleep and one run) it was categorized as a "Run On" pyramidal cell.

In order to study Run activity of robust pyramidal cells, low firing rate units were eliminated from the study. Thus all subsequent analysis of Run active pyramidal cells were restricted to cells that fired a minimum of 1 Hz during the entire run period (Mehta, 1997) as defined by total number spikes divided by the total amount of time spent in the run period apparatus.

2.13 Behavioral paradigm: linear track and recording session protocols.

Mice were housed in a 12hr light/dark cycle and given food ad lib. Chocolate sprinkles were mashed onto food pellets in order to acclimate the mice to the taste. At the end of a daily adjusting period, the mice were also given small crushed amounts chocolate sprinkles by hand. After tetrodes were stable for more than one day, we began recording spike data during mouse behavior.

Recordings were started 3-6 hours before the dark cycle of the mouse in order to capture the mouse's mostly inactive/immobile sleep behavior. Recordings attempted during the dark cycle resulted in very poor sleep/immobile behavior because the mice would incessantly run and explore the sleep box incessantly. All recordings were done in a room 12'x12' with distinct visual cues on all four walls with medium bright ambient lighting focused away from the behavioral apparatus towards the cues on the walls. For the first epoch of a daily recording schedule the mice were placed in a familiar black cylindrical box 1.5' tall. The sleep box was filled with 2 cm of cage bedding which had acquired the scent of the mouse from the prior two weeks of adjusting. The linear track was created in an "L" shape configuration with one arm of the L physically blocked off for all sessions analyzed. Each arm was 100 cm long

(approximately 175 pixels long) and was daily cleaned with 70% EtOH and laid down with a clean blue bench top cloth.

Mice were allowed to sit/sleep in the sleep box for up to 45 minutes or until the mouse was immobile or sleeping and sharp wave activity was persistent. Recording of sleep would continue for at least 25 minutes, after which the mouse was placed into a blocked off end of the linear track. Recording was continued and then the blocked off area was opened to allow the mouse to explore. Mice were allowed to run for a total of a minimum of 30 traversals (15 round trips). Crushed chocolate sprinkles (~1/4 of a sprinkle) were placed sparingly every 4-5 laps at both ends of the linear track in a small plastic dish in order to induce the mouse to continue to explore/run the full length of the track. Interestingly, mouse behavior was markedly worse if chocolate sprinkles were given for every traversal of the linear track since the mice tended to spend a lot of time eating/grooming. The additional time spent would not only slow down the recording session but would also produce some limited noise artifacts in the EEG signals. After the run recording session, mice were placed back into the sleep box. It was common for most mice to be fairly active and exploratory in the sleep box for 10-30 minutes. We continued to record the entire session as sleep and only analyzed the last 20-30 minutes of immobile behavior which was SPW abundant recorded during the second sleep period.

To this author's knowledge, this study collected in total the largest numbers of hippocampal units in a mouse compared to all other studies published to this date. In total two homozygous PSD-95 KO mouse and three control mouse data sets were separated in to mutant and control running sessions. While there are fewer mice in this study, it is offset by the over all efficiency of pyramidal cell collection. There is an order of magnitude more cells in this study than others that would preclude the need for larger numbers of animals as was previously argued

by other groups (Buzsaki, 2003). Linear track data was collected for 3-5 days. After which the second arm of the linear track was opened for a novel exposure. All linear track data sessions were equivalently compared with each other. An equivalent number of sessions were compared between mutants (d=13) and controls (d=16). I clustered a total of 352 pyramidal cells and 32 interneurons in the control mice. I also clustered 161 pyramidal and 14 interneurons in the mutant animals. In both the mutants and controls approximately 10% of the total number of cells were interneurons. This was a typical yield suggesting equivalent interneuron/pyramidal cell distributions during neocortical development of the mutants. If each cell was further divided by direction of running into two place fields (Mehta, 1997), I collected a total of ~700 control and ~300 mutant place fields for a grand total of 1000 place fields! However if these fields were eliminated from the analysis based on firing rate many more mutant fields would disappear from the analysis for reasons that will be explained in section 3.9-3.11. An equivalent number of cells were compared between mutants and controls for the majority of the analysis for balancing reasons. Statistical differences and similarities were unchanged though slightly improved with the larger n.

CHAPTER 3: PSD-95 KO EXPERIMENTAL RESULTS

3.1 Defining the question.

If we were to eliminate LTP/LTD in the hippocampal system, how would spatial representations of memory be affected? This question was posed by McHugh et al., and was satisfactorily answered and will be extensively compared in the discussion section with this animal model. The question we are posing with the PSD-95 KO mouse is the following: if we were to eliminate LTD altogether, while only allowing an enhanced form of LTP to exist in the mouse, how will spatial representations formed by CA1 pyramidal cells be altered?

By inspection the mice will give us some level of prediction for what we might expect in awake-behaving electrophysiology. Many mutant mice are visibly different than their wildtype counterparts, such as NT-3 transgenics or TSDn65 mutants (data not shown). Either they are poorly groomed, or hyperexcitable – nonetheless these mice make for a poor model for place cell electrophysiology studies. However, by gross inspection of adult mice, it is nearly impossible to distinguish the difference between the mutants and controls. They are not hyper-excitable or aggressive, nor are they larger as adults though some runting in litters has been reported in Migaud et al. (1998).

We know from Migaud et al., that the mice have a spatial learning deficit as assayed in the Morris water maze. Thus there is a prediction that these mice will have some altered physiological representation of space by their CA1 pyramidal neurons. However we don't know a priori what those changes would be. One prediction we might have is that by lacking a mechanism to depress synaptic connections, the pyramidal cells would continuously enhance their synaptic strengths causing a positive feedback loop which would quickly overrun the

network system and cause widespread over-excitation. This over-excitation might lead to seizure activity. This was the case for a CamKII knockout mouse (personal communication, M.A.Wilson), BDNF over-expressing transgenic mouse (unpublished results, LDS). Luckily, the PSD-95 KO mouse does not show any seizure activity, and thus it seems that we can predict that the mechanisms which regulate overall network activity will be maintained.

Additional control analysis must be completed in order to assess what potentially significant changes are occurring in these mice. If every measure we compare between mutants and controls are different, then we can generally conclude that we have a "screwed up" animal. However if we can further restrict the relevant synaptic differences between the animals, we will be more confident and have fewer correlations to link an explaination to the observed phenotype.

3.2 Equivalent percentage of pyramidal cells are active during run.

Other enhanced LTP mice have reported significantly fewer cells active during run (Yan, 2002). However in our study the ratio of run active cells for mutant sessions (0.68+/-0.06, n = 10) and control sessions (0.8+/-0.04, n = 16) were not significantly different ($p>0.05$, Students T-test). Pyramidal cells were considered "run-active" if they fired a minimum of 200 spikes during both sleep sessions and minimum of 50 spikes during run. They were "sleep-only" active if they fired a minimum of 200 spikes during both sleep sessions and less than 50 spikes during run. Sessions were only included if at least 6 pyramidal cells were identified.

3.3 Firing rates are not significantly different.

The first order of comparison between mutants and controls is to compare the general firing rates of the CA1 pyramidal cells and interneurons. Firing rates were calculated for entire

epoch periods of Sleep 1, Run 1, and Sleep 2. All spikes were divided by the total time period spent during those epochs. Sleep epochs were chosen to reflect immobile activity of the mouse. Firing rate analysis during run epochs included times during which the animal was running, grooming, eating, and some immobile behavior.

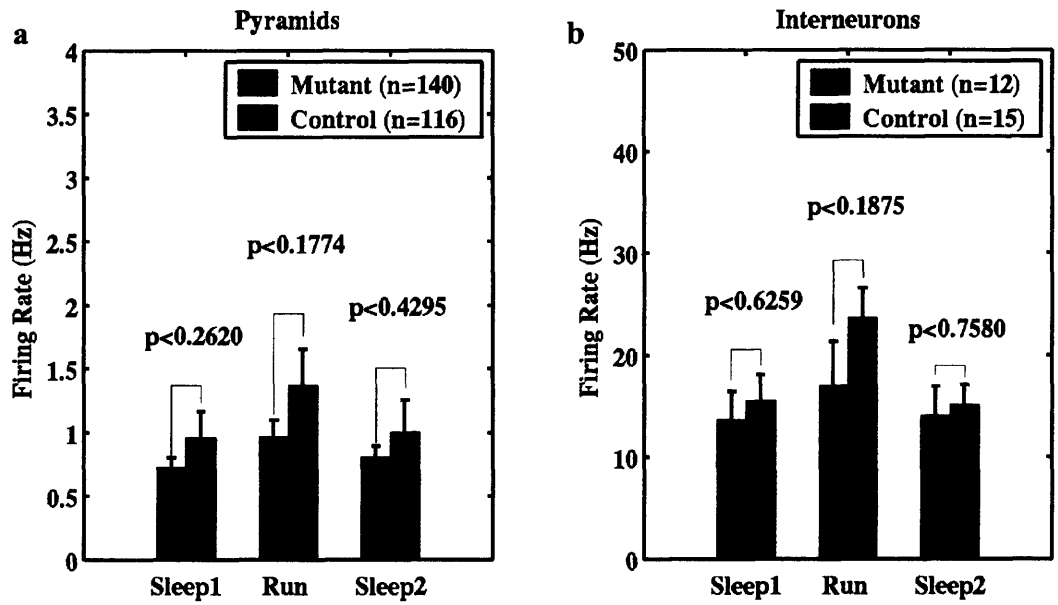

Figure 3.3.1 **(a)** Pyramidal cells for Mutants (red) and Controls (blue) were not significantly different in overall firing rates during the sleep or run epochs. **(b)** Interneurons were also not significantly different.

During Sleep 1, Run, and Sleep 2 epochs, pyramidal cell firing rates between mutants (n =140) and controls (n = 116) were not significantly different ($p<0.26$, $p<0.18$, $p<0.43$ respectively; Students T-test). During the same three epochs, interneuronal firing rates between mutants (n =12) and controls (n = 15) were also not significantly different ($p<0.62$, $p<0.19$, $p<0.76$ respectively; Students T-test; Figure 3.3.1). Pyramidal cells had an average firing rate of 1Hz and interneurons approximately 17Hz which is consistent with previous values in McHugh et al. (1996). The fact that overall firing rates were not altered in the mutants provides evidence that

network wide regulation of activity is not altered. Specifically, there was not a system-wide over-excitation that was occurring in the mutants which leads to overall higher firing rates.

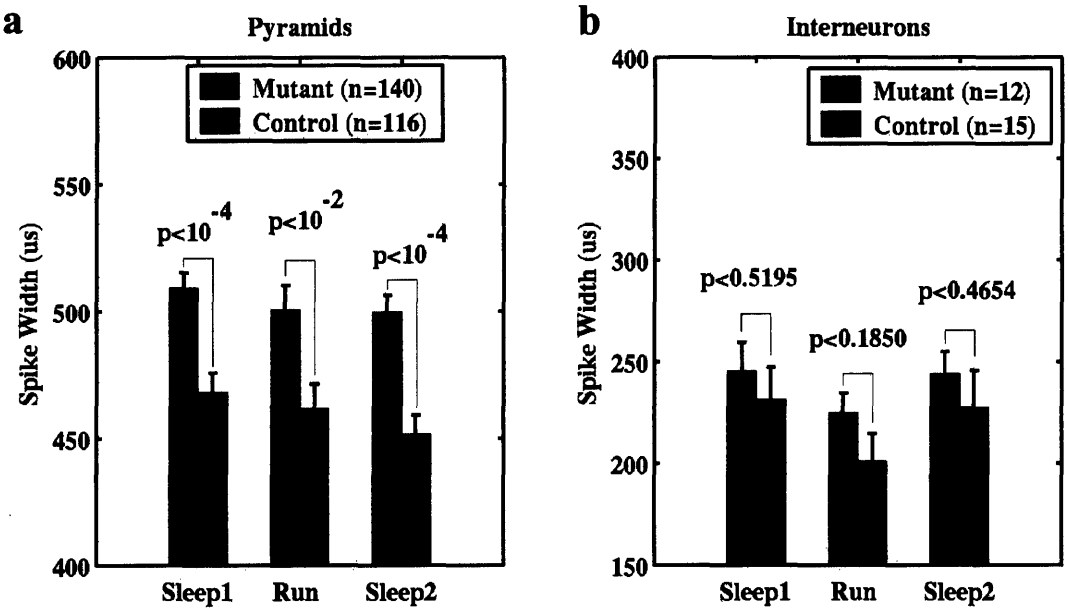

Figure 3.4.1. **(a)** Pyramidal cell spike widths are wider in the mutants than controls. **(b)** Interneuronal spike widths are not significantly wider than pyramidal cells.

3.4 Spike widths are significantly wider in mutants than in controls.

Spike widths are computed from the 32 pixel samples from one of the four waveforms recorded from a tetrode which had the maximum amplitude. The width was calculated from the peak of the waveform to the trough. If a waveform was larger than the 32 pixels and the minimum value was the 32nd pixel, then the peak to trough distance was calculated from the peak to the 32nd pixel. This would happen more frequently for pyramidal cells which typically had longer lasting spike waveforms than interneurons.

Pyramidal cell peak to trough spike widths in all three epochs for mutants (n = 140) compared to controls (n = 116), were significantly wider ($p<10^{-4}$, $p<10^{-2}$, $p<10^{-4}$, Students T-test;

Figure 3.4.1). However for Interneurons the peak to trough widths for mutants (n = 12) compared to controls (n = 15), were not significantly different for the datasets compared ($p<0.52$, $p<0.19$, $p<0.47$, Students T-test). Potassium channels have been suggested as the sole component for which causes the peak to trough width to vary and is a potential mechanism to explain the differences in spike width.

3.5 Bursting properties are not significantly different.

Complex spikes are a typical property of pyramidal cells (Ranck, 1973; McNaughton, 1983). The complex spike index (CSI) is an estimate of the bursting characteristics of a pyramidal cell (McHugh, 1996). To calculate CSI every spike pair is analyzed that are within 15 ms of each other but no less than 2 ms apart. If the second spike amplitude is lower than the first, then a +1 is added to the sum. If the second spike amplitude is higher than a –1 is added to the sum. The total sum is divided by the total number of spike pairs and multiplied by 100 to achieve a "percentage" CSI value. In other words, if a CSI value of 15 is obtained, we would say that approximately 15% of the spike pairs compared have decreasing amplitude spikes over time beyond that expected by chance. A high positive CSI value is typical of pyramidal cells, while a low near zero CSI value is typical of interneurons.

Pyramidal cell CSI values in all three epochs for mutants (n = 140) compared to controls (n = 116), were not significantly different ($p<0.052$, $p<0.26$, $p<0.12$, Students T-test; Figure 3.5.1). Pyramidal cell CSI values averaged approximately 17, typical of bursting CA1 pyramidal cell. Also for interneurons the CSI values for mutants (n = 12) compared to controls (n = 15), were not significantly different ($p<0.52$,$p<0.19$,$p<0.47$, Students T-test). Note that CSI values for the interneurons were significantly lower than the pyramidal cells averaging near zero.

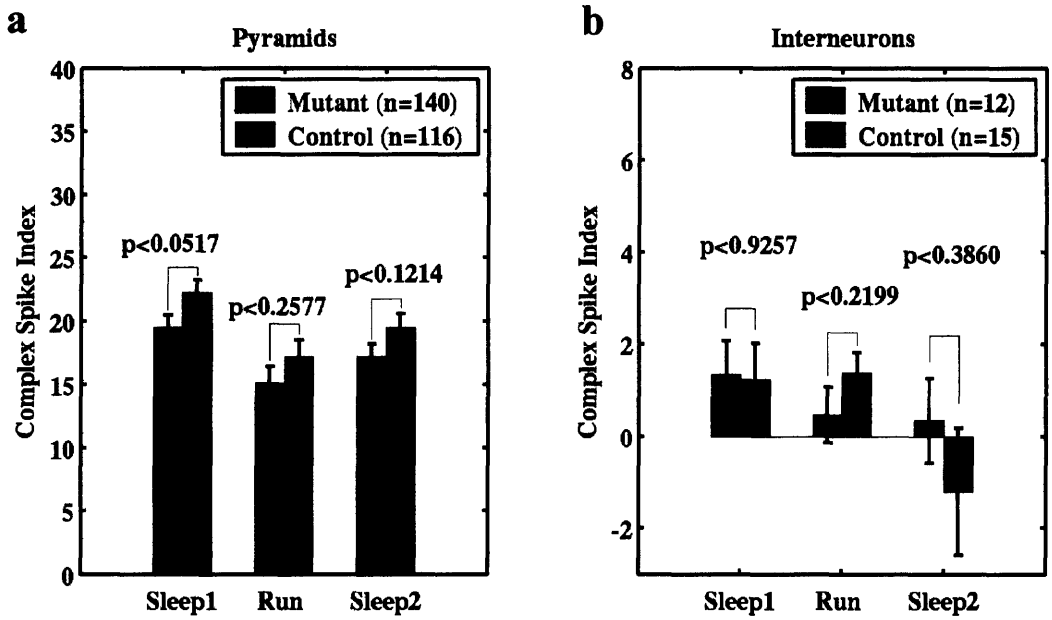

Figure 3.5.1. **(a)** Pyramidal cells Complex Spike Index (CSI) are not significantly different between mutants and controls for all three epochs. CSI values are equivalently high in both mutants and controls. **(b)** The same is true for interneurons between mutants and controls, however the CSI values are much lower.

Complex Spike Index was not used as a determinant for cell identification. Only spike width was used, and CSI values were calculated post cell classification. The similar CSI values between mutants and controls provides evidence that the basic cellular mechanisms that regulate bursting activity remain unchanged in the mutants.

3.6 Covariance of firing is enhanced during post-run sleep in the mutants.

Overlapping place fields have been reported to increase their covariance of firing after experience. CA1-NMDA knockout mice, which lack LTP & LTD, have also been reported to lack covariance of firing during spatial exploration (McHugh, 1996). It would be curious to

know how the PSD-95 KO mouse, which exhibits enhanced LTP and lacks LTD, would be affected in co-firing rate properties. The first order properties of LTP would predict that the PSD-95 KO will at least retain but perhaps increase its covariance of firing. While examining fields which fired over at least 10% of the linear track ($270cm^2$) and their pairs which overlapped a minimum of $40cm^2$ (as in McHugh et al.), we found that there was indeed an increased co-variance of firing during the post-run sleep session. The mean covariance coefficient of the mutants during Sleep 1 (0.035+/-0.007, n = 141) and Run (0.078+/-0.011 n = 141) were not different than the controls during Sleep 1 (0.036+/-0.007, n = 173, $p<0.89$, Students T-test) and Run (0.086+/-0.009, n = 173, $p<0.60$, Students T-test). However during the Sleep 2 session, the mutants show an enhanced covariance compared to controls (0.085+/-0.01, n = 141; 0.057+/-0.007, n = 173, $p<0.0219$, Students T-test) as shown in Figure 3.6.1. Correlation coefficient of interneuronal field pairs of mutants and controls were not significantly different ($p>0.05$, data not shown).

When we examined the mean correlation coefficient of *non-overlapping* fields using the same 10% minimum size criteria, mutant field pairs were not significantly different (Figure 3.6.1; Students T-test) than control field pairs in Sleep 1 (0.034+/-0.021, n = 12; 0.014+/-0.005, n = 31; $p>0.19$), Run (-0.024+/-0.006, n = 12; -0.022+/-0.006, n = 31; $p>0.91$), or Sleep 2 (0.065+/-0.021, n = 12; 0.032+/-0.011, n = 31; $p>0.14$). However when comparing relative differences of correlation between overlapping and non-overlapping fields in Sleep 2 within genotype, there is no significant trend seen. Thus, while PSD-95 KO mice have equivalent co-variance of firing compared to control mice during the encoding of space, they also have enhanced post-run correlations during the second sleep session. Thus, unidirectional LTP might be enhancing co-firing of pyramidal cells in Sleep 2. It is also interesting to note that over a 24-

hour period, covariance of firing decreases again as is reflected in equivalent Sleep 1 correlations. Therefore there must be a mechanism other than LTD that decreases the covariance over the 24-hour period that spans Sleep 2 to Sleep 1 periods.

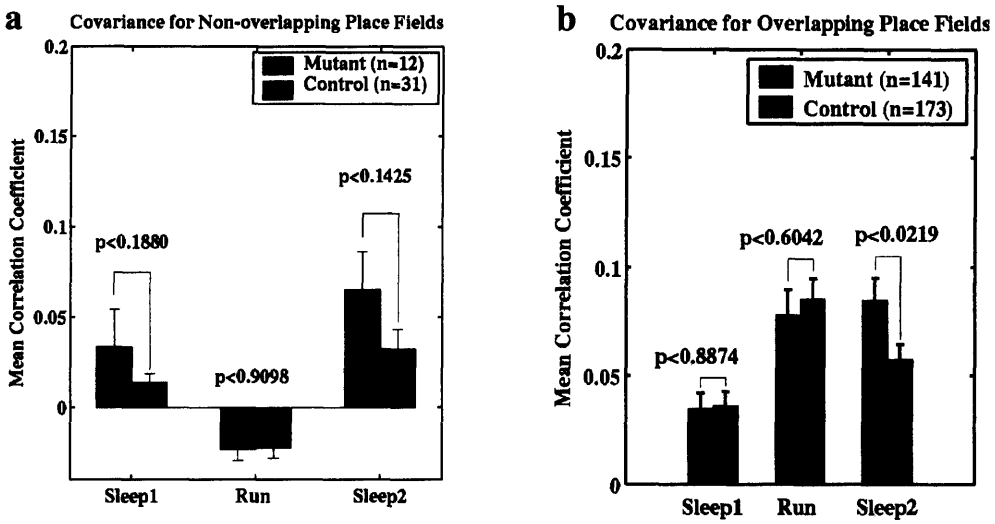

Figure 3.6.1. Pyramidal Cell mean correlation coefficients for overlapping place fields on the linear track during Sleep and Run Sessions. Mutants and controls are not significantly different during Sleep 1 and Run. However during post-run Sleep 2 mutant correlation stays enhanced while control correlations subside. The same cells pairs were maintained analyzed for all three epochs.

We also used other traditional methods for assessing co-variance of firing such using the distance between the center-of-mass of place field pairs as a criterion to categorize "overlapping" or "not-overlapping" pairs. Various distances were examined to determine the best distance which showed the greatest difference of mean correlation between overlapping and non-overlapping place field pairs in the controls as well as the mutants. By the Student's T-test measure at 15 cm distance criterion, overlapping mutant pairs (n = 192) and control pairs (n =

299) were not significantly different from each other in Sleep 1 (0.027+/-0.0056; 0.040+/-0.006; p>.05), Run (0.042+/-0.008; 0.059+/-0.007; p>.05), or Sleep 2 (0.0623+/-0.008; 0.065+/-0.006; p>.05). While comparing non-overlapping pairs, although there was a slightly lower and unexplainable covariance in Sleep 1 (0.023+/-0.004; 0.033+/-0.002; p>.05), pairs were also not significantly different in Run (0.008+/-0.004; 0.013+/-0.004; p>.05), or Sleep 2 (0.045+/-0.006; 0.051+/-0.003; p>.05). The problem with using distance as a criterion for categorizing overlapping mouse place fields on the linear track is that mouse fields tend to vary in shape not always spatially gaussian-distributed. Additionally, field size was not taken into account thus adding additional noise and unpredictable correlations between very different types of place fields. This can be readily observed in the distance criterion Run pair correlations for non-overlapping fields which are net-positive. However, Run place field pairs using the original criteria (actual place field size and actual place field overlap in square cm) leads to a net-negative correlation as expected for a non-overlapping place field and a more consistent data. By choice, the original criterion presented is preferred.

3.7 Mutant place fields are larger.

Place field size was determined by summing 15 laps (30 total traversals) of the run epoch of the linear track recording session. Forward and reverse traversals were treated as separate fields. Rate maps were calculated by taking the total number of spikes and dividing by total occupancy. Because we desired to compare running behavior only, all occupancies and positions for which the animal was not moving at a one second averaged mean velocity of 1.0 cm/second were eliminated from the calculations of the rate map. Additionally, all activity that occurred

within the "end" boxes of the linear track were eliminated from the analysis because a significant number of spikes would fire within them during immobile sharp wave (SPW) activity. Rate maps were calculated raw per pixel, however the final rate maps were gaussian smoothed over the pixel space and used for field size comparisons. Place field size in this measure was calculated by counting pixels that were greater than 10% of the peak firing rate value for each rate map. In convention with Mehta et al. (1997), we were interested in robustly firing pyramidal cells, thus all cells that were firing less than a mean average of 1.0 Hz were eliminated from the study for comparison. This eliminated a number of mutant fields due to their low firing rates, which will be further explained in section 3.9. Nonetheless, all place fields which had a mean minimum firing rate of 1.0 Hz were compared. For all subsequent sections of place field comparisons, this standard was maintained unless otherwise mentioned.

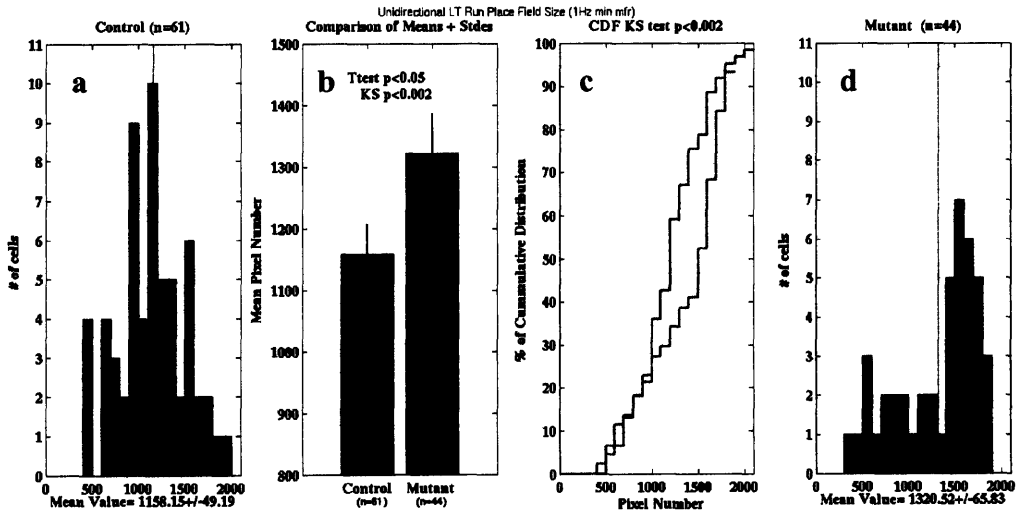

Figure 3.7.1. **(a,d)** Distributions of place field size (pixels) for pyramidal cells of controls and mutants. **(b)** comparison of means of place field sizes in pixels. **(c)** cumulative distribution function for mutants. Red = mutant, Blue = control.

Pyramidal cell place field sizes as determined by number of raw tracker pixels for mutants during the Run period of the linear track (1158+/-49, n = 44) compared to controls (1321+/-66, n = 61), were significantly larger ($p<0.05$, Students T-test; $p<0.002$, Non-parametric Kolmorogorov-Smirnov Test; Figure 3.7.1). Thus, uni-directional place fields that encoded for space at a high firing rate were active for a larger amount of space on the linear track in the mutants than in the control mice (Figure 3.7.2).

While place fields can vary between mutants and controls, it is possible that the behavior of the mice will also vary between mutants and controls. Thus it important to compare overall running velocity between mutants and controls which were not significantly different (Figure 3.7.3).

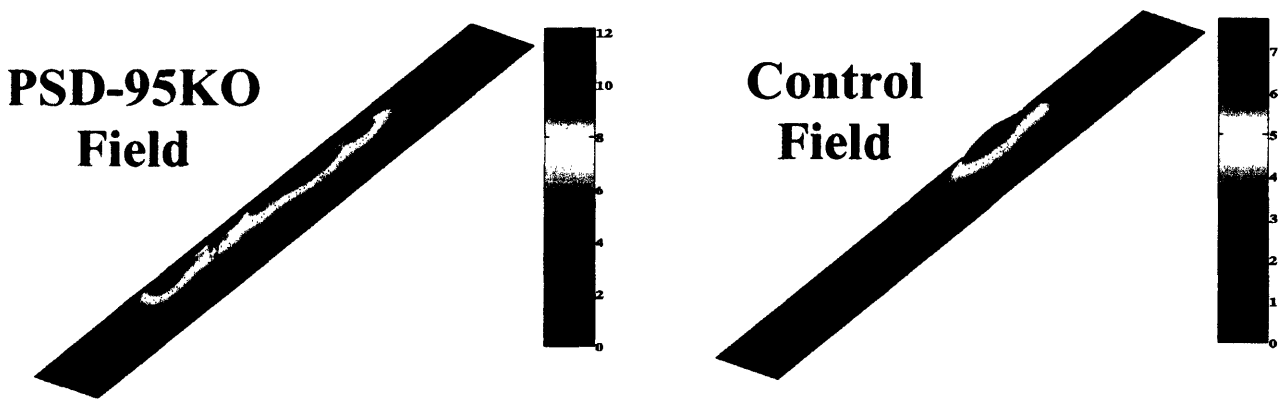

Figure 3.7.2. Example place fields on the linear track with ends cut off and a minimum of 1.0 cm/sec velocity. It was typical to find mutant pyramidal cells that fired the full length of a linear track, while they were almost absent from the control animals.

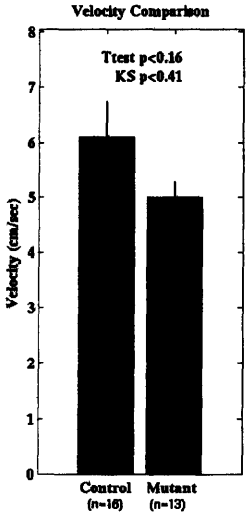

Figure 3.7.3. Mean+/-SEMs of average velocity during running periods for all the linear track recording sessions were compared. Mean velocities of the controls (6.1+/-0.6) were not significantly different compared to the mutants (5.0+/-0.3, $p<0.16$, Students T-test; $p<0.41$ Kolmorogorov-Smirnov Test).

3.8 Mutant place field sizes are established on the second traversal of a linear track for every day the mouse was run on the linear track.

As an additional measure of place field size, I measured the distance between the first and last positions of a gaussian smoothed place field which fired at 10% of the peak firing rate. Thus, this is a measure that is a one-dimensional value of "length of a place field" in centimeters. When examining each trip individually across all recording sessions. Place field size for the first trip of the day was not different between the mutants and controls however the mutant fields quickly established larger place fields on the second trip and beyond (Figure 3.8.1).

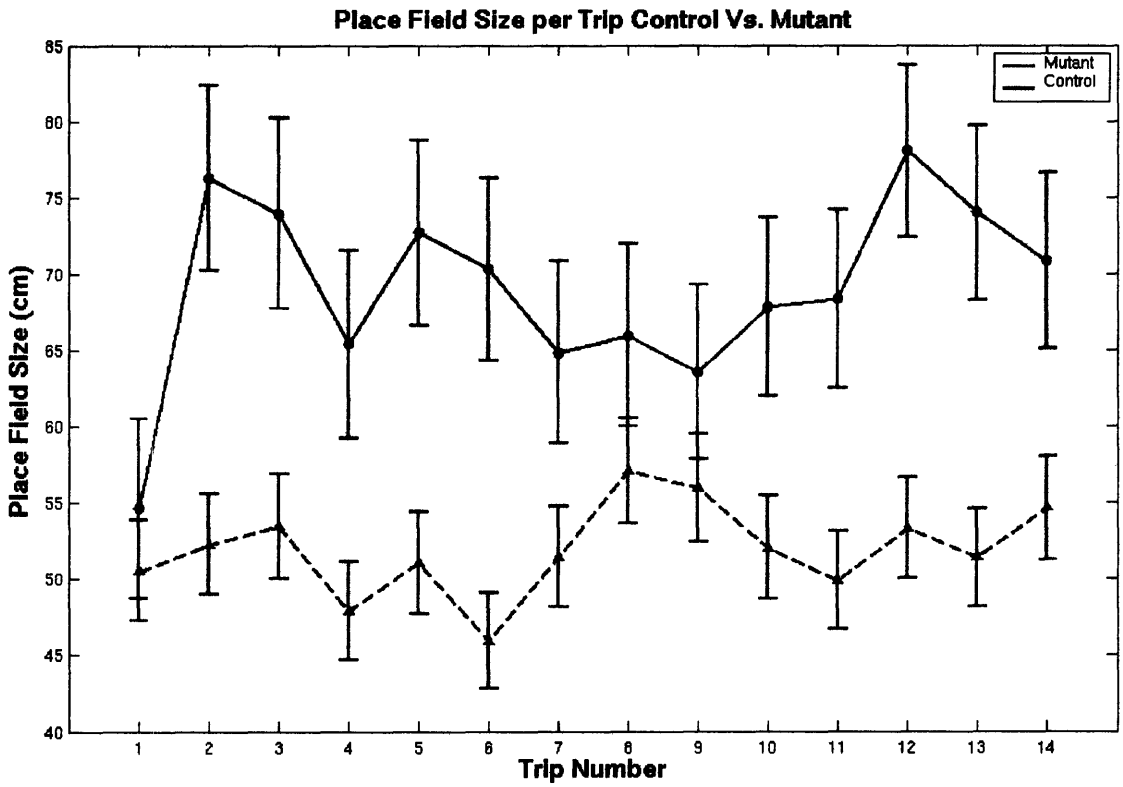

Figure 3.8.1. Place field size of high firing-rate unidirectional place fields were plotted on a per trip basis across all experiments. Red = mutant. Blue = control. Mean+/-SEM plotted.

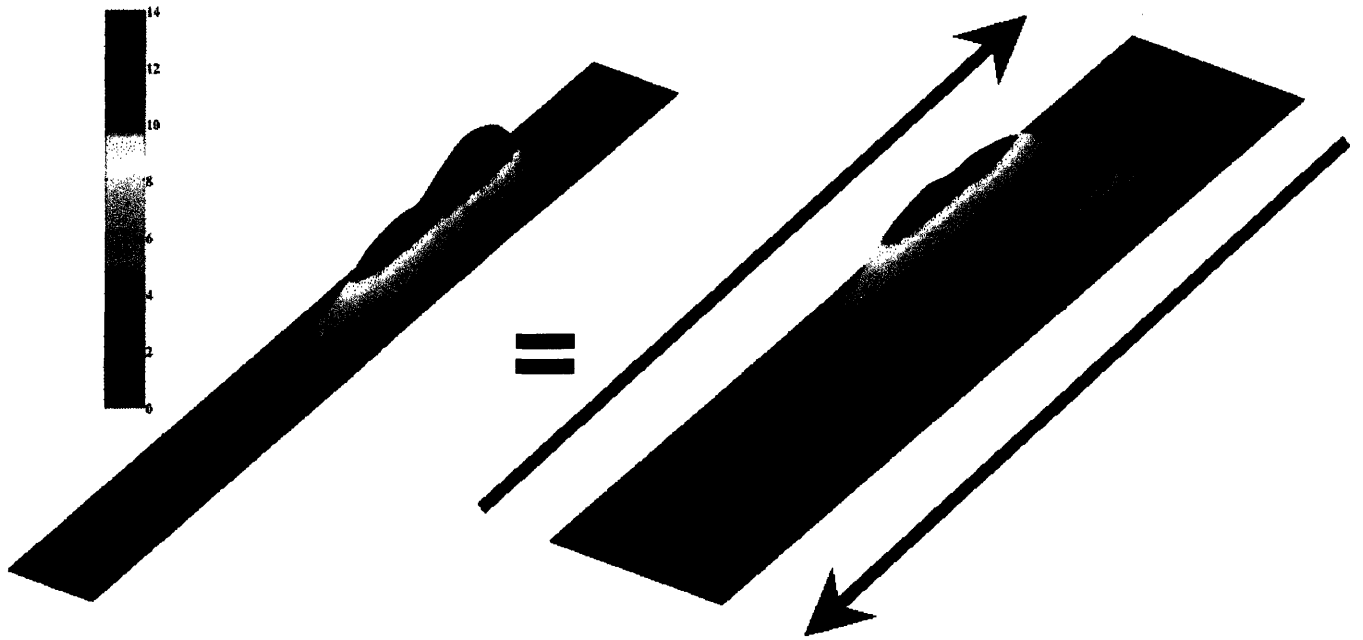

$$\text{Directionality Index} = \frac{|\,FR1-FR2\,|}{(FR1+FR2)}$$

Figure 3.9.1. Example of how a single place field when split by direction of running for the mouse can be bias in one direction more so that the opposite direction. The Directionality Index (DI) ranges from values of 0 to 1, where 0 is a field which fires equally in both directions and a value of 1 is represented by a highly directional field which preferentially fires spikes only in one direction.

3.9 Directionality of pyramidal cell and interneuron place fields is enhanced in mutants.

Figure 3.9.1 shows a representative place field rate map for all running behavior 15 laps (or 30 traversals). However, when place fields are separated by direction there is sometimes an apparent bias in firing rate for a northwards vs. a southwards direction or vice verse. The directionality for a pyramidal cell is measured by the Directionality Index (DI) measure which is

calculated by taking the difference between firing rates of opposite running directions, then dividing the absolute value by the sum of both.

When comparing pyramidal cell place field directionality of the mutants (0.62+/-0.05, n = 54) with the controls (0.41+/-0.03, n = 83), the mutant fields showed enhanced directionality ($p<0.0002$, Students T-test, $p<10^{-5}$, Kolmorogorov-Smirnov Test; Figure 3.9.2). This result was highly significant and quite unexpected.

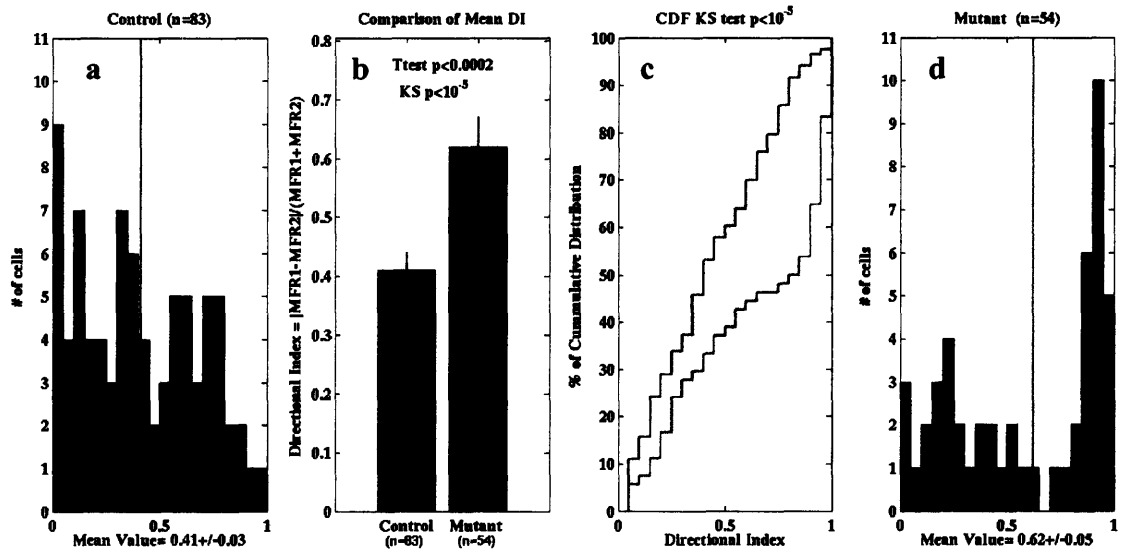

Figure 3.9.2 (a,d) Distributions of place field DI for pyramidal cells of controls and mutants. **(b)** comparison of means of place field DI. **(c)** cumulative distribution function for mutants. Red = mutant, Blue = control.

When comparing the interneuron place field directionality of the mutants (0.15+/-0.03, n = 12) with the controls (0.08+/-0.01, n = 32), the mutant fields showed enhanced directionality ($p<0.005$, Students T-test, $p<0.006$, Kolmorogorov-Smirnov Test; Figure 3.9.3). This result was also highly significant and unexpected.

The fact that both the pyramidal cells and interneurons have enhanced directionality suggested that there was a possible interaction between interneurons and pyramidal cells in a network level behavior that governs directionality. In other words, the pyramidal cells that have greater integrated firing rates are stimulating interneurons thus accounting for their increased DI. Perhaps, the increased directional input to the interneurons are subsequently acting as the feedback mechanism which gradually suppresses local hippocampal pyramidal cells.

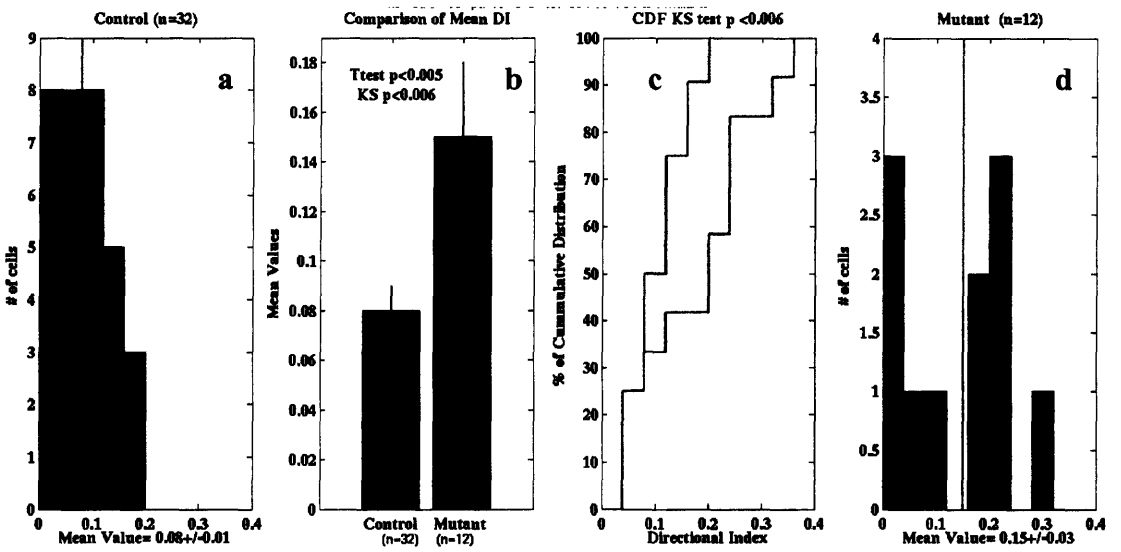

Figure 3.9.3 (a,d) Distributions of place field DI for interneurons of controls and mutants. **(b)** comparison of means of place field DI. **(c)** cumulative distribution function for mutants. Red = mutant, Blue = control.

3.10 Directionality is established on second traversal of a linear track for each day.

When examining each trip individually across all recording sessions. Place field directionality for the first trip of the day was not different between the mutants and controls ($p>0.05$, Students T-test). However the mutant fields quickly established their enhanced

directionality on the second trip and beyond (Figure 3.10.1). The first five traversals of the mutant seemed to steadily enhance the directional value of all the place fields. Similar to the place field size measure over a trip by trip basis, it seemed as if place field dynamics were quickly established in the both the mutants and controls, and in the mutants, there was a consistent and rapid rise in the directional bias of its pyramidal cells while they were encoding for space.

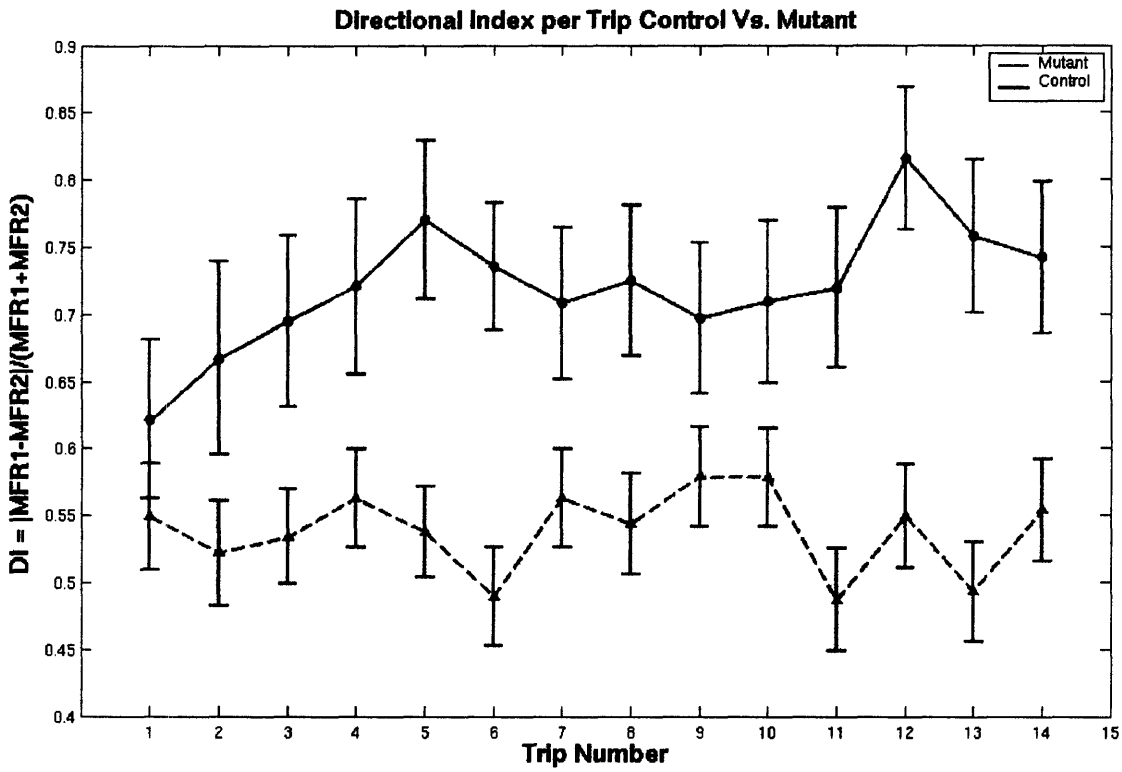

Figure 3.10.1. The Directionality Index (DI) of high firing-rate unidirectional place fields sizes were plotted on a per trip basis across all recording sessions. Red = mutant. Blue = control. Mean+/-SEM plotted.

3.11 Averaged place fields summaries.

For every place field, the higher firing rate direction was defined as the dominant directional field while the lower firing rate direction was defined as the minor field. All dominant fields were centered on their center of mass and were averaged across all place fields. The same was done with all the minor fields. The average place fields are plotted in Figure 3.11.1. Integrated Firing Rate differences (IFR) between the dominant fields and minor fields of each genotype shows that the difference in mean fields is more than two fold greater in the mutants than in the controls. This summary reflects the general higher bias in directional firing for the mutants, and shows how the controls are mildly biased compared to the mutants.

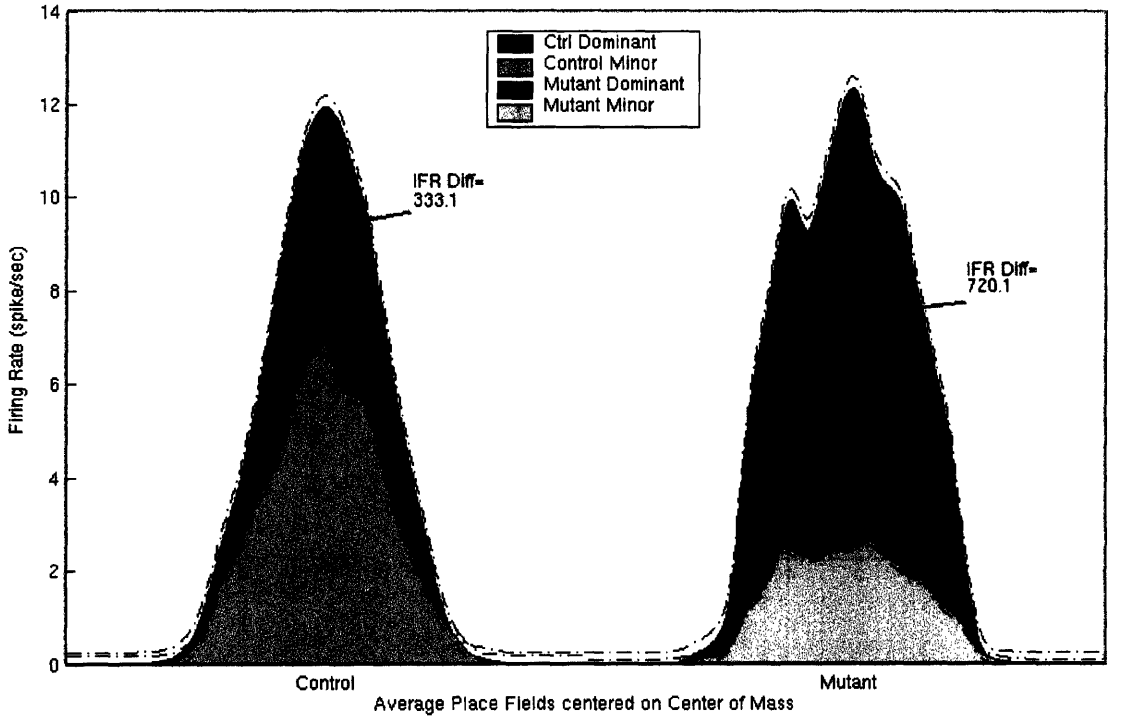

Figure 3.11.1. Comparison of dominant versus minor fields reflects increased directional firing bias in mutants over controls. The mean place fields for controls (blue) and mutants (red) were generated from all fields centered over their center of masses. Mutant fields are more biased by direction than their control counterparts.

3.12 Mutant place fields are not-asymmetric compared to wildtype controls.

Place field asymmetry was compared between mutants and controls. The firing rate asymmetry index (FRAI; Mehta, 1997) was defined by the first and last spikes as the boundary of a place field and dividing the field into two equal portions. The integrated firing rate (IFR) of the first half of the place field was subtracted from the IFR with the last half of the field was divided by the sum of the IFR of both fields. Thus negative values are equivalent to negatively asymmetric place field (the first half of the field fires at lower firing rate than the second half of the field). Figure 3.12.1a shows two examples of place fields, one from the mutant (red) and one from the control (blue). In the mutant example the place field is non-asymmetric while in the control example the place field exhibits a triangular asymmetrical shape. The FRAI of the place fields for the mutants (0.05+/-0.06, n = 36) were significantly non-asymmetric ($p<0.005$, Students T-test; Figure 3.12.1b) compared to the negatively asymmetric control fields (-0.11+/-0.03, n = 83).

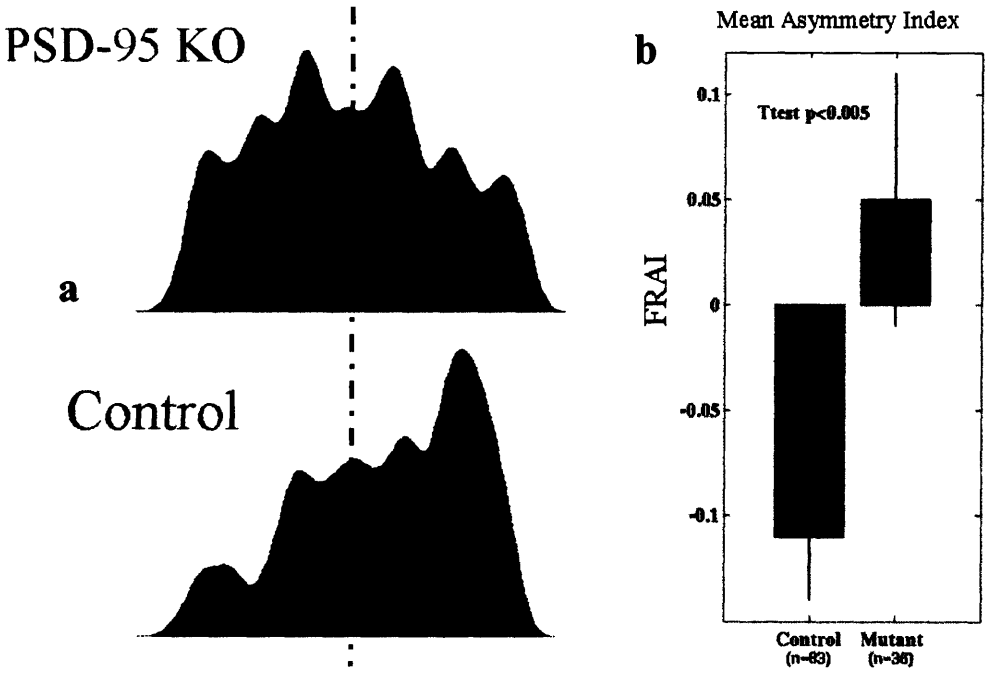

Figure 3.12.1. **(a)** Two example place fields of the mutant and control mice. The mean FRAI of the mutants was not significantly different from zero. **(b)** The control mice showed significantly negative asymmetry values compared to the mutants.

The Mehta, Lee, and Wilson (2002) model proposed that the asymmetrical place field in the presence of a theta rhythm is a possible mechanism that can describe the phase precession effect first described by (O'Keefe, 1993). Because the PSD-95 KO mice have non-asymmetric place fields, it begs the question to ask whether or not the mutant mice also have defective phase precession. However one possibility that must be eliminated to describe a phase precession effect is to make sure that the theta rhythm is not defective in the mutants compared to the controls. The following sections will attempt to do this as well as describe the general methodology of how the theta rhythm was acquired.

3.13 Theta EEG for mutants and controls are normal.

During recording of place cells, a dedicated computer was continuously acquiring EEG local field potentials of the tetrodes. The EEG signals were bandpass filtered between 1 Hz and 3 kHz at a sampling rate of 6.25 kHz. A single channel was chosen per recording session and was determined by best signal to noise of the theta frequency (6-12 Hz) compared to the wideband frequency range. The subsequent signals were down sampled to between 100-200Hz. The down-sampled signal was then bandpass filtered between 6-12 Hz. Using a peak detection algorithm, the peaks of the theta cycle were identified and used as a measure to determine the relative phase of a theta cycle, which a pyramidal cell might fire (Figure 3.13.1). Autocorrelograms of the theta peaks identified for mutants and controls show that both the mutants and controls have similarly robust theta frequency behavior (Figure 3.13.2). Additionally, the mean theta frequency identified by the first autocorrelogram peak for each recording session for the mutants (8.92+/-0.08Hz, n = 9) and controls (9.02+/-0.08Hz, n = 15) were not significantly different ($p<0.37$, Students T-test). In conclusion, the mutant has normal theta rhythmic activity during exploratory behavior.

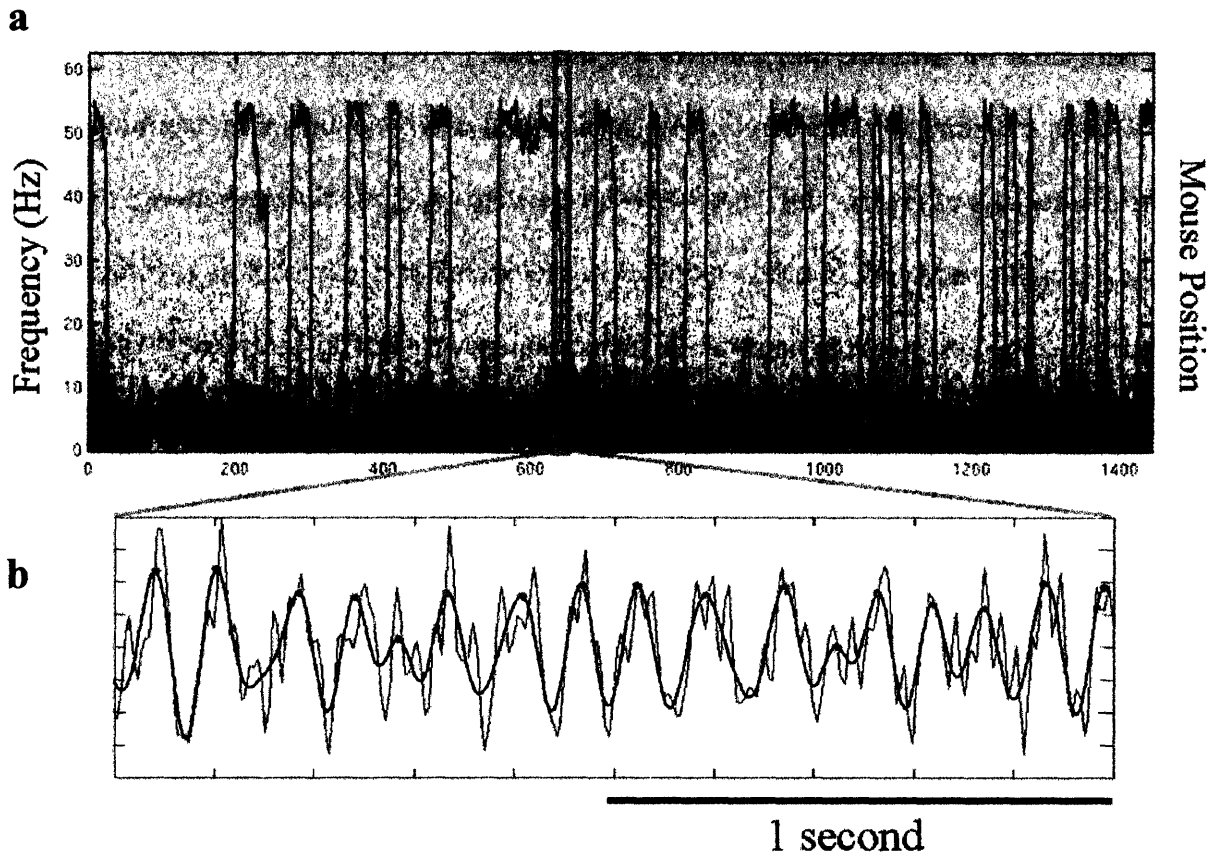

Figure 3.13.1. Example EEG theta peak extraction. (a) The upper plot are two plots superimposed on each other. Time (seconds) vs. mouse position on a linear track is plotted as a blue line. The background is a spectrogram of an example EEG signal; it is plotted as time vs. frequency content. The dark red pixels represent stronger the frequency content at that particular frequency. Notice that there is a strong red band between 6-12 Hz representing theta activity while the mouse is engaged in exploratory behavior throughout the behavioral period displayed. **(b)** The raw trace of a two-second wideband EEG signal is plotted time versus amplitude in black which looks very similar to rat EEG signals (O'Keefe, 1993). Overlaid on top of it is a trace of the 6-12 Hz bandpassed filtered EEG signal (Red). The identified peaks of the theta are displayed as green dots on the peaks of the EEG filtered theta.

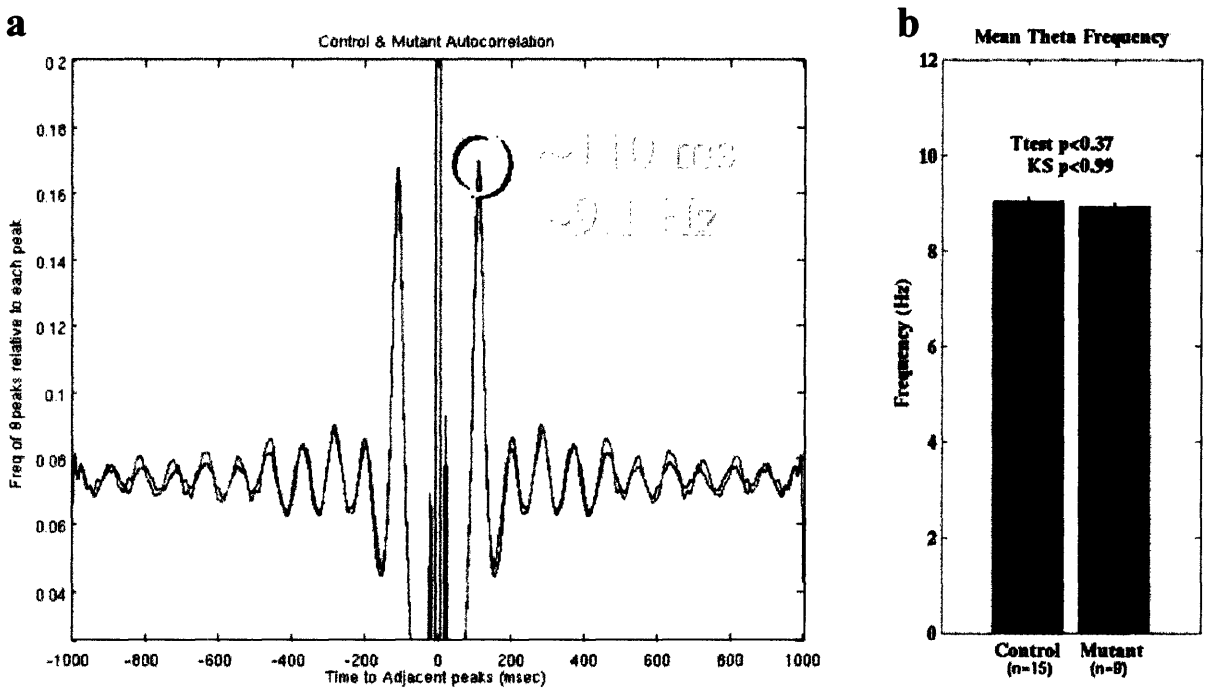

Figure 3.13.2. **(a)** Autocorrelograms for the control theta peaks (blue) are superimposed with the mutant autocorrelogram (red) for a two second period and are not significantly different. **(b)** Mean theta frequency for mutant and control recording sessions are not significantly different.

3.14 Phase precession is specifically abnormal in the mutants

While the theta frequency mechanisms seemed to be maintained in the mutant, the question now is to ask whether or not phase precession exists in the mutant mice and if so whether it is affected. First of all, I demonstrated that phase precession does exist in the mouse. Three representative examples of place fields phase precession are displayed in Figure 3.14.1a. Phase precession plots were calculated from methods obtained in O'Keefe & Reece (1993). Linear regression statistics were calculated per unidirectional field. A minimum of 100 spikes fired during behavior was required of a field in order for it to be included in the calculations of

phase precession. Theta peaks were determined by bandpass filtering EEG between 6-15Hz, and strictly limiting the inter-peak interval of the theta peaks between 83-166ms (6-12 Hz). Spikes that fell within intervals shorter or longer than the inter-peak interval range, or which fired when the mouse was moving at less than 1.0cm/second were eliminated from the analysis. If the resulting field had less than 100 spikes total, it was entirely removed from the study. Correlation coefficients from the linear regression plots of position vs. phase were compared between mutants ($r = 0.014+/-0.028$, $n = 26$) and controls ($r = -0.062+/-0.018$, $n = 85$) and were shown to be significantly different ($p<0.018$; Kolmorogorov-Smirnov Test (KS); Figure 3.14.2a). Slope from the linear regression plots of position vs. phase were compared between mutants ($0.098+/-0.115$, $n = 26$) and controls ($-0.304+/-0.081$, $n = 85$) and were also shown to be significantly different ($p<0.014$; KS Test; Figure 3.14.2b). Correlation coefficients were also calculated for spatial firing rate vs. phase between mutants ($r = 0.017+/-0.027$, $n = 27$) and controls ($r = -0.063+/-0.018$, $n = 86$) and were also significantly different ($p<0.01$; KS Test; Figure 3.14.2c). Finally, slopes were also compared for spatial firing rate vs. phase between mutants ($0.138+/-0.118$, $n = 27$) and controls ($-0.392+/-0.119$, $n = 86$) and were also significantly different ($p<0.008$; KS Test; Figure 3.14.2). Note that the number of mutant fields was significantly reduced because the enhanced directionality of their fields caused one direction to fire so few spikes that it was occluded from the analysis. The control place cells were much more balanced in bidirectional firing and thus the control group n was larger.

To the author's knowledge, this is the first report of the existence of phase precession in the mouse. This report is also a novel demonstration of a measured ablation of phase precession by a genetic modification of a synaptic protein, which specifically causes unidirectional synaptic plasticity.

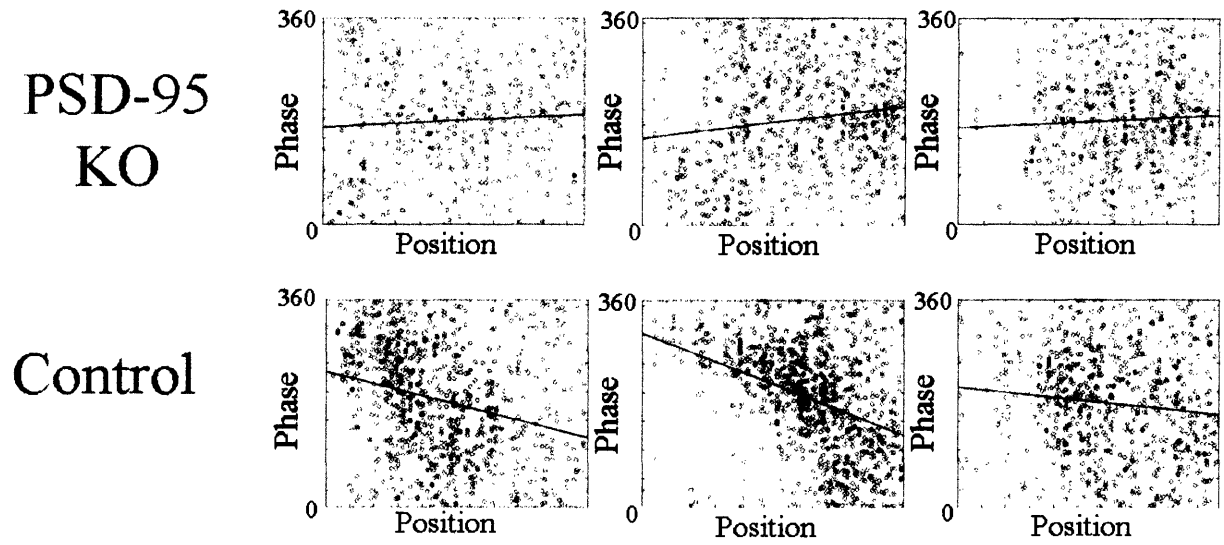

Figure 3.14.1. Three representative cells from mutants (top row) and controls (bottom row). Spikes from fifteen traversals were summed up for each position vs. phase plot. As the mouse runs across its place field from the left to the right, it's CA1 pyramidal cell will fire at a particular phase of the theta cycle, which is plotted on the y-axis. A linear regression for all the spikes is plotted in red. The control mouse fields show a particularly strong phase precession effect while the mutant fields show relatively arbitrary position vs. phase firing.

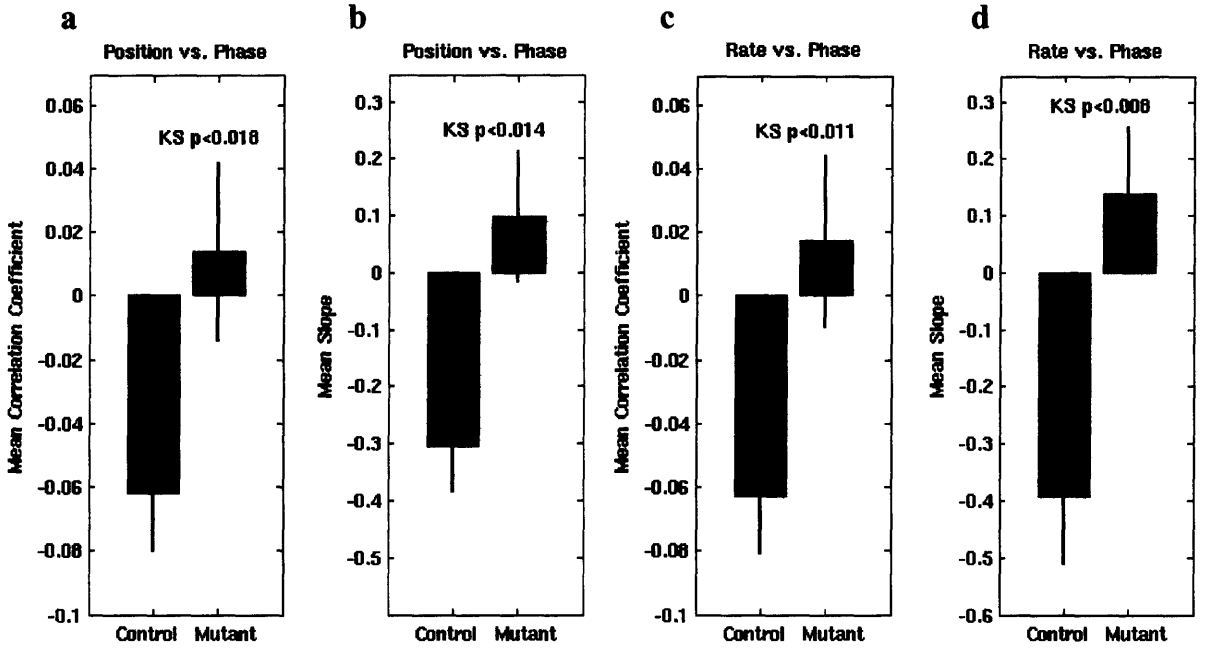

Figure 3.14.2. **(a)** Correlation coefficients from the linear regression plots of position vs. phase for mutants (r = 0.014+/-0.028, n = 26) and controls (r = -0.062+/-0.018, n = 85) were significantly different ($p<0.018$; Kolmorogorov-Smirnov Test (KS)). **(b)** Slope of position vs. phase of mutants (0.098+/-0.115, n = 26) and controls (-0.304+/-0.081, n = 85) were significantly different ($p<0.014$; KS Test). **(c)** Correlation coefficients for spatial firing rate vs. phase between mutants (r = 0.017+/-0.027, n = 27) and controls (r = -0.063+/-0.018, n = 86) were significantly different ($p<0.01$; KS Test). **(d)** Slopes of spatial firing rate vs. phase between mutants (r = 0.138+/-0.118, n = 27) and controls (-0.392+/-0.119, n = 86) and were also significantly different ($p<0.008$; KS Test).

3.15 Summary of Results.

In summary, the enhanced LTP/eliminated LTD in the PSD-95 KO mouse resulted in *differences* characterized by:

- Larger place fields.
- Enhanced directional fields in pyramidal cells & interneurons.
- Enhanced post-run sleep correlations.
- Less asymmetrical place fields.
- Altered phase precession.
- Wider spikes.

Mutants and Controls were identical in the following measures:

- General locomotive behavior (velocity).
- Overall firing rate (homeostatic regulation maintained).
- Sparsity of pyramidal firing during run encoding periods.
- Pyramidal cell bursting (Complex Spike Index).
- Normal pre-run sleep and during-run correlations.
- Theta EEG activity (rhythmic modulation is unperturbed).

CHAPTER 4: DISCUSSION

4.1 In Conclusion PSD-95 KO mice and controls are specifically different.

We saw in Chapter 3 that the mutant PSD-95 KO mice were actually affected in a very specific manner and the mice did not exhibit a generalized deficit in neuronal place field function. The importance of having a good set of controls to show equivalence between mutants and controls is to help isolate the true effects of the mutation and thus improve our understanding of the cause and effect of our manipulation.

In many ways the PSD-95 KO mouse is normal as determined by control experiments. Most importantly of these controls was that the mutant mice were determined to be behaviorally normal: their mean running velocities were statistically the same. A naïve assumption we made for an enhanced LTP/reduced LTD mouse was that a network of neurons would not be able to down-regulate its own activity and thus fire continuously out of control. However not only does the mutant lack seizure-like activity that would belie such a condition, the overall firing rates were equivalent between mutants and controls. When examining the sparsity of activity of pyramidal cells during run behavior, mutants and controls were not significantly different. Additionally, the mechanism that regulates bursting and complex spiking behavior of CA1 pyramidal cells seems to be maintained in the mutant. It was significant to note that the first order prediction for LTP to be the mechanism that regulates increased covariance of firing of overlapping place fields was maintained in the mutants during run spatial encoding, unlike the CA1-NMDA KO mouse which lacked LTP & LTD. Previously it was argued by McHugh and colleagues that covariance of firing was a possible mechanism by which place fields can be used by mice to navigate. *However, because mutant covariance of overlapping place fields is normal*

during the encoding of run, we can now conclude that poor spatial learning behavior of the PSD-95 mutants is not due to the lack of covariance of firing of CA1 pyramidal cells during active spatial encoding. Finally, theta activity of the hippocampus was compared between mutants and controls and was determined be normal in the mutants. The overall theta frequency was also equivalent. In conclusion, having an enhancement of LTP and a lack of LTD in the PSD-95 KO mouse did not affect a large number of first order and second-order pyramidal cell, interneuronal, and network wide properties.

Yet, there were very specific differences between mutants and controls. Mutant place fields were larger than control fields for repeated trips down a linear track. This result was not too surprising, and provided some evidence that increased field size might account for poor behavior in the Morris Watermaze. Interestingly, the post-run sleep covariance for overlapping place fields was enhanced in the mutants. Perhaps this enhanced covariance and that the inability to de-correlate these units during post-run sleep causes memory consolidation errors. However, in pre-run sleep the following day, units are non-correlated, suggesting that there is some type of de-correlation that is occurring during the 22 hour period we didn't record. Mutant place fields also showed *enhanced directionality,* which was a very unexpected and novel result. This is the first report of such a phenomena in rodent awake behaving electrophysiology. The enhanced DI was seen in pyramidal cells as well as interneurons, which suggested network-wide phenomena instead of a single-neuron phenotype.

However, directionality was not the only greater than first-order property that was different in pyramidal cell activity for the mutants. Bi-directional synaptic plasticity was discovered to be regulated by the relative timing of APs and EPSPs (Markram, 1997; Bi, 1998). The relative timing of spikes predicted that asymmetric fields would form within the

hippocampus for unidirectional travel (Mehta, 1997) and was later verified to be dependent on NMDA-mediated synaptic function (Mehta, 2000). By altering synaptic plasticity to a uni-directional model in the PSD-95 KO mice, we can test whether or not asymmetric place fields would still form. In fact, the mutant place fields showed less asymmetry than controls after a number of traversals across a linear track. The important prediction of the Mehta, Lee and Wilson (2002) model that asymmetric place fields generated the phenomena of phase precession, begged the question of whether there existed a phase precession effect in the mutant mice. We demonstrated for the first time that phase precession does exist in the mouse. And after showing that theta generation is normal in the mutants, I presented data that shows that phase precession is abolished in the mutants.

One of the more unusual and unexplainable differences in the mutant was that the peak-to-trough spike widths were wider in mutants. Perhaps potassium K+ channels are functionally up-regulated in the mutant. Though unclear, one such mechanism maybe altered K+ clustering (see section 1.5.10). Because the PSD-95 fragment is in a truncated form, yet still contains the critical PDZ2 domain responsible for K+ channel clustering, the altered form of PSD-95 may increase total K+ density at the synapse. However, while larger spikes might contribute to a major change in network physiology, the fact that a significant number physiological properties were unchanged suggests that wider spikes do not cause a major problem in basic cellular physiology nor in network wide firing rate dynamics. Still one cannot exclude the possibility that spike width may be a major determinant of the major differences seen.

Altogether, I have produced a large set of data that shows that the PSD-95 KO mutants have very specific set of phenotypic differences, which do not belie a generalized synaptic/cognitive or behavioral problem in the mutants.

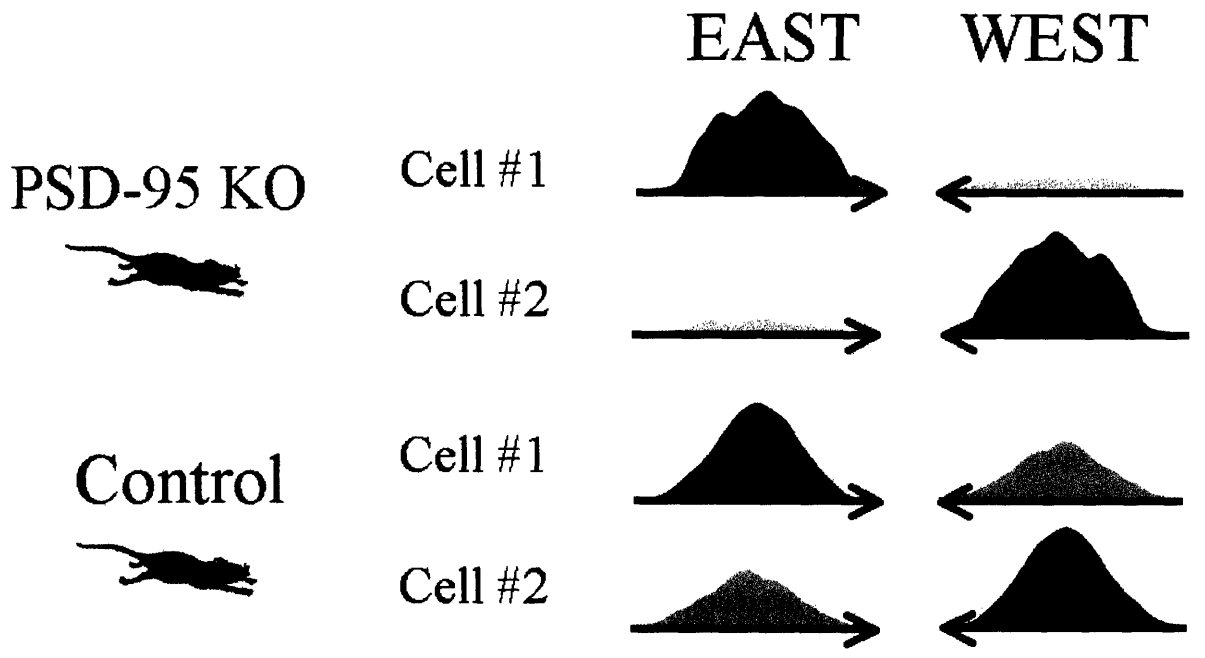

Figure 4.2.1. Two hypothetical examples of place cells from mutants and controls. On average the mutant cells firing in one direction will be much more bias in total integrated firing rate compared to the controls which show a more balanced amount of firing in each direction.

4.2 A unified network model to explain enhanced directionality, reduced asymmetry, phase precession and poor spatial learning.

If we are to imagine an entire network of mouse CA1 pyramidal cells active during the entire traversal of a linear track, approximately 30% of that network will have been engaged while encoding for space (Wilson, 2002). If we are to imagine single cell activity in the mutant while it is running across that linear track, some of the cells will be firing very dominantly while an equivalent subset will be firing very weakly. This is the most reasonable conclusion that can be drawn from section 3.9-10. The control cells will be doing the same but the degree to which the strength of the place fields will vary, will be much less between the stronger direction place field and weaker direction place fields. This is best illustrated in Figure 4.2.1. On average the

mutant cells firing in one direction will exist as a bimodal distribution of cells with very large and very small Integrated Firing Rates (IFRs). While the controls cells firing in one direction will exist as a distribution of cells firing with medium-large IFRs and medium-small IFRs. But a hippocampus is made up of more than two cells. Thus if we are to compare two active hippocampal structures that are actively encoding space as the mouse runs across a linear track, the mutant structures will continue to look bimodal with a distribution of cells that seem like they are high in contrast with their neighboring CA1 pyramidal cells, while the control cells are less in contrast with each other in overall IFRs (Figure 4.2.2).

But what does this mean for the mouse? Is it relevant? I propose that the increased contrast between "neighboring" cells is causing a reduction of the overall capacity for the hippocampal circuit to process information. My proposal is based on the assumption that the resting state of the hippocampus is off where most of the cells are not firing or firing at very low firing rates. By increasing the contrast between cells within the mutant, one set of cells fires to a large degree while opposing set fires to a much lesser degree and sometimes not at all. The assumption is that the very low firing rate cells are indistinguishable from the background noise of the other silent cells in the hippocampus. It has fewer active pyramidal cells at its disposal to describe its current experience and thus the mutant has a lower information-processing rate in its hippocampus (Figure 4.2.3). In other words the sparsity of the hippocampus is higher in the mutants.

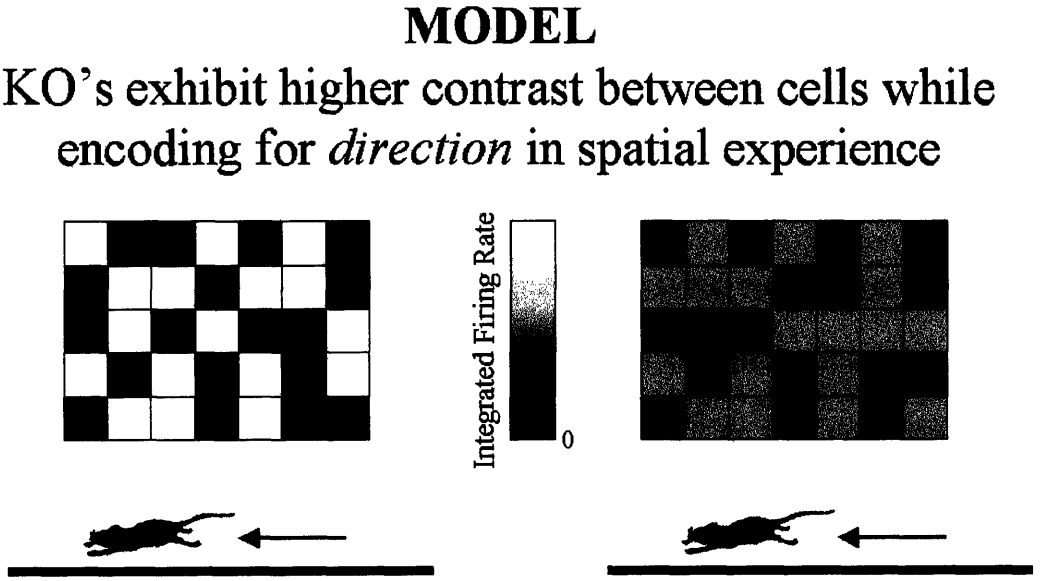

Figure 4.2.2. Grid of squares represents hypothetical CA1 pyramidal cells that are active during the encoding of space while the mouse is running across a linear track environment. Integrated firing rate (IFR) is represented by brightness of squares, white being the largest fields. Increased directionality of the mutant (red) cells exhibit higher contrast difference between other cells also encoding for space during run. Control cells also exhibit directional bias, however the overall differences are much less between cells than in the mutants.

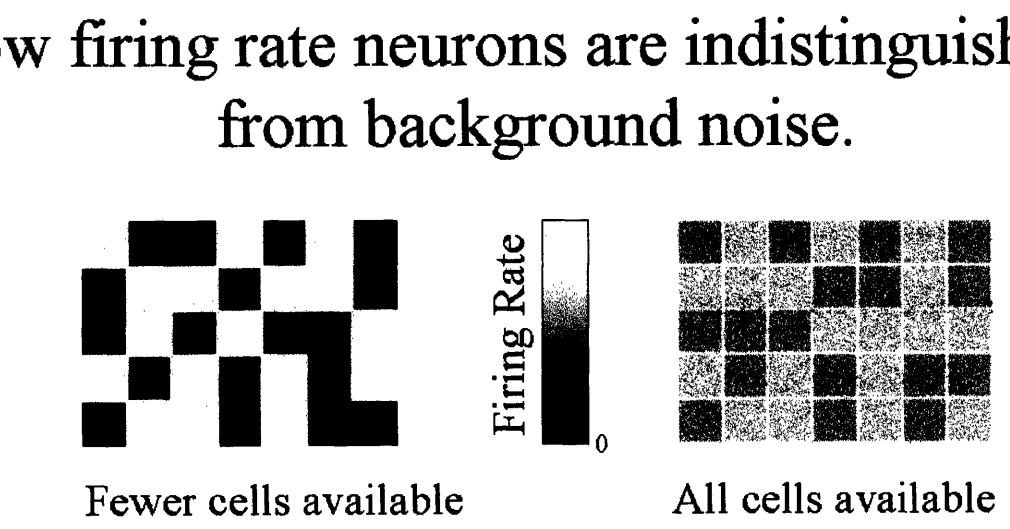

Figure 4.2.3. Model's Conclusion. If we assume that low firing rate cells are indistinguishable from background noise of the hippocampus. Then there are fewer active high firing rate cells available in the mutant to encode for space while the mouse is actively exploring. (Yellow squares = high firing rate active pyramidal cells).

It is quite possible that this lower rate of coding/increased sparsity could be causing a lack of asymmetry in place field encoding during successive experiences by not providing too few cells at a reasonable firing rate necessary for proper spatial encoding. The lack of high firing rate pyramidal cells for encoding of space can readily explain the poor spatial learning in the Morris Watermaze.

A potential first-order synaptic mechanism to explain this phenotype can be the simple "winner take all" dendritic model which could be a potential mechanism to explain directionality in the hippocampus. Suppose a CA1 pyramidal cell is receiving inputs from external cues on one set of dendrites if the mouse runs in direction A. The same cell also receives inputs onto another set of dendrites from inputs created from running in direction B. In the mutant animal, the first traversal of a linear track in both directions is not enough to establish a directional bias yet. However, because of the enhanced LTP phenotype and lack of LTD, one of the two directions will "win" all of the synaptic change and will only further strengthen the winner. However, in the controls which have normal LTP & LTD, dendritic connections on a single neuron are balanced and there is infrequently a "winner take all" scenario which lumps all the response of a post synaptic neuron to a single set of dendritic inputs.

4.3 Comparison with CA1-NMDA Knockout Mouse.

Because of the similarity between the experimental conditions and animals, making a direct comparison between the CA1-NMDA knockout mouse and the PSD-95 knockout mouse is a very valuable opportunity. Although, not all measures are comparable, many interesting comparisons can be made in an attempt to compare two uniquely genetically manipulated animal models, that have distinctly opposing synaptic properties. The CA1-NMDA knockout mouse

lacks of LTP & LTD (Tsien, 1996). The PSD-95 KO mouse has an enhanced version of LTP while lacking LTD. Thus one can actually isolate a single unidirectional synaptic property and ask the question upon comparing these two animals, "what does LTP do?" The summary of relevant comparisons is shown in Figure 4.3.1.

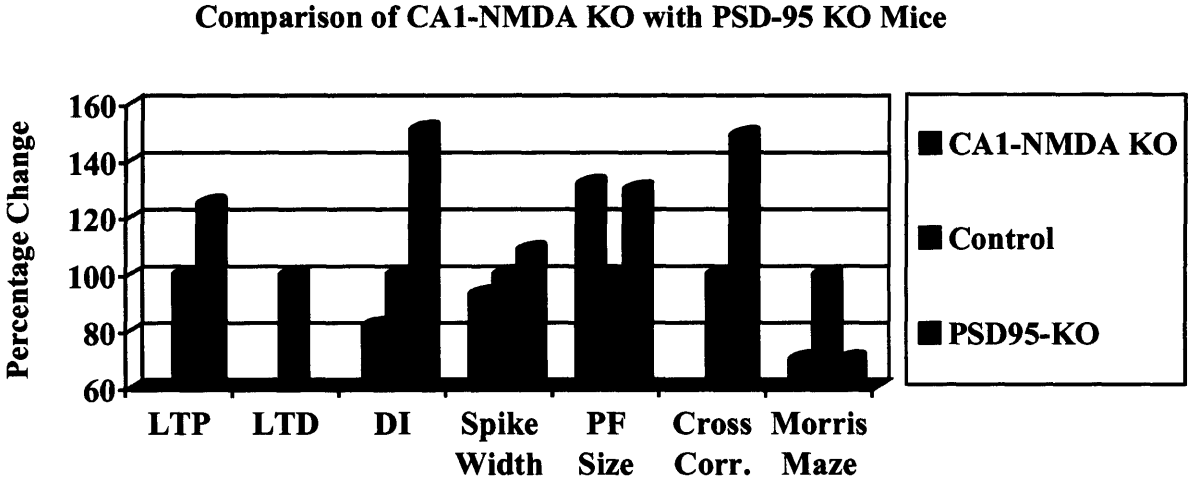

Figure 4.3.1. Summary of percentage change that occurred in PSD95-KO mice relative to its control and changes in CA1-NMDA KO mouse relative to its control. Values that are at bottom of 3d plot are equal to zero (CA1-NMDA KO LTP, LTD, Cross Correlation = 0 percent; PSD-95 KO LTD = 0 percent). LTP = Long Term Potentiation. LTD = Long Term Depression. DI = Directional Index. Spike Width = Peak to trough spike width. PF Size = Place field size. Morris Maze = Morris Watermaze target platform crossing. Cross Corr. = correlation coefficient for overlapping place fields. Data taken from McHugh et al. (1996) for comparison.

There are a few measures that are directly proportional to the relative strength of LTP. As LTP is enhanced in the PSD-95 mutants, the directionality index (DI) of place fields is enhanced and the spike widths are lengthened. Interestingly in the CA1-NMDA KO mice, the DI was decreased (but not strongly significantly different). Directionality is one of the most

striking and unexpected measures to have been affected by an enhanced LTP phenotype and thus its significance should be emphasized again because there is no obvious mechanism that would produce such a change. One such mechanism I proposed is the "synaptic contrast model". I argued that the amount of input that the CA3 pyramidal cells drive into the CA1 pyramidal cell layer is maintained between controls and mutants, as evidenced by equivalent overall hippocampal CA1 pyramidal cell and interneuronal firing rates. However, there exists an increased "contrast" between the firing rates of neurons that are actively coding for space, as evidenced by enhanced directionality in neurons actively coding for space. This increased contrast between cells might be a result of an enhanced LTP phenotype in the PSD-95 KO mice, where the "north-run-direction" inputs into one CA1 pyramidal cell representing a place is the winner that dominates all of the output of that cell to the detriment of the "south-run-direction" input. While in the control mice, the normal LTP phenotype causes some bias in northern vs. southern firing rates, however one direction does not completely eliminate the opposite direction. While DI is one of the more unexpected results, there are others as equally as interesting if not more puzzling results.

Peak to trough spike widths were also not expected to be wider in the mutants. This result was one of the most statistically significant results in this study as were thinner spike widths in the CA1-NMDA KO mice study. It's true to say that spike width is one of the best predictors of genotype! One possible explanation for wider spikes, which would seem to be a fundamental characteristic change of a synaptic network could be the regulation of potassium K+ channels expressed on the surface membrane of a neuron. This altered regulation or cluster of K+ channels could be the result of postsynaptic clustering alterations caused by the PSD-95 mutation (Tejedor, 1997). By having lower numbers of K+ channels, the repolarization of the

membrane potential would in theory be slower, and thus possibly wider. This is a prediction that could be tested in vitro. One of the possible reasons that interneurons have thinner spikes than pyramidal cells is because they have higher concentrations of K+ channels expressed on their surface membranes. The fact that peak to trough widths were wider in pyramidal cells as well as interneurons argues for a conserved mechanism of regulating the overall stimulation times that the pyramidal cells are engaging in, and possibly wider interneuronal spike widths are evidence that the mouse's brain was attempting to regulate the overall stimulation strength offered by the altered pyramidal cells (data for wider interneuronal spike widths not shown- because of balancing issues a subset was compared, if the entire set is compared, interneurons of mutants also have wider spikes). One additional fascinating possibility is the fact that LTP and LTD phenotypes can be entirely accounted for by the balance of excitation and inhibition of a pyramidal cell (as proposed by G. Liu, PCLM, 2002). This excitation and inhibition could be regulated by synaptic stimulation that would presumably be occurring within CA3 as well as CA1 pyramids. Yet for such a fundamental change in spiking characteristic, overall firing rates were not altered, nor was seizure activity increased, nor behavioral mobility. Thus having altered peak to trough spike widths did not cause significant detrimental changes to the mutant's general homeostatic mechanisms which regulate overall network excitability.

Still, I did observe unidirectional place field sizes increase in size. A bimodal distribution of place fields is slightly evident in the mutant population as determined by directional bias, with one population of cells firing highly in one direction and not at all in the opposite. Our place field size measure only included place cells that fired more than a mean firing rate of 1 Hz in a particular direction. Because of this restriction, we were eliminating the "minor" directional place fields of the mutants because they were firing at a very low firing rate.

Thus the mutant cells that were examined tended to have very high firing rates and larger place fields existing for the length of the linear track while firing in one preferred direction. Again one possibility for this larger firing behavior could be explained by the "winner take all" hypothesis of synaptic dominance of the northern directional information compared to the southern directional information entering a CA1 pyramidal, where the dominant direction causes increased total integrated firing across the entire length of a linear track in that preferred direction. While in the minor place field direction, firing rates were suppressed and were overall decreased in total integrated firing rate. The CA1-NMDA KO mouse lack of LTP & LTD causes increased place field size. The PSD-95 KO mouse equivalent lack of LTD but having enhanced LTP also increases place field size to a similar degree. Thus, the naïve conclusion is that LTP is not sufficient in place field size tuning, but instead LTD might be the necessary and sufficient mechanism.

One of the striking features of the CA1-NMDA KO mouse was the complete lack of cross correlation of firing (equivalent to zero) between overlapping place fields during running behavior. This means that cells were not firing in a consistent manner across repeated passes on a linear track and thus overlapping place fields would not co-vary in their firing patterns. McHugh et al. proposed that this covariance of firing might be the central mechanism to explain network level learning where cells that fired together, wired together in a temporally and spatially specific pattern. Interestingly, in the PSD-95 KO mice, by reintroducing LTP into these animals, cross correlation between overlapping place fields during run is not different from the controls. *Thus we can conclude that LTP is a necessary and sufficient for producing covariance of firing for overlapping place fields during run. However, we must also conclude that the covariance of firing is not necessary and sufficient for the mutant animal to form normal place*

fields, nor sufficient to provide the mouse the ability to solve spatial memory tasks such as the Morris Watermaze. An alternative mechanism is necessary to explain the inability to form spatial and temporal patterns necessary to solve spatial learning tasks. One such mechanism we proposed was the lack of asymmetry and thus lack of phase precession due to altered synaptic properties of the PSD-95 KO mouse. Another mechanism, however unlikely, might be the enhanced post-run sleep correlations seen in the mutants. For our final conclusion on this topic we can fairly conclude that LTP alone is not enough during the active process of encoding, but instead bi-directional synaptic plasticity is necessary for proper place field formation, directionality, and the formation of spatial memories.

4.4 Commentary on Mouse Genetics and Learning and Memory

Admittedly, it is beyond the scope of the PSD-95 global knockout mouse to pose the question about the role of PSD-95 in the hippocampus alone because the gene is manipulated in every cell of the mouse. Though the CA1-NMDA KO mouse still represents the state of the art technology of current mouse genetic manipulations, the obsolete older methods of producing straight knockouts can still be scientifically useful. For example, knockouts of genes that are normally expressed in the adult such as those regulated by the CamKII promoter, would not be significantly different than knocking out that gene in the mouse's postnatal forebrain. Additionally, promoter driven expression of CRE recombinase is rarely ideal and a range of expression patterns have been observed between different transgenic founder lines; it not uncommon to see only 50% of pyramidal cells expressing CRE recombinase. Current gene expression induction protocols have also shown varying degrees of penetrance and time course. While advanced forms of regulated gene manipulation allows us the experimental opportunity to

assay for gene function in specific brain regions, they are frequently scrutinized for their conclusive power as much as for the scientific question the mouse originally posed. Thus, in all mouse genetic studies, there is a fine balance between specificity, effect and conclusive power of a manipulation based on its region specificity.

While attempting to causally link molecules to behavior, we must also be careful as to how strongly we can make conclusions that molecule 'X' causes a learning and memory deficit. For example, a mutation which caused a non-specific behavior such as slower swimming speed, can lead us to conclude from the watermaze result that slow swimming mice are also poor learners. Or perhaps a learning and memory deficit is discovered in a mutant mouse whose real problem is excessive hyperactivity. It's important to keep in mind that a priori we cannot causally conclude that a genetic manipulation is solely responsible for a learning and memory result we have assayed for in a specific behavioral task, especially one as complex as the Morris watermaze. In the learning and memory field we are limited to pieces of evidence that are correlated, but are not necessarily full proof of causality. The same was true for the discovery of the neuronal structures by Ramon Cajal and his prediction of neuronal function in the early 1900's. However many years later and thousands of repeated experiments later, original hypotheses are repeated and confirmed with improved resolution and improved technology. We are more comfortable with the result that an NMDAR1 knockout is the causative agent for an LTP and memory deficit precisely because a significant amount of previous experimental literature that established a specific role for NMDARs and the formation of LTP. While control experiments are always necessary to increase specificity of a finding, additional skepticism must be levied again if we are to evaluate a novel protein X and unexpected learning deficit. However this does not preclude that this result should not be presented to the scientific world for

evaluation, because over time each scientific study's contribution will be evaluated by the community's subsequent support or rejection.

Appendix A: Collaborative Contributions to "Hippocampal CA3 NMDA Receptors Are Crucial for Memory Acquisition of One-Time Experience"

Nakazawa, K., Sun, L. D., Quirk, M. C., Rondi-Reig, L., Wilson, M. A., and Tonegawa, S. (2003). Neuron *38*, 305-315.

Abstract:

Lesion and pharmacological intervention studies have suggested that in both human patients and animals the hippocampus plays a crucial role in the rapid acquisition and storage of information from a novel one-time experience. However, how the hippocampus plays this role is poorly known. Here, we show that mice with NMDA receptor (NR) deletion restricted to CA3 pyramidal cells in adulthood are impaired in rapidly acquiring the memory of novel hidden platform locations in a delayed matching-to-place version of the Morris water maze task but are normal when tested with previously experienced platform locations. CA1 place cells in the mutant animals had place field sizes that were significantly larger in novel environments, but normal in familiar environments relative to those of control mice. These results suggest that CA3 NRs play a crucial role in rapid hippocampal encoding of novel information for fast learning of one-time experience.

My Contribution:

In this paper I developed a novel method to count the number of peaks within a place field rate map. This method utilized the MATLAB image processing toolbox to identify local maxima within a given rate map. We showed that mutant place fields in a degraded cue

environment had altered place field representations which were larger in size and integrated firing rate. However, my "place field peak" analysis provided statistically the strongest evidence ($p<0.01$) that mutant fields were altered during our environmental manipulation (Figure 2D). Additionally, I also provided assistance to showing statistical significance of CA1 pyramidal cell place field recordings on the Linear Track (Figure 2), as well as provided sufficient rebuttal evidence to reviewers.

Neuron, Vol. 38, 305–315, April 24, 2003, Copyright ©2003 by Cell Press

Hippocampal CA3 NMDA Receptors Are Crucial for Memory Acquisition of One-Time Experience

Kazu Nakazawa,[1,2,3,4] Linus D. Sun,[2,4]
Michael C. Quirk,[2,4,5] Laure Rondi-Reig,[1,2,3,4,6]
Matthew A. Wilson,[2,4] and Susumu Tonegawa,[1,2,3,4,*]
[1]Howard Hughes Medical Institute
[2]Picower Center for Learning and Memory and
RIKEN-MIT Neuroscience Research Center
[3]Center for Cancer Research
[4]Departments of Biology and Brain
and Cognitive Sciences
77 Massachusetts Avenue
Massachusetts Institute of Technology
Cambridge, Massachusetts 02139

Summary

Lesion and pharmacological intervention studies have suggested that in both human patients and animals the hippocampus plays a crucial role in the rapid acquisition and storage of information from a novel one-time experience. However, how the hippocampus plays this role is poorly known. Here, we show that mice with NMDA receptor (NR) deletion restricted to CA3 pyramidal cells in adulthood are impaired in rapidly acquiring the memory of novel hidden platform locations in a delayed matching-to-place version of the Morris water maze task but are normal when tested with previously experienced platform locations. CA1 place cells in the mutant animals had place field sizes that were significantly larger in novel environments, but normal in familiar environments relative to those of control mice. These results suggest that CA3 NRs play a crucial role in rapid hippocampal encoding of novel information for fast learning of one-time experience.

Introduction

One-trial or one-experience learning is crucial for both human and nonhuman animals for the normal maintenance of day-to-day life and even for survival. In the ever changing world, events occur only once and, therefore, episodic memory—memory of an event that enables an explicit recollection (see Tulving, 1972, 2002, for reviews)—is based on this rapid form of learning. Other examples include poison avoidance (Garcia and Koelling, 1966), recognition memory (Ennaceur and Delacour, 1988), spatial learning (Morris, 1983; Panakhova et al., 1984; Whishaw, 1985; reviewed by Morris, 2001), and food caching (Clayton and Dickinson, 1998; reviewed by Griffiths et al., 1999). Studies on amnesic patients and lesioned animals have demonstrated that in both human and nonhuman animals, the hippocampus plays a crucial role in some types of one-trial learning (Zola-Morgan et al., 1986; Rempel-Clower et al., 1996; Steele and Morris, 1999; Xavier et al., 1999). In the case of rodents, it was shown that intrahippocampal infusion of NMDA receptor (NR) antagonist, AP5, results in an impairment in delay-dependent acquisition of one-trial spatial learning (Steele and Morris, 1999; Morris and Frey, 1997). However, little is known about the hippocampal subfields and their circuits in which NRs play a crucial role in this or any other types of rapid one-trial learning.

Based on theoretical grounds, Marr and others have suggested that a recurrent network with modifiable synaptic strength could support rapid acquisition of memories of one-time experiences (Marr, 1971; McClelland et al., 1992, Soc. Neurosci., abstract; McClelland et al., 1995). The CA3 subfield of the hippocampus is known to have just such a type of network, with its pyramidal cells receiving synaptic contacts from ~2% of other CA3 pyramidal cells (MacVicar and Dudek, 1980; Miles and Traub, 1986). Furthermore, NR-dependent, Hebbian-type synaptic plasticity in the form of long-term potentiation (LTP) has also been demonstrated at the recurrent collateral-CA3 synapses (Harris and Cotman, 1986; Williams and Johnston, 1988; Zalutsky and Nicoll, 1990; Berger and Yeckel, 1991). However, there has been no experimental evidence supporting the hypothesis that the recurrent CA3 network plays a crucial role in rapid one-trial learning.

Recently, we generated a conditional knockout mouse strain in which the deletion of the gene encoding the NR subunit 1 (NR1) of NRs is targeted to the CA3 pyramidal cells of adult mice (refereed to as CA3-NR1 KO mice) (Nakazawa et al., 2002). These mice were indeed deficient in evoked LTP specifically at the recurrent collateral-CA3 synapses but were normal in the spatial reference memory that is acquired incrementally over several days of repeated trials. We also demonstrated that this normal acquisition of spatial reference memory in the mutants correlated well with their normal place-related activities of CA1 pyramidal cells in a simulated familiar spatial environment.

The availability of the CA3-NR1 KO mice provided an opportunity to test the hypothesis that the recurrent CA3 network with modifiable synaptic strength supports hippocampus-dependent, rapid one-trial learning. For this purpose, we subjected the mutant mice to the delayed matching-to-place (DMP) version of the Morris water maze task in which the animal's ability to acquire a novel location of the hidden platform with just one visiting trial is tested by its performance in the second trial conducted a few minutes later. We also sought physiological correlates of the behavioral phenotype by monitoring place-related activities of CA1 pyramidal cells.

Results

CA3-NR1 KO Mice Are Impaired in Acquiring Memory of Novel Platform Locations in the DMP Task

The setup of the DMP task was similar to that of the standard hidden platform version of Morris water maze

*Correspondence: tonegawa@mit.edu
[5]Present address: Cold Spring Harbor Laboratories, 1 Bungtown Road, Cold Spring Harbor, New York 11724.
[6]Present address: LPPA-UMR CNRS 9950, Collège de France, 11 place Marcelin Berthelot, 75005 Paris, France.

except that the location of the platform was altered each day in a pseudo-random way (Figure 1A). We followed the trial protocol previously employed for rats with minor modifications (Steele and Morris, 1999); on each day, four trials were given with an intertrial interval of 5 min, and the time needed to reach the platform (escape latency) was recorded. The mean latencies were relatively long for the first trial of a day because the animals had no prior knowledge of the platform location. However, they can potentially shorten the mean latencies on the second trial based on the memory rapidly acquired during the first visit, and the reduced latencies in the second trial reflect the "savings" accrued from memory of the first trial (see Experimental Procedures for more details). For the data analysis and presentation, the DMP training session was subdivided into three blocks of 4 consecutive days (Figure 1B; blocks 1–3). Similarly, the data obtained during the 4 day-long testing session were combined (Figure 1C; days 13–16 for block 4). For each of the four trials (trials 1–4) conducted each day, the escape latencies were averaged over multiple animals for each genotype and over the 4 days of each training or testing block.

The mean latency curves for the DMP training session (blocks 1–3) and the testing session (block 4) are shown in Figures 1B and 1C, respectively. In Figure 1E, the latencies of trials 1 and 2 across the blocks are replotted. There were no significant differences of latencies between the two genotypes in any of the trials during the training session except for a small but significant reduction of block 3 trial 2 latencies in the mutants relative to controls. In the testing block, however, the mutants' mean latencies of the second and subsequent trials were clearly longer than controls' mean latencies of the corresponding trials (Figure 1C), and the mutants' mean savings between trials 1 and 2 was significantly shorter than the controls' (t test, $p < 0.04$). These results are consistent with the interpretation that CA3-NR1 KO mice are impaired in the rapid acquisition of spatial memory of novel locations of the hidden platform with just one visiting trial. However, prior to making a firm conclusion we evaluated several other possibilities. First, Figure 1D shows that the saving difference cannot be accounted for by a swim speed difference. Second, there is no significant difference in the time spent near the wall between two genotypes (Figure 1D), indicating that the mutants' reduced saving is not due to augmented thigmotaxis. Third, mutant mice did not search the platform at or near the locations of the previous day any more than control mice (Figure 1D), indicating that the mutants' latency prolongations are not due to increased memory interference or perseveration. This last point is also suggested by the lack of genotype-dependent latency difference in the first trials in which one expects memory interference, if any, would be most pronounced (Figure 1E). On the basis of these results, we conclude that the reduced savings observed in the mutants relative to controls during the testing session (block 4) is most probably a consequence of the mutants' impaired capability in rapidly acquiring the spatial memory of the novel location of the platform.

Why didn't the impairment in savings appear in the early stages of the training session (blocks 1 and 2)? Like any other task, the DMP task demands learning of a variety of basic rules. For instance, the animals will have to learn to swim away from the walls (i.e., overcome thigmotaxis), to climb on the platform once they find it (i.e., incentive learning), and most importantly, learn that there is a single place to escape and that this place varies from one day to another. Learning these basic rules is the prerequisite for the acquisition of the robust memory of the accurate location of the novel platform. In block 1, the effect of the first trials on the mean latencies of the second trials was minimal. In block 2, it was more pronounced, but the second trial latencies were still quite long (60 and 59 s for controls and mutants, respectively), suggesting that the saving was primarily due to rule learning rather than robust acquisition of spatial memory. In blocks 3 and 4, the second trial latencies of the mutants remained at the levels attained in block 2 while those of the control mice progressively shortened, resulting in genotype-specific differences in saving (Figure 1E). Also, the fact that the first trial latencies are the same for both genotypes across all four blocks suggests normal rule learning. These data suggest that CA3 NRs are involved primarily in the rapid spatial learning rather than in DMP rule learning.

CA3-NR1 KO Mice Are Normal in Recalling the Memory of Familiar Platform Locations in the DMP Task

One of the salient features of an association to be learned rapidly with one trial or one experience is its novelty. In the water maze DMP task, the animals are required to rapidly and accurately acquire the association of the novel location of the platform with the configuration of distal cues. In order to investigate further the role of the CA3 NR and recurrent network in the novelty-associated mnemonic process, we subjected other sets of pretrained mice ($n = 15$ and 13 for mutant and control animals, respectively) to a similar testing session except that on each of the 4 days in block 4 the platform locations were those experienced 4 days earlier during training rather than novel ones (Figures 1F and 1G). Under these conditions, the first trials can serve as a reminder of the spatial memory acquired 4 days earlier, and the performance improvement (saving) in the second trials would reflect the animals' ability to retrieve this reference memory. As shown in Figure 1F, we observed no difference in the mean latencies of not only first trials but also of the subsequent three trials between the two genotypes. Again, no significant differences were observed in the swim speed (Figure 1G), nor the time near the wall (data not shown), nor perseveration index between the two genotypes (data not shown).

A three-way ANOVA for escape latencies (KO versus control X novel versus familiar platform location X trials 2–4) based on the data from Figures 1C and 1F revealed a high significance in genotype effect [$F_{(1,220)} = 13.4$, $p < 0.0003$] as well as in the interaction between "genotype" versus "novel versus familiar platform location" [$F_{(1,220)} = 7.7$, $p < 0.006$]. Post hoc tests showed that mutant mean escape latencies of trials 2–4 were significantly longer ($p < 0.05$) than those of controls when the platform was placed at novel locations. In contrast, in trial 1 the latency differences were not significant [genotype effect, $F_{(1,220)} = 0.48$, $p = 0.49$; interaction between "geno-

type" versus "novel versus familiar platform location," $F_{(1,220)} = 0.06$, $p = 0.81$]. No significant interaction was observed in three-way ANOVA for swim speed (KO versus control X novel versus familiar platform location X trials 2–4) based on the data from Figures 1D and 1G (interaction between "genotype" versus "novel versus familiar platform location," $F_{(1,220)} = 0.02$, $p = 0.90$). These data demonstrate differential effects of the CA3 NR knockout on the acquisition and retrieval of reference memory and on the acquisition of single trial memory: CA3 NRs are dispensable in the acquisition of spatial memory by repeated trials and in its retrieval, but play a crucial role in rapid, one-trial acquisition of accurate memory involving novel and spatially dependent information.

Normal CA1 Place Cell Activity of Mutant Mice during Exploration in Familiar Linear Tracks

In order to investigate the cellular mechanisms that might underlie the specific behavioral impairment observed in the mutant mice, we examined the effect of novelty on spatial representations in area CA1—the output of the hippocampus proper. We chose this area because our primary goal was to determine the downstream effect of the disruption of CA3 activity that could be related to the behavioral output of hippocampus-dependent tasks. Using the tetrode recording technique (Wilson and McNaughton, 1993; Nakazawa et al., 2002), we compared the activity of CA1 pyramidal cells on familiar (track A) and novel (track B) regions of an L-shaped track (Figure 2A). After animals were familiarized with track A by running back and forth for 15 min for 1 day, data were collected from 108 complex spiking (pyramidal) cells and 21 putative interneurons from five mutant mice, and 89 complex spiking cells and eight putative interneurons from five control mice. As summarized in Table 1, under these conditions, we detected no effect of the CA3 NR1 knockout on the basic cellular properties of CA1 pyramidal cells such as spike width, complex spike index, mean firing rate, and peak firing rate, nor on the spatial tuning properties of individual place cells such as mean in-field firing rate, integrated firing rate, and place field size (see Experimental Procedures for the definition of each of these parameters). However, burst spike frequency in pyramidal cells and mean firing rate of CA1 interneurons were significantly diminished in the mutants relative to controls, presumably reflecting the reduced CA3 drive onto CA1 as a consequence of the NR1 knockout in CA3 (Nakazawa et al., 2003, in press).

Impaired Spatial Tuning of Mutant CA1 Place Cells in Novel Regions of Familiar Environment

To examine the effect of the mutation on the spatial tuning properties of CA1 place cells when animals are introduced to a novel region of the familiar environment, we let randomly chosen subsets of mutant and control mice enter into the perpendicularly attached novel track (track B) by removing the partition. We then compared the properties of CA1 place cells during the first 15 min in novel track B with those of the last 15 min in familiar track A (Figure 2A). Twenty seven and twenty nine complex spiking cells were recorded in the familiar track A, and twenty two and twenty nine cells were recorded in the novel track B from mutant and control mice, respectively. We found that three spatial tuning measures, integrated firing rate, place field size, and number of place field peaks (see Experimental Procedures) in CA1 complex spiking cells were all significantly greater for the mutant mice in the novel track compared to the familiar track, while those of the CA1 cells of the control mice did not change significantly upon entry into the novel track (Figures 2B–2D, "Day N"). In contrast, mean in-field firing rate was not elevated in the mutants (Figure 2E), indicating that impaired spatial tuning was not simply due to over excitation but due specifically to the enlargement of the field size of the mutant CA1 place cells upon entering into the novel track.

To confirm that the observed impairment in spatial tuning was related to the novelty of exposure, the same set of mutant and control mice were subjected to another recording session on the next day in familiar track A immediately followed again by a recording session in track B. In this second pair of recording sessions, the data were collected from 24 and 26 complex spiking cells in track A and 23 and 23 complex spiking cells in track B from the mutant and control mice, respectively. In this case, there was no indication of an increase in any of the three spatial tuning measures upon reentry into track B from track A in either the control or mutant mice (Figures 2B–2D, "Day N+1"). Running velocity could affect place cell firing properties (McNaughton et al., 1983). However, average running velocity did not differ for either genotype under any of the four conditions (Figure 2F). In addition, we did not observe any overt behavioral changes in either the mutant or control mice upon any of the track shifts. Figures 2I and 2J show two examples each of the place fields of CA1 complex spiking cells from the control and mutant mice in tracks A and B, respectively. In these examples, the place fields were relatively compact in the familiar track A for both control and mutant cells (Figure 2I), while they were spatially less tuned when the mutant mice were exposed to track B for the first time (Figure 2J, "Day N") and returned to normal on the next day (Figure 2J, "Day N+1"). We also conducted the statistical analysis per mouse and found significant interaction between "genotype" versus "condition" (four recording conditions) in integrated firing rate [$F_{(3,16)} = 7.6$, $p < 0.03$], and in place field size [$F_{(3,16)} = 3.3$, $p < 0.05$].

It is interesting to find out whether the improved spatial tuning observed in the mutant mice upon the revisit of track B on day N+1 reflects a certain consolidation process which may occur during the 24 hr-long resting period between the day N and day N+1 recording sessions. An alternative possibility is that the extent of spatial tuning depends on the amount of experience in track B throughout the day N and day N+1 recording sessions (15 min each and 30 min total). In order to address this issue, we calculated the mean integrated firing rate and the place field size every 3 min during the day N and day N+1 recording sessions. As shown in Figures 2G and 2H, there were no significant changes in either of these two spatial tuning parameters within the day N or day N+1 recording session. Thus, the levels of mutant spatial tuning were discontinuous between the last 3 min of the day N recording session and the first 3 min

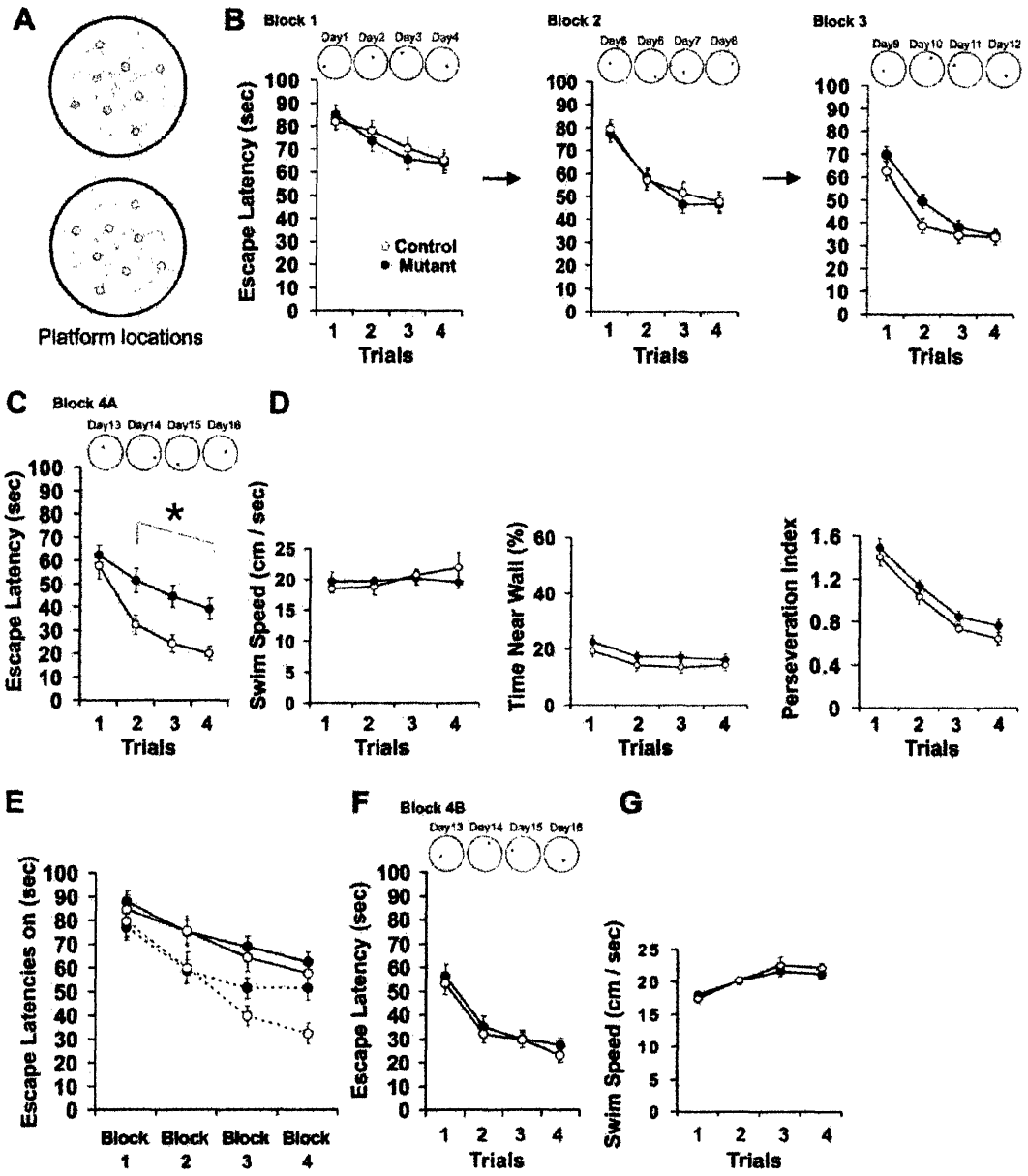

Figure 1. A Delayed Version of Matching-to-Place Task in Water Maze

(A) Sixteen platform locations employed during the 16 day-long training and testing experiments (one location per day) are displayed in two groups to avoid over crowding.

(B) Eighteen- to twenty-two-week-old male CA3-NR1 KO mice (filled circles, N = 31) and their fNR1 control littermates (open circles, N = 25) were subjected to delayed version of matching-to-place (DMP) training for 12 days, four trials per day with an intertrial interval of 5 min. The training session was subdivided into three blocks (blocks 1–3), each consisting of 4 consecutive days. The escape latencies (s) of mice of one genotype (mutant or control) were averaged for the first, second, third, and fourth trial over 4 days for each block. In this panel and in panels (C) and (F), the locations of platforms employed on each day are indicated at the top.

(C) About a half of the pretrained CA3-NR1 KO mice (filled circles, N = 16) and their fNR1 control littermates (open circles, N = 12), both randomly chosen, were subjected to 4 more days of trials, each day with a novel platform location (block 4A, days 13–16). Mutants' escape latencies were indistinguishable from those of controls in the first trial (t test, $p = 0.513$) but were significantly longer in subsequent trials (trials 2–4) compared to controls' latencies of the corresponding trials [repeated measure of ANOVA for trials 2–4, genotype effect, $F_{(1,110)} = 16.00$, $^*p < 0.001$].

(D) In block 4A, there were no differences between the two genotypes in swim speed [genotype effect, $F_{(1,110)} = 0.06$, $p = 0.8$], in time (%) spent near the pool wall [genotype effect, $F_{(1,110)} = 1.9$, $p = 0.17$], and in perseveration index [genotype effect, $F_{(1,110)} = 2.8$, $p = 0.97$; see Experimental Procedures].

(E) Escape latencies of the first (solid lines) and second (dotted lines) trials during the training and testing were replotted only for those mice that received the block 4A testing (mutants, filled circles, N = 16; controls, open circles, N = 12). There was no difference in the first trial latencies between the two genotypes, suggesting no effect of the mutation on perseveration. The mutants' second trial latencies dropped in block 2 compared to block 1, but no further shortening was observed in the subsequent blocks. In contrast, controls' second trial latencies continued to drop throughout blocks, resulting in genotype-specific differences.

of the day N+1 recording session, suggesting a certain consolidation process is at work between the two sessions.

The results described in this section suggest that mutants' CA1 place cell activities are less spatially tuned compared to those of control animals, at least during the first 15 min of animals' exploration in a novel region of a familiar environment. This spatial tuning impairment is, however, restored by the time the animals explore the same region on the next day through some sort of consolidation process that occurs during the intervening resting period.

Exposure of Mutant Mice to a Novel Environment Exhibits Poor Spatial Tuning

Similar recordings were performed using a single open-field testing environment. We recorded from CA1 for 20 min as the mutant (n = 6) or control mice (n = 5) explored a novel open arena and compared the data with those obtained when the animals were returned to the same environment on the following days. The total numbers of cells recorded were 33 and 43 for day 1, 22 and 36 for day 2, and 102 and 102 for day 3 and after, for control and mutant animals, respectively. We found that the controls' place field sizes were compact on day 1 and remained compact throughout the subsequent several days, while the mutants' place field sizes were significantly greater on day 1, became compact on day 2, and remained compact on the subsequent days (Figures 3A and 3B). Similar pattern of abnormalities was found in the integrated firing rate of the mutants (Figures 3C), while neither mean in-field firing rate (Figure 3D) nor several intrinsic properties of complex spiking cells (Figure 3E and 3F) nor the animals' running velocity (Figure 3G) differed between the two genotypes.

We examined whether the mutant spatial tuning developed continuously during the day 1 and day 2 recording sessions or discontinuously between the two sessions. We found that the levels of mutant spatial tuning were discontinuous between the last 10 min of the day 1 recording session (24 cells) and the first 10 min of the day 2 recording session (16 cells) (t test, $p < 0.05$ for integrated firing rate; $p < 0.03$ for place field size). This again suggests that certain consolidation events may be at work during the intermittent resting period in the home cages.

The increases in integrated firing rate, place field size, and place field peak number observed in the mutants upon exposure to novel spatial information suggest that these animals are indeed impaired in the rapid incorporation of novel spatial information into CA1 spatial representations. The observation that the mutant's integrated firing rate, place field size, and place field shape assessed by the number of place field peaks are normal in the familiar track or arena indicate that CA3 NRs are dispensable for reactivation of established memory representations (Brun et al., 2002). Furthermore, the observation that in mutants, these place cell parameters are normal from the very first moment upon reentry to the now familiar track or arena which was novel 1 day earlier, indicates that these mice are capable of forming memory representations of novel experiences, although they are impaired in doing so rapidly.

Discussion

In the present study, we demonstrated that CA3-NR1 KO mice were impaired in the DMP task when the escape platform was placed at a novel location and the animals were required to rapidly incorporate this novel spatially dependent information into spatial representations of the environment. In contrast, the behavior of the mutant mice was indistinguishable from the control mice when previously experienced locations of the platform were used. These results may relate to the recent finding that rats which received the NR antagonist, AP5, in CA3 displayed short-term memory deficit in a task involving a novel environment (Lee and Kesner, 2002). We also showed that spatial tuning of CA1 place cell activity in the mutant mice was impaired when they visited novel regions of an environment. This impairment was, however, overcome by the following day, showing the correlation between the time courses of behavioral deficits and impaired spatial tuning in the mutant animals.

Correlations of the Behavioral and Physiological Data

Our evaluation of the efficacy and time course of acquisition of novel information required comparison of behavioral and physiological measurements. In the DMP task, novelty lies in the new associations between the escape behavior and spatial locations within the water maze. These spatial behavioral associations were not necessarily made with novel spatial locations; the novelty arises from the specific conjunction of spatial and nonspatial information. Previous studies have shown that place cell response can reflect this type of specific conjunction (Fyhn et al., 2002; Louie, 2002). In those studies, novel spatial behavioral associations, such as stopping at a location that was previously encountered during active locomotion as a neutral site but subsequently marked by nonspatial information, resulted in establishment of distinct place cell representations, with individual place cells expressing the conjunction of both the spatial and nonspatial information present in these tasks. They demonstrated that formation of robust spatially dependent place cell responses reflects acquisition of novel spatial behavioral associations such as those established during active locomotion on the linear

(F) The other half of the pretrained mutants (filled circles, N = 15) and fNR1 control littermates (open circles, N = 13) were also subjected to 4 more days of trials, but in this case with platform locations that were experienced 4 days earlier, namely during block 3 (block 4B, day 13–16). There were no differences between the two genotypes in escape latencies throughout the trials [$F_{(1,110)} = 0.547$, $p = 0.461$ for trials 2–4; t test, $p = 0.751$ for trial 1].

(G) Swim speeds in block 4B were also indistinguishable between the two genotypes [genotype effect, $F_{(1,110)} = 0.7$, $p = 0.39$]. All the data were expressed as mean ± SEM.

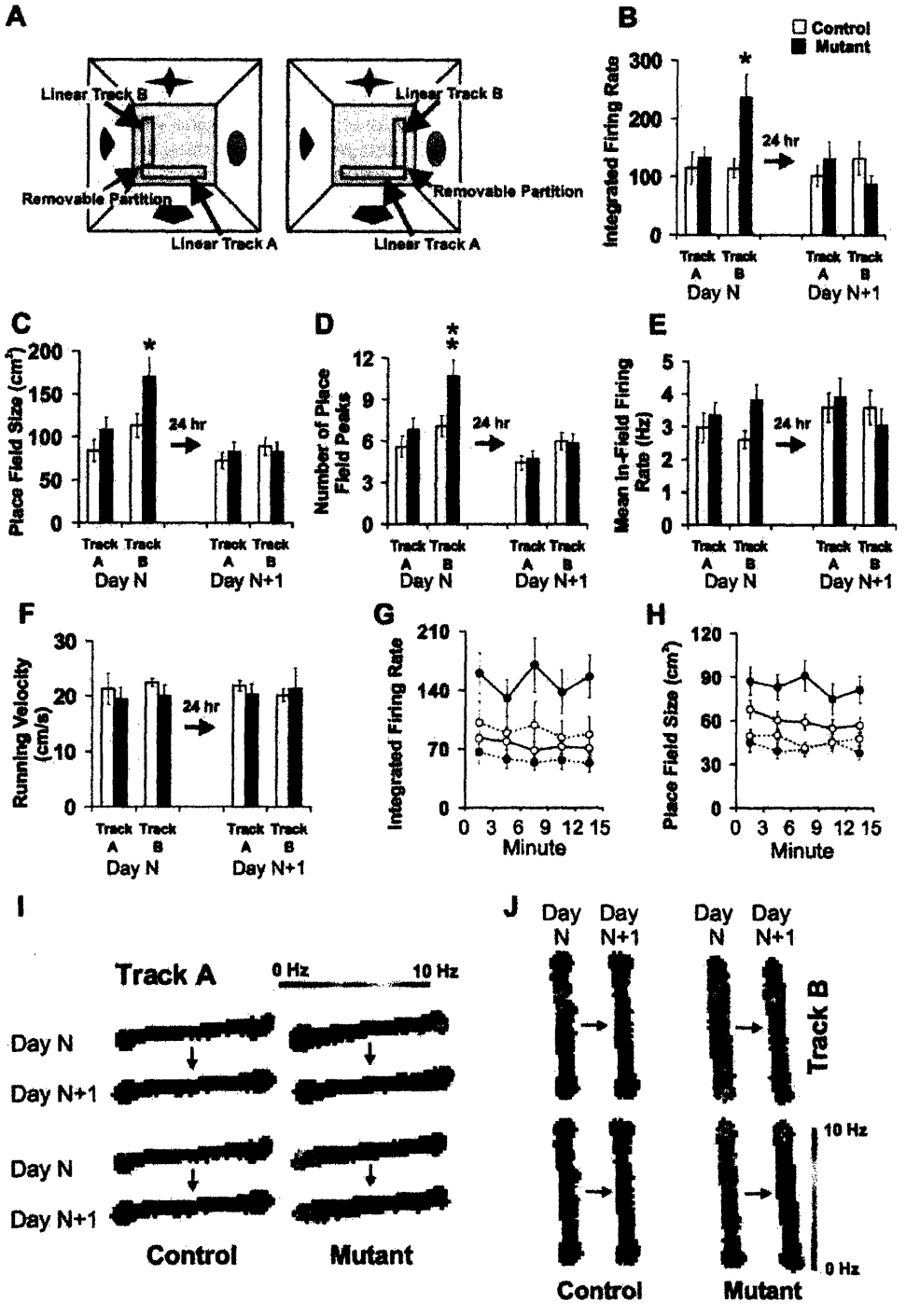

Figure 2. CA1 Place Cell Activities in Novel and Familiar Tracks

(A) Designs of the in vivo tetrode recording space (top-down view). Two linear tracks A and B were placed in an L shape in a square room. The two versions shown were alternated to counterbalance differential effects of the cue versus track configurations. Tracks A and B were used as familiar and novel areas, respectively, on day N. Immediately after the animals entered track B from track A, the partition was reinstalled to prevent them from returning to track A.

(B–E) Open bars, fNR1 controls (N = 3); solid bars, mutants (N = 3). (B) Mutants' integrated firing rates in track B on day N were significantly greater compared to all other combinations of genotype, day and track [genotype effect, $F_{(1,195)} = 3.3$, $p < 0.05$, interaction between genotype and condition, $F_{(3,195)} = 3.8$, $^*p < 0.02$]. (C) Mutants' place field sizes in track B on day N were also significantly larger compared to all other combinations of genotype, day, and track [genotype effect, $F_{(1,195)} = 7.1$, $p < 0.009$; interaction between genotype and condition, $F_{(3,195)} = 2.6$, $^*p < 0.05$]. (D) The number of place field peaks of the mutants in track B on day N was significantly greater compared to other combinations of day and track, while that of controls was not (Kruskal-Wallis ANOVA for number of place field peaks, $H = 16.7$, $p < 0.01$ for mutant, $H = 7.5$, $p = 0.06$ for control). Mann-Whitney U test comparison gave a highly significant difference between the genotypes in track B on day N ($U = 178.5$, $^{**}p < 0.008$). (E) Mean in-field firing rates did not differ significantly among different combinations of conditions [genotype effect, $F_{(1,195)} = 1.1$, $p = 0.29$, interaction between genotype and condition, $F_{(3,195)} = 1.1$, $p = 0.34$].

Table 1. Properties of CA1 Pyramidal Cells and Interneurons in Familiar Linear Track

	Pyramidal Cells		Interneurons	
	Control (n = 89, D = 17, N = 5)	Mutant (n = 108, D = 18, N = 5)	Control (n = 8, D = 16, N = 5)	Mutant (n = 21, D = 15, N = 5)
Spike width (μs)	336.1 ± 4.4	339.7 ± 4.6	192.0 ± 9.8	185.5 ± 5.5
Complex spike index	19.9 ± 1.4	18.3 ± 1.1	−0.7 ± 1.3	0.7 ± 0.3
Mean firing rate (Hz)	1.79 ± 0.14	2.03 ± 0.17	30.4 ± 5.4	16.2 ± 3.3[a]
Peak firing rate (Hz)	9.68 ± 0.7	9.82 ± 0.7	ND	ND
Mean in-field firing rate (Hz)	3.35 ± 0.26	3.28 ± 0.23	ND	ND
Integrated firing rate [Σ(Hz/pixel)]	119.7 ± 13.8	128.6 ± 12.0	ND	ND
Place field size (cm^2)	85.2 ± 6.4	98.3 ± 5.8	ND	ND
Burst spike frequency (%)	52.1 ± 1.3	48.2 ± 1.4[a]	ND	ND

All measurements are mean ± SEM. n, number of cell; D, number of recording session; N, number of animal. ND, not determined.
[a]Significantly different from fNR1 control (Student's t-test, $p < 0.05$).

track as well as during the type of behavior that is expressed in the DMP task.

Ideally, evaluation of place cell response during the acquisition of the memory of novel spatial behavioral contingency in the DMP task would be carried out during the task itself. Unfortunately, the limited and biased nature of spatial sampling inherent in this type of navigational task, and the sensitivity of place cell activity to changes in behavior per se, complicates the interpretation of place cell response under those conditions. While place cell recording has been performed during tasks of this type (Hollup et al., 2001; Fyhn et al., 2002), the desire to examine the time course of novelty effects combined with the constraints imposed by limited sampling, and the difficulty in assessing the direct contribution of behavioral changes dictated the use of a separate protocol to robustly assess the impact of novelty on place cell response. This was achieved through the comparison of place cell activity on two separate linear tracks which allowed repeated measurement of place cell activity during exposure to novelty. Under these conditions that permit the control for sampling and behavioral variation, novelty lies in the new associations between distal cues on the second track. Therefore, in both the DMP and linear track tasks, there is the expectation that the hippocampal spatially dependent place cell representations are altered to incorporate novel associations.

While it remains possible that the mechanisms and dynamics of novel spatial behavioral associations may differ dependent upon the history of exposure to the spatial component of the association, our results suggest a strong correlation in the characteristics and time course of the behavioral and electrophysiological phenotypes, and point to the common involvement of CA3 NRs in both conditions.

Impaired Place Cells and Their Recovery

How does the lack of CA3 NRs lead to the decreased spatial specificity of CA1 pyramidal cells in the novel space? CA1 receives inputs both from the layer III stellate cells of entorhinal cortex (EC) via the temporoammonic pathway, and from CA3 pyramidal cells via the Schaffer collaterals. During spatial exploration, cells in the superficial layer of the EC show spatially related responses with significantly lower spatial specificity than that observed in CA3 (Barnes et al., 1990; Quirk et al., 1992; Frank et al., 2000). It has been suggested that these EC cells provide a major source of input to CA1 (Vinogradova, 1975; McNaughton et al., 1989; Brun et al., 2002), particularly during tasks that require encoding of novel information (Sybirska et al., 2000). Furthermore, the activity of the temporoammonic pathway has been shown to regulate the gating of CA1 spikes in EC-hippocampal slices (Remondes and Schuman, 2002). Our result showing that CA1 place fields are less spatially tuned in the mutant animals when new spatial representation is required is consistent with the notion that new spatial context is conveyed via temporoammonic pathway. Moreover, our finding supports a long-standing hypothesis that CA1 network acts as a comparator: detecting novelty or mismatches between actual sensory information from entorhinal cortex and expectation from memory in CA3 (Sokolov, 1963; Vinogradova, 1970; O'Keefe and Nadel, 1978; Gray, 1982; Moser and Paulsen, 2001; Fyhn et al., 2002), while the memory seems to be retrieved from area CA1 itself in the CA3-NR1 KO mice.

(F) Average running velocities during whole recording session did not differ significantly between genotypes under any of the four conditions (Kruskal-Wallis ANOVA for running velocity: $H = 3.1$, $p = 0.38$ for mutant; $H = 0.15$, $p = 0.98$ for control).
(G and H) Time courses of spatial tuning parameters averaged over 3 min bins within individual recording sessions in track B. (G), integrated firing rate; (H), place field size. Filled circles with solid lines, mutants on day N; Open circles with solid lines, controls on day N; Filled circles with dotted lines, mutants on day N+1; Open circles with dotted lines, controls on day N+1. The values for mutants on day N were consistently greater than those of other conditions [repeated measure of ANOVA, $F_{(3,93)} = 5.3$, $p < 0.003$ for integrated firing rate; $F_{(3,93)} = 7.9$, $p < 0.0001$ for place field size]. The values for mutants during the last 3 min on day N were significantly greater that those during the first 3 min on day N+1 (t test, $p < 0.004$ for integrated firing rate; $p < 0.002$ for place field size).
(I and J) Two representative place fields for each genotype recorded from the same complex spiking cells on two consecutive days in track A and track B. They were smoothed for visualization. The track A was familiar to the animals on both day N and day N+1, while the track B was novel on day N and familiar on day N+1. $N > 3$ and $N < 9$. All the data were expressed as mean ± SEM on a per-cell basis.

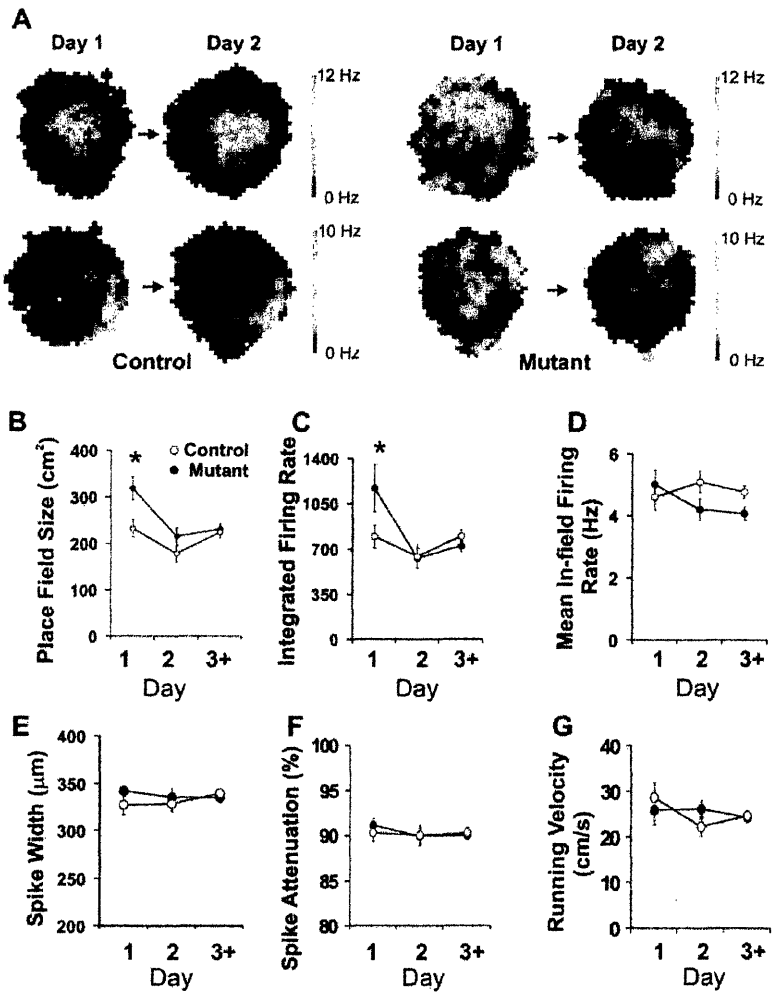

Figure 3. CA1 Place Cell Activities in Novel and Familiar Open Arena

(A) Representative place fields of the same complex spiking cells on day 1 (novel) and day 2 (familiar). They were smoothed for visualization.

(B–F) Day-to-day time course of place cell parameters. (B) The mutants' place field sizes were larger on day 1, but were indistinguishable on day 2 or subsequent days compared to the control animals [two-way ANOVA, interaction between genotype and day, $F_{(2,328)} = 3.1$, $^*p < 0.045$]. (C) The mutants' integrated firing rates were greater on day 1, but were indistinguishable on day 2 or subsequent days compared to the control animals [interaction between genotype and day, $F_{(2,328)} = 3.7$, $^*p < 0.026$]. (D) Mutants' in-field firing rate was indistinguishable from that of controls on day 1 and on subsequent days [interaction between genotype and day, $F_{(2,328)} = 2.0$, $p = 0.14$]. Mutants' spike width (E) and spike attenuation (F) were also indistinguishable from those of controls throughout the days of recording.

(G) The running velocity of the mutants and controls were also indistinguishable throughout the days. In (B)–(G), open circles are fNR1 controls (N = 5) and filled circles are mutants (N = 6). All the data were expressed as mean ± SEM on a per-cell basis.

We hypothesize that during exposure to a novel context, CA1 response is initially driven by the spatially broadly tuned, direct EC input. In control animals, NR function in CA3, perhaps via recurrent connections, allows rapid formation of more spatially specific responses that can then drive correspondingly specific response in CA1 as the input through the Schaffer collaterals comes to dominate or shape the input from the EC. In CA3-NR1 KO mice, CA3 NR ablation leading to the lack of dominant CA3 input (Nakazawa et al., 2003, in press) may result in a more gradual spatial refinement of CA1 place fields implemented by other hippocampal circuit plasticity. In fact, our preliminary recording from CA3 place cells revealed a robust reduction of CA3 activity in the familiar environment, suggesting generally decreased output from CA3 (K.N., unpublished data). CA1 place field enlargement may be due to the prolonged influence of direct EC input to CA1 during this slow spatial refinement process.

Place Cells as Memory Traces

For any cellular or cell ensemble activities to qualify as memory traces, several conditions have to be met. The activities must be formed in an experience-dependent manner and be specific to the acquired information. They must outlast the period in which the animals are exposed to the information and be reactivatable upon the presentation of recalling cues. A large number of studies have provided evidence for the qualifications of place cells as memory traces at the neuronal ensemble level (O'Keefe and Nadel, 1978; Wilson and McNaughton, 1993, 1994; Eichenbaum et al., 1999; Poucet et al., 2000; Louie and Wilson, 2001; Moser and Paulsen, 2001; Lee and Wilson, 2002). However, among these efforts, establishing the experience dependency has been most difficult. The reason is that place cells are formed so rapidly when an animal is exposed to a novel space or situation that it is difficult to catch them in the midst of making. Indeed, our data shown in Figures 2G and 2H confirmed a rapid formation of high spatial tuning place cells upon entry of control animals into the novel track, which prevented our capturing their earlier state. In contrast, the NR knockout in CA3 slowed down the process of place cell formation drastically and allowed us to catch them in an immature state (Figure 2). Although we do not know the exact time course nor the mechanism of the maturation of these place cells, our data showed that they do eventually acquire normal high spatial tuning by the time the animals reenter the space 1 day later. Assuming that these immature place cells observed in the mutant mice represent an early state of place cells in normal animals, they may provide insights into the

mechanisms that contribute to the formation of place cells. Our having captured these immature place cells reinforces evidence for the memory trace role of place cells.

Another intriguing aspect of the mutants' place cells is the rare dissociation of spatial representation and spatial encoding on day 1 (or day N). Since spatial representation is normal on day 2 (or day N+1), the animals must have encoded a sufficient amount of spatial information on day 1 that permits the subsequent formation of robust spatial representation. How this improvement of spatial representation can be achieved without a continued supply of external cues is a matter of great interest for future studies.

Conclusions

Our results have demonstrated that a specific ablation of functional elements within the hippocampal system can selectively alter the time course of acquisition of novel information and the formation of spatial memory representations. In particular, the present results provide evidence for a crucial role of CA3 NRs in the rapid formation of memory representations in CA1 as a specific pattern of place cell activities and for the rapid acquisition of one-time experience or one-trial memory. Given our previous findings demonstrating the requirement of CA3 NRs in associative memory recall, NRs expressed in the same CA3 pyramidal cells seem to play multiple roles in the hippocampus-dependent mnemonic process.

Experimental Procedures

Animals

All the experiments were carried out using male CA3-NR1 KO mice (strain C57BL/6) of 18–20 weeks of age and their floxed- NR1 (fNR1; control) littermates. By these ages, NR proteins were abolished in the mutant mice specifically in CA3 pyramidal cells (Nakazawa et al., 2002). Two to five mice were housed per cage under the conditions of a 12 hr light/dark cycle and ad libitum access to food and water. All the experiments were conducted by operators who were blind to the genotypes of the mice used. All procedures relating to animal care and treatment conformed to the Institutional and NIH guidelines.

A Delayed Matching-to-Place Task for Mice in Water Maze

The task protocol used was similar to that reported for rats (Steele and Morris, 1999). The water maze (1.6 min in diameter) and its surrounding set up was as previously described (Nakazawa et al., 2002). The experiments were conducted in a series of three phases: (1) pretraining on a cued platform task; (2) training on the delayed matching-to-place (DMP) task; and (3) DMP testing. Throughout training and testing phases, the single escape platform (10 cm in diameter) was located 1.5 cm below the surface of the water, on successive days, in 1 of 16 separate places within the pool, located symmetrically near the side wall (8 places, outer ring) or near the center (8 places, inner ring) (Figure 1A). The centers of these 16 different places were at least 26.6 cm away from the wall and separated from each other by at least 20 cm. Throughout the three behavioral phases, the locations of the platform were altered from one day to the next in a pseudo-random fashion, and the use of two locations in the same quadrant on 2 successive days was avoided. Throughout the experimental phases, the trials began at N, E, S, and W in a pseudo-random sequence with mice facing the pool wall. The experiment began with pretraining with a cued platform, which lasted for 3 days, four trials per day, with the location of the platform altered each day but marked by an attached flag (10 cm high). The flag was removed the next day (day 1) to begin DMP training, which lasted for 12 days (days 1–12), each day with a novel location of the hidden platform. Four trials were given per day with an intertrial interval of 5 min and the four release sites (N, E, S, and W) used in a different order each day. Between trials, mice were kept in home cages under a warming light. In each trial, a mouse was allowed to search the platform for up to 120 s. In the first trial of a day, if an animal found the platform, it was allowed to stay on it for 30 s prior to transfer to the home cage. Otherwise, the search was interrupted and the animal was gently hand picked, placed on the platform, and allowed to stay there for 30 s. In the subsequent trials (trials 2–4), the same procedure was followed except that the platform-stay period was reduced to 15 s. After completion of the training phase, the mice were randomly divided into two groups for the DMP testing phase, which lasted 4 days (days 13–16). One group of mice continued to receive the DMP task, four trials per day with a new platform location each day, and the escape latency (time to reach platform), the swimming speed, time spent in an area near the wall (up to 18% radius from the wall), and averaged perseveration index were recorded. The perseveration index was defined as a ratio of averaged distance from the today's platform center to that from the previous day's platform center. The second group of mice also underwent 4 more days of the DMP task, but the platform location was the same as that experienced 4 days earlier (i.e., the platform location on day 13 was the same as that on day 9, the platform location on day 14 was the same as that on day 10, and so on). For these experiments, the mouse release sites and their order were also the same as those used 4 days earlier. The data from obvious "floaters" (less than 10% of all the mice tested) were excluded.

In Vivo Tetrode Recording

Experimental procedure for in vivo tetrode recording was previously described (Nakazawa et al., 2002). Briefly, male mice (18–24 weeks of age) were implanted with a microdrive array consisting of six independently adjustable tetrodes (stereotaxic coordinates from bregma: 2.0 mm lateral; 1.8 mm posterior). As animals randomly explored linear tracks (77 × 7 cm for each track; Figure 2A) or a low-walled open field arena (50 cm in diameter) placed near the center of a black-curtained rectangular chamber, extracellular action potentials in CA1 cell layers were recorded while the animal's position was tracked using a pair of infrared diodes above the animal's head. Following data acquisition, action potentials were assigned to individual cells based on a spike's relative amplitudes across the four recording wires of a tetrode. Putative pyramidal cells were defined as cells with relatively broad waveforms (peak to trough width > 300 μs) and a strong tendency to produce complex spike bursts (complex spike index [CSI] $> 3\%$; defined as the percentage above chance of spikes with first lag interspike intervals that fall between 2 and 15 ms and whose second spike is smaller than the first), whereas putative interneurons had relatively narrow waveforms (peak to trough width < 240 μs) and few if any complex spike bursts (CSI $< 3\%$).

Firing properties of CA1 pyramidal cells were characterized using three measures: (1) mean firing rate (Hz), (2) peak firing rate (Hz), and (3) burst spike frequency (%)—percentage of the number of spikes involved in a burst relative to the total number of spikes produced by the cell. Those pyramidal cells with mean firing rates over 0.5 Hz, indicating spatial responsiveness during running, were selected for place field analysis. Individual pixels were excluded if the animal's total occupancy time within that pixel did not exceed 0.5 s. Spatial tuning of individual cells was assessed by four measures: (1) mean in-field firing rate, defined as the average firing rate across all pixels with mean pixel firing rate exceeding 10% of the cell's peak firing rate; (2) integrated firing rate, defined as the sum of mean pixel firing rates across pixels; (3) place field size, defined as the area of pixels whose firing rate exceeding 10% of the peak firing rate; and (4) number of place field peaks (Figure 2D). Mean pixel firing rate was calculated by dividing the total number of spikes detected at a pixel location by the total occupancy time within that pixel. Place field peak number analysis was carried out by analyzing the individual firing rate maps of each place cell in the linear track. Significant peaks were counted only if their firing rates were above 20% of the cell's peak firing rate. Peaks were identified as local

maxima (locations with all surrounding pixels having lower values, Matlab image processing toolbox). As a measure of the intrinsic properties of pyramidal cells, we determined spike width (peak to trough width), and the degree of amplitude attenuation within a three spike burst. For linear track data, analysis was restricted to periods during which the animal's running speed exceeded 2.0 cm/s. Place cell examples shown were identified as the same cells with waveform profiles that remained stable across the 2 days' recording sessions (Figures 2I, 2J, and 3A). The inherently more variable behavior in the open field precluded analysis of multiple peaks.

Novelty experiment in linear tracks in Figure 2 was conducted as follows. The familiarization of track A consisted of at least two sessions of running in the track A, each session lasting for 15 min and taking place on an independent day within the maximum total period of 8 days. Immediately after the completion of the last 15 min familiarization session on day N, animals were allowed to enter the novel track B by a temporary removal of the partition and to explore it for 15 min. The activities of complex spiking cells in CA1 were recorded during the entire 30 min period before and after the track shift. The animals were then transferred to home cages and returned 1 day later (i.e., day N+1) to the track A followed by track B and the recording conducted as before.

Acknowledgments

We thank Dr. Richard G.M. Morris for valuable advice for the mouse DMP task; Frank Bushard, Candice Carr, and Lorene Leiter for help with the experiments; and many members of both Tonegawa and Wilson labs, particularly Ray Kelleher and David Foster, for valuable advice and discussions during the course of this study and manuscript preparation. Supported by NIH grant RO1-NS32925 (S.T.), RIKEN (S.T. and M.A.W.), NIH grant P50-MH58880 (S.T. and M.A.W.), HHMI (S.T.), and Human Frontier Science Program long-term fellowship (K.N.).

Received: October 25, 2002
Revised: March 7, 2003
Accepted: March 8, 2003
Published: April 23, 2003

References

Barnes, C.A., McNaughton, B.L., Mizumori, S.J.Y., Leonard, B.W., and Lin, L.-H. (1990). Comparison of spatial and temporal characteristics of neuronal activity in sequential stages of hippocampal processing. Prog. Brain Res. *83*, 287–300.

Berger, T.W., and Yeckel, M.F. (1991). Long-term potentiation of entorhinal afferents to the hippocampus enhanced propagation of activity through the trisynaptic pathway. In Long-Term Potentiation: A Debate of Current Issues, M. Baudry and J.L. Davis. eds. (Cambridge, MA; MIT Press), pp. 327–356.

Brun, V.H., Otnæss, M.K., Molden, S., Steffenach, H.-A., Witter, M.P., Moser, M.-B., and Moser, E.I. (2002). Place cells and place recognition maintained by direct entorhinal-hippocampal circuitry. Science *296*, 2243–2246.

Clayton, N.S., and Dickinson, A. (1998). Episodic-like memory during cache recovery by scrub jays. Nature *395*, 272–274.

Eichenbaum, H., Dudchenko, P., Wood, E., Shapiro, M., and Tanila, H. (1999). The hippocampus, memory, and place cells: is it spatial memory or a memory space? Neuron *23*, 209–226.

Ennaceur, A., and Delacour, J. (1988). A new one-trial test for neurobiological studies of memory in rats. 1: behavioral data. Behav. Brain Res. *31*, 47–59.

Frank, L.M., Brown, E.N., and Wilson, M.A. (2000). Trajectory encoding in the hippocampus and entorhinal cortex. Neuron *27*, 169–178.

Fyhn, M., Molden, S., Hollup, S., Moser, M.-B., and Moser, E.I. (2002). Hippocampal neurons responding to first-time dislocation of a target object. Neuron *35*, 555–566.

Garcia, J., and Koelling, R.A. (1966). Relation of cue to consequence in avoidance learning. Psychon. Sci. *4*, 123–124.

Gray, J.A. (1982). The neuropsychology of anxiety: an enquiry into functions of the septo-hippocampal system. (Oxford, UK: Oxford University Press).

Griffiths, D., Dickinson, A., and Clayton, N. (1999). Episodic memory: what can animals remember about their past? Trends Cogn. Sci. *3*, 74–80.

Harris, E.W., and Cotman, C.W. (1986). Long-term potentiation of guinea pig mossy fiber response is not blocked by N-methyl D-aspartate antagonist. Neurosci. Lett. *70*, 132–137.

Hollup, S.A., Molden, S., Donnett, J.G., Moser, M.-B., and Moser, E.I. (2001). Accumulation of hippocampal place fields at the goal location in an annular watermaze task. J. Neurosci. *21*, 1635–1644.

Lee, I., and Kesner, R.P. (2002). Differential contribution of NMDA receptors in hippocampal subregions to spatial working memory. Nat. Neurosci. *5*, 162–168.

Lee, A.K., and Wilson, M.A. (2002). Memory of sequential experience in the hippocampus during slow wave sleep. Neuron *36*, 1183–1194.

Louie, K. (2002). Mnemonic information in the rodent hippocampus during wake and sleep states. PhD thesis, Department of Biology, Massachusetts Institute of Technology, Cambridge, Massachusetts.

Louie, K., and Wilson, M.A. (2001). Temporally structured replay of awake hippocampal ensemble activity during raid eye movement sleep. Neuron *29*, 145–156.

MacVicar, B., and Dudek, F. (1980). Local synaptic circuits in rat hippocampus: interaction between pyramidal cells. Brain Res. *184*, 220–223.

Marr, D. (1971). Simple memory: a theory for archicortex. Philos. Trans. R. Soc. Lond. B Biol. Sci. *262*, 23–81.

McClelland, J.L., McNaughton, B.L., and O'Reilly, R.C. (1995). Why there are complementary learning systems in the hippocampus and neocortex: insights from the success and failures of connectionist models of learning and memory. Psychol. Rev. *102*, 419–457.

McNaughton, B.L., Barnes, C.A., and O'Keefe, J. (1983). The contributions of position, direction, and velocity to single unit activity in the hippocampus of freely-moving rats. Exp. Brain Res. *52*, 41–49.

McNaughton, B.L., Barnes, C.A., Meltzer, J., and Sutherland, R.J. (1989). Hippocampal granule cells are necessary for normal spatial learning but not for spatially-selective pyramidal cell discharge. Exp. Brain Res. *76*, 485–496.

Miles, R., and Traub, R. (1986). Excitatory synaptic interactions between CA3 neurons in the guinea-pig hippocampus. J. Physiol. *373*, 397–418.

Morris, R.G.M. (1983). An attempt to dissociate "spatial-mapping" and "working-memory" theories of hippocampal function. In Neurobiology and Hippocampus, W. Seifert, ed. (London: Academic Press).

Morris, R.G.M. (2001). Episodic-like memory in animals: psychological criteria, neural mechanisms and the value of episodic-like tasks to investigate animal models of neurodegenerative disease. Philos. Trans. R. Soc. Lond. B Biol. Sci. *356*, 1453–1465.

Morris, R.G.M., and Frey, U. (1997). Hippocampal synaptic plasticity: role in spatial learning or the automatic recording of attended experience? Philos. Trans. R. Soc. Lond. B Biol. Sci. *352*, 1489–1503.

Moser, E.I., and Paulsen, O. (2001). New excitement in cognitive space: between place cells and spatial memory. Curr. Opin. Neurobiol. *11*, 745–751.

Nakazawa, K., Quirk, M.C., Chitwood, R.A., Watanabe, M., Yeckel, M.F., Sun, L.D., Kato, A., Carr, C.A., Johnston, D., Wilson, M.A., et al. (2002). Requirement for hippocampal CA3 NMDA receptors in associative memory recall. Science *297*, 211–218.

Nakazawa, K., Wilson, M.A., and Tonegawa, S. (2003). On crucial roles of hippocampal NMDA receptors in acquisition and recall of associative memory. In Neurobiology of Perception and Communication, L. Squire, ed. (Cambridge, UK: Cambridge University Press), in press.

O'Keefe, J., and Nadel, L. (1978). The Hippocampus as a Cognitive Map (Oxford, UK: Oxford University Press).

Panakhova, E., Buresova, O., and Bures, J. (1984). Persistence of spatial memory in the Morris water tank task. Int. J. Psychophysiol. *2*, 5–10.

Poucet, B., Save, E., and Lenck-Santini, P.-P. (2000). Sensory and memory properties of hippocampal place cells. Rev. Neurosci. *11*, 95–111.

Quirk, G.J., Muller, R.U., Kubie, J.L., and Ranck, J.B., Jr. (1992). The positional firing properties of medial entorhinal neurons: description and comparison with hippocampal place cells. J. Neurosci. *12*, 1945–1963.

Remondes, M., and Schuman, E.M. (2002). Direct cortical input modulates plasticity and spiking in CA1 pyramidal neurons. Nature *416*, 736–740.

Rempel-Clower, N.L., Zola, S.M., Squire, L.R., and Amaral, D.G. (1996). Three cases of enduring memory impairment after bilateral damage limited to the hippocampal formation. J. Neurosci. *16*, 5233–5255.

Sokolov, E.N. (1963). Perception and the Conditioned Reflex (London, UK: Pergamon).

Steele, R.J., and Morris, R.G.M. (1999). Delay-dependent impairment of a matching-to-place task with chronic and intrahippocampal infusion of the NMDA-antagonist D-AP5. Hippocampus *9*, 118–136.

Sybirska, E., Davachi, L., and Goldman-Rakic, P.S. (2000). Prominence of direct entorhinal-CA1 pathway activation in sensorimotor and cognitive tasks revealed by 2-DG functional mapping in nonhuman primate. J. Neurosci. *20*, 5827–5834.

Tulving, E. (1972). Episodic memory and semantic memory. In Organization of Memory, E. Tulving and W. Donaldson, eds. (New York: Academic Press), pp. 381–403.

Tulving, E. (2002). Episodic memory: from mind to brain. Annu. Rev. Psychol. *53*, 1–25.

Vinogradova, O. (1970). Registration of information and the limbic system. In Short-term Changes in Neural Activity and Behavior, G. Horn and R.A. Hinde, eds. (Cambridge, UK: Cambridge Univ. Press), pp. 95–140.

Vinogradova, O.S. (1975). Functional organization of the limbic system in the process of registration of information: facts and hypothesis. In The Hippocampus, Volume 2: Neurophysiology and Behavior, R.L. Isaacson and K.H. Pribram, eds. (New York and London: Plenum Press), pp.3–69.

Whishaw, I.Q. (1985). Formation of a place learning-set by the rat: a new paradigm for neurobehavioral studies. Physiol. Behav. *35*, 139–143.

Williams, S., and Johnston, D. (1988). Muscarinic depression of long-term potentiation in CA3 hippocampal neurons. Science *242*, 84–87.

Wilson, M.A., and McNaughton, B.L. (1993). Dynamics of the hippocampal ensemble code for space. Science *261*, 1055–1058.

Wilson, M.A., and McNaughton, B.L. (1994). Reactivation of hippocampal ensemble memories during sleep. Science *265*, 676–679.

Xavier, G.F., Oliveira-Filho, F.J.B., and Santos, A.M.G. (1999). Dentate gyrus-selective colchicine lesion and disruption of performance in spatial tasks: difficulties in "place strategy" because of a lack of flexibility in the use of environmental cues? Hippocampus *9*, 668–681.

Zalutsky, R.A., and Nicoll, R.A. (1990). Comparison of two forms of long-term potentiation in single hippocampal neurons. Science *248*, 1619–1624.

Zola-Morgan, S., Squire, L.R., and Amaral, D.G. (1986). Human amnesia and the medial temporal region: enduring memory impairment following a bilateral lesion limited to field CA1 of the hippocampus. J. Neurosci. *6*, 2950–2967.

Appendix B: Collaborative Contributions to "Requirement for hippocampal CA3 NMDA receptors in associative memory recall."

Nakazawa, K., Quirk, M. C., Chitwood, R. A., Watanabe, M., Yeckel, M. F., Sun, L. D., Kato, A., Carr, C. A., Johnston, D., Wilson, M. A., and Tonegawa, S. (2002). Science *297*, 211-218.

Abstract:

Pattern completion, the ability to retrieve complete memories on the basis of incomplete sets of cues, is a crucial function of biological memory systems. The extensive recurrent connectivity of the CA3 area of hippocampus has led to suggestions that it might provide this function. We have tested this hypothesis by generating and analyzing a genetically engineered mouse strain in which the N-methyl-D-aspartate (NMDA) receptor gene is ablated specifically in the CA3 pyramidal cells of adult mice. The mutant mice normally acquired and retrieved spatial reference memory in the Morris water maze, but they were impaired in retrieving this memory when presented with a fraction of the original cues. Similarly, hippocampal CA1 pyramidal cells in mutant mice displayed normal place-related activity in a full-cue environment but showed a reduction in activity upon partial cue removal. These results provide direct evidence for CA3 NMDA receptor involvement in associative memory recall.

My Contribution:

The conclusion of this paper required detailed behavioral analysis of mutant and control mouse behavioral in the Morris Watermaze as summarized in Figure 5. Utilizing my own

custom software written for MATLAB, I thoroughly analyzed all of the mouse behavioral data collected in this study and provided critical analysis which wasn't previously available by other Morris Watermaze studies. I showed that the mutants acquired the standard reference memory task equivalently to control animals (Figure 5A-E). However when the mice were reintroduced during the probe trial to a reduced environment I showed that the mutants had much lower platform occupancy than control mice. Platform occupancy had not been used before as a measure for spatial learning and memory. This subtle effect was further emphasized by occupancy histogram plots I generated (Figure 5H).

Requirement for Hippocampal CA3 NMDA Receptors in Associative Memory Recall

Kazu Nakazawa,[1,2,3] Michael C. Quirk,[1,3]* Raymond A. Chitwood,[4] Masahiko Watanabe,[5] Mark F. Yeckel,[4]† Linus D. Sun,[1,3] Akira Kato,[1,2,3]‡ Candice A. Carr,[1,2,3] Daniel Johnston,[4] Matthew A. Wilson,[1,3] Susumu Tonegawa[1,2,3]§

Pattern completion, the ability to retrieve complete memories on the basis of incomplete sets of cues, is a crucial function of biological memory systems. The extensive recurrent connectivity of the CA3 area of hippocampus has led to suggestions that it might provide this function. We have tested this hypothesis by generating and analyzing a genetically engineered mouse strain in which the *N*-methyl-D-asparate (NMDA) receptor gene is ablated specifically in the CA3 pyramidal cells of adult mice. The mutant mice normally acquired and retrieved spatial reference memory in the Morris water maze, but they were impaired in retrieving this memory when presented with a fraction of the original cues. Similarly, hippocampal CA1 pyramidal cells in mutant mice displayed normal place-related activity in a full-cue environment but showed a reduction in activity upon partial cue removal. These results provide direct evidence for CA3 NMDA receptor involvement in associative memory recall.

In both humans and animals, the hippocampus is crucial for certain forms of learning and memory (*1, 2*). Anatomically, the hippocampus can be divided into several major areas: the dentate gyrus, CA3, and CA1 (*3*). In area CA3, the pyramidal cells, which project to CA1 pyramidal cells via Schäffer collaterals, receive excitatory inputs from three sources: the mossy fibers of the dentate gyrus granule cells, the perforant path axons of the stellate cells in the superficial layers of the entorhinal cortex, and the recurrent collaterals of the CA3 pyramidal cells themselves, which are the most numerous type of input to the CA3 pyramidal cells (*4*). The prominence of these recurrent collaterals has led to suggestions that CA3 might serve as an associative memory network. Associative networks, in which memories are stored through modification of synaptic strength within the network, are capable of retrieving entire memory patterns from partial or degraded inputs, a property known as pattern completion (*5–10*). In CA3, the strength of the recurrent collateral synapses along with perforant path synapses can be modified in an NMDA receptor (NR)–dependent manner (*11–14*). In this study, we have examined the role of these synapses in memory storage, retrieval, and pattern completion by generating and analyzing a mouse strain in which the NMDAR subunit 1 (NR1) is specifically and exclusively deleted in the CA3 pyramidal cells of adult mice.

CA3 NMDA receptor knockout mice. To generate CA3 pyramidal cell–specific NR1 knockout mice (CA3-NR1 KO mice), we used the bacteriophage P1–derived Cre/*loxP* recombination system (*15*). Because the CA3 pyramidal cell layer is a robust site of expression of KA-1, one of the kainate receptor subunits (*16*), we created transgenic mice in which the transcriptional regulatory region of the KA-1 gene drives the expression of the Cre transgene (*17*). In one transgenic line (G32-4), the level of Cre immunoreactivity (IR) was robust in the CA3 pyramidal cell layer in mice older than 4 weeks of age (*17*) (Fig. 1A). The spatial and temporal pattern of Cre/*loxP* recombination in the G32-4 Cre transgenic mouse line was examined by crossing it with a *lacZ* reporter mouse (Rosa26) and staining brain sections derived from the progeny with X-gal (*17*) (Fig. 1, B to D). Cre/*loxP* recombination was first detectable at postnatal day 14 in area CA3 of the hippocampus. At 8 weeks of age, recombination had occurred in nearly 100% of pyramidal cells in area CA3 (Fig. 1C). Recombination also occurred in a few other brain areas, but at distinctly lower frequencies: in about 10% of dentate gyrus (Fig. 1C) and cerebellar granule cells (Fig. 1D) and in about

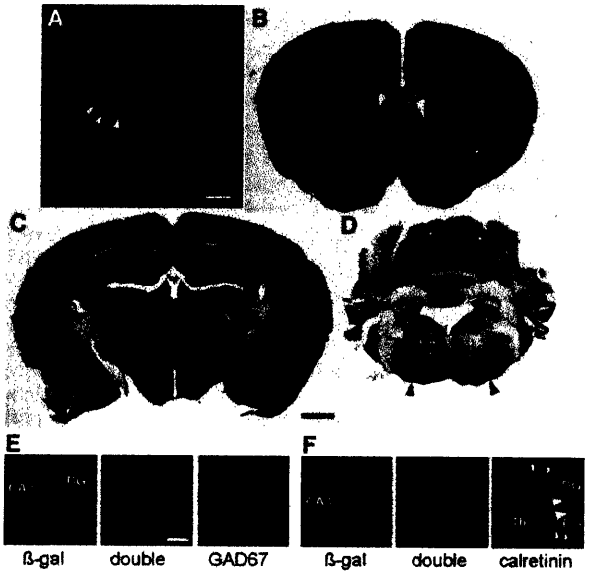

Fig. 1. Distribution of Cre immunoreactivity and Cre/*loxP* recombination in G32-4 mice. (**A**) A parasagittal Vibratome section from the brain of a 4-week-old male G32-4 mouse was stained with a rabbit antibody against Cre, and Cre IR was visualized with fluorescein isothiocyanate. Arrowheads, CA3 pyramidal cell layer. Scale bar, 50 μm. (**B** to **D**) Coronal sections from the brain of an 8-week-old male G32-4/Rosa26 double-transgenic mouse stained with X-gal and Nuclear Fast Red. In forebrain (B and C), arrow, CA3 cell layer; arrowhead, dentate granule cell layer. In hindbrain (D), arrowheads, facial nerve nuclei. Scale bar, 100 μm. (**E** and **F**) Parasagittal hippocampal sections from the brain of an 8-week-old G32-4/Rosa26 double-transgenic mouse subjected to double immunofluorescence staining with (E) antibodies against β-galactosidase (visualized by Alexa488) and GAD67 (visualized by Cy3), or (F) with antibodies against β-galactosidase and calretinin (visualized by Cy3). Green, β-galactosidase IR; red in (E) GAD67-IR; red in (F), calretinin-IR. DG, dentate gyrus; Th, thalamus; white arrows, somata of mossy cells; white arrowheads, axon terminals of mossy cells. Scale bar, 10 μm.

[1]Picower Center for Learning and Memory, RIKEN-MIT Neuroscience Research Center, [2]Howard Hughes Medical Institute, and [3]Department of Biology and Department of Brain and Cognitive Sciences, Massachusetts Institute of Technology, Cambridge, MA 02139, USA. [4]Division of Neuroscience, Baylor College of Medicine, Houston, TX 77030, USA. [5]Department of Anatomy, Hokkaido University School of Medicine, Sapporo 060-8638, Japan.

*Present address: Cold Spring Harbor Laboratories, Cold Spring Harbor, NY 11724, USA.
†Present address: Department of Neurobiology, Yale University School of Medicine, New Haven, CT 06520–8001, USA.
‡Present address: Shionogi Research Laboratories, Shionogi & Co., Ltd., Koka-gun, Shiga 520-3423, Japan.
§To whom correspondence should be addressed. E-mail: tonegawa@mit.edu

50% of cells in the facial nerve nuclei of the brain stem (Fig. 1D). Recombination frequency did not change in older mice. No recombination was detected in the cerebral cortex or in the hippocampal CA1 and subicular regions (Fig. 1, B to D). We determined the type of the recombination-positive cells in the hippocampus with double immunofluorescence staining using a set of antibodies specific for β-galactosidase (a marker for the Cre/*loxP* recombination), glutamic acid decarboxylase (GAD)-67 (a marker for interneurons), and calretinin (a marker for dentate gyrus mossy cells in the mouse hippocampus) (*17*, *18*). Minimal overlapping staining was observed with antibodies against β-galactosidase and GAD67 (Fig. 1E) and with antibodies against β-galactosidase and calretinin (Fig. 1F). These results indicate that in area CA3 and the dentate gyrus, Cre/*loxP* recombination is restricted to the pyramidal cells and the granule cells, respectively.

We crossed the G32-4 mice with floxed-NR1 (*fNR1*) mice (*15*, *17*) in order to restrict the NR1 knockout to those cell types targeted by the G32-4 Cre transgene. Floxed refers to a genetic allele in which a gene or gene segment is flanked by *loxP* sites in the same orientation; Cre recombinase excises the segment between the *loxP* sites. Homozygous floxed, Cre-positive progeny (CA3-NR1 KO) were viable and fertile, and they exhibited no gross developmental abnormalities. In situ hybridization data (*17*) suggested that in the CA3 pyramidal cell layer of these mice, the NR1 gene is intact until about 5 weeks of age, starts being deleted thereafter, and is nearly completely deleted by 18 weeks (white arrowheads in Fig. 2D) of age (Fig. 2, A to D). There was no indication of deletion of the NR1 gene elsewhere in the brain throughout the animal's life. Specifically, the NR1 gene seemed to be intact in granule cells of the dentate gyrus (Fig. 2, E and F) and the cerebellum (Fig. 2, A to D), as well as in the facial nerve nuclei (Fig. 2, G and H). These results are in contrast to the Cre/*loxP* recombination–dependent expression of the *lacZ* gene (see Fig. 1, C and D), likely due in part to differences in the sensitivity of detection of the Cre/*loxP* recombination and in part to differences in the susceptibility of the *loxP* substrates to the recombinase.

Performing NR1-immunocytochemistry with an antibody against the COOH-terminus of mouse NR1 (*17*) confirmed that the selective and late-onset deletion of the NR1 gene in the CA3 region of the mutant mice resulted in loss of the protein. The protein distribution was normal for the first 7 weeks after birth. By the 18th postnatal week, however, NR1 protein had disappeared from both the apical and basal dendritic areas in the CA3 region (Fig. 2, I to L). In contrast, normal levels of NR1 protein were maintained in the CA1 region and the dentate gyrus of the 18-week-old mutant mice. The reduction of NR1 protein in the CA3 region was observed in both dorsal and ventral hippocampus (Fig. 2, K and L), suggesting that the NR1 gene is deleted uniformly along the longitudinal axis of the hippocampus.

We carried out a set of immunocytochemical and cytochemical experiments to investigate the integrity of the cytoarchitecture of the mutant hippocampus (*17*). No significant differences could be detected in the patterns of postsynaptic density-95 (PSD-95) (*19*) or GluR1 [α-amino-3-hydroxy-5-methyl-4-isoxazol propionate (AMPA)-type glutamate receptor subunit 1] expression (Fig. 2, M and N). Also normal was the IR distribution of calbindin$_{D28k}$, a Ca^{2+}-binding protein expressed at high levels in dentate gyrus granule cells but not in cells in the CA3 region, suggesting that mossy fibers from dentate gyrus granule cells project normally to their target in the CA3 region (the stratum lucidum) (*19*). Nissl staining did not reveal any obvious abnormalities (Fig. 2, O and P). We also used the Golgi-impregnation technique to assess dendritic structures and found no significant differences between the mutant and the *fNR1* control mice (24 weeks of age) with respect to the dendritic length, the number of dendritic branching points, or the spine density of CA3 pyramidal cells (*20*).

Thus, in the mutant mice, the NR1 gene is

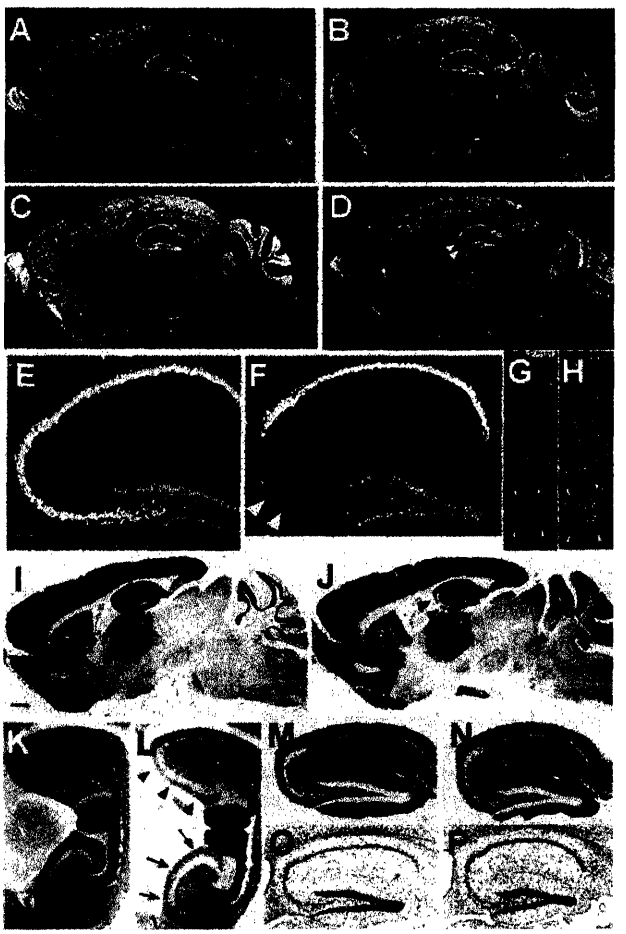

Fig. 2. Distributions of NR1 mRNA, NR1 protein, and other proteins in brains of CA3-NR1 KO mice. (**A** to **H**) Dark field images of in situ hybridization on parasagittal brain sections with a ^{33}P-labeled NR1 cRNA probe. The sources of the brains were (A) a 5-week-old male *fNR1* control; (B) a 5-week-old male mutant [a littermate of the mouse in (A)]; (C, E, and G) an 18-week-old male *fNR1* control; (D, F, and H) an 18-week-old male mutant [a littermate of the mouse in (C), (E), and (G)]. Scale bar, 100 μm. (E and F) The hippocampal regions of (C) and (D), respectively, are enlarged. (G and H) The areas of the facial nerve nuclei are enlarged. In the CA3 pyramidal cell layer of the mutant, the level of NR1 mRNA was normal until 5 weeks of age, started to decline thereafter, and reached the lowest and stable level by 18 weeks of age [arrowheads in (D)]. There was no indication of a reduced NR1 mRNA level in the mutant mice relative to the control littermates in any other brain area throughout the postnatal development. In particular, the levels of NR1 mRNA in the mutants' dentate gyrus (F), cerebellum (B and D), and the facial nerve nuclei (H) are indistinguishable from those of the control littermates (A, C, E, and G). (F) Arrowheads indicate scattered hybridization signals that are likely derived from CA3 interneurons. (G and H) Arrowheads, the facial nerve nuclei. In (E) to (H), scale bar, 25 μm. (**I** to **N**) Immunoperoxidase staining of paraffin sections of brains derived from 18-week-old male mice visualized with 3,3'-diaminobenzidine. The primary antibodies used are specific for NR1 (I to L) and for GluR1 (M and N). The genotypes of the mice are *fNR1* (control) (I, K, M), and CA3-NR1 KO (mutant) (J, L, N). Medial parasagittal sections were used for experiments other than those in (K) and (L), for which lateral parasagittal sections were used. In the mutants, NR1-IR was selectively deficient in the dorsal [arrowheads in (J) and (L)], as well as ventral [arrows in (L)] area CA3. Scale bar in (I), 100 μm. (K to P) See scale bar in (K), 50 μm. (**O** and **P**) Nissl staining of hippocampal sections derived from an 18-week-old male *fNR1* mouse (O) and a male CA3-NR1 KO littermate (P). The mutant exhibited no gross morphological alteration.

selectively deleted in the CA3 pyramidal cells of the hippocampus. This deletion occurs only in adult mice (older than 5 weeks of age) and does not affect the hippocampal cytoarchitecture.

NMDA receptor activation. To evaluate whether functional NRs are present in CA3 pyramidal cells in CA3-NR1 KO mice, whole-cell patch-clamp recordings were performed on visually identified cells in freshly prepared hippocampal slices obtained from adult *fNR1* control and mutant mice (*17*). We compared the basic intrinsic properties and synaptically evoked responses of CA3 and CA1 pyramidal cells. In all but two experiments, the experimenters were blind to whether the animals were control or mutant mice. There were no differences in the intrinsic properties of CA3 pyramidal cells in control (n = 14) or mutant mice (n = 23) [resting membrane potential (*RMP*): control, −67.0 ± 2.0 mV; mutant, −67.8 ± 1.6 mV; input resistance (R_N): control, 200.8 ± 17.9 MΩ; mutant, 183 ± 12.6 MΩ]. Similarly, *RMP* and R_N did not differ for CA1 pyramidal cells in control and mutant mice (*RMP*: control, n = 7, −62.3 ± 1.4 mV; mutant, n = 12, −62.3 ± 0.7 mV; R_N: control, 189.8 ± 30.0 MΩ; mutant, 171.1 ± 10.8 MΩ).

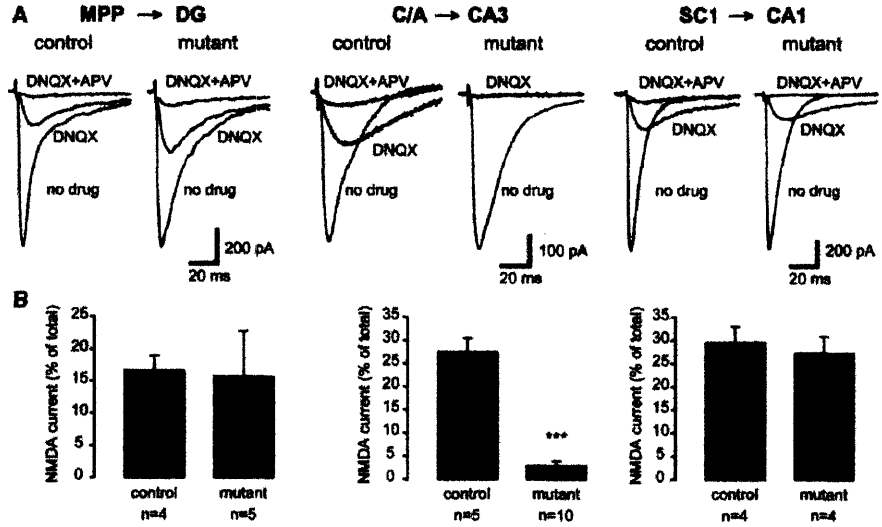

Fig. 3. NMDAR function is absent only in the C/A-CA3 pathway of CA3-NR1 KO mice. (**A**) Synaptic responses were evoked and NMDA currents pharmacologically isolated. Details in the Materials and Methods section (*17*). (Left) Representative data from a control (*fNR1*) dentate gyrus granule cell (DG) showing a medial perforant path evoked NMDA current (isolated with DNQX and blocked by APV). (Middle) C/A-evoked NMDA current. (Right) In a CA1 pyramidal cell, SC stimulation-elicited NR-mediated excitatory postsynaptic current. (**B**) Summary data for NMDA currents in *fNR1* and mutant animals (***$P < 0.0001$).

We next isolated synaptically evoked NMDA currents (*17*) (Fig. 3). At the medial perforant path (MPP)–dentate gyrus (DG) synapse, there were no differences in the 6-cyano-7-dinitroquinoxalline-2,3-dione (DNQX)-insensitive component of the total synaptic current (control, 15.8 ± 7%, n = 5; mutant, 16.7 ± 2.3%, n = 4; P = 0.96; Fig. 3B). A similar relationship was observed at the Schäffer collateral (SC)-CA1 synapse (control, 26.7 ± 6%, n = 4; mutant, 29.3 ± 4%, n = 4; P = 0.78) (Fig. 3B). However, consistent with the immunohistochemical characterization of an absence of NR1 in CA3-NR1 KO mice, the DNQX-insensitive component was significantly reduced at the recurrent commissural/associational (C/A) synapse in the mutant animals relative to controls (control, 27.5 ± 3%, n = 10; mutant, 3.0 ± 1%, n = 5; $P < 0.0001$) (Fig. 3B).

We also tested the prediction that long-term potentiation (LTP) would be impaired at C/A–CA3 synapses in CA3-NR1 KO mice (Fig. 4). At the mossy fiber–CA3 synapse (MF-CA3), in which LTP does not depend on NR activation (*11–14*), there was no significant difference in

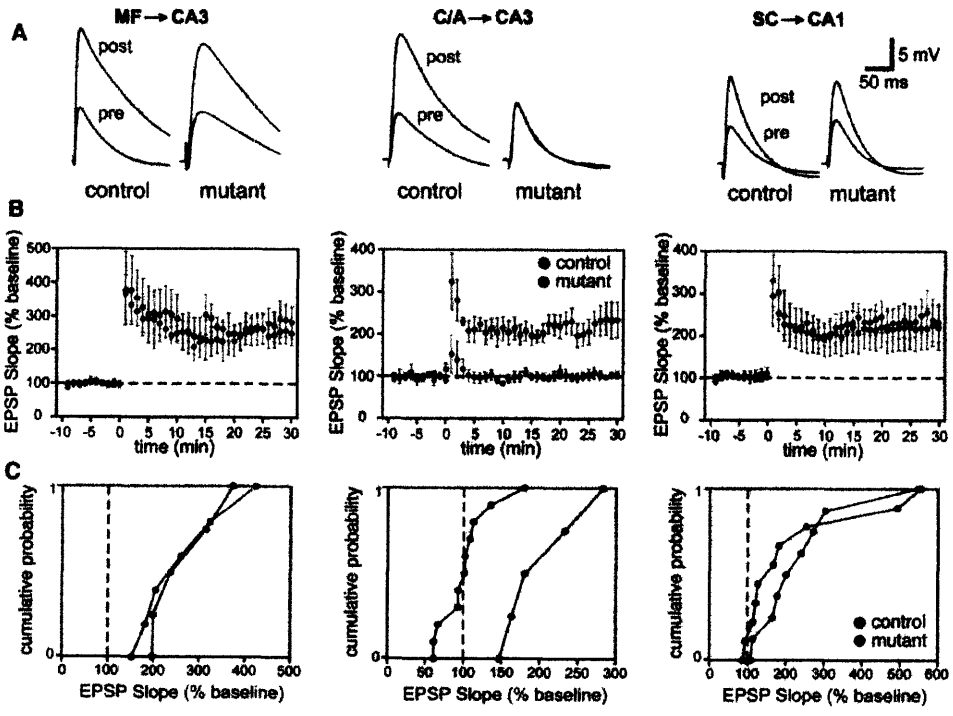

Fig. 4. NMDA-dependent LTP at the recurrent CA3 synapses in CA3-NR1 KO mice. (**A**) Representative waveforms (averages of five consecutive responses recorded at 0.05 Hz) show that C/A-CA3 LTP was selectively prevented in mutant animals. (**B**) Summary graphs showing the time course of potentiation after three long trains of stimulation (100 pulses at 100 Hz concomitant with a 1-s depolarizing pulse 1 train every 20 s). (**C**) Cumulative probability plots; each point represents the magnitude of change relative to baseline (abscissa) as a cumulative fraction of the total number of experiments (ordinate) for a given experiment 20 to 25 min (average) after high-frequency stimulation. EPSP, excitatory postsynaptic potential.

the induction or expression of LTP between control and mutant mice (control, 265 ± 39%, $n = 5$; mutant, 259 ± 45%, $n = 6$). Additionally at the SC-CA1 synapse, where NRs were intact, LTP was similar in both groups of animals (control, 232 ± 37%, $n = 9$; mutant, 219 ± 53%, $n = 10$). Similarly, in control animals, LTP was induced at C/A-CA3 synapses in all the animals examined (202 ± 28%, $n = 5$). In contrast, LTP was nearly absent at C/A-CA3 synapses in 9 out of 11 CA3-NR1 KO mice (101 ± 11%, $n = 11$). In two cases, we observed LTP, which may have been due to calcium influx from voltage-dependent calcium channels. These data provide functional evidence that NR1 knockout in CA3 pyramidal cells selectively disrupts NR-dependent LTP in CA3 at the recurrent C/A synaptic input, but not NR-independent mossy fiber LTP in CA3 or NR-dependent LTP in area CA1.

Spatial reference memory. We subjected the CA3-NR1 KO mice and their control littermates to the hidden platform version of the Morris water maze task (*17*, *21*) to assess the effect of the selective ablation of NRs in CA3 pyramidal cells on the animals' ability to form a spatial reference memory. No significant differences were observed between the control and mutant mice in the escape latency, path length, average swimming velocity, or wall-hugging time (Fig. 5, A to D). We subjected the mutant, *fNR1*, Cre, and wild-type littermates to a probe trial on day 2 (*P1*), day 7 (*P2*), and day 13 (*P3*), and assessed spatial memory by monitoring the relative radial-quadrant occupancy (Fig. 5E). There was no difference in the acquisition rate of spatial learning among the four genotypes. By day 13 (*P3*), all four mouse strains spent significantly more time in the target radial-quadrant than in any of the nontarget quadrants. This result for three types of mice

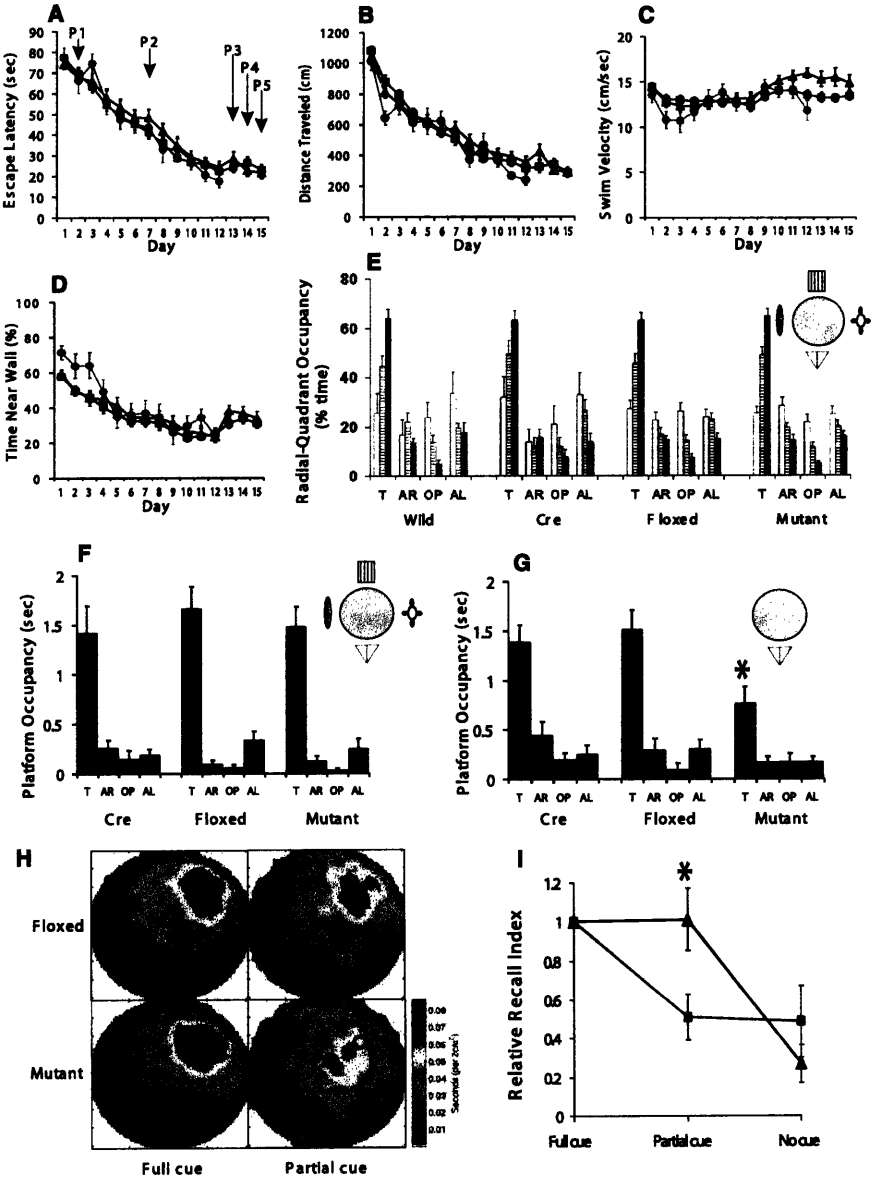

Fig. 5. Performance of CA3-NR1 KO mice in the standard Morris water maze task and recall capability under various cue conditions. (**A** to **D**) 18- to 24-week-old male CA3-NR1 KO mice (mutant, red, $n = 44$), *fNR1* (blue, $n = 37$), Cre ($n = 14$, not shown), and their wild-type littermates (green, $n = 11$) were subjected to training trials under full-cue conditions. The four types of mice did not differ significantly in (A) escape latency, (B) distance traveled, (C) swimming velocity, or (D) time spent near the pool wall [genotype effect for each measure, $F(3,102) < 2.5$, $P > 0.05$; genotype x trial interaction for each measure, $P > 0.05$]. (**E**) Probe trials on day 2 (*P1*, open bars), day 7 (*P2*, hatched bars), and day 13 (*P3*, solid bars) under full-cue conditions, monitored by relative radial-quadrant occupancy [time (%) the mice spent in the target radial-quadrant relative to the total time spent in the four radial-quadrants]. On day 13, all the genotypes spent significantly more time in the target radial-quadrant than other quadrants [wild, $F(3,40) = 84.1$, $P < 0.0001$; Cre, $F(3,52) = 52.7$, $P < 0.0001$; *fNR1*, $F(3,144) = 130.4$, $P < 0.0001$; mutant, $F(3,172) = 163.4$, $P < 0.0001$; Newman-Keuls post hoc comparison (the trained quadrant compared to all the other quadrants); $P < 0.01$ for all genotypes]. (**F**) Day 13 probe trial (*P3*) of randomly selected subsets of Cre ($n = 14$), *fNR1* ($n = 20$) and mutant ($n = 23$) mice by absolute platform occupancy [time (sec) the mice spent in the area which corresponded exactly to the area occupied by the platform during the training session] [Cre, $F(3,52) = 15.8$, $P < 0.0001$; *fNR1*, $F(3,76) = 37.4$, $P < 0.0001$; mutant, $F(3,88) = 35.5$, $P < 0.0001$; Newman-Keuls post hoc comparison (the target platform position compared to all the other platform positions); $P < 0.01$ for all genotypes]. (**G**) The same sets of mice as in (F) were subjected to partial-cue probe trials on day 14 (*P4*) and absolute platform occupancy assessed. Cre and fNR1 mice exhibited similar recall under partial-cue conditions as under full-cue conditions (paired t test, $P > 0.9$ for each genotype), while recall by the mutant mice was impaired (paired t test, $^*P < 0.01$). (**H**) Spatial histograms of the animals' location during the full-cue (*P3*) and partial-cue (*P4*) probe trials. *fNR1*, $n = 20$; mutant, $n = 23$. (**I**) Relative recall index [RRI, averaged ratio of the target platform occupancy of the partial-cue (*P4*) or no-cue (*P5*) probe trial to that of the full-cue (*P3*) probe trial for each animal (*17*)] of *fNR1* mice ($n = 18$, blue) and mutant mice ($n = 22$, red). The RRI value difference between the *fNR1* and the mutant mice under the partial-cue conditions was significant ($^*P < 0.009$; Mann-Whitney U test), while that under no-cue conditions was not ($P = 0.9$; Mann-Whitney U test). T, target quadrant; AR, adjacent right quadrant; OP, opposite quadrant; AL, adjacent left quadrant.

was also shown by the criterion of absolute platform occupancy (Fig. 5F). Thus, the selective ablation of NRs in adult hippocampal CA3 pyramidal cells has no detectable effect on the animal's ability to form and retrieve spatial memory as determined by the standard hidden platform version of the Morris water maze task. Further, the CA3-NR1 KO mice are not impaired in motivation, motor coordination, or the sensory functions required to carry out this spatial memory task.

Partial cue removal. In order to assess the role of CA3 NRs in pattern completion at the behavioral level, we examined the dependence of spatial memory recall on the integrity of distal cues in the CA3-NR1 KO mice and their control littermates (*17*). We first subjected randomly selected subsets of the mice that had gone through the training and probe trial sessions to one more block (4 trials) of training 1 hour after the day 13 probe trial (*P3*) in order to counteract any extinction that may have occurred during the probe trial. On day 14, we subjected these animals to a fourth probe trial (*P4*) in the same water maze except that three out of the four extramaze cues had been removed from the surrounding wall. In the partial-cue probe trial, both the *fNR1* control and Cre control mice searched the phantom platform location as much as they did in the full-cue probe trial. In contrast, the search preference of the mutant mice for the phantom platform location was significantly reduced by the partial cue removal (Fig. 5, F and G).

We also monitored the effect of the partial cue removal by the criterion of relative radial-quadrant occupancy. The target radial-quadrant occupancy of the Cre, *fNR1*, and mutant mice were 63.0 ± 4%, 65.9 ± 4%, and 66.4 ± 4% under the full cue conditions (*P3*), respectively, and 55.8 ± 5%, 58.8 ± 5%, and 44.6 ± 5% under the partial-cue conditions (*P4*), respectively. The effect of the partial cue removal was significant for mutant (paired t test, $P < 0.002$) but not for Cre ($P > 0.2$) or *fNR1* mice ($P > 0.2$).

The differential effect of partial cue removal on search behaviors of *fNR1* control and mutant mice was also indicated by a difference in the distribution of the animal's occupancy of locations during the probe trials (Fig. 5H): In the full-cue environment (*P3*), both mutant and *fNR1* control mice focused their search at or near the location of the phantom platform, as did the *fNR1* mice searching for the platform in the partial-cue environment. By contrast, the mutant mice spent the majority of the time at or near the release site at the center of the pool and significantly less time at or near the location of the phantom platform in the partial-cue environment (*P4*).

For each individual mouse, we also determined the occupancy time at the phantom platform location in the partial-cue probe trial and compared that with the phantom platform occupancy time in the earlier full-cue probe trial, yielding a "relative recall index (RRI)" measure (*17*). There was no effect of partial cue removal on this parameter in the *fNR1* control mice, whereas the effect was highly significant for the mutant mice (Fig. 5I).

It is possible that the mutant mice performed poorly in the partial-cue probe trial because they had lost the spatial memory faster than the control mice. To test this possibility, we restored the full-cue training environment by returning the three missing cues and the platform, then subjected the same set of animals that had gone through the training and probe trials to one more block (four trials) of training on day 14, 1 hour after the *P4* partial-cue probe trial. Both the mutant and *fNR1* control animals found the platform as fast as they did on day 12 and day 13, and there was no significant difference between the latencies of the mutant and control animals ($P = 0.32$) (Fig. 5A). There were also no significant differences between mutant and control mice in the total path length traveled and in their thigmotaxic tendency to remain close the walls of the maze ($P > 0.4$ for both measures) (Fig. 5, B and D). These results indicated that the reason why the mutant mice performed poorly in the partial-cue probe trial was not faster memory loss. The results also confirmed that both the mutant and control animals had reached the asymptotic level of learning by day 12.

To test whether the recall in the partial-cue environment depended on the remaining spatial cue, we carried out a fifth no-cue probe trial (*P5*) on day 15 after removal of all of the extramaze cues. We found robust recall deficits in *fNR1* control and mutant mice under these conditions (Fig. 5I). Both types of mice must have retained the memory of the platform location during this no-cue probe trial, because they reached the platform efficiently in a final block of training in the full-cue environment 1 hour after *P5* (Fig. 5, A to D, at day 15) ($P > 0.15$ for any of four measures).

We also tested whether the mutants' deficit in the partial-cue probe trial was due to impairment in perceiving the platform-distal cue. When mutants and *fNR1* littermates were trained and probed with only one platform-distal cue, the mutants acquired the spatial memory, as well as the controls [mutant, $F(3,36) = 5.5$, $P < 0.005$; *fNR1*, $F(3,36) = 17.7$, $P < 0.005$; Newman-Keuls post hoc comparison (the trained radial-quadrant compared to all the other quadrants); $P < 0.05$ for both genotypes]. These results indicate that mutants are not defective in perceiving the platform-distal cue.

In summary, under the full-cue conditions both mutant and control mice exhibited robust memory recall. When three out of the four major extramaze cues were removed, control mice still exhibited the same level of recall, whereas the mutants' recall capability was severely impaired.

Spatial coding in CA1. To investigate the neural mechanisms that might underlie this deficit in memory recall, we examined the neurophysiological consequences of CA3-NR1 disruption by analyzing CA1 place cell activity with in vivo tetrode recording techniques (*17*). Although genetic deletion was confined to CA3 pyramidal cells, place cell recordings were made from CA1 for two reasons. First, CA1 is the final output region of the hippocampus proper and, as a consequence, CA1 activity is more likely to reflect behavioral performance than CA3 activity. Second, most previous relevant electrophysiological tetrode recording studies have been performed in CA1 (*22, 23*), so CA1 recordings are most suited for comparison with published findings of place cell activity in other genetically altered mice (*24*).

We recorded from 188 complex spiking (pyramidal) cells and nine putative interneurons from five mutant mice (24 sessions) and from 155 pyramidal cells and 8 interneurons

Table 1. Properties of CA1 pyramidal cells and interneurons in familiar open field. Values are means ± SEM. For pyramidal from *fNR1* controls cells in 19 recording sessions with three animals, n (cells) = 155; for mutant pyramidal cells in 24 recording session with five animals, n = 188; for *fNR1* interneurons in 19 recording sessions with three animals, n = 8; for mutant interneurons in 24 recording sessions with five animals, n = 9. NA, not applicable.

Measurement	Pyramidal cells		Interneurons	
	fNR1	Mutant	*fNR1*	Mutant
Mean firing rate (Hz)	1.175 ± 0.097	1.179 ± 0.082	30.96 ± 5.27	12.62 ± 1.73*
Spike width ($_{\mu}$s)	328.5 ± 4.31	326.8 ± 3.70	186.6 ± 9.7	167.2 ± 4.8
Spike attenuation (%)	90.44 ± 0.56	90.45 ± 0.40	NA	NA
Complex spike index	24.26 ± 1.21	16.84 ± 0.83†	1.66 ± 0.52	1.67 ± 0.39
Burst spike frequency (%)	52.93 ± 1.17	42.18 ± 1.28†	NA	NA
Integrated firing rate [Σ(Hz/pixel)]	549.5 ± 48.2	544.7 ± 40.0	NA	NA
Place field size (no. of pixels)	125.6 ± 8.28	133.1 ± 7.27	NA	NA
Covariance coefficient	0.0359 ± 0.007	0.0410 ± 0.005	NA	NA

*Significantly different from *fNR1* control (t test, $P < 0.003$). †Significantly different from *fNR1* control (t test, $P < 10^{-4}$).

from three *fNR1* control mice (19 sessions) while the mice were engaged in open-field foraging (*25*). Although an analysis of the basic cellular properties of CA1 pyramidal cells revealed no difference in mean firing rate, spike width, or spike amplitude attenuation within bursts (*26*), pyramidal cells from mutant animals showed a significant decrease in complex spike bursting properties (complex spike index and burst spike frequency) (Table 1). This reduction may reflect a decrease in excitatory input from CA3 (*27, 28*) where NR1 is ablated. If so, the reduced CA3 input would also alter the coding properties of CA1 place cells in mutant animals. However, under full-cue conditions, we found no significant differences between *fNR1* control and mutant animals in either place field size (number of pixels above a 1 Hz threshold) or average firing rate within a cell's place field (integrated firing) (Table 1). Furthermore, the ability of cells with overlapping place fields to fire in a coordinated manner did not differ between *fNR1* and mutant mice (covariance coefficient) (Table 1), in contrast with CA1-NR1 KO mice in which there was a complete lack of coordinated firing (*24*). Thus, spatial information within CA1 is relatively preserved despite the loss of CA3 NRs, providing a physiological correlate of the intact spatial performance of CA3-NR1 KO mice in the Morris water maze under full-cue conditions.

CA1 pyramidal cells also receive inhibitory input from local interneurons, and CA1 output reflects a balance between excitatory and inhibitory inputs (*29*). The CA3-NR1 KO mice showed a decrease in the firing rate of putative CA1 interneurons (Table 1), which could be due either to a decrease in direct feed-forward input from CA3 onto inhibitory interneurons (*30, 31*) as a consequence of the CA3-NR1 knockout, or to a decrease in local feedback drive from CA1 pyramidal cells onto interneurons (*32*). This reduction in inhibition in mutant mice may compensate for the reduction of excitatory drive from CA3, thereby allowing CA1 pyramidal cells to maintain robust spatial coding. This hypothesis is consistent with previous theoretical (*5*) and experimental (*33*) studies.

CA1 place cells. We next determined whether CA1 output would be maintained after partial cue removal (*34, 35*). Mice were allowed to explore an area for 20 to 30 minutes in the presence of four distal visual cues and then removed to their home cage. After a 2-hour delay, mice were returned to the open field with either the same four cues present (4 to 4 condition), or with three of the four cues removed (4 to 1 condition). Using three *fNR1* control mice, we identified 28 and 26 complex spike cells during five "4 to 4" sessions and five "4 to 1" sessions, respectively. From five mutant mice we were able to isolate 43 and 47 complex spike cells during six "4 to 4" and six "4 to 1" recording sessions, respectively (Fig. 6, A and B)

To quantify relative changes in place field properties of these cells, we calculated, for each cell, a relative change index (RCI) (*17*). Using this index, we measured three properties of CA1 output: burst spike frequency, place field size, and integrated firing rate (Fig. 6, C to E). Despite individual cell variation, on average in *fNR1* mice there was no change in burst spike frequency, field size, or integrated firing rate of cells from the cue removal conditions relative to those from the no-cue removal conditions. Thus, at the population level, the net output from CA1 was maintained for *fNR1* mice under cue removal conditions. In contrast, mutant cells showed significant reductions in burst spike frequency, place field size, and integrated firing rate after cue removal. It is important to note that mutant place cells showed no significant changes when mice were returned to the recording environment in the presence of all four distal cues. Average running velocity in the open field across all conditions was not different in both genotypes (Kruskal-Wallis test, $P = 0.70$). When we examined whether the location of individual place fields shifted across conditions, we found no significant differences between mutant and *fNR1* mice for either cue removal or no-cue removal conditions, suggesting that some reflection of past experience is maintained in the firing of mutant CA1 place cells even under conditions of partial cue removal (Fig. 6F).

These physiological results are compatible with the behavioral results, suggesting that reductions in CA1 output as a consequence of reduced CA3 drive resulting from cue removal may make it more difficult for mutants to retrieve spatial memories. This impairment may underlie the inability of mutants to solve spatial memory tasks, such as the water maze, when only partial distal cues are available.

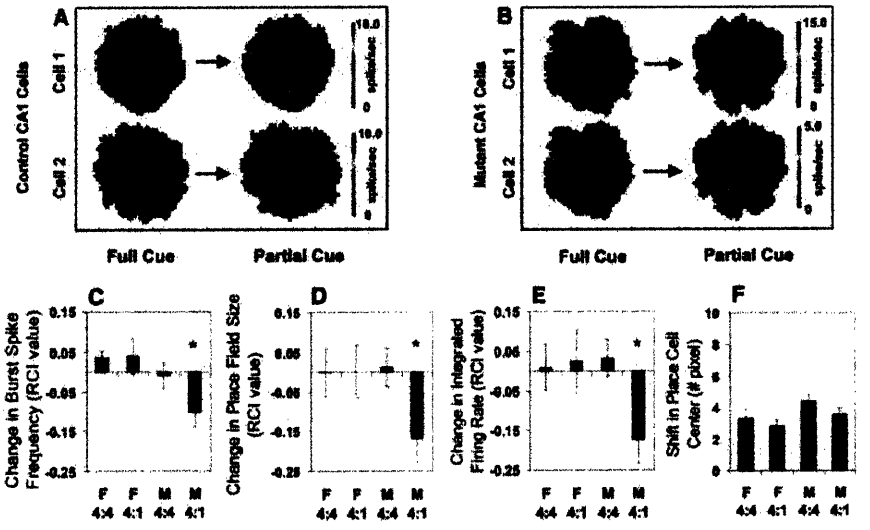

Fig. 6. CA1 place cell activity in CA3-NR1 KO mice. (**A** and **B**) Examples of place fields that are representative of cells that showed no reduction [*fNR1* (A)] and a reduction of field size [mutant (B)] before and after partial cue removal. (**C** to **E**) Relative change in the place field properties for each cell recorded across two conditions quantified with a relative change index (RCI, defined as the difference between the cell's firing between two conditions divided by the sum of the cell's firing across the two conditions) (*17*). Among the cells that were identified as the same cells throughout the two recording sessions, the average burst spike frequency [(C): $F(3,140) = 4.16$, $P < 0.007$; Fisher's post hoc comparison (mutant 4:1 vs. all the other three paradigms), $^*P < 0.05$], place field size over 1 Hz [(D): $F(3,140) = 2.68$, $P < 0.049$; Fisher's post hoc comparison (mutant 4:1 versus all the other three paradigms), $^*P < 0.05$], and the integrated firing rate [(E): $F(3,140) = 3.20$, $P < 0.025$; Fisher's post hoc comparison (mutant 4:1 versus all the other three paradigms), $^*P < 0.05$], were significantly reduced in the mutant animals (red bars) only after partial cue removal (4:1). In contrast, partial cue removal did not affect CA1 place cell activity in the control mice (blue bars). (**F**) Location of CA1 place field center between the two recording sessions was not shifted regardless of genotype and cue manipulation (F): $F(3,140) = 2.15$, $P = 0.097$. F, *fNR1* control mice; M, mutant mice.

Discussion. The formation of hippocampus-dependent memories of events and contexts involves incorporating complex configurations of stimuli into a memory trace that can be later recalled or recognized (*1, 2*). The subregions of the hippocampus likely serve complementary but computationally distinct roles in this process (*3*). For example, NRs in area CA1 are critical for the formation of spatial reference memory and normal CA1 place cells under conditions of fully cued memory retrieval (*15, 24*). In contrast, CA3-NR1 KO mice exhibit intact spatial reference memory under conditions of fully cued mem-

ory retrieval with normal behavior and normal CA1 place cell activity. Thus, area CA1 is a major site involved in the storage of spatial reference memory and that this memory can be formed without CA3 NRs.

Although previous studies of memory formation and recall under fully cued conditions (*15*) provided basic insights into the mechanisms of memory formation, in day-to-day life, memory recall almost always occurs from limited cues in real-life situations, as pattern completion (*5*). In the past, computational analyses have pointed out that a recurrent network with modifiable synaptic strength, such as that in hippocampal area CA3, could provide this pattern completion ability (*5–10*). The impairment exhibited by CA3-NR1 KO mice in recalling the spatial memory after partial cue removal provides a direct demonstration of a role for CA3 and CA3 NRs in pattern completion at the behavioral level. At the neuronal network level, pattern completion was indicated by intact CA1 place cell activity under cue removal conditions in control mice, demonstrating the ability of intact CA3-CA1 networks to carry out this function. By contrast, under the same partial-cue conditions, CA1 place field size in mutant mice without CA3 NRs was reduced, demonstrating incomplete memory pattern retrieval.

The residual search preference for the phantom platform location exhibited by mutant mice after partial cue removal (Fig. 5, G and H) reflects the degradation rather than the complete loss of spatial memory retrieval. This is consistent with the complementary observation of reduced place cell responses with preserved place field location (Fig. 6F), indicating a decrease rather than complete disruption of reactivation of the memory trace. This result may also reflect the existence of additional recall mechanisms independent of CA3 NR function.

Although plasticity at mossy fiber-CA3 synapses is NR-independent (*11–14*), plasticity at perforant path-CA3 synapses is NR-dependent (*14*). Therefore, we cannot exclude the possibility that the feed-forward input to CA3 via the perforant path contributes to the observed pattern completion effects. However, the substantially greater strength of recurrent synaptic inputs relative to the contribution of the perforant path (*36*) suggests a dominant role for the recurrent system.

It has been proposed that memory can be stored in associative memory networks whose synapses are modifiable (*5–10*) (Fig. 7). In this model, inputs arriving via dentate mossy fibers or perforant path afferents (or both) would produce a pattern of CA3 ensemble output that reflects the pattern of inputs received. During normal memory acquisition under full-cue conditions, recurrent fiber synapses are modified in an NR-dependent manner to reinforce this ensemble pattern by strengthening connections between coactive neurons within the ensemble. This reflects storage of the memory trace within CA3 (Fig. 7, B and C). This complete CA3 pattern, driven by full-cue input and reinforced by recurrent connections, activates CA1 neurons and produces a pattern that serves as the output of the hippocampal circuit. The strengthening of connections between the CA3 and CA1 neurons that participated in this process reflects storage of the memory trace within CA1 (Fig. 7, B and C). Under full-cue conditions in mutant animals, the lack of NRs in the CA3 pyramidal cells prevents storage of the memory trace in the CA3 recurrent network but does not impair storage in CA1 (Fig. 7, D and E). The input for the memory storage in CA1 could also arrive via perforant path afferents directly from the entorhinal cortex.

Under conditions of normal recall, presentation of the full set of cues activates CA3 neurons in a pattern corresponding to the original CA3 memory trace, thereby leading to reactivation of the memory trace in CA1 (Fig. 7B). In mutant animals without CA3 NRs under full-cue conditions, although the CA3 memory trace is absent, the CA1 memory trace is reactivated directly by the incoming cues that correspond in their configuration to the pattern of the memory trace (Fig. 7D). Reactivation of previously strengthened recurrent synapses is unnecessary for recall under full-cue conditions, as indicated in the model (Fig. 7, B and D) and confirmed by our results from recordings in CA1. Nevertheless, the reactivation may contribute to the recall process in control animals by producing a more robust input to CA1 from CA3. This possibility would be consistent with the observed reduction in CA1 inhibitory cell activity in mutant animals, suggesting that even under full-cue conditions, the strength of input from CA3 might be diminished and compensated for through homeostatic reduction of feedback or feedforward inhibitory drive. In this way, a complete but weakened CA3 output pattern can provide sufficient drive to CA1 (*33*). Direct measurement of CA3 output may clarify some of these issues.

Under conditions of partial cue removal, limited input activity provides only partial activation of the CA3 output pattern in both control and mutant animals (green lines, Fig. 7, C to E). In control animals, this limited output activates previously strengthened recurrent synapses onto CA3 neurons that had participated in the original full-cue pattern (Fig. 7C). These recurrently driven cells complete the output pattern of CA3 (red lines, Fig. 7C), which can then drive the full output pattern in CA1. In mutant animals, limited input drives a correspondingly limited CA3 output pattern (green line in Fig. 7E). However, because of the lack of a memory trace in recurrent synapses, their activation is unable to drive neurons that had participated in the original full-cue pattern. This circumstance leads to a limited output pattern from CA3 that leads to a limited output pattern in CA1 in the form of smaller place fields with reduced firing rates (Fig. 7E).

Because CA3 NR function is absent during both memory formation and retrieval in CA3-NR1 KO mice, retrieval itself may be

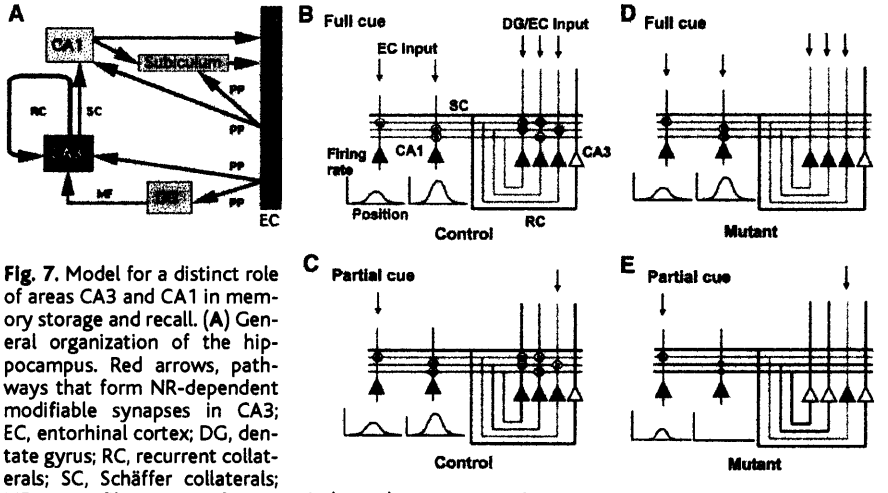

Fig. 7. Model for a distinct role of areas CA3 and CA1 in memory storage and recall. (**A**) General organization of the hippocampus. Red arrows, pathways that form NR-dependent modifiable synapses in CA3; EC, entorhinal cortex; DG, dentate gyrus; RC, recurrent collaterals; SC, Schäffer collaterals; MF, mossy fibers; PP, perforant path. (**B** to **E**) Basic wiring of CA3 and CA1, illustrating the proposed mechanisms for pattern completion. In control (B) and mutant (D), full cue input (downward arrows) is provided to CA3 from DG or EC and to CA1 from EC. Although the nature of these inputs is likely to be different, we do not consider this difference in this model. In control (C) and mutant (E), a fraction of the original input is provided to activate the memory trace during recall. For detailed explanation, see Discussion. Red dots, CA3 RC synapses or SC-CA1 synapses participating in memory trace formation; red circles, memory traces that are activated during recall; red dots without red circles, memory trace not activated during recall; red triangles and lines, CA3 pyramidal cell activity resulting from pattern completion through recurrent collateral firing; green triangles and lines, CA3 pyramidal cell response to external cue information; open triangles and black lines, silent CA3 pyramidal cells and inactive outputs; blue triangles, CA1 pyramidal cells.

affected by NR manipulation. Infusion of AP5 selectively into the hippocampus impairs spatial memory acquisition but shows no effect on retrieval of previously trained spatial reference memory in the water maze (*37*), suggesting that our results reflect a primary deficit in NR-dependent memory formation in CA3 that is then revealed as a deficit in recall under limited cue conditions.

A substantial proportion of aged individuals exhibit deficits of memory recall (*38*). In early Alzheimer patients, retrieval is the first type of memory function to decline; such retrieval deficits may serve as an early predictor of Alzheimer disease (*39, 40*). Normal aging produces a CA3-selective pattern of neurochemical alterations (*41–43*). Exposure to chronic stress, which can lead to memory deficits, also selectively causes atrophy in the apical dendrites of CA3 pyramidal cells (*44*). These results are consistent with our findings in mice that the CA3 region is critical for cognitive functions related to memory recall through pattern completion.

This study along with our previous study with CA1-NR1 KO mice (*15, 24*) illustrates the power of cell type-restricted, adult-onset gene manipulations in the study of molecular, cellular, and neuronal circuitry mechanisms underlying cognition. The same neurotransmitter receptors (i.e., NMDA receptors) can play distinct roles in the mnemonic process depending on where and in which neural circuitry in the hippocampus they are expressed. It is expected that other genetically engineered mice with precise spatial and/or temporal specificity will help dissect mechanisms for a variety of cognitive functions.

References and Notes

1. J. O'Keefe, L. Nadel, *The Hippocampus as a Cognitive Map* (Clarendon Press, Oxford, UK, 1978).
2. L. R. Squire, *Psychol. Rev.* **99**, 195 (1992).
3. D. G. Amaral, M. P. Witter, *Neuroscience* **31**, 571 (1989).
4. N. Ishizuka, J. Weber, D. G. Amaral, *J. Comp. Neurol.* **295**, 580 (1990).
5. D. Marr, *Philos. Trans. R. Soc. London Ser. B* **262**, 23 (1971).
6. A. R. Gardner-Medwin, *Proc. R. Soc. London Ser. B* **194**, 375 (1976).
7. J. J. Hopfield, *Proc. Natl. Acad. Sci. U.S.A.* **79**, 2554 (1982).
8. B. L. McNaughton, R. G. M. Morris, *Trends Neurosci.* **10**, 408 (1987).
9. E. T. Rolls, in *The Computing Neuron*, R. Durbin, C. Miall, G. Mitchison, Eds. (Addison-Wesley, Wokingham, UK, 1989), pp. 125–159.
10. M. E. Hasselmo, E. Schnell, E. Barkai, *J. Neurosci.* **15**, 5249 (1995).
11. E. W. Harris, C. W. Cotman, *Neurosci. Lett.* **70**, 132 (1986).
12. S. Williams, D. Johnston, *Science* **242**, 84 (1988).
13. R. A. Zalutsky, R. A. Nicoll, *Science* **248**, 1619 (1990).
14. T. W. Berger, M. F. Yeckel, in *Long-Term Potentiation: A Debate of Current Issues*, M. Baudry, J. L. Davis, Eds. (MIT Press, Cambridge, MA, 1991), pp. 327–356.
15. J. Z. Tsien, P. T. Huerta, S. Tonegawa, *Cell* **87**, 1327 (1996).
16. W. Wisden, P. H. Seeburg, *J. Neurosci.* **14**, 3582 (1993).
17. Relevant data and experimental procedures can be found at *Science* Online.
18. Y. Liu, N. Fujise, T. Kosaka, *Exp. Brain Res.* **108**, 389 (1996).
19. M. Watanabe *et al.*, unpublished data.
20. S. Chattarji, B. S. S. Rao, K. Nakazawa, S. Tonegawa, unpublished data.
21. R. G. M. Morris, P. Garrud, J. N. P. Rawlins, J. O'Keefe, *Nature* **297**, 681 (1982).
22. R. Muller, *Neuron* **17**, 813 (1996).
23. P. J. Best, A. M. White, A. Minai, *Annu. Rev. Neurosci.* **24**, 459 (2001).
24. T. J. McHugh, K. I. Blum, T. Z. Tsien, S. Tonegawa, M. A. Wilson, *Cell* **87**, 1339 (1996).
25. R. U. Muller, J. L. Kubie, *J. Neurosci.* **7**, 1951 (1987).
26. M. C. Quirk, K. I. Blum, M. A. Wilson, *J. Neurosci.* **21**, 240 (2001).
27. P. A. Schwartzkroin, D. A. Prince, *Brain Res.* **147**, 117 (1978).
28. R. K. S. Wong, R. D. Traub, *J. Neurophysiol.* **49**, 442 (1983).
29. O. Paulsen, E. I. Moser, *Trends Neurosci.* **21**, 273 (1998).
30. G. Buzsaki, *Prog. Neurobiol.* **22**, 131 (1984).
31. S. J. Y. Mizumori, C. A. Barnes, B. L. McNaughton, *Brain Res.* **50**, 99 (1989).
32. J. Csicsvari, H. Hirase, A. Czurko, G. Buzsaki, *Neuron* **21**, 179 (1998).
33. S. J. Y. Mizumori, B. L. McNaughton, C. A. Barnes, F. B. Fox, *J. Neurosci.* **9**, 3915 (1989).
34. J. O'Keefe, D. H. Conway, *Exp. Brain Res.* **31**, 573 (1978).
35. P. A. Hetherington, M. L. Shapiro, *Behav. Neurosci.* **111**, 20 (1997).
36. N. N. Urban, D. A. Henze, G. Barrionuevo, *Hippocampus* **11**, 408 (2001).
37. R. G. M. Morris, *J. Neurosci.* **9**, 3040 (1989).
38. M. Gallagher, P. R. Rapp, *Annu. Rev. Psychol.* **48**, 339 (1997).
39. H. Tuokko, R. Vernon-Wilkinson, J. Weir, B. L. Beattie, *J. Clin. Exp. Neuropsychol.* **13**, 871 (1991).
40. L. Backman, *et al.*, *Neurology* **52**, 1861 (1999).
41. H. Le Jeune, D. Cecyre, W. Rowe, M. J. Meaney, R. Quirion, *Neuroscience* **74**, 349 (1996).
42. T. Kadar, S. Dachir, B. Shukitt-Hale, A. Levy, *J. Neural Transm.* **105**, 987 (1998).
43. M. M. Adams *et al.*, *J. Comp. Neurol.* **432**, 230 (2001).
44. B. S. McEwen, *Annu. Rev. Neurosci.* **22**, 105 (1999).

45. We thank P. Soriano, F. Tronche, T. Furukawa, R. J. DiLeone, F. Bushard, S. Chattarji, and M. Fukaya for reagents, assistance, and/or advice. We also thank the many members of the Tonegawa and Wilson Labs for valuable advice and discussions. Supported by an NIH grant RO1-NS32925 (S.T.), RIKEN (S.T. and M.W.), NIH grant P50-MH58880 (S.T. and M.W.), HHMI (S.T.), and Human Frontier Science Program (K.N.).

Supporting Online Material

www.sciencemag.org/cgi/content/full/1071795/DC1
Materials and Methods
Fig. S1

12 March 2002; accepted 17 May 2002
Published online 30 May 2002;
10.1126/science.1071795
Include this information when citing this paper.

Surface Melt–Induced Acceleration of Greenland Ice-Sheet Flow

H. Jay Zwally,[1]* Waleed Abdalati,[2] Tom Herring,[3] Kristine Larson,[4] Jack Saba,[5] Konrad Steffen[6]

Ice flow at a location in the equilibrium zone of the west-central Greenland Ice Sheet accelerates above the midwinter average rate during periods of summer melting. The near coincidence of the ice acceleration with the duration of surface melting, followed by deceleration after the melting ceases, indicates that glacial sliding is enhanced by rapid migration of surface meltwater to the ice-bedrock interface. Interannual variations in the ice acceleration are correlated with variations in the intensity of the surface melting, with larger increases accompanying higher amounts of summer melting. The indicated coupling between surface melting and ice-sheet flow provides a mechanism for rapid, large-scale, dynamic responses of ice sheets to climate warming.

The time scale for dynamic responses of ice sheets to changes in climate (e.g., snow accumulation and surface temperature) is typically considered to be hundreds to thousands of years (*1*). Because most ice-sheet motion occurs by ice deformation in the lower layers, basal sliding, or deformation in basal till, the effects of changes in surface climate must be transmitted deep into the ice to affect the ice flow markedly. In particular, changes in the surface-mass balance alter the ice thickness slowly, and therefore the driving stresses in the deforming layers, as thickness changes accumulate. Changes in surface temperature can also affect the rate of ice deformation or basal sliding, but only after the very slow conduction of heat to the lower layers (*2*). In contrast to the flow of grounded ice, both floating glacier tongues (*3*) and Antarctic ice

[1]Oceans and Ice Branch, Code 971, NASA Goddard Space Flight Center, Greenbelt, MD 20771, USA. [2]Code YS, NASA Headquarters, 300 E Street, SW, Washington, DC 20546, USA. [3]Department of Earth, Atmospheric, and Planetary Sciences, MIT Room 54-618, 77 Massachusetts Avenue, Cambridge, MA 02139, USA. [4]Department of Aerospace Engineering Sciences, University of Colorado, Boulder, CO 80309, USA. [5]Raytheon Inc., Code 971, NASA Goddard Space Flight Center, Greenbelt, MD 20771, USA. [6]CIRES, University of Colorado, CB 216, Boulder, CO 80309, USA.

*To whom correspondence should be addressed. E-mail: jay.zwally@gsfc.nasa.gov

Appendix C: Collaborative Contributions to "APP Processing and Synaptic Plasticity in Presenilin-1 Conditional Knockout Mice"

Yu, H., Saura, C. A., Choi, S. Y., Sun, L. D., Yang, X., Handler, M., Kawarabayashi, T., Younkin, L., Fedeles, B., Wilson, M. A., *et al.* (2001). Neuron *31*, 713-726.

Abstract:

We have developed a presenilin-1 (PS1) conditional knockout mouse (cKO), in which PS1 inactivation is restricted to the postnatal forebrain. The PS1 cKO mouse is viable and exhibits no gross abnormalities. The carboxy-terminal fragments of the amyloid precursor protein differentially accumulate in the cerebral cortex of cKO mice, while generation of beta-amyloid peptides is reduced. Expression of Notch downstream effector genes, Hes1, Hes5, and Dll1, is unaffected in the cKO cortex. Although basal synaptic transmission, long-term potentiation, and long-term depression at hippocampal area CA1 synapses are normal, the PS1 cKO mice exhibit subtle but significant deficits in long-term spatial memory. These results demonstrate that inactivation of PS1 function in the adult cerebral cortex leads to reduced Abeta generation and subtle cognitive deficits without affecting expression of Notch downstream genes.

My Contribution:

The creation of a PS1 conditional null in the postnatal forebrain provided the first rodent model to study the effects of the first identified early-onset Alzheimer's Disease gene. While the biochemical pathway of PS1 was satisfactorily mapped in this study, it was a mystery as to how

this mutation would manifest itself in the behavior of the mouse; in other words is normal PS1 function important to the mouse's behavior. I provided evidence that showed that normal PS1 function is necessary for spatial learning and memory. I conducted the reference Morris Watermaze experiment for this study. I showed that while early spatial memory is not impaired in the mutants, a subtle late phase refinement of spatial memory was impaired in the mutants as summarized in Figure 8. After ten days of Watermaze training, upon removal of the hidden platform during the probe trial, the cKO mice crossed the target platform significantly fewer times than controls indicating poorer spatial memory recall. Next, by reversing platform positions for additional training, I showed that mutant mice have subtly impaired abilities to learn the new platform positions. Finally, by making the hidden platform visible by placing a flag on it, I showed that mutants and controls are indistinguishable from each other and both groups performed very well in this easier non-spatial variant of the Watermaze. Thus my contributions showed that normal PS1 function is necessary specifically for the formation of spatial memories; and I successfully eliminated the possibility that the effect observed is due to a nonspecific underlying locomotor or vision deficit.

Neuron, Vol. 31, 713–726, September 13, 2001, Copyright ©2001 by Cell Press

APP Processing and Synaptic Plasticity in *Presenilin-1* Conditional Knockout Mice

Huakui Yu,[1,8] Carlos A. Saura,[1,8] Se-Young Choi,[3] Linus D. Sun,[4] Xudong Yang,[1] Melissa Handler,[1] Takeshi Kawarabayashi,[5] Linda Younkin,[5] Bogdan Fedeles,[4] Matthew A. Wilson,[4] Steve Younkin,[5] Eric R. Kandel,[6] Alfredo Kirkwood,[3] and Jie Shen[1,2,7]

[1]Center for Neurologic Diseases
Brigham and Women's Hospital
[2]Program in Neuroscience
Harvard Medical School
Boston, Massachusetts 02115
[3]Mind/Brain Institute
Johns Hopkins University
Baltimore, Maryland 21218
[4]Department of Brain and Cognitive Sciences
Center for Learning and Memory
Massachusetts Institute of Technology
Cambridge, Massachusetts 02138
[5]Mayo Clinic Jacksonville
Jacksonville, Florida 32224
[6]Howard Hughes Medical Institute
Center for Neurobiology and Behavior
Columbia University
New York, New York 10032

Summary

We have developed a *presenilin-1* (*PS1*) conditional knockout mouse (cKO), in which PS1 inactivation is restricted to the postnatal forebrain. The *PS1* cKO mouse is viable and exhibits no gross abnormalities. The carboxy-terminal fragments of the amyloid precursor protein differentially accumulate in the cerebral cortex of cKO mice, while generation of β-amyloid peptides is reduced. Expression of Notch downstream effector genes, *Hes1*, *Hes5*, and *Dll1*, is unaffected in the cKO cortex. Although basal synaptic transmission, long-term potentiation, and long-term depression at hippocampal area CA1 synapses are normal, the *PS1* cKO mice exhibit subtle but significant deficits in long-term spatial memory. These results demonstrate that inactivation of PS1 function in the adult cerebral cortex leads to reduced Aβ generation and subtle cognitive deficits without affecting expression of Notch downstream genes.

Introduction

Mutations in Presenilin-1 (PS1) are the most common cause of early-onset familial Alzheimer's disease (FAD). Accumulation and deposition of β-amyloid (Aβ) peptides in the cerebral cortex is an early and central process in the pathogenesis of AD. The Aβ peptides are generated from the amyloid precursor protein (APP) as a result of sequential proteolytic cleavages by β- and γ-secretases, which are therefore prime targets for therapeutic intervention. β-secretase (BACE) was recently identified as a novel aspartyl protease, while γ-secretase was found to be closely associated with PS1. The generation of Aβ peptides is markedly reduced in cultured *PS1*$^{-/-}$ neurons (De Strooper et al., 1998). Conversely, FAD-linked PS1 mutations invariably lead to increased production of the particularly amyloidogenic species Aβ42 (Duff et al., 1996; Jarrett et al., 1993; Scheuner et al., 1996). It has been postulated that PS1 may itself possess γ-secretase activity (Wolfe et al., 1999), a notion that is supported by the direct binding of PS1 by peptidomimetic γ-secretase inhibitors (Esler et al., 2000; Li et al., 2000). These findings have raised the possibility that PS1 may represent an attractive target for anti-amyloidogenic therapy.

The feasibility of PS1 as a therapeutic target for AD depends critically on the effects of reduced PS1 function in the adult brain. Due to the perinatal lethality of *PS1*$^{-/-}$ mice, however, previous studies on APP processing in the absence of PS1 have relied on cultured neurons derived from the embryonic *PS1*$^{-/-}$ brain. In addition to its role in APP processing, our previous studies of *PS1*$^{-/-}$ mice showed that PS1 exerts pleiotropic effects during brain development, including the regulation of neurogenesis and Notch signaling (Handler et al., 2000; Shen et al., 1997). In the absence of PS1, neural progenitor cells differentiate prematurely into postmitotic neurons, leading to early depletion of the progenitor cells and subsequently a smaller neuronal population (Handler et al., 2000). Furthermore, Notch signaling is reduced in the *PS1*$^{-/-}$ embryonic brain, as indicated by reduced *Hes5* expression and increased *Dll1* expression (Handler et al., 2000). PS1 appears to influence Notch signaling by regulating the generation of the intracellular domain of Notch1 (NICD) (De Strooper et al., 1999; Song et al., 1999), which translocates to the nucleus to stimulate transcription of downstream effector genes. The role of PS1 in the adult brain, however, remains unknown due to the perinatal lethality of the *PS1*$^{-/-}$ mouse. Recently, mutations in the PS1 homologs in *C. elegans*, sel-12 and hop-1, have been found to lead to defects in temperature memory and the neuritic morphology of two cholinergic interneurons, indicating an involvement of PS1 in neuronal function (Wittenburg et al., 2000).

To investigate the effects of PS1 inactivation on APP processing, the Notch signaling pathway, and synaptic and cognitive function in the adult brain, we employed the Cre/loxP recombination system to develop a *PS1* conditional knockout (cKO) mouse. Using this strategy, PS1 expression is progressively eliminated in the cortex of cKO mice beginning in the third postnatal week. In the adult cerebral cortex of cKO mice, levels of Aβ40 and Aβ42 are differentially reduced, while levels of the APP C-terminal fragments (CTFs) are differentially increased. Surprisingly, expression of the Notch downstream effector genes, *Hes1*, *Hes5*, and *Dll1*, is unaffected in the cortex of cKO mice. Basal synaptic transmission and synaptic plasticity in hippocampal area CA1 are normal, but the *PS1* cKO mice exhibit

[7]Correspondence: jshen@rics.bwh.harvard.edu
[8]These authors contributed equally to this work.

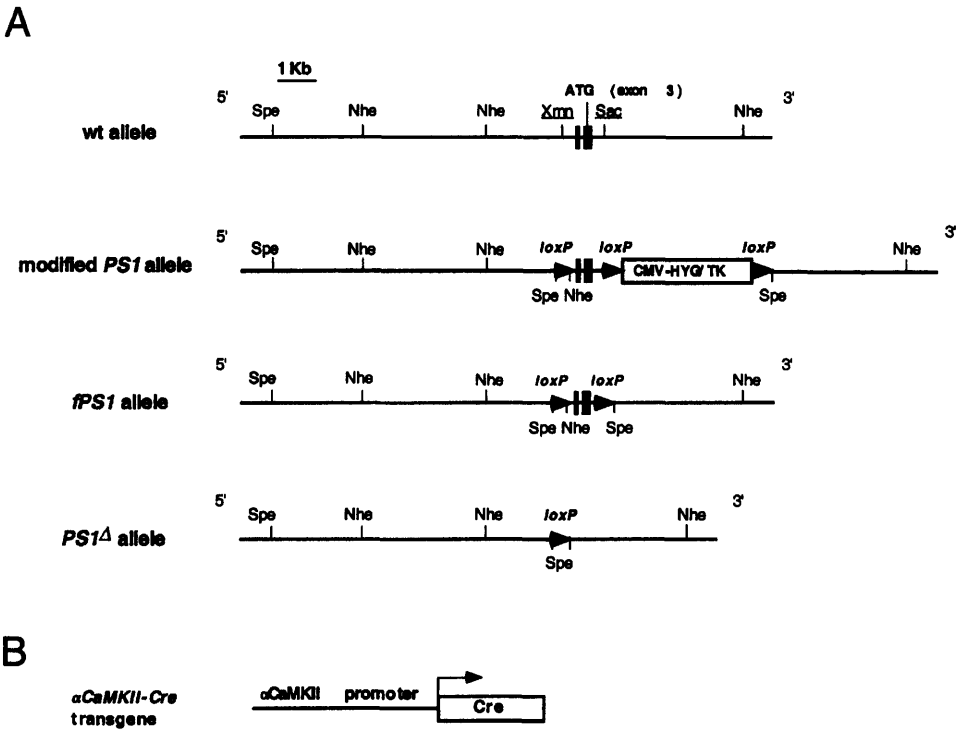

Figure 1. Generation of the Floxed *PS1* and the α*CaMKII-Cre* Transgenic Mice

(A) Schematic representation of the wild-type *PS1* genomic region encompassing exons 2 and 3 and the modified *PS1* alleles. The black boxes represent *PS1* exons 2 and 3, and exon 3 contains the start ATG codon. The modified *PS1* allele contains a loxP site in *PS1* intron 1 and a floxed CMV-HYG/TK selection cassette in intron 3. The floxed selection cassette is removed in the *fPS1* allele, while the entire floxed region including *PS1* exons 2 and 3 is excised in the *PS1*$^{\Delta}$ allele.

(B) Schematic representation of the α*CaMKII-Cre* transgene (not drawn to scale). The transgene contains a ~8.5 kb segment of the α*CaMKII* promoter, a hybrid 5′ intron, cDNA encoding Cre recombinase, and the SV40 polyadenylation signal.

subtle deficits in spatial reference memory. These results indicate that disruption of PS1 function in the adult brain results in reduced Aβ generation and subtle cognitive impairment.

Results

Generation and Characterization of the *PS1* cKO Mouse

To achieve the selective disruption of PS1 in the cerebral cortex (neocortex and hippocampus) during postnatal life, we employed the recently developed Cre/loxP recombination technology. We first generated a floxed *PS1* mouse, in which *PS1* exons 2 and 3 are flanked by two *loxP* sites (Figure 1A). Using homologous recombination in embryonic stem (ES) cells, we generated a modified *PS1* allele, in which a *loxP* site and a floxed drug selection cassette were introduced into *PS1* introns 1 and 3, respectively (Figure 1A). The floxed *PS1* allele (*fPS1*) and the *PS1*$^{\Delta}$ allele were then generated by transient transfection of a cDNA encoding Cre recombinase, which mediates site-specific recombination between two *loxP* sites (Yu et al., 2000). ES cells carrying either the *fPS1* or the *PS1*$^{\Delta}$ allele were injected into mouse blastocysts to generate chimeric mice, which were then used to generate heterozygous and homozygous *fPS1* and *PS1*$^{\Delta}$ mice. We also generated a *Cre* transgenic mouse (*CaM-Cre*), in which Cre recombinase is expressed selectively in pyramidal neurons of the postnatal forebrain under the control of the α-calcium-calmodulin-dependent kinase II promoter (Figure 1B) (Mayford et al., 1996; Minichiello et al., 1999). The *PS1* conditional knockout (cKO) mouse was then generated by crossing the *fPS1* mouse to the *CaM-Cre* transgenic mouse.

To determine whether the introduction of the *loxP* sites into *PS1* introns affects transcription and/or splicing of *PS1* mRNA, we performed Northern and RT-PCR analyses and found that the level and the size of *PS1* transcripts are unaltered in homozygous *fPS1* mice (Figure 2A and data not shown). The homozygous *PS1*$^{\Delta}$ mice exhibit phenotypes indistinguishable from those of the *PS1*$^{-/-}$ mice that we previously reported, confirming that excision of the floxed region results in a *PS1* null allele (Shen et al., 1997). Northern analysis of *PS1*$^{\Delta}$ mice revealed greatly reduced levels of a smaller *PS1* transcript, indicating that the *PS1* transcript lacking exons 2 and 3 is highly unstable or that important transcriptional regulatory sequences reside within this region (Figure 2A).

Spatial and temporal inactivation of *PS1* expression in cKO mice was examined by Northern, Western, and in situ hybridization analyses. Northern analysis showed a marked reduction in the level of *PS1* mRNA in the cortex (neocortex and hippocampus) of cKO mice at the age of 6 weeks, though residual *PS1* transcripts were

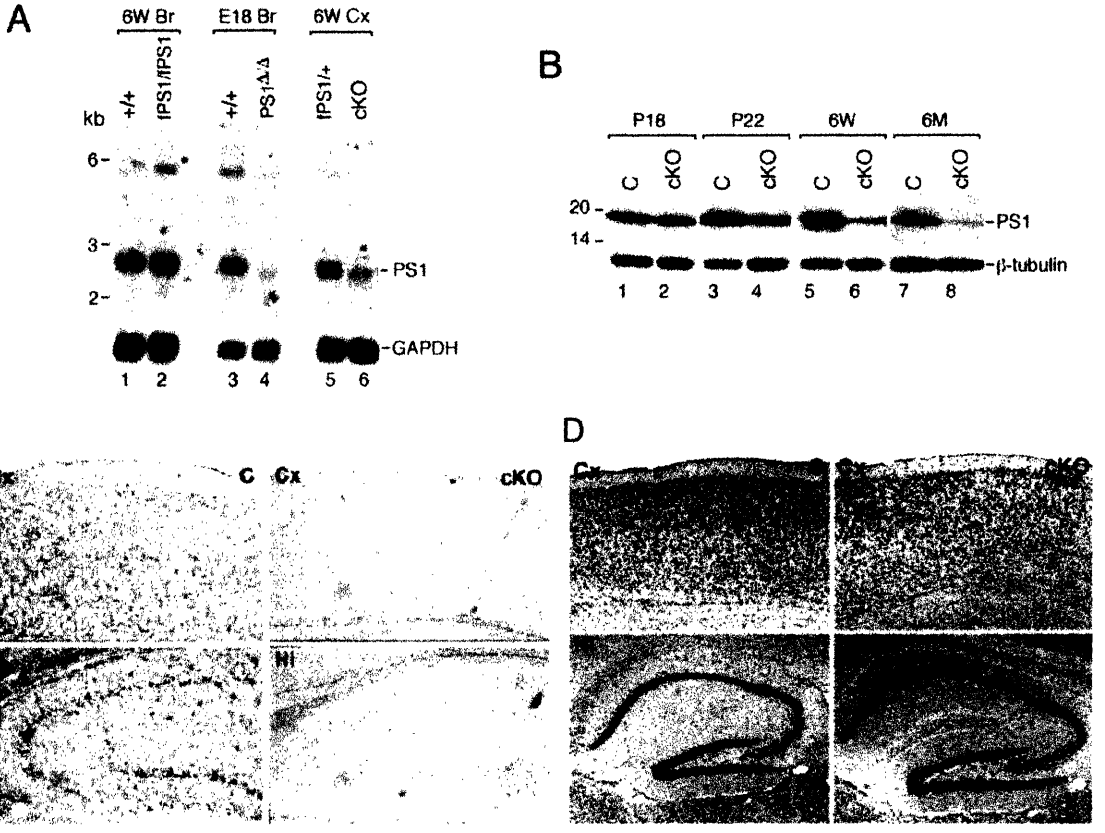

Figure 2. Spatially and Temporally Specific Inactivation of *PS1* in cKO Mice

(A) Northern analysis of *PS1* transcripts in *fPS1/fPS1*, *PS1*$^{\Delta/\Delta}$, and *PS1* cKO mice. Total RNA was prepared from the brains of *fPS1/fPS1* and littermate control (+/+) mice at the age of 6 weeks (lanes 1 and 2), the brains of *PS1*$^{\Delta/\Delta}$ and littermate control (+/+) mice at embryonic day 18 (lanes 3 and 4), and the cortex (neocortex and hippocampus) of cKO (*PS1*$^{\Delta}$*/fPS1;CaM-Cre*) and littermate control (*fPS1/+*) mice at the age of 6 weeks (lanes 5 and 6), and then hybridized with a *PS1* cDNA probe. The same blot was then hybridized with a control probe, *GAPDH*, to normalize the amounts of RNA in each lane.

(B) Progressive elimination of PS1 CTFs in the cKO cortex. Brain homogenate from the cortex of cKO (*PS1*$^{\Delta}$*/fPS1;CaM-Cre*) and littermate control (C) (*fPS1/+* or *fPS1/fPS1*) mice at the ages of P18, P22, 6 weeks, and 6 months was immunoblotted with antiserum raised against the loop region of PS1 (Thinakaran et al., 1996). The blot was then incubated with β-tubulin antibody to normalize the amounts of protein in each lane.

(C) In situ hybridization analysis of *PS1* expression in the neocortex and hippocampus of *PS1* cKO and control mice. Sagittal brain sections (10 μm) of *PS1* cKO (*PS1*$^{\Delta}$*/fPS1;CaM-Cre*) and littermate control (*PS1*$^{\Delta}$*/fPS1*) mice at the age of 3 months were hybridized with a digoxigenin-labeled probe specific for *PS1* exons 2 and 3. Expression of *PS1* transcripts is largely eliminated in the hippocampus and neocortex of the *PS1* cKO brain.

(D) Normal gross morphology of the hippocampus and neocortex of the cKO mouse. Sagittal brain sections (12 μm) of *PS1* cKO and littermate control mice at the age of 3 months were stained with cresyl violet. The gross morphology of the cKO brain is indistinguishable from that of the control.

still detectable (Figure 2A). Since the majority of endogenous PS1 undergoes endoproteolytic processing into 27 kDa N-terminal and 18 kDa C-terminal fragments (CTF), we examined the level of PS1 CTF by Western analysis. The level of PS1 CTF in the cortex is slightly reduced at postnatal day 18 (P18) and further reduced at P22 (Figure 2B). By the ages of 6 weeks and 6 months, very low levels of PS1 CTF were detected in the cortex of cKO mice, while the level of PS1 CTF was unchanged in the cerebellum and brain stem (Figure 2B and data not shown). These results indicate a selective elimination of PS1 expression in the cortex of *PS1* cKO mice beginning at P18. The residual amount of PS1 observed in the cortex of cKO mice is due to its expression in glial cell types (Lah et al., 1997) and possibly a small population of neurons lacking Cre expression. We further performed in situ hybridization on brain sections of *PS1* cKO and control mice at the age of 3 months using a digoxigenin-labeled probe specific for *PS1* exons 2 and 3. We found that *PS1* is expressed at high levels in the hippocampus and at lower levels in the neocortex of the control brain, while its expression in the cKO brain is eliminated (Figure 2C).

In contrast to *PS1*$^{-/-}$ mice, the *PS1* cKO mouse is viable with no obvious phenotypic abnormalities. Nissl staining of the brain sections of cKO mice at the ages of P18, 20, 22, and 3 months (Figure 2D) also revealed no gross abnormalities. Despite large numbers of reports that have suggested a role for PS1 in apoptosis using various cell culture systems, we failed to detect an increase in apoptosis in the cerebral cortex of cKO mice. Bisbenzimide staining and TUNEL analysis of the

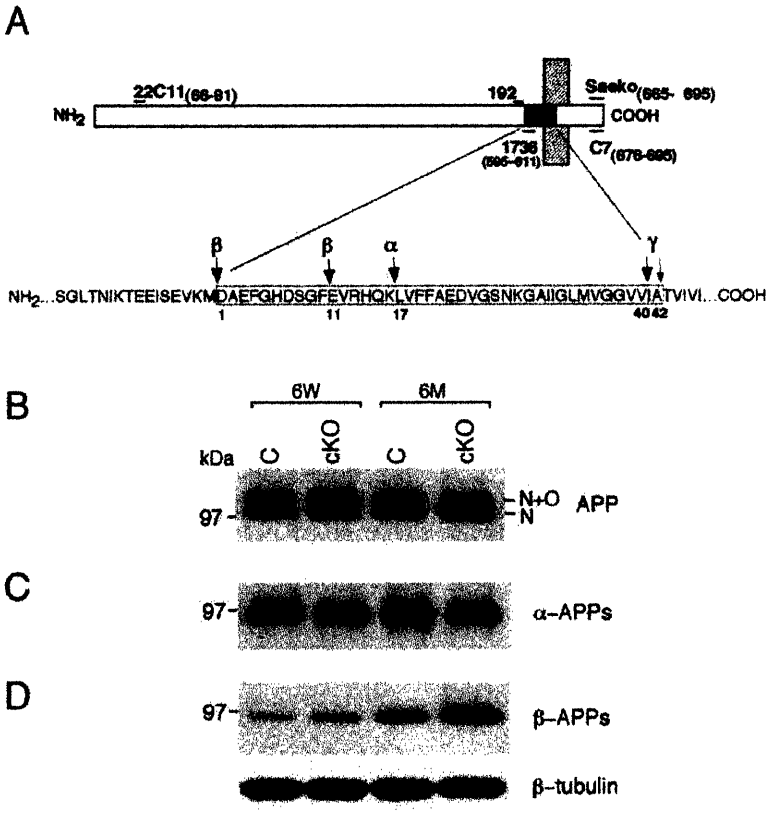

Figure 3. Unchanged Levels of α- and β-APPs in *PS1* cKO Mice

(A) Schematic representation of APP and the amino acid sequence comprising the Aβ region. A single transmembrane domain is indicated by the vertical hatched bar, while the Aβ region is indicated by the filled black box. Antibodies raised against various regions of APP are shown. The α-, β-, and γ-cleavage sites on APP are indicated by vertical arrows.

(B) Western analysis of full-length APP. Levels of full-length APP, which were measured by Western using the "Saeko" antiserum (Kawarabayashi et al., 1996), are similar in the cortex of both *PS1* cKO and control mice at the ages of 6 weeks (6W) and 6 months (6M). "N" and "O" denote glycosylation at the NH_2 and OH groups of Asn and Ser/Thr residues, respectively.

(C) IP-Western analysis of α-APPs. α-APPs was detected by IP with antiserum 1736 followed by Western using antibody 22C11. Levels of α-APPs are similar in the cortex of cKO and control mice at the ages of 6 weeks and 6 months.

(D) Western analysis of β-APPs. β-APPs was detected by antibody 192, which is specific for the C terminus of β-APPs. Levels of β-APPs are similar in the cortex of *PS1* cKO and control mice at the ages of 6 weeks and 6 months. The level of β-APPs is upregulated in the cortex of both *PS1* cKO and control mice from the age of 6 weeks to the age of 6 months. The same immunoblot was incubated with β-tubulin antibody to confirm similar amounts of total protein loaded in each lane. I^{125}-labeled antibodies were also used in Western analysis to measure levels of β-APPs more quantitatively, and no significant differences between the cKO and control cortex were found.

cortex of control and cKO mice at the ages of P18, P20, P22, and 3 months showed no significant difference in the low number of apoptotic cells detected for each genotype (data not shown).

Altered APP Processing and Reduced Aβ Generation

To investigate the role of PS1 in APP processing in the adult cerebral cortex, we used a panel of well-characterized antibodies against APP to examine levels of the APP ectodomains (α-APPs and β-APPs) and membrane bound CTFs (α-CTF and β-CTF) generated by α- and β-secretase cleavage (Figure 3A). β-secretase (BACE1) has been shown to cleave APP at the +1 (Asp) and +11 (Glu) sites of Aβ (Figure 3A) (Cai et al., 2001; Luo et al., 2001). Western analysis showed that the level of the full-length APP is unchanged in the adult cortex lacking PS1 (Figure 3B). Immunoprecipitation (IP) with an antiserum specific for the α-APPs, followed by Western blotting using the antibody 22C11, showed similar levels of the α-APPs in the cortex of cKO and littermate control mice (Figure 3C). Western analysis of β-APPs using an antiserum specific for β-APPs also showed similar levels of the β-APPs in the cKO cortex compared to the control (Figure 3D). These results indicate that PS1 is not involved in the regulation of α- and β-secretase cleavage of APP.

We then performed Western analysis using an antiserum ("Saeko") raised against the C-terminal region of APP to measure the level of the APP CTFs in the cortex, and found that the CTFs accumulate in the cortex of cKO mice in an age-dependent manner (Figure 4A). At P18, the level of the CTFs is slightly higher in the cKO cortex relative to the littermate control. At P22, levels of the CTFs are further increased, consistent with the reduction in the level of PS1 (Figure 2B). At the ages of 6 weeks and 6 months, there is a striking progressive accumulation of the CTFs in the cKO cortex (Figure 4A). Five distinct CTF species were detected in the cortex of cKO and littermate control mice (Figure 4A, lanes 1–8), as previously reported (Buxbaum et al., 1998), while only three APP CTF species were detected in CHO cells transfected with the human wild-type *APP* cDNA (Figure 4A, lane 11). The additional APP CTF species in the brain are phosphorylated forms of the α- and β-CTFs, as they disappear following phosphatase treatment (Figure 4A, lanes 9 and 10). The three CTF species in CHO cells and mouse cortex following phosphatase treatment represent the α-CTF (C83), which is cleaved at +17 (Leu) of Aβ, and the β-CTFs (C99 and C89), which are cleaved at +1 (Asp) and +11 (Glu) of Aβ, respectively (Figure 3A) (Cai et al., 2001; Luo et al., 2001; Simons et al., 1996).

To quantify the increase of the APP CTFs, we performed Western analysis using serial dilutions of cKO brain lysate at the age of 6 months (Figure 4B). We estimate that the levels of C83 and C89 are increased approximately 30-fold, relative to the control, while the increase in the level of C99 is approximately 3-fold. Since

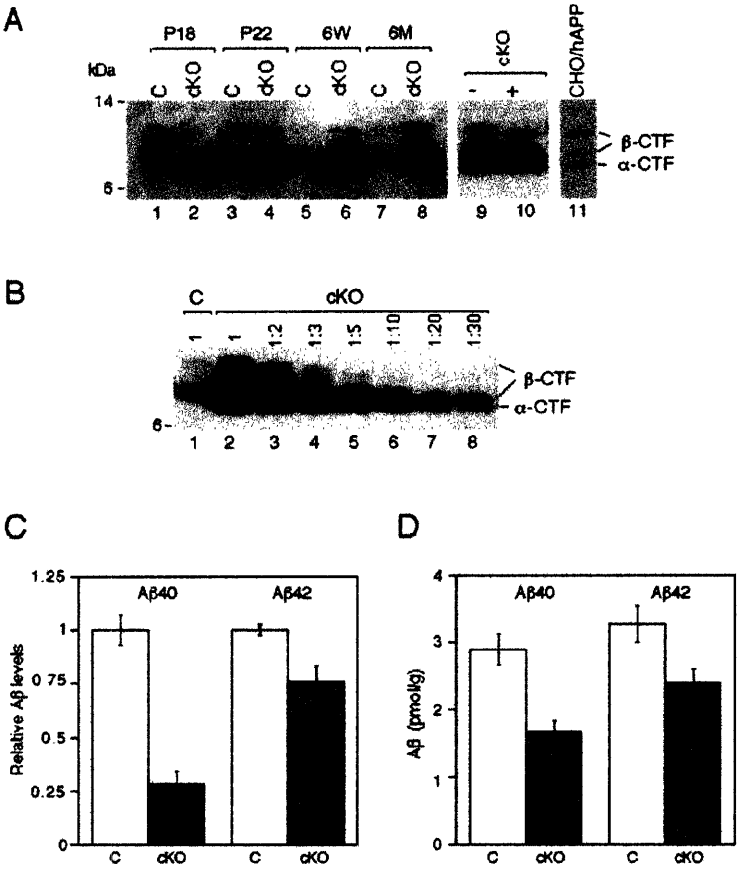

Figure 4. Differential Accumulation of the APP CTFs and Reduction of Aβ peptides in *PS1* cKO Mice

(A) Western analysis of the APP CTFs in *PS1* cKO and littermate control mice. Western analysis was performed using lysate prepared from the cortex of cKO and littermate control mice (lanes 1–8) and CHO cells transfected with human wild-type *APP* cDNA (lane 11). The "Saeko" antiserum was used to detect the CTFs. At least five species of the CTFs were detected in the mouse brain (lanes 1–8), while one α-CTF (C83) and two β-CTF (C89 and C99) species were detected in the transfected CHO cells (lane 11). The two additional CTF bands were eliminated after treatment with potato acid phosphatase (lanes 9 and 10). The level of the CTFs is slightly higher in the cKO cortex at P18 (lane 2), and further increased at P22 (lane 4). The accumulation of the CTFs (C83 and C89) in the cKO cortex is very striking at the ages of 6 weeks (lane 6) and 6 months (lane 8), while the increase of the β-CTF (C99) is modest, compared to the control.

(B) Differential accumulation of the α- and β-CTFs in the cKO cortex. Brain lysate prepared from the cortex of *PS1* cKO mice at the age of 6 months was diluted as indicated (lanes 2–8), and immunoblotted with the "Saeko" antiserum along with the undiluted homogenate of the control cortex (lane 1). The level of the α-CTF (C83) and β-CTF (C89) in the cKO cortex is increased about 30-fold while the level of the β-CTF (C99) in the cKO cortex is increased about 3-fold relative to the control.

(C) Reduction of endogenous mouse Aβ40 and Aβ42 peptides in the cKO cortex. Relative levels of mouse Aβ40 and Aβ42 in the cortex of the cKO (n = 9) and control (n = 9) mice at the age of 3–6 months were determined by the BNT-77/BA27 and BNT-77/BC05 ELISA assays following immunodepletion of the APP CTFs using the "Saeko" antiserum, respectively. Levels of Aβ40 and Aβ42 in the cKO cortex are shown as relative values to that of the control, which are designated as 1.

(D) Reduction of human Aβ40 and Aβ42 peptides in the cKO cortex. The level of human Aβ40 and Aβ42 in the cortex of the cKO (n = 7) and control (n = 6) mice at the age of 6–9 weeks was measured by the 2G3/3D6 and 21F12/3D6 ELISA assays, respectively. In the control mice overexpressing human mutant APP, levels of human Aβ42 are slightly higher than that of Aβ40, most likely due to the Indiana mutation that is known to increase the production of Aβ42. In the cKO mice overexpressing human mutant APP, levels of both Aβ40 and Aβ42 are significantly reduced ($p < 0.01$, Student's t test). The reduction of Aβ40 (~42%) is more marked than that of Aβ42 (~27%) in the cKO cortex.

elimination of PS1 expression does not affect α- and β-secretase cleavages, these results indicate that PS1 is required for γ-secretase activity, and that lack of PS1 results in accumulation of γ-secretase substrates.

To investigate PS1 function in the generation of Aβ peptides in the adult cerebral cortex, we measured levels of Aβ40 and Aβ42 in the cortex of the cKO and the littermate control mice at the ages of 6 weeks and 6 months by enzyme-linked immunosorbent assay (ELISA). Well-characterized antibodies specific for Aβ40 and Aβ42—BA27 and BC05, respectively—were used for the assay (Duff et al., 1996; Suzuki et al., 1994). We found that levels of Aβ40 are reduced in the cortex of *PS1* cKO mice at both ages examined (Table 1). Surprisingly, we detected higher levels of Aβ42 in the cortex of cKO mice than in the control, and the increase becomes more substantial by the age of 6 months (Table 1). Given the pronounced age-dependent accumulation of the CTFs (as much as 30-fold by 6 months) in the cKO cortex, we then examined whether the antibodies used for ELISA detection, BA27 and BC05, crossreact with the CTFs by Western, IP-Western, and IP-ELISA. Western analysis showed that neither BA27 nor BC05 recognizes the high levels of the accumulated CTFs in the *PS1* cKO cortex (data not shown). Immunoprecipitation using either BA27 or BC05 followed by Western analysis, however, revealed that BC05 crossreacts with the APP CTFs, while BA27 does not, suggesting that levels of Aβ42

Table 1. Cortical Levels of Aβ40 and Aβ42 in the Control and cKO Mice

Genotype	Age	Aβ40 (pmol/g)	Aβ42 (pmol/g)
Control	6 weeks	1.67 ± 0.19	0.47 ± 0.09
cKO		0.92 ± 0.08	0.96 ± 0.08
(n = 4 ea.)			
Control	6 months	1.53 ± 0.28	0.49 ± 0.06
cKO		0.96 ± 0.15	1.29 ± 0.10
(n = 3 ea.)			

All values shown are mean ± SD. Levels of Aβ40 and Aβ42 were determined by the BNT-77/BA27 and BNT-77/BC05 ELISA assays, respectively. Similar changes in the level of Aβ40 and Aβ42 in the cKO and control mice were observed in three independent experiments.

Table 2. Relative Cortical Levels of Aβ40 and Aβ42 following CTF Immunodepletion (ID)

		Aβ40		Aβ42	
Genotype	Age (Months)	Control ID	ID	Control ID	ID
Control (n = 9)	3–6	1.00 ± 0.07	0.83 ± 0.06	1.00 ± 0.02	0.70 ± 0.02
cKO (n = 9)	3–6	0.46 ± 0.04[a]	0.23 ± 0.05[a]	1.66 ± 0.04[a]	0.53 ± 0.05[a]

All values (mean ± SEM) represent relative levels of Aβ40 and Aβ42 measured by the BNT-77/BA27 and BNT-77/BC05 ELISA assays, respectively, following immunodepletion with beads alone (Control ID) or with beads and the "Saeko" antiserum (ID). Similar changes in the level of Aβ40 and Aβ42 in the cKO and control mice were observed in three independent experiments.
[a] $p < 0.004$ compared to control by Mann Whitney test.

detected by BC05 may be artificially elevated in the cKO cortex due to the presence of high levels of the APP CTFs. To measure levels of Aβ40 and Aβ42 accurately, we removed the APP CTFs from the lysate by immunodepletion using the "Saeko" antiserum, and then determined the level of Aβ40 and Aβ42 in the supernatant by ELISA (Table 2). The complete removal of the CTFs in the supernatant was confirmed by Western analysis. Using this method, we found that the level of both Aβ40 and Aβ42 is reduced in the cKO cortex relative to the control (Table 2, Figure 4C). We recently generated cKO mice that overexpress the human mutant APP containing the Swedish and the Indiana (V717F) mutations (Mucke et al., 2000). The level of human Aβ40 and Aβ42 was determined by ELISA assays using antibodies that are specific for human Aβ40 and Aβ42 peptides and do not crossreact with APP CTFs (Johnson-Wood et al., 1997). We found that the level of human Aβ40 and Aβ42 is also reduced in the cKO cortex (Figure 4D). Together, our results showed that elimination of PS1 expression in most neurons of the adult mouse cerebral cortex markedly reduces the production of Aβ peptides, supporting the notion that targeting PS1 is an effective strategy for anti-amyloidogenic therapy in AD.

Normal Expression of Notch Downstream Effector Genes

Our previous studies of *PS1*$^{-/-}$ mice showed that PS1 is involved in the regulation of the Notch signaling pathway during neural development (Handler et al., 2000; Song et al., 1999). In the developing brain of both *PS1*$^{-/-}$ mice and *Notch1*$^{-/-}$ mice, the expression of the Notch downstream target gene *Hes5* is reduced and the expression of *Dll1* is increased, while *Hes1* expression is unaffected (de la Pompa et al., 1997; Handler et al., 2000). PS1 appears to regulate Notch signaling at the level of posttranslational activation since the level of Notch1 mRNA and protein is unchanged in the absence of PS1 (Handler et al., 2000). More specifically, PS1 is involved in the proteolytic production of NICD, based on the in vitro findings that NICD production is reduced in cultured *PS1*$^{-/-}$ cells transfected with truncated Notch1 constructs (De Strooper et al., 1999; Song et al., 1999). However, a direct in vivo assessment of PS1 function in NICD generation has not been possible because endogenous levels of NICD fall below the limits of detection with currently available methods. We therefore investigated PS1 function in Notch signaling in the adult cerebral cortex by examining expression of the Notch downstream target genes, *Hes1*, *Hes5*, and *Dll1*. Northern analysis of poly(A)$^+$ RNA derived from the cortex of cKO and littermate control mice at the age of 6 weeks showed similar levels of *Hes1*, *Hes5*, and *Dll1* expression (Figure 5). Quantitative comparison of the level of the *Hes1*, *Hes5*, and *Dll1* transcripts in the cortex of multiple mice (n = 4–5) from multiple experiments (n = 3) confirmed normal expression of these Notch downstream target genes in the cKO cortex. These re-

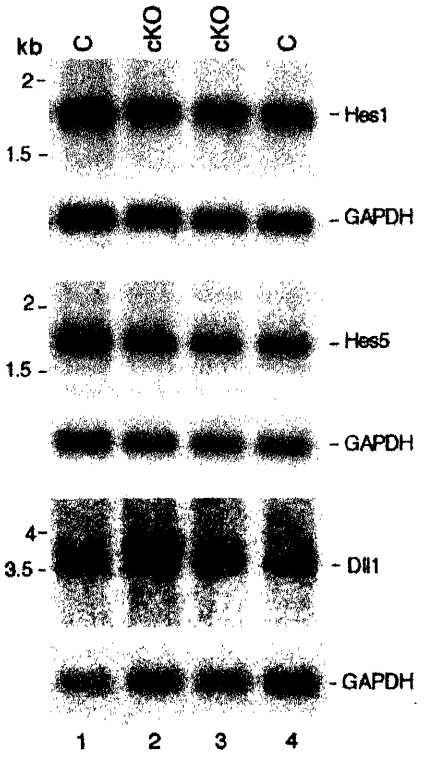

Figure 5. Unchanged Expression of *Hes1*, *Hes5*, and *Dll1* Transcripts in *PS1* cKO Mice

Northern analysis of *Hes1*, *Hes5*, and *Dll1* transcripts in *PS1* cKO and littermate control mice. Poly(A)$^+$ RNA was prepared from the cortex of cKO and control mice at the age of 6 weeks, and then hybridized with a *Hes1*, *Hes5*, or *Dll1* cDNA probe (Sasai et al., 1992; Takebayashi et al., 1995). The same blots were then hybridized with a control probe, *GAPDH*, to normalize the amounts of RNA in each lane. The level of each transcript was quantified using NIH Image software. Multiple experiments (n = 3) using poly(A)$^+$ RNA prepared from the cortex of cKO and control mice (n = 4–5) showed unchanged expression of *Hes1*, *Hes5*, and *Dll1* in the cKO cortex.

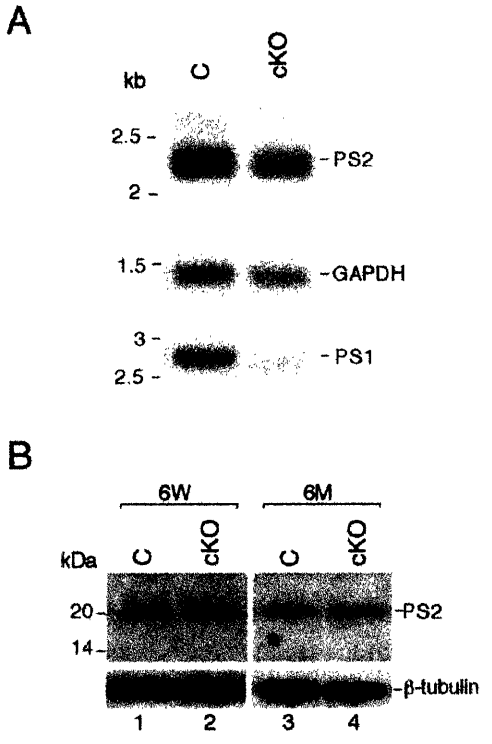

Figure 6. Unchanged Expression of PS2 in *PS1* cKO Mice

(A) Similar levels of *PS2* transcripts in *PS1* cKO and littermate control mice. Total RNA was prepared from the cortex of cKO and control mice at the age of 6 weeks, and then hybridized with a *PS2* cDNA probe. The same blot was then hybridized with a control probe, *GAPDH*, to normalize the amounts of RNA in each lane. (B) Similar levels of the PS2 CTF in *PS1* cKO and littermate control mice. Brain homogenate of the cortex of cKO and control mice at the age of 6 weeks was immunoblotted with the antiserum raised against the loop region of PS2 (Tomita et al., 1998). The same immunoblot was then incubated with the β-tubulin antibody to confirm similar amounts of total protein loaded in each lane.

sults demonstrate that the regulation of the Notch downstream effector genes differs in the embryonic and adult brain with respect to its dependence on PS1 function.

One possible explanation for the failure of PS1 inactivation to affect expression of Notch downstream genes in the adult brain could be a compensatory upregulation of presenilin-2 (PS2) expression. Alternatively, loss of PS1 could lead to an increase in the proteolytic processing of PS2 since the cleavage of PS proteins appears to be tightly regulated (Thinakaran et al., 1997; Tomita et al., 1997). To address these possibilities, we examined expression of PS2 by Northern and Western analyses. Northern analysis using total RNA derived from the cortex of *PS1* cKO and control mice at the age of 6 weeks showed no change in the level of *PS2* transcripts in the cKO cortex (Figure 6A). The level of the C-terminal fragment of PS2 is also unchanged in the cKO cortex (Figure 6B). These results indicate that elimination of PS1 function in the adult cortex does not result in a compensatory overproduction of PS2. It remains possible, however, that normal expression levels of PS2 in the adult cortex, which are higher than those in the embryonic brain relative to PS1, are sufficient to maintain the normal expression of the Notch downstream target genes. Alternatively, the regulation of Notch downstream genes in the adult brain might be independent of PS proteins.

Normal Synaptic Transmission and Plasticity in the Schaeffer Collateral Pathway

Our previous studies of $PS1^{-/-}$ mice revealed a critical role for PS1 in neurogenesis, neuronal differentiation, and migration during neural development, which is consistent with high levels of PS1 expression in the ventricular zone and the developing cortical plate (Handler et al., 2000; Shen et al., 1997). In the adult brain, PS1 is also expressed at relatively high levels in the hippocampus and neocortex (Figure 2C). To investigate whether PS1 is involved in the modulation of synaptic function in the adult brain, we examined the *PS1* cKO mice for deficits in synaptic transmission and plasticity in the Schaeffer collateral/commissural pathway of acute hippocampal slices.

We first evaluated the impact of PS1 inactivation on basal synaptic transmission. Input/output (I/O) curves were obtained by plotting the amplitude of the fiber volley (a measure of the number of recruited axons) versus the initial slope of the evoked field excitatory postsynaptic potential (fEPSP) response. As shown in Figure 7A, there is no significant difference in the I/O curve of the *PS1* cKO and control mice ($p > 0.5$, t test). In addition, the magnitude of the maximal response is similar in the cKO (1.286 ± 1.96 V/s) and in the control (1.376 ± 0.37 V/s). To assess possible effects on the presynaptic contribution to synaptic transmission, we next examined paired-pulse facilitation (PPF), a form of short-term plasticity. The cKO and control mice exhibited similar degrees of facilitation at all inter-stimulus intervals tested ($F_{7,259} = 0.280$; $p = 0.961$) (Figure 7B). These data indicate that basal synaptic transmission and short-term plasticity are normal in hippocampal area CA1 in the absence of PS1.

Subsequently, we examined the effect of PS1 inactivation on long-term potentiation (LTP) and long-term depression (LTD) in the CA1 region of the hippocampus, which are the best understood models of the synaptic modifications involved in learning and memory (reviewed in Bailey et al., 2000; Malenka and Nicoll, 1999). Previous studies have shown that LTP is enhanced in transgenic mice overexpressing FAD-linked mutant PS1 (Parent et al., 1999; Zaman et al., 2000). To determine whether PS1 plays a role in the initiation and maintenance of LTP, we induced LTP with theta burst stimulation (TBS) or a series of high frequency stimulation (HFS, 100 Hz tetanus). The magnitude of LTP induced by 5 TBS (measured 60 min after TBS) was essentially the same in the *PS1* cKO (144.9 ± 10) and in the control (148.5 ± 7.3; $p = 0.94$, t test) (Figure 7C). A series of HFS (three 100 Hz tetani), which is a stronger but less physiological LTP induction protocol (Baranes et al., 1998), produced a larger and longer lasting form of LTP. The magnitude of LTP, including the late phase of LTP measured 140 min after the last tetanus, was comparable in *PS1* cKO (167 ± 16) and control mice (148 ± 15; $p = 0.26$) (Figure 7D). LTD has been proposed to provide a complementary mechanism to LTP for the bidirectional

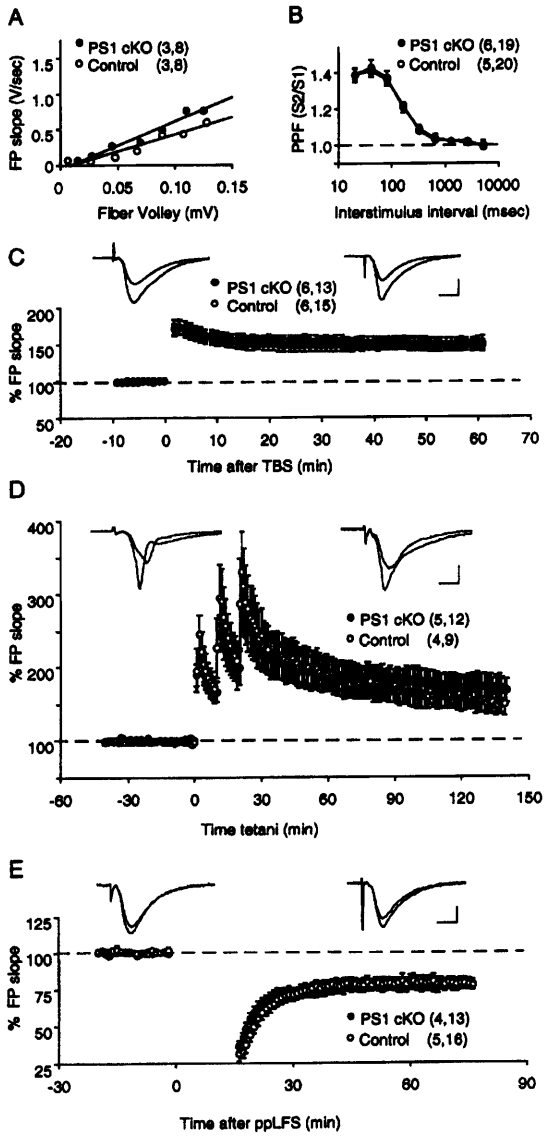

Figure 7. Normal Synaptic Transmission and Plasticity in Hippocampal Area CA1 of *PS1* cKO Mice

(A) Normal input/output curve of synaptic transmission in *PS1* cKO mice. The amplitude of the fiber volley (FV) is plotted against the initial slope of the evoked fEPSP for the cKO and littermate control mice. Each point represents data averaged across all slices for a narrow bin of FV amplitude. The lines represent the best linear regression fit (cKO: 6.6x-0.5, r2 = 0.97; control: 4.6x-0.04, r2 = 0.93).

(B) Normal paired pulse facilitation (PPF) in *PS1* cKO mice. The graph depicts the paired-pulse response ratio (2^{nd} fEPSP/1^{st} fEPSP) obtained at different interstimuls intervals (in m).

(C–E) Normal synaptic plasticity in *PS1* cKO mice. (C) Time course of the effects of 5 TBS on the fEPSP initial slope. Shown on top are examples of robust LTP induced in slices from control (left) and cKO (right) mice. Superimposed traces are averages of four consecutive responses recorded before (−1 min) and 60 min after TBS. (D) Normal late phase LTP induced by three tetanic trains (100 Hz, 1 s) in *PS1* cKO mice. The graph depicts the time course of the effects of three trains of HFS on the fEPSP initial slope. Traces on top, as in (C), were recorded before (−1 min) and 140 min after the first tetanus. (E) Normal LTD induced by paired-pulse low frequency stimulation (ppLFS) in *PS1* cKO mice. Time course of the effects of ppLFS on the fEPSP initial slope is shown. Traces on top, as in (C), were recorded before (−1 min) and 60 min after ppLFS. For all the panels, the results are expressed as average ± SEM. Filled circles represent *PS1* cKO and open circles represent controls. The number of mice (left) and slices (right) used in each experiment is indicated in parenthesis. Calibration bar: 0.5 mV, 5 ms.

modulation of synaptic efficacy (Bear, 1999). To investigate further whether PS1 plays a role in the modulation of synaptic plasticity in hippocampal area CA1, we induced LTD with a paired-pulse low frequency stimulation (ppLFS), a protocol effective in inducing LTD in slices from mature mice (Krezel et al., 1999). As shown in Figure 7E, the magnitude of LTD (measured 60 min after conditioning) was identical in the *PS1* cKO (78 ± 4) and the control (78 ± 4; p = 0.94) (Figure 7E). These results demonstrate that PS1 is not required for the induction and maintenance of LTP and LTD in the Schaeffer collateral pathway of the hippocampus.

Subtle Long-Term Spatial Memory Deficits in *PS1* cKO Mice

To assess the neuronal function of PS1 more globally, we used the Morris water maze task, a hippocampus-dependent paradigm for spatial learning and memory (Morris et al., 1982). During the acquisition phase of the task, mice learn the position of a hidden escape platform in a circular pool using distal spatial cues. Their performance is measured by the time required to locate the platform (escape latency) and by the distance traveled to reach the platform (path length). During the first 7 days of training, both groups of mice improved their performance at a similar rate, as indicated by the decreasing escape latencies and path lengths (Figures 8A and 8B). However, during the last 3 to 5 days of training, the control mice continued to improve while the performance of the cKO mice plateaued, resulting in significantly longer escape latencies and path lengths for the cKO group (Figures 8A and 8B). A two-way ANOVA showed a significant interaction effect of group x days ($F(9,261) = 2.06$; $p = 0.03$). Subsequent pairwise comparisons (Student's t tests) showed significantly longer latencies and path lengths for the cKO group versus the control group on days 8, 9, and 10 ($t(29)$; $p < 0.05$). Swimming speed and the degree of thigmotaxis (wall hugging) were similar in the cKO and control mice (data not shown), arguing against nonspecific effects due to impaired motor function and/or anxiety.

The *PS1* cKO and control mice were further tested in probe trials, in which the platform is removed from the pool, after 1, 5, and 10 days of training. If the mice have learned the position of the hidden platform using the distal cues, they tend to search preferentially in the quadrant (target quadrant) where the platform was previously located, and they swim across the precise platform location more frequently than the corresponding locations in other quadrants (platform crossings). After 1 and 5 days of training, the cKO and control mice showed no preference for the target quadrant (quadrant occupancy) and the platform location (platform crossing) relative to the remaining quadrants. After 10 days of training, both groups of mice searched preferentially in the target quadrant (Figures 8C and 8D). The total number of platform crossings by the cKO mice (2.27 ±

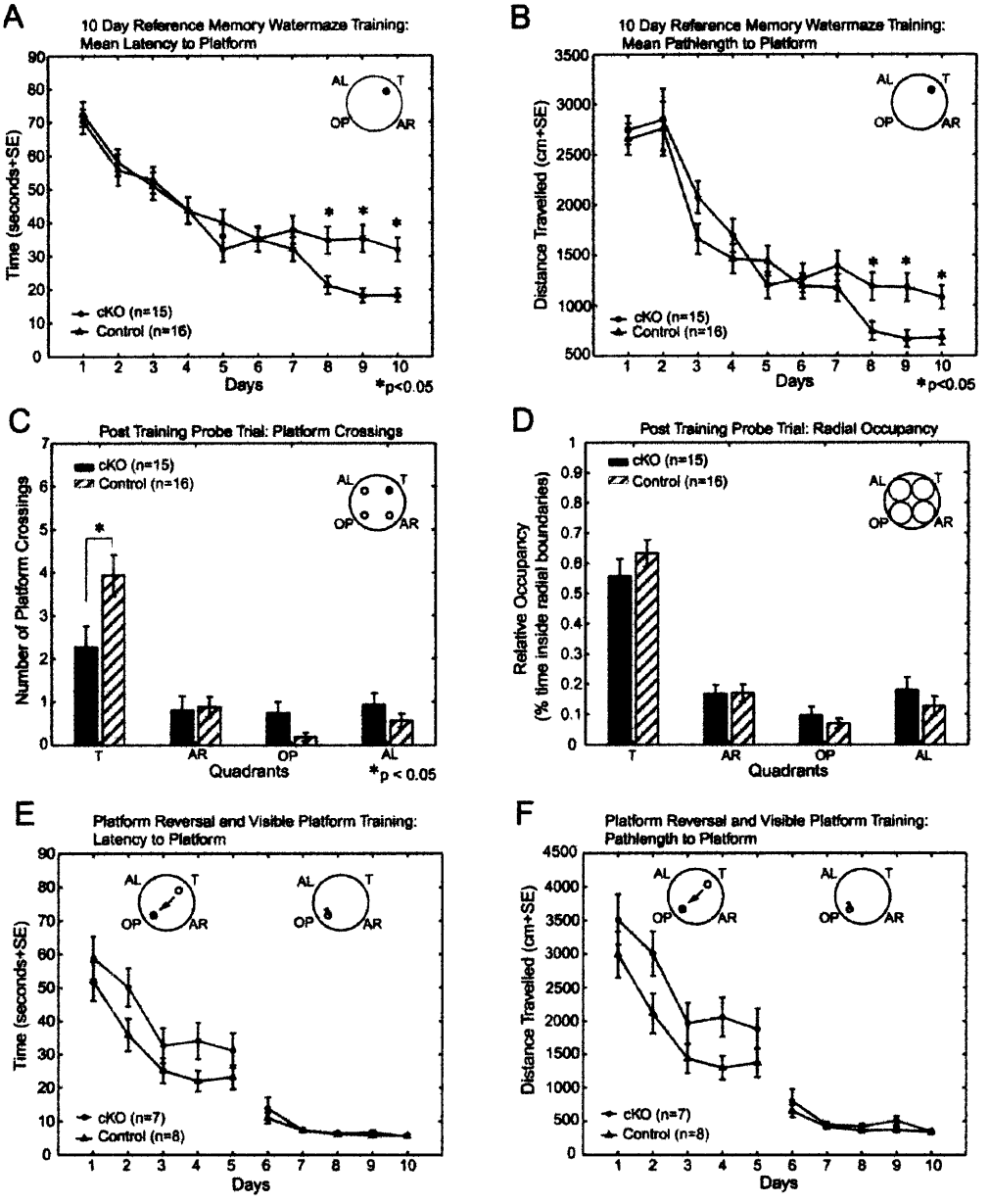

Figure 8. Mild Impairment of Spatial Learning and Memory in *PS1* cKO Mice

(A and B) Delayed escape latencies and longer path lengths exhibited by *PS1* cKO mice in the hidden platform version of the Morris water maze task. Escape latencies and path lengths of cKO and control mice over 10 days of training (four trials per day) were plotted. Both cKO and control mice learned similarly up to day 7, after which the cKO mice showed significantly longer latencies and path lengths (Student's t test, $p < 0.05$).

(C and D) Reduced platform crossings by *PS1* cKO mice in the probe trial after 10 days of training. Data were collected during the probe trial (90 s) immediately following the 10th day of training. The mean number of crossings through the target platform location was significantly lower in the cKO group (2.27 ± 0.49) than in the control group (3.94 ± 0.88) (Student's t test, $p < 0.05$). This difference indicates a subtle but significant deficit in the ability of the cKO mice to find the target using a higher spatial resolution strategy. However, radial quadrant occupancy, which is measured by the time spent in the target radial quadrant relative to the time spent in all four radial quadrants, was similar for cKO (0.557 ± 0.058) and controls (0.633 ± 0.044), indicating no significant difference in gross spatial navigation strategies between the two groups.

(E and F) Hidden platform reversal and visible platform tasks. Escape latencies and path lengths of cKO and control mice over 5 days of training (four trials per day) in the platform-reversal phase of the hidden platform water maze task were plotted. The cKO mice showed longer latencies and path lengths, particularly on days 2 and 4 ($p < 0.05$). The platform-reversal phase was followed by a 5 day visible platform version of the task. Both the cKO and control mice performed extremely well with indistinguishable latencies of ~5 s and path lengths of ~350 cm. This result indicates that the cKO mice do not exhibit a general motivational or physical deficit in swimming performance to the target location. For all the panels, the results are expressed as average ± SEM. Filled circles represent *PS1* cKO, and triangles represent controls. Abbreviations: T, target quadrant; OP, opposite quadrant; AL, adjacent left quadrant; AR, adjacent right quadrant.

0.49), however, was significantly lower than that of the control mice (3.94 ± 0.88; $p < 0.05$), though the target radial quadrant occupancies of cKO (0.557 ± 0.058) and control (0.633 ± 0.044) mice were similar ($p = 0.3$) (Figures 8C and 8D).

We then moved the hidden platform to a different location in the opposite quadrant of the pool (platform-reversal phase), and repeated the acquisition experiment for 5 more days. The displacement of the platform resulted in an initial increase in the mean escape latency and path length of both groups of mice (Figures 8E and 8F). The cKO mice again exhibited poorer performance than the controls with longer escape latencies and path lengths (e.g., $p < 0.05$ at day 4) (Figures 8E and 8F). To determine whether the delayed escape latencies of the cKO mice might be caused by deficits in motivation, sensory, and/or motor abilities, both groups of mice were also tested in the visible platform version of the task. The escape latencies and path lengths of the cKO and control mice were very low and essentially indistinguishable (Figures 8E and 8F). Taken together, these results demonstrate a mild but specific impairment in spatial learning and memory in the *PS1* cKO mice.

Discussion

Recent studies using *PS1*$^{-/-}$ cells and transition state analog inhibitors provided strong evidence that PS1 is required for γ-secretase activity (De Strooper et al., 1998; Esler et al., 2000; Li et al., 2000). It is therefore critically important to test the feasibility of targeting PS1 for anti-amyloidogenic therapies in vivo. Although germline *PS1* inactivation has been shown to reduce the production of Aβ peptides markedly in cultured embryonic neurons, a requirement for PS1 in Aβ generation in the adult cerebral cortex remained to be demonstrated. Furthermore, our previous studies showed that PS1 is required for neurogenesis and Notch downstream target genes during brain development (Handler et al., 2000; Shen et al., 1997), but it remained unclear whether PS1 played a similar role in the regulation of Notch downstream target genes in the adult brain.

To address these questions, we developed a conditional *PS1* KO mouse, in which expression of *PS1* is selectively eliminated in most neurons of the cerebral cortex beginning at postnatal day 18 (Figure 2). Here we show that the adult cerebral cortex of the *PS1* cKO mouse is morphologically normal, in contrast to the pleiotropic phenotypes associated with PS1 deficiency in the embryonic brain. Despite the differential effects of PS1 inactivation in the embryonic and adult brain, the role of PS1 in the generation of Aβ peptides appears similar. Consistent with previous studies using cultured *PS1*$^{-/-}$ neurons (De Strooper et al., 1998), we found a substantial reduction in the level of both mouse and human Aβ40 and Aβ42 in the adult cortex of *PS1* cKO mice (Table1, Figures 4C and 4D). This result provides important in vivo confirmation of the requirement for PS1 in the generation of Aβ peptides in the adult cerebral cortex, where accumulation and deposition of Aβ peptides are important and invariant features of AD. Interestingly, the reduction of Aβ40 is more significant than that of Aβ42 in the cKO mice, raising the possibility that PS2 may play a more important role in the production of Aβ42. Recent studies using embryonic stem cells derived from *PS1*$^{-/-}$;*PS2*$^{-/-}$ mice showed that in the absence of both presenilins, the level of Aβ peptides was undetectable (Herreman et al., 2000; Zhang et al., 2000). We plan to investigate whether the generation of Aβ peptides is abolished completely in the adult cerebral cortex of *PS1* cKO mice in the *PS2*$^{-/-}$ background.

The most striking feature of the disrupted APP processing is the 30-fold accumulation of the APP CTFs in *PS1* cKO mice by the age of 6 months (Figure 4). Interestingly, the APP β-CTFs (C89 and C99) accumulate differentially in the absence of PS1, with the increase in the level of C89 and C99 measuring approximately 30- and 3-fold, respectively (Figure 4). The levels of the α-CTF (C83) are also elevated by as much as 30-fold (Figure 4). Since the CTFs represent the substrates for γ-secretase cleavage, these results are consistent with a requirement of PS1 for γ-secretase activity. The differential accumulation of the CTFs, particularly C89 and C99, which are cleavage products of β-secretase, is likely due to the differences in their half lives. Alternatively, C99 could be converted to C89 by β-secretase, resulting in much lower levels of C99 relative to C89 in the cKO mice. Furthermore, we found that all APP CTFs are present in phosphorylated and nonphosphorylated forms in the brain of both control and cKO mice (Figure 4 and data not shown). The cytoplasmic domain of full-length APP has been shown to be phosphorylated in cultured neurons and adult rat brain by cdk5 on Thr668, which resides in the C-terminal region common to all APP CTF species (Iijima et al., 2000; Oishi et al., 1997). This phosphorylation event may therefore account for the observed phosphorylation of the CTFs. Although the physiological significance of APP phosphorylation is unclear, there is evidence suggesting that it may be associated with the regulation of Aβ generation and neurite extension (Ando et al., 1999; Buxbaum et al., 1993).

Identification of the close association between PS1 and the γ-secretase activity has sparked interest in the use of PS1 as a therapeutic target in AD. The critical role of PS1 in Notch signaling during neural development, however, raised the possibility that inhibition of PS1 function in the adult brain might be deleterious. In contrast to the reduction of Notch1 activity in the *PS1*$^{-/-}$ embryonic brain, as evidenced by reduced expression of *Hes5* and increased expression of *Dll1*, expression of the Notch1 downstream effector genes *Hes1*, *Hes5*, and *Dll1* is unchanged in the cortex of *PS1* cKO mice (Figure 5). It is possible that expression of PS2 in the adult cortex, which is relatively high compared to its expression in the embryonic brain, is sufficient to maintain normal expression of these Notch downstream genes. Alternatively, it is also possible that the regulation of expression of these genes in the adult brain differs from that in the embryonic brain and is independent of presenilins.

A recent report showed that the *C. elegans* PS1 homologs, sel-12 and hop-1, are required for the proper morphology and function of cholinergic interneurons (Wittenburg et al., 2000). To investigate whether PS1 plays a role in the regulation of synaptic function in the mammalian nervous system, we studied the *PS1* cKO mice for

subtle behavioral abnormalities and deficits in synaptic transmission and plasticity. Thorough examination of the cKO and littermate control mice failed to identify any significant deficits in basal synaptic transmission and plasticity in the Schaeffer collateral pathway of the hippocampus (Figure 7). However, the Morris water maze task revealed a mild delayed deficit in spatial learning and memory in the *PS1* cKO mice (Figure 8). Although the performance of the cKO mice during initial stages of learning was not significantly different from that of the control mice, the performance of the cKO mice plateaued during the later stages of this reference memory task, while the control mice continued to improve (Figure 8). In addition, the platform crossings of the cKO mice were much lower than the control in the probe trial after 10 days of training, but the target quadrant occupancy was similar in both groups of mice. The cKO mice are thus able to learn the general location of the platform, but with less spatial precision than the control mice. These findings suggest a deficit in detailed spatial navigation in the cKO mice, though gross spatial navigation is normal.

The platform-reversal phase of the task also elicited a poorer performance by the cKO mice in the escape latencies and path length from the first training day, indicating a mild learning deficit (Figure 8). The identical performance by the cKO and control mice in the visible platform task indicates that the deficits exhibited by the cKO are due to spatial learning and memory rather than a visual, motor, or motivational impairment. Elimination of PS1 expression in the adult cortex thus leads to subtle but significant deficits in learning and memory, indicating a requirement for PS1 in normal neuronal function. The normal synaptic transmission and plasticity in the Schaeffer collateral pathway in the cKO mice, however, suggest that the observed cognitive impairment may be mediated by selective abnormalities in other hippocampal or cortical circuits. It will be interesting to determine whether the absence of both presenilins will evoke more severe impairments in learning and memory.

Although loss of PS1 function did not lead to impaired synaptic transmission and plasticity in the Schaeffer collateral pathway, previous studies indicated that overexpression of FAD-linked mutant PS1, but not wild-type PS1, in transgenic mice results in enhanced LTP in this pathway (Parent et al., 1999; Zaman et al., 2000). It is unclear whether the enhancement of LTP in these transgenic mice influences their behavior, but the present results suggest that altered PS1 activity can produce alterations in learning and memory. The mechanism by which PS1 may regulate synaptic function is unknown. Recent reports have shown that the C-terminal region of PS1 interacts with PDZ domain-containing proteins, including X11α and X11β (Lau et al., 2000; Tomita et al., 1999; Xu et al., 1999). X11 proteins form a complex with Munc18-1 in the brain, which is essential for synaptic vesicle exocytosis (Borg et al., 1998; Okamoto and Sudhof, 1997; Verhage et al., 2000). In addition, X11α is part of an evolutionarily conserved heterotrimeric complex CASK/X11α/Veli, which is thought to be involved in coupling synaptic vesicle exocytosis and neuronal cell adhesion (Borg et al., 1998, 1999; Butz et al., 1998). Alternatively, PS1 may be involved in synaptic function indirectly through its role in APP processing. An interaction has been reported between the cytoplasmic YENPTY motif of APP and the PTB domain of X11α (Borg et al., 1996; Zhang et al., 1997). Although the normal physiological role of APP in the interaction of X11α and Munc18-1 and the formation of the CASK/X11α/Veli complex is unclear, the striking accumulation of the APP CTFs in the cortex of *PS1* cKO mice may disrupt these complexes and lead to deficits in synaptic function.

In summary, our analysis of the *PS1* cKO mice provides direct in vivo evidence of the requirement for PS1 in normal APP processing and the generation of amyloid peptides. Surprisingly, the regulation of the Notch downstream genes in the adult brain is independent of PS1, in contrast to the regulation of Notch activity by PS1 during brain development. It is therefore likely that therapeutic γ-secretase inhibitors will be able to achieve reduced production of Aβ peptides in the adult brain without unwanted side effects on the expression of the Notch target genes. PS1 also appears to be required for normal neuronal function in the adult brain, but the observed cognitive deficits in the *PS1* cKO mice are relatively subtle and may be restricted to specific neural circuits. In support of this notion, synaptic transmission and plasticity in hippocampal area CA1 of the cKO mice was entirely normal. It will be important, however, to determine whether mice lacking both presenilins exhibit any additional abnormalities since therapeutic γ-secretase inhibitors are likely to inhibit both PS1- and PS2-mediated activities. Based on our current study, the benefits of therapeutic γ-secretase inhibitors may outweigh the potentially detrimental effects associated with targeting PS1 function.

Experimental Procedures

Generation of Floxed *PS1*, *CaMKII-Cre*, and *PS1* cKO Mice

The targeting vector was transfected into J1 (129/Sv) ES cells, and the ES cells carrying the modified *PS1*, *fPS1*, and *PS1*$^{\Delta}$ allele were generated as described in Yu et al., 2000. The ES cells carrying the *fPS1* or the *PS1*$^{\Delta}$ allele were injected into mouse blastocysts to generate chimeric mice, which were bred to C57BL/6J to generate heterozygous *fPS1* and *PS1*$^{\Delta}$ mice, respectively. The construction of the α*CaMKII-Cre* transgene was similar to that described in Mayford et al., 1996. The α*CaMKII* promoter segment contains ~8.5 kb genomic DNA upstream of the transcription initiation site of the α*CaMKII* gene and 84 bp of the 5′ noncoding exon, which is followed by a hybrid intron, *Cre* cDNA, and the SV40 polyadenylation signal. The α*CaMKII-Cre* (*CaM-Cre*) transgene was injected into the pronucleus of C57BL/6J and CBA hybrid embryos. The transgenic mice were then backcrossed several generations to C57BL/6J. The *fPS1* mice were bred to *CaM-Cre* transgenic mice to obtain *PS1* cKO (*fPS1/fPS1;CaM-Cre* or *PS1*$^{\Delta}$*/fPS1;CaM-Cre*) and littermate control (*fPS1/fPS1* or *PS1*$^{\Delta}$*/fPS1*) mice used in the study.

In Situ Hybridization

A 260 bp sense or antisense riboprobe specific for *PS1* exons 2 and 3 was synthesized using an in vitro transcription kit (Boehringer Mannheim). In situ hybridization was carried out as previously described (Schaeren-Wiemers and Gerfin-Moser, 1993).

Western and IP-Western

The αPS1Loop antiserum (1:10,000) was raised against amino acid residues 320–375 of human PS1, and recognizes both human and mouse PS1 (Thinakaran et al., 1996). The PS2 antiserum (1:1000), G2L, was raised against a GST-PS2loop (301–361) fusion protein (Tomita et al., 1998). The following APP antibodies were used: polyclonal C7 (residues 676–695) (Knops et al., 1995); C-terminal polyclonal "Saeko" (1:10,000) (Kawarabayashi et al., 1996); monoclonal

192 (0.25 μg/ml), which specifically recognizes the C terminus of β-APPs (Knops et al., 1995); polyclonal 1736 antisera raised against N-terminal of Aβ (residues 595–611) (Haass et al., 1992); and monoclonal antibody 22C11 (0.15 μ/ml; Roche), which recognizes an N-terminal epitope (residues 66–81) of APP.

Mouse cortex was dissected on ice and homogenized in cold lysis buffer (50 mM Tris HCl, pH 7.4, 150 mM NaCl, 1% NP-40, 2 mM EDTA, protease inhibitors). Protein extracts (40 μg) of cKO and control cortex were separated on 4%–12%, 4%–20% Tris-Glycine (Invitrogen) or 16% Tris-tricine SDS-PAGE, and transferred to PVDF membrane. The blots were incubated with appropriate primary antibody and developed with enhanced chemiluminescence (ECL Plus, Amersham). For Western blotting, the same blot was also incubated with anti-tubulin antibody to normalize the amounts of total protein loaded in each lane.

ELISA Assays

For the detection of mouse endogenous Aβ peptides, the cortex of cKO and control mice was dissected on ice, and then homogenized in RIPA buffer containing complete protease inhibitors. The samples were analyzed using the BNT-77/BA27 and BNT-77/BC05 quantitative sandwich ELISA assays (Duff et al., 1996) to determine the level of Aβ40 and Aβ42, respectively. Levels of the human Aβ40 and Aβ42 peptides in the cortex of cKO and control mice that overexpress the human mutant APP transgene were measured by the 2G3/3D6 and 21F12/3D6 ELISA assays, respectively, as previously described (Johnson-Wood et al., 1997). The experimenters were blind to the genotypes of the samples.

Electrophysiology

Hippocampal slices (400 μm) from cKO and littermate control mice (aged 3–6 months) were prepared as described (Kirkwood et al., 1999). The slices were maintained in an interface storage chamber containing artificial cerebrospinal fluid (ACSF) at 30°C for at least an hour prior to recording. Stimulation (200 μs) pulses were delivered with a bipolar concentric metal electrode. Synaptic strength was quantified as the initial slope of field potentials recorded with ACSF filled microelectrodes (1 to 2 MΩ). Baseline responses were collected at 0.07 Hz with a stimulation intensity that yielded a half-maximal response. Two conditioning protocols were used to induce LTP. One was five episodes of theta burst stimulation (TBS) delivered at 0.1 Hz. TBS consisted of ten stimulus trains delivered at 5–7 Hz; each train consisted of four pulses at 100 Hz. The other protocol was three 100 Hz tetani delivered every 10 min. LTD was induced with 900 paired-pulses (40 ms apart) delivered at 1 Hz. Average responses (± SEM) are expressed as percent of pre-TBS baseline response (at least 10 min of stable responses). A repeated measures ANOVA and nonpaired t test were used to asses statistical significance. The experimenters were blind to the genotypes of the mice.

Morris Water Maze Task

The water maze is a circular pool 160 cm in diameter. Mouse position in the maze was tracked by a ceiling mounted Dragon Tracker system (60 Hz) connected to a computer. Position information was analyzed by custom Matlab software (Linus Sun and Bogdan Fedeles). Mice were housed in a standard 12 hr light-dark cycle and were tested at 2 p.m. every day. Each mouse was given four trials daily with a maximum duration of 90 s separated by a minimum of 15 min. If mice did not find the hidden platform, they were guided to the platform and allowed to remain on it for 15 s. Two groups of mice at the ages of 5 or 8 months (~eight mice per genotype per age group) were trained in the hidden platform task for 10 or 12 days, respectively. Similar results were obtained from these two independent experiments, and so the data were combined. After 1, 5, and 10 days of training, the hidden platform was removed and a 90 s probe trial was performed on both age groups. After 12 days of training in the hidden platform task, the platform was transferred to the corresponding location of the opposite quadrant (reversal of platform), and the older groups of mice (8 months, N = 7,8) were trained with four trials daily for 5 days to locate the new platform position. The same groups of mice were further tested for 5 days in the visible platform task, where a proximal cue was added to the reversed platform position. The experimenters were blind to the genotypes of the mice.

Acknowledgments

The authors would like to thank Wen Cheng and Eddie Meloni for technical assistance, Dennis Selkoe and Bing Zheng for APP antibodies and ELISA measurements of human Aβ peptides, Lennart Mucke for the APP transgenic mice, Mikio Shoji for the "Saeko" antiserum, Gopal Thinakaran for PS1 and Takeshi Iwatsubo for PS2 antisera, Peter St. George-Hyslop for PS2, and Ryoichiro Kageyama for Hes1, Hes5, and Dll1 plasmids. This work was supported in part by grants from NIH and Alzheimer's Association.

Received August 14, 2000; revised June 12, 2001.

References

Ando, K., Oishi, M., Takeda, S., Iijima, K., Isohara, T., Nairn, A., Kirino, Y., Greengard, P., and Suzuki, T. (1999). Role of phosphorylation of Alzheimer's amyloid precursor protein during neuronal differentiation. J. Neurosci. *19*, 4421–4427.

Bailey, C.H., Giustetto, M., Huang, Y.Y., Hawkins, R.D., and Kandel, E.R. (2000). Is heterosynaptic modulation essential for stabilizing Hebbian plasticity and memory? Nat. Rev. Neurosci. *1*, 11–20.

Baranes, D., Lederfein, D., Huang, Y.Y., Chen, M., Bailey, C.H., and Kandel, E.R. (1998). Tissue plasminogen activator contributes to the late phase of LTP and to synaptic growth in the hippocampal mossy fiber pathway. Neuron *21*, 813–825.

Bear, M.F. (1999). Homosynaptic long-term depression: a mechanism for memory? Proc. Natl. Acad. Sci. USA *96*, 9457–9458.

Borg, J., Straight, S., Kaech, S., De Taddeo-Borg, M., Droon, D., Karnak, D., Turner, R., Kim, S., and Margolis, B. (1998). Identification of an evolutionarily conserved heterotrimeric protein complex involved in protein targeting. J. Biol. Chem. *273*, 31633–31636.

Borg, J., Lopez-Figueroa, M., De Taddeo-Borg, M., Kroon, D., Turner, R., Watson, S., and Margolis, B. (1999). Molecular analysis of the X11-mLin-2/CASK complex in brain. J. Neurosci. *19*, 1307–1316.

Borg, J.P., Ooi, J., Levy, E., and Margolis, B. (1996). The phosphotyrosine interaction domains of X11 and FE65 bind to distinct sites on the YENPTY motif of amyloid precursor protein. Mol. Cell. Biol. *16*, 6229–6241.

Butz, S., Okamoto, M., and Sudhof, T. (1998). A tripartite protein complex with the potential to couple synaptic vesicle exocytosis to cell adhesion in brain. Cell *94*, 773–782.

Buxbaum, J.D., Koo, E.H., and Greengard, P. (1993). Protein phosphorylation inhibits production of Alzheimer amyloid beta/A4 peptide. Proc. Natl. Acad. Sci. USA *90*, 9195–9198.

Buxbaum, J., Thinakaran, G., kolliatsos, V., O'Callahan, J., Slunt, H., Price, D., and Sisodia, S. (1998). Alzheimer amyloid protein precursor in the rat hippocampus transport and processing through the perforant path. J. Neurosci. *18*, 9629–9637.

Cai, H., Wang, Y., McCarthy, D., Wen, H., Borchelt, D., Price, D., and Wong, P. (2001). BACE1 is the major b-secretase for generation of Ab peptides by neurons. Nat. Neurosci. *4*, 233–234.

de la Pompa, J.L., Wakeham, A., Correia, K.M., Samper, E., Brown, S., Aguilera, R.J., Nakano, T., Honjo, T., Mak, T.W., Rossant, J., and Conlon, R.A. (1997). Conservation of the Notch signalling pathway in mammalian neurogenesis. Development *124*, 1139–1148.

De Strooper, B., Saftig, P., Craessaerts, K., Vanderstichele, H., Guhde, G., Annaert, W., Von Figura, K., and Van Leuven, F. (1998). Deficiency of presenilin-1 inhibits the normal cleavage of amyloid precursor protein. Nature *391*, 387–390.

De Strooper, B., Annaert, W., Cupers, P., Saftig, P., Craessaerts, K., Mumm, J.S., Schroeter, E.H., Schrijvers, V., Wolfe, M.S., Ray, W.J., et al. (1999). A presenilin-1-dependent gamma-secretase-like protease mediates release of Notch intracellular domain. Nature *398*, 518–522.

Duff, K., Eckman, C., Zehr, C., Yu, X., Prada, C.-M., Perez-Tur, J., Hutton, M., Buee, L., Harigaya, Y., Yager, D., et al. (1996). Increased

amyloid-β42(43) in brains of mice expressing mutant presenilin 1. Nature *383*, 710–713.

Esler, W., Kimberly, W., Ostaszewski, B., Diehl, T., Moore, C., Tsai, J.-Y., Rahmati, T., Xia, W., Selkoe, D., and Wolfe, M. (2000). Transition-state analogue inhibitors of γ-secretase bind directly to presenilin-1. Nat. Cell Biol. *2*, 428–434.

Haass, C., Schlossmacher, M.G., Hung, A.Y., Vigo-Pelfrey, C., Mellon, A., Ostaszewski, B.L., Lieberburg, I., Koo, E.H., Schenk, D., Teplow, D.B., and Selkoe, D.J. (1992). Amyloid β-peptide is produced by cultured cells during normal metabolism. Nature *359*, 322–325.

Handler, M., Yang, X., and Shen, J. (2000). Presenilin-1 regulates neuronal differentiation during neurogenesis. Development *127*, 2593–2606.

Herreman, A., Serneels, L., Annaert, W., Collen, D., Schoonjans, L., and De Strooper, B. (2000). Total inactivation of γ-secretase activity in presenilin-deficient embryonic stem cells. Nat. Cell Biol. *2*, 461–462.

Iijima, K., Ando, K., Takeda, S., Satoh, Y., Seki, T., Itahara, S., Greengard, P., Kirino, Y., Naim, A., and Suzuki, T. (2000). Neuron-specific phosphorylation of Alzheimer's β-amyloid precursor protein by cyclin-dependent kinase 5. J. Neurochem. *75*, 1085–1091.

Jarrett, J.T., Berger, E.P., and Lansbury, P.T., Jr. (1993). The carboxy terminus of the beta amyloid protein is critical for the seeding of amyloid formation: Implications for the pathogenesis of Alzheimer's disease. Biochemistry *32*, 4693–4697.

Johnson-Wood, K., Lee, M., Motter, R., Hu, K., Gordon, G., Barbour, R., Khan, K., Gordon, M., Tan, H., Games, D., Lieberburg, I., Schenk, D., Seubert, P., and MConlogue, L. (1997). Amyloid precursor protein processing and Aβ42 deposition in a transgenic mouse model of Alzheimer disease. Proc. Natl. Acad. Sci. USA *94*, 1550–1555.

Kawarabayashi, T., Shoji, M., Sato, M., Sasaki, A., Ho, L., Eckman, C.B., Prada, C.M., Younkin, S.G., Kobayashi, T., Tada, N., et al. (1996). Accumulation of beta-amyloid fibrils in pancreas of transgenic mice. Neurobiol. Aging *17*, 215–222.

Kirkwood, A., Rozas, C., Kirkwood, J., Perez, F., and Bear, M.F. (1999). Modulation of long-term synaptic depression in visual cortex by acetylcholine and norepinephrine. J. Neurosci. *19*, 1599–1609.

Knops, J., Suomensaari, S., Lee, M., McConlogue, L., Seubert, P., and Sinha, S. (1995). Cell-type and amyloid precursor protein-type specific inhibition of a beta release by Bafilomycin A1, a selective inhibitor of vacuolar ATPases. J. Biol. Chem. *270*, 2419–2422.

Krezel, W., Giese, K.P., Silva, A.J., and Chapman, P.F. (1999). Long-term depression is unpaired in hippcampus of adult a-CAMKIIT286A. Abstr. Soc. Neurosci. *25*, 987.

Lah, J.J., Heilman, C.J., Nash, N.R., Rees, H.D., Yi, H., Counts, S.E., and Levey, A.I. (1997). Light and electron microscopic localization of presenilin1 in primate brain. J. Neurosci. *17*, 1971–1980.

Lau, K., McLoughlin, D., Standen, C., and Miller, C. (2000). X11a and X11b interact with presenilin-1 via their PDZ domains. Mol. Cell. Neurosci. *16*, 557–565.

Li, Y.-M., Xu, M., Lai, M.-T., Huang, Q., Castro, J., DiMuzio-Mower, J., Harrison, T., Lellis, C., Nadin, A., Neduvelil, J., Register, R., Sardana, M., Shearman, M., Smith, A., Shi, X.-P., Yin, K.-C., Shafer, J., and Gardell, S. (2000). Photoactivated γ-secretase inhibitors directed to the active site covalently label presenilin 1. Nature *405*, 689–694.

Luo, Y., Bolon, B., Kahn, S., Bennett, B., Babu-khan, S., Denis, P., Fan, W., Kha, H., Zhang, J., Gong, Y., et al. (2001). Mice deficient in BACE1, the Alzheimer's b-secretase, have normal phenotype and abolished b-amyloid generation. Nat. Neurosci. *4*, 231–232.

Malenka, R.C., and Nicoll, R.A. (1999). Long-term potentiation—a decade of progress? Science *285*, 1870–1874.

Mayford, M., Bach, M.E., Huang, Y., Wang, L., Hawkins, R.C., and Kandel, E. (1996). Control of memory formation through regulated expression of a CaMKII transgene. Science *274*, 1678–1683.

Minichiello, L., Korte, M., Wolfer, D., Kuhn, R., Unsicker, K., Cestari, V., Rossi-Arnaud, C., Lipp, H., Bonhoeffer, T., and Klein, R. (1999). Essential role of TrkB receptors in hippocampus-mediated learning. Neuron *24*, 401–414.

Morris, R., Garrud, P., Rowlins, J., and O'Keefe, J. (1982). Place navigation impaired in rats with hippocampal lesions. Nature *297*, 681–683.

Mucke, L., Masliah, E., Yu, G.O., Mallory, M., Rockenstein, E., Tatsuno, G., Hu, K., Kholodenko, D., Johnson-Wood, K., and McConlogue, L. (2000). High-level neuronal expression of Ab1–42 in wild-type human amyloid protine precursor transgenic mice: synaptotoxicity without plaque formation. J. Neurosci. *20*, 4050–4058.

Oishi, M., Nairn, A., Czernik, A., Lim, G., Isohara, T., Gandy, S., Greengard, P., and Suzuki, T. (1997). The cytoplasmic domain of Alzheimer's amyloid precursor protein is phosphorylated at Thr654, Ser655, and Thr668 in adult brain and cultured cells. Mol. Med. *3*, 111–123.

Okamoto, M., and Sudhof, T. (1997). Mints, Munc18-interacting proteins in synaptic vesicle exocytosis. J. Biol. Chem. *272*, 31459–31464.

Parent, A., Linden, D., Sisodia, S., and Borchelt, D. (1999). Synaptic transmission and hippocampal long-term potentiation in transgenic mice expressing FAD-linked presenilin 1. Neurobiol. Dis. *6*, 56–62.

Sasai, Y., Kageyama, R., Tagawa, Y., Shigemoto, R., and Nakanishi, S. (1992). Two mammalian helix-loop-helix factors structurally related to *Drosophila hairy* and *Enhancer of split*. Genes Dev. *6*, 2620–2634.

Schaeren-Wiemers, N., and Gerfin-Moser, A. (1993). A single protocol to detect transcripts of various types and expression levels in neural tissue and cultured cells: *in situ* hybridization using digoxigenin-labelled cRNA probes. Hisotchemistry *100*, 431–440.

Scheuner, D., Eckman, C., Jensen, M., Song, X., Citron, M., Suzuki, N., Bird, T.D., Hardy, J., Hutton, M., Kukull, W., et al. (1996). Secreted amyloid β protein similar to that in the senile plaques of Alzheimer's disease is increased *in vivo* by the presenilin 1 and 2 and *APP* mutations linked to familial Alzheimer's disease. Nat. Med. *2*, 864–870.

Shen, J., Bronson, R.T., Chen, D.F., Xia, W., Selkoe, D.J., and Tonegawa, S. (1997). Skeletal and CNS defects in presnilin-1 deficient mice. Cell *89*, 629–639.

Simons, M., de Strooper, B., Multhaup, G., Tienari, P.J., Dotti, C.G., and Beyreuther, K. (1996). Amyloidogenic processing of the human amyloid precursor protein in primary cultures of rat hippocampal neurons. J. Neurosci. *16*, 899–908.

Song, W., Nadeau, P., Yuan, M., Yang, X., Shen, J., and Yankner, B.A. (1999). Proteolytic release and nuclear translocation of Notch-1 are induced by presenilin-1 and impaired by pathogenic presenilin-1 mutations. Proc. Natl. Acad. Sci. USA *96*, 6959–6963.

Suzuki, N., Iwatsubo, T., Odaka, A., Ishibashi, Y., Kitada, C., and Ihara, Y. (1994). High tissue content of soluble β1–40 is linked to cerebral amyloid angiopathy. Am. J. Pathol. *145*, 452–460.

Takebayashi, K., Akazawa, C., Nakanishi, S., and Kageyama, R. (1995). Structure and promoter analysis of the gene encoding the mouse helix-loop-helix factor HES-5. Identification of the neural precursor cell-specific promoter element. J. Biol. Chem. *270*, 1342–1349.

Thinakaran, G., Borchelt, D.R., Lee, M.K., Slunt, H.H., Spitzer, L., Kim, G., Rotovitsky, T., Davenport, F., Nordstedt, C., Seeger, M., et al. (1996). Endoproteolysis of presenilin 1 and accumulation of processed derivatives in vivo. Neuron *17*, 181–190.

Thinakaran, G., Harris, C.L., Ratovitski, T., Davenport, F., Slunt, H.H., Price, D.L., Borchelt, D.R., and Sisodia, S.S. (1997). Evidence that levels of presenilins (PS1 and PS2) are coordinately regulated by competition for limiting cellular factors. J. Biol. Chem. *272*, 28415–28422.

Tomita, T., Maruyama, K., Saido, T.C., Kume, H., Shinozaki, K., Tokuhiro, S., Capell, A., Walter, J., Grunberg, J., Haass, C., et al. (1997). The presenilin 2 mutation (N141I) linked to familial Alzheimer disease (Volga German families) increases the secretion of amyloid β protein ending at the 42nd (or 43rd) residue. Proc. Natl. Acad. Sci. USA *94*, 2025–2030.

Tomita, T., Tokuhiro, S., Hashimoto, T., Aiba, K., Saido, T.C., Maruyama, K., and Iwatsubo, T. (1998). Molecular dissection of domains in mutant presenilin 2 that mediate overproduction of amyloidogenic forms of amyloid beta peptides. Inability of truncated forms of PS2 with familial Alzheimer's disease mutation to increase secretion of Abeta42. J. Biol. Chem. *273*, 21153–21160.

Tomita, T., Tokikawa, R., Morchashi, Y., Takasugi, N., Saido, T.C., Maruyama, K., and Iwatsubo, T. (1999). Carboxyl terminus of presenilin is required for overproduction of amyloidogenic Aβ42 through stabilization and endoproteolysis of presenilin. J. Neurosci. *19*, 10627–10634.

Verhage, M., Maia, A., Plomp, J., Brussaard, A., Heeroma, J., Vermeer, H., Toonen, R., Hammer, R., van den Berg, T., Missler, M., et al. (2000). Synaptic assembly of the brain in the absence of neurotransmitter secretion. Science *287*, 864–869.

Wittenburg, N., Eimer, S., Lakowski, B., Rohrig, S., Rudolph, C., and Baumeister, R. (2000). Presenilin is required for proper morphology and function of neurons in *C. elegans*. Nature *406*, 306–309.

Wolfe, M.S., Xia, W., Ostaszewski, B.L., Diehl, T.S., Kimberly, W.T., and Selkoe, D.J. (1999). Two transmembrane aspartates in presenilin-1 required for presenilin endoproteolysis and γ-secretase activity. Nature *398*, 513–517.

Xu, X., Shi, Y., Wu, X., Gambett, P., Sui, D., and Cui, M. (1999). Identification of a novel PSD-95/Dlg/Zo-1 (PDZ)-like protein interacting with the C-terminus of presenilin-1. J. Biol. Chem. *274*, 32543–32546.

Yu, H., Kessler, J., and Shen, J. (2000). Heterogeneous populations of ES cells in the generation of a floxed *Presenilin-1* allele. Genesis *26*, 5–8.

Zaman, S., Parent, A., Laskey, A., Lee, M., Borchelt, D., Sisodia, S., and Malinow, R. (2000). Enhanced synaptic potentiation in transgenic mice expressing presenilin-1 familial Alzheimer's disease mutation is normalized with a benzodiazepine. Neurobiol. Dis. *7*, 54–63.

Zhang, Z., Lee, C., Mandiyan, V., Borg, J., Margolis, B., Schlessinger, J., and Kuriyan, J. (1997). Sequence-specific recognition of the internalization motif of the Alzheimer's amyloid precursor protein by the X11 PTB domain. EMBO J. *16*, 6141–6150.

Zhang, Z., Nadeau, P., Song, W., Donoviel, D., Yuan, M., Bernstein, A., and Yankner, B. (2000). Presenilins are required for γ-secretase cleavage of β-APP and transmembrane cleavage of Notch-1. Nat. Cell Biol. *2*, 463–465.

Appendix D: Collaborative Contributions to "An Important Role for Neural Activity-Dependent CaMKIV Signaling in the Consolidation of Long-Term Memory"

Kang, H., Sun, L. D., Atkins, C. M., Soderling, T. R., Wilson, M. A., and Tonegawa, S. (2001). Cell *106*, 771-783.

Abstract:

Calcium/calmodulin-dependent protein kinase IV (CaMKIV) has been implicated in the regulation of CRE-dependent transcription. To investigate the role of this kinase in neuronal plasticity and memory, we generated transgenic mice in which the expression of a dominant-negative form of CaMKIV (dnCaMKIV) is restricted to the postnatal forebrain. In these transgenic mice, activity-induced CREB phosphorylation and c-Fos expression were significantly attenuated. Hippocampal late LTP (L-LTP) was also impaired, whereas basic synaptic function and early LTP (E-LTP) were unaffected. These deficits correlated with impairments in long-term memory, specifically in its consolidation/retention phase but not in the acquisition phase. These results indicate that neural activity-dependent CaMKIV signaling in the neuronal nucleus plays an important role in the consolidation/retention of hippocampus-dependent long-term memory.

My Contribution:

In the study of the dnCaMKIV mouse, we had no a priori knowledge of the mutation's behavioral consequences. Thus I conducted the Morris Watermaze behavioral analysis of these animals. I showed that these mice had a selective impairment in the formation of spatial

memories. While the animals did learn the Watermaze task, their learning performance was significantly slower and never quite matched the controls (Figure 4A,B). Upon examination of the probe trial at the end of the training session, it was clear that these mice had a selective impairment in the ability to form precise spatial memories because: the time spent in the target quadrant and number of platform crossings was significantly attenuated (Figure 4D). When I built the occupancy histograms of Watermaze probe trial performance, we can readily see from the mutant's behavior that while the mutants seemed to generally know which quadrant the target platform was located, they were entirely unable to develop a spatial strategy that would allow them to locate the hidden platform in the middle of the pool's target quadrant area (Figure 4E). Additionally when I examined the behavior of the mutants in the fixed location/visible platform task, wildtype mutants clearly employed a spatial strategy while the mutants were unable to utilize the spatial strategy and instead adopted a non-spatial strategy to find the location of the platform (Figure 5C).

Cell, Vol. 106, 771–783, September 21, 2001, Copyright ©2001 by Cell Press

An Important Role of Neural Activity-Dependent CaMKIV Signaling in the Consolidation of Long-Term Memory

Hyejin Kang,[1,2] Linus D. Sun,[2] Coleen M. Atkins,[3] Thomas R. Soderling,[3] Matthew A. Wilson,[2] and Susumu Tonegawa[1,2,4]
[1]Howard Hughes Medical Institute
[2]Center for Learning and Memory
RIKEN-MIT Neuroscience Research Center
Departments of Biology and Brain and Cognitive Sciences
Massachusetts Institute of Technology
Cambridge, Massachusetts 02139
[3]Vollum Institute
Oregon Health Sciences University
Portland, Oregon 97201

Summary

Calcium/calmodulin-dependent protein kinase IV (CaMKIV) has been implicated in the regulation of CRE-dependent transcription. To investigate the role of this kinase in neuronal plasticity and memory, we generated transgenic mice in which the expression of a dominant-negative form of CaMKIV (dnCaMKIV) is restricted to the postnatal forebrain. In these transgenic mice, activity-induced CREB phosphorylation and c-Fos expression were significantly attenuated. Hippocampal late LTP (L-LTP) was also impaired, whereas basic synaptic function and early LTP (E-LTP) were unaffected. These deficits correlated with impairments in long-term memory, specifically in its consolidation/retention phase but not in the acquisition phase. These results indicate that neural activity-dependent CaMKIV signaling in the neuronal nucleus plays an important role in the consolidation/retention of hippocampus-dependent long-term memory.

Introduction

Activity-dependent synaptic plasticity is thought to be the cellular mechanism for storing new information in the brain. Previous studies have indicated that activity-dependent increases in postsynaptic Ca^{2+} and subsequent activation of Ca^{2+}-dependent enzymes play a critical role in the relatively early phase of synaptic plasticity that may serve as a cellular cognate of memory acquisition (Bliss and Collingridge, 1993; Soderling and Derkach, 2000). The enduring phases of synaptic plasticity (e.g., L-LTP) and long-term memory seem to require cellular mechanisms that link synaptic signaling to nuclear events involving transcriptional activation and consequent protein synthesis (Frey et al., 1988; Nguyen et al., 1994). For these mechanisms, Ca^{2+} and cAMP-mediated signaling, including the cAMP-response element binding protein (CREB) and cAMP-responsive element (CRE)-dependent transcription, have been implicated in systems ranging from *Aplysia* to mammals (Bartsch et al., 1995; Bourtchuladze et al., 1994; Impey et al., 1996; Yin et al., 1994, 1995).

In mammals, the roles of Ca^{2+} and CREB in LTP and long-term memory were first addressed with a global knockout mouse in which the expression of the α and δ isoforms of CREB was disrupted (Bourtchuladze et al., 1994; Kogan et al., 1996). Under certain behavioral and electrophysiological protocols, deficits in long-term memory and synaptic plasticity were observed in these mice, however, the interpretation of these results was difficult because these mutant mice harbored compensatory increases in the level of several other CREB isoforms (Blendy et al., 1996). In addition, the confounding effects inherent to global knockout mice have made it difficult to establish a direct link between CREB function in an adult brain and the enduring form of synaptic plasticity or long-term memory.

Subsequently, a role of cAMP signaling in L-LTP and in memory consolidation was investigated by analyzing double knockout mice lacking calmodulin (CaM)-stimulated adenylyl cyclases, AC1 and AC8 (Wong et al., 1999), or transgenic mice expressing an inhibitory form (*R(AB)*) of protein kinase A (PKA) (Abel et al., 1997). Characterization of these mice revealed significant deficits in both L-LTP and long-term memory. However, L-LTP induced in hippocampal slices of these mice decayed significantly faster than that induced in control slices in the presence of a protein synthesis inhibitor, suggesting an additional role of the cAMP signaling pathway in the protein synthesis-independent, early component of L-LTP. Recent studies indeed demonstrated that PKA plays a part in the protein synthesis-independent form of LTP as well as in protein synthesis-dependent L-LTP (Blitzer et al., 1995; see discussion in Winder et al., 1998). In addition, although separate pharmacological studies implicated the cAMP signaling pathway in CREB activation (Impey et al., 1996; Yamamoto et al., 1988), it was not shown whether CREB activation was impaired in either AC1/AC8 double knockout mice or R(AB) transgenic mice. Thus, understanding the relationship between protein synthesis-dependent LTP and long-term memory, and the role of CREB in L-LTP require further studies.

The phosphorylation of CREB at Ser^{133} is essential to the transcriptional activation of CREB/CRE-mediated signaling pathway (Bito et al., 1996). Among several Ca^{2+}-dependent protein kinases that phosphorylate CREB at Ser^{133} (Sun et al., 1996), CaMKIV is the only one detected predominantly in the nuclei of neurons in adult brain (Jensen et al., 1991; Nakamura et al., 1995) and thus must be accessible to transcription factors like CREB. In cultured neurons, inhibition of endogenous CaMKIV activity by transfection with either an antisense oligonucleotide or a catalytic mutant of CaMKIV attenuates nuclear CREB phosphorylation and CRE-dependent transcription (Bito et al., 1996; Finkbeiner et al., 1997). In another study, transfection with a dominant-negative form of CaMKIV inhibited depolarization-

[4]Correspondence: tonegawa@mit.edu

induced synthesis of brain-derived neurotrophic factor (BDNF) in a CRE-dependent manner (Shieh et al., 1998). Furthermore, constitutively active CaMKIV was shown to increase the activity of CREB binding protein (CBP) and thereby stimulate CRE-dependent gene transcription. (Chawla et al., 1998; Hardingham et al., 1999; Hu et al., 1999).

Recently, two independently derived global CaMKIV knockout mice were reported and their phenotypes were very different (Ho et al., 2000; Wu et al., 2000). One of them was severely impaired in viability, fertility, and motor control and displayed poor development of cerebellar Purkinje cells (Ribar et al., 2000; Wu et al., 2000). Obviously, this mutant mouse strain is not ideal for LTP or memory studies. In contrast, the other CaMKIV knockout mouse strain exhibited no gross abnormality or motor defects, although the mice displayed some alterations in cerebellar Purkinje cell development and hippocampal physiology (Ho et al., 2000). Both basal and depolarization-induced CREB phosphorylation were reduced, and hippocampal E-LTP and L-LTP were impaired. The early onset of L-LTP deficit, namely that observed within the first 5 min after induction, suggests alterations in resident synaptic molecules in addition to those in CREB/CRE-mediated nuclear transcription events. These knockout mice showed no detectable impairment in spatial learning despite clear deficits in hippocampal LTP and cerebellar L-LTD. However, the mutant mice carried truncated transcripts and it was not clear whether the CaMKIV activity was entirely eliminated. Multiple effects that can occur in global knockout mice, including compensation during development, complicate the interpretation of these results.

To identify more specifically the role of CaMKIV in long-term memory, we generated and analyzed transgenic mice in which a dominant-negative form of CaMKIV (dnCaMKIV) inhibits Ca^{2+}-stimulated CaMKIV activity only in the postnatal forebrain.

Results

Generation of Transgenic Mice Expressing dnCaMKIV in the Postnatal Forebrain

We constructed a vector with the following components from 5′ to 3′ (Figure 1A): αCp-FLAG-*dnCaMKIV*-SV40 intron-SV40 pA, where αCp is the 8.5 kb DNA fragment derived from the 5′ flanking region of the *αCaMKII* gene and FLAG-*dnCaMKIV* encodes an epitope tag fused to the amino terminus of dnCaMKIV. We produced ten transgenic founders (C57BL/6) and chose three lines, C7, C15, and C34, carrying approximately 15, 2, and 1 copies of the transgene, respectively. Northern blot analysis of forebrain RNA, using a probe specific for the 3′ end of the transgene, revealed that a transgene transcript of about 2.4 kb was expressed in all three lines (Figure 1B). As a control, we examined the endogenous levels of *αCaMKII* transcripts and found no discernable difference between the transgenic and control mice (Figure 1B). To minimize the risk of nonspecific effects of the transgene, we selected C34, the lowest expressor among the three transgenic lines, for further characterization. The expression of the transgene in line C34 was relatively high in the cerebral cortex and hippocampal formation, lower in the striatum, amygdala, and olfactory bulb, and undetectable in the cerebellum (Figure 1C). Within area CA1 of the hippocampus, transgene expression was confined to the pyramidal cell layer (Figure 1D).

Western blot analysis carried out using anti-FLAG antibody detected the epitope tag of the transgenic dnCaMKIV protein in the forebrain of C34 mice but not in that of control littermates (Figure 1E). The anti-CaMKIV catalytic domain antibody detected the endogenous CaMKIV protein in control mice, and both the endogenous CaMKIV and the transgenic dnCaMKIV protein in transgenic mice. The total level of CaMKIV immunoreactivity in the forebrain of C34 mice was at least 2- to 3-fold higher than that in wild-type littermates. The level of the expression of other synaptic proteins such as αCaMKII and actin did not seem to be affected by the transgene (Figure 1E).

There was no difference in basal CaMKIV activity in the hippocampal homogenates of wild-type and C34 transgenic mice (Figure 1F). However, when the hippocampal slice was treated with KCl, CaMKIV activity was significantly lower (~80% reduction) in the homogenates derived from transgenic mice compared to those from the wild-type littermates. We also examined the activity of CaMKII in the hippocampal homogenates. As shown in Figure 1F, neither basal activity nor the activity induced by KCl treatment was significantly affected by the presence of the *dnCaMKIV* transgene in C34 mice. The transgenic animals appear healthy, are fertile, and exhibit no obvious behavioral abnormalities. Furthermore, terminal deoxynucleotidyl transferase-mediated biotinylated-dUTP nick-end labeling (TUNEL) assay revealed that the expression of the *dnCaMKIV* transgene did not alter the viability of cells in the adult hippocampus (see Supplmental Data available online at http://www.cell.com/cgi/content/full/106/6/771/DC1).

Suppression of CREB Phosphorylation and CRE-Dependent Gene Expression

We first tested the ability of dnCaMKIV to prevent CREB/CRE-mediated transcription using COS7 cells. Constitutively active forms of CaMKIV (caCaMKIV) and CaMK kinase (caCaMKK) were used to assess CRE-mediated transcription to avoid the complex effects of elevated intracellular Ca^{2+} on other endogenous Ca^{2+}-activated enzymes (Enslen et al., 1996). Cells were transfected with plasmids as indicated in Figure 2A and CRE-mediated transcription was assayed using a CRE-luciferase reporter construct (Grewal et al., 2000). Transfection with caCaMKIV alone had no effect, whereas cotransfection with caCaMKK gave a 5- to 6-fold increase in luciferase activity (Figure 2A). This increase in CRE-mediated transcription was almost completely blocked by cotransfection with dnCaMKIV or a CREB mutant in which Ser^{133} was mutated to Ala (Figure 2A).

We next examined the ability of dnCaMKIV to inhibit activity-induced CREB phosphorylation in hippocampal slices of C34 transgenic mice. For this purpose, we perfused C34 or wild-type hippocampal slices with saline containing 90 mM KCl or 100 μM glutamate, and 30 min later determined the levels of Ser^{133}-phosphorylated CREB (pCREB) by Western blot analysis. In wild-type slices, both KCl and glutamate treatments resulted in robust increases in CREB phosphorylation, whereas

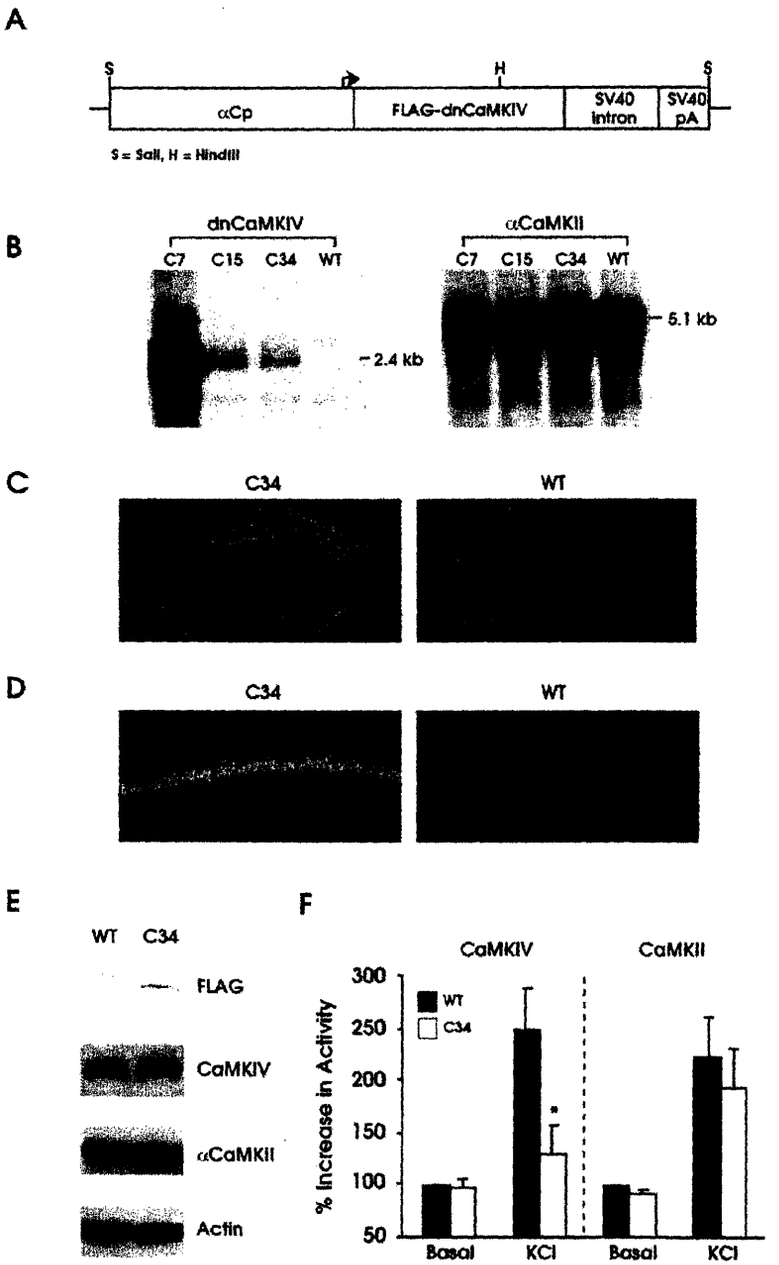

Figure 1. Expression of the *dnCaMKIV* Transgene Inhibits Depolarization-Induced Activation of Endogenous CaMKIV

(A) Schematic representation of the *dnCaMKIV* transgenic construct.

(B) Northern blot analysis of total RNA from the forebrain of three transgenic lines, C7, C15, and C34. The SV40 probe detects the 2.4 kb transgenic mRNA. The α*CaMKII* probe reveals the normal expression of 5.1 kb α*CaMKII* mRNA in the transgenic mice.

(C) Regional distribution of the *dnCaMKIV* transgene in line C34 revealed by in situ hybridization. Sagittal sections from the brains of transgenic (C34, left) and wild-type (WT, right) mice were hybridized with the SV40 probe specific to the transgene.

(D) Expression of the transgene in CA1 region of the hippocampus.

(E) Western blot analysis of forebrain extracts from wild-type and C34 mice. Both anti-FLAG and anti-CaMKIV antibodies detect ~66 kDa transgenic protein, which is slightly bigger than the endogenous form of CaMKIV. The *dnCaMKIV* transgene does not alter the expression of other synaptic proteins.

(F) Enzyme activity determined in hippocampal extracts from wild-type and C34 mice. The activity of immunoprecipitated CaMKIV (left) or CaMKII (right) was measured by the phosphorylation of a specific peptide substrate. Depolarization-induced CaMKIV activity is significantly inhibited in the hippocampus of transgenic mice (wild-type [WT]: 249.6 ± 41%, n = 8; C34: 129.5 ± 27.8%, n = 5, $p < 0.05$). The activity of CaMKII appears normal in C34 transgenic mice (WT: 223.4 ± 39%, n = 7; C34: 193.7 ± 37.5%, n = 4, ns). *$p < 0.05$ for C34 versus control group.

only modest increases were observed in C34 slices (Figures 2B and 2C). The effects of the transgenic dnCaMKIV were specific for stimulation-induced CREB phosphorylation and no difference was observed in the basal levels of CREB phosphorylation. Furthermore, the total amount of CREB was not affected either by the presence of dnCaMKIV or by the stimulation treatments.

It is known that activation of some of the immediate early genes such as *c-fos* depends on CREB phosphorylation (Sheng and Greenberg, 1990). We therefore examined whether transgenic dnCaMKIV inhibits activity-dependent c-Fos expression. We found that the levels of KCl- and glutamate-induced c-Fos were significantly lower in C34 slices compared to wild-type slices 3 hr after KCl or glutamate treatments (Figures 2B and 2C). The effect of dnCaMKIV was specific to the inhibition of CaMKIV-mediated CREB phosphorylation and c-Fos expression. We did not observe any effect of transgenic dnCaMKIV on the level of pCREB or c-Fos induced by an activator of PKA signaling pathway, forskolin (50 μM; Figures 2B and 2C). In addition, KCl-induced phosphorylation of mitogen-activated protein kinase (MAPK) was not affected (Figure 2D). Taken together, these data indicate that CaMKIV signaling is crucially involved in Ca^{2+}-stimulated CREB phosphorylation and activation of CRE-dependent transcription in the adult hippocampus, and that this signaling is significantly impaired in *dnCaMKIV* transgenic mice.

Normal Synaptic Transmission and Impaired L-LTP

We examined basal synaptic transmission at Schaffer collateral-CA1 synapses of hippocampal slices derived

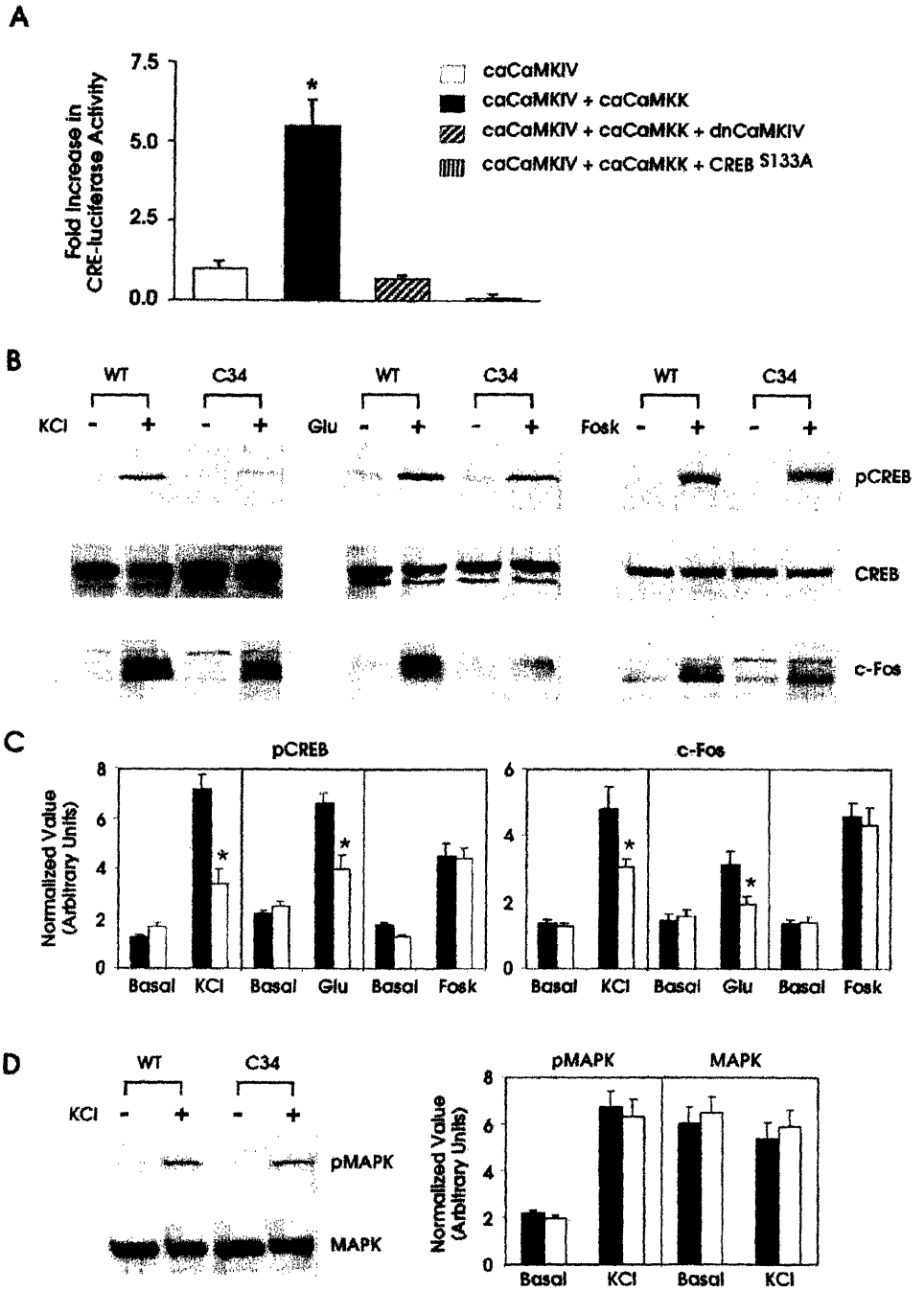

Figure 2. Expression of dnCaMKIV Suppresses Activity-Induced CREB Phosphorylation and CRE-Dependent Gene Expression

(A) Effects of dnCaMKIV on CRE-mediated transcription. COS7 cells were transfected with plasmids expressing the reporter gene CRE-luciferase and caCaMKIV alone (open bar) or with (all others) caCaMKK. DnCaMKIV or CREB^{S133A} was transfected as indicated. Luciferase activity was measured in the cell extracts: caCaMKIV alone (1.0 ± 0.20, n = 12) or with caCaMKK (5.5 ± 0.79, n = 12, $p < 0.001$). This CaMKIV/CaMKK stimulation of luciferase expression was completely inhibited when cells were transfected with either dnCaMKIV (0.67 ± 0.11, n = 6) or CREB^{S133A} (0.08 ± 0.10, n = 6).

(B) Immunoblot analysis of hippocampal extracts from wild-type and C34 transgenic slices stimulated with KCl, glutamate (Glu), or forskolin (Fosk). The blots were probed with anti-pCREB, anti-CREB, or anti-c-Fos antibodies, respectively.

(C) Quantification of average pCREB and c-Fos immunoreactivity obtained from three independent experiments. *$p < 0.05$ for C34 versus control group.

(D) Immunoblot analysis of hippocampal extracts from either unstimulated or KCl-stimulated wild-type and C34 transgenic slices. The blots were probed with anti-pMAPK or anti-MAPK antibodies. Right panel, quantification of average pMAPK and MAPK immunoreactivity obtained from two independent experiments.

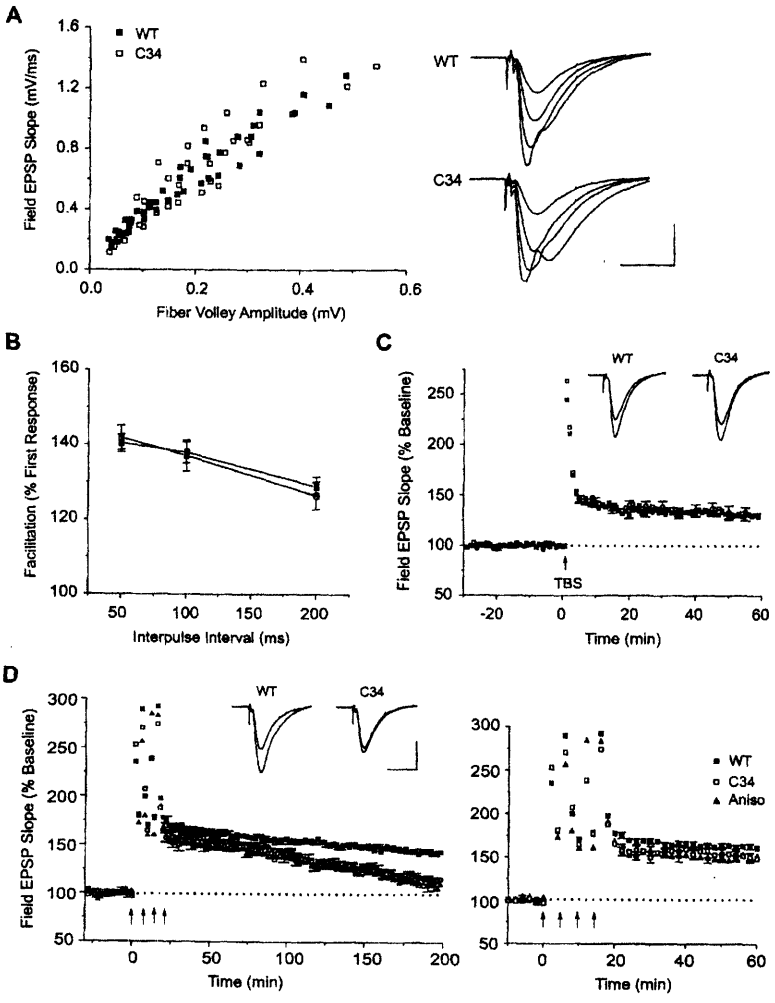

Figure 3. L-LTP Is Disrupted in *dnCaMKIV* Transgenic Mice

(A) Input-output curves plotting the fEPSP slopes and their corresponding presynaptic fiber volley amplitudes in wild-type (filled squares) and C34 transgenic (open squares) slices (n = 8 mice, 41 slices). Superimposed representative EPSPs shown were obtained at stimulation strength 15, 20, 30, and 50 μA. Calibration bars, 1 mV and 20 ms.

(B) Paired-pulse facilitation is not altered. The facilitation ratio (slope of second EPSP/slope of first EPSP) was plotted as a function of interpulse interval, 50, 100, and 200 ms (n = 9 mice, 16 slices). For each group, the mean ± SEM is indicated.

(C) LTP induced by theta-burst stimulation (TBS). Significant LTP was elicited in both groups after TBS. Superimposed representative EPSPs shown were recorded 5 min before and 1 hr after LTP induction.

(D) Late-phase LTP (L-LTP) induced by four trains of tetanic stimulation spaced by 5 min intervals. Right panel, magnified view of the first 60 min of L-LTP. Filled triangles indicate L-LTP obtained with wild-type slices in the presence of anisomycin (Aniso). Superimposed representative EPSPs shown were recorded 5 min before and 3 hr after L-LTP induction. Calibration bars, 1 mV and 20 ms.

from wild-type and transgenic animals. The synaptic input-output relationship, namely field EPSP (fEPSP) slopes versus their corresponding presynaptic fiber volley amplitudes elicited at different stimulus strengths, was not different between wild-type and C34 slices (Figure 3A). The mean ratios of fEPSP slope to fiber volley sizes for wild-type (3.45 ± 0.11, n = 41) and C34 transgenic mice (3.43 ± 0.12, n = 41) were comparable, indicating that the transgenic dnCaMKIV did not perturb basic synaptic response properties.

Because the transgene is expressed in both CA1 and CA3 pyramidal neurons in C34 transgenic line (see Figure 1C), we examined the integrity of the presynaptic machinery by analyzing two forms of short-term synaptic plasticity, paired-pulse facilitation (PPF) and posttetanic potentiation (PTP). At all interpulse intervals, PPF was indistinguishable in wild-type and mutant slices (Figure 3B). The peak PTP elicited by 100 Hz stimulation was also normal in C34 transgenic mice (WT: 256.1 ± 8.7%, n = 9; C34: 263.3 ± 12.1%, n = 9, ns). These data suggest that presynaptic neurotransmitter release processes are not affected by the expression of *dnCaMKIV* transgene.

We next explored the role of CaMKIV in LTP induction. Administration of theta burst stimulation (TBS) at 100 Hz produced LTP that was similar in wild-type and transgenic mice (Figure 3C). The magnitude of potentiation measured at 1 hr after stimulation was 129.9 ± 3.0% (n = 10) for wild-type and 131.5 ± 5.9% (n = 9) for C34 transgenic mice. We then addressed the role of CaMKIV in L-LTP, especially its protein synthesis-dependent late phase, by applying repeated tetanization to the Schaffer collateral pathway. Wild-type slices showed stable L-LTP for at least 200 min, whereas the same stimulation protocol produced a continually decaying potentiation in C34 mutant slices (Figure 3D). The potentiation observed in mutant slices was significantly less than that observed in wild-type at 3 hr (WT: 145.5 ± 1.5%, n = 9; C34: 117.9 ± 2.7%, n = 9, $p < 0.05$), and this significance appeared from 1 hr posttetanization (WT: 162.0 ± 1.9%, n = 9; C34: 147.9 ± 5.5%, n = 9, $p < 0.05$). The decay kinetics of L-LTP in C34 transgenic mice was similar to that observed with L-LTP in wild-type slices in the presence of a protein synthesis inhibitor, anisomycin (Aniso, 40 μM, at 1 hr: 150.4 ± 8.1%; at 3 hrs: 115.5 ± 7.9%, n = 7, ns for C34 versus Aniso) (Figure 3D). Anisomycin (40 μM) did not exert any effect on a nonpotentiated baseline synaptic transmission (at 1 hr: 101.6 ±

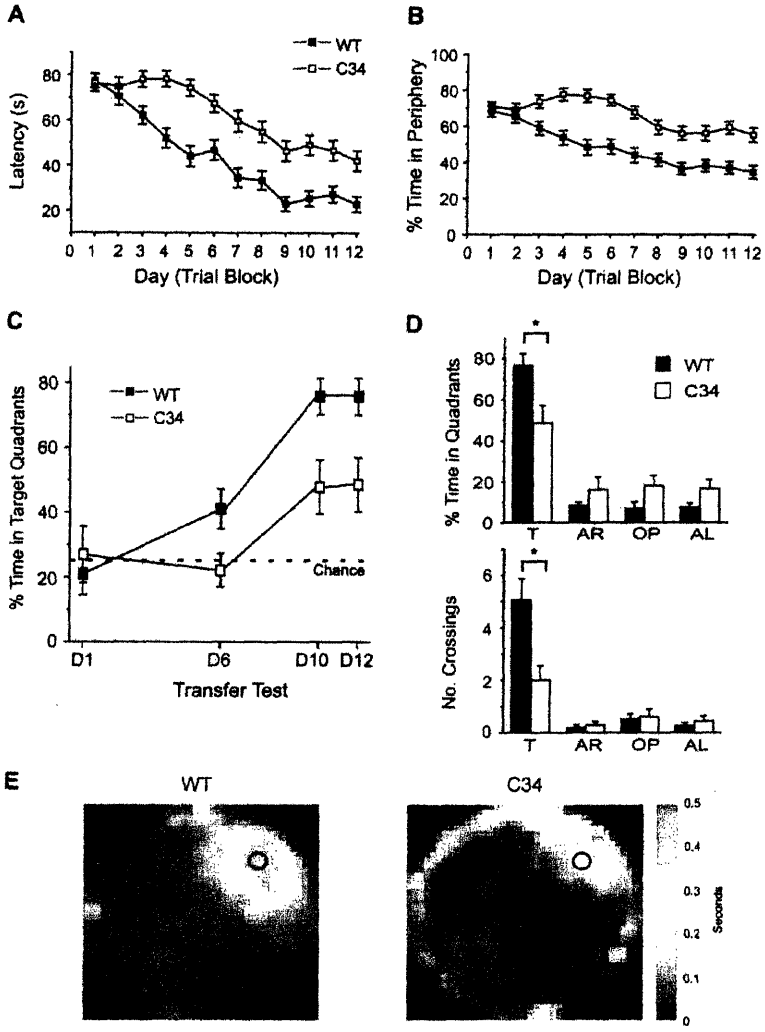

Figure 4. The Performance of *dnCaMKIV* Transgenic Mice in a Spatial Memory Task—Morris Water Maze

The transgenic mice are impaired in the hidden platform version of the Morris water maze. Mean ± SEM values are plotted against the training day for the wild-type (filled squares, n = 15) and C34 transgenic (open squares, n = 13) mice.

(A) Mean escape latencies for each group to reach the hidden platform. The transgenic mice display a longer latency in every block (4 trials per day) than the wild-type mice. On the last day of training (12th day), the transgenic mice took 42 ± 4.5 s to find the platform whereas the wild-type controls required only 22.8 ± 3.4 s ($p < 0.05$).

(B) Mean percentage of swim time spent in the peripheral portion (outer 40% of the total volume) of the pool for each group. The transgenic mice show a higher tendency of thigmotaxis than the wild-type controls from the 3rd day of training.

(C) Comparison of mean percentage of time (± SEM) spent in target quadrant by wild-type and C34 mice in probe trials on day 1 (WT: 20.9 ± 6.5%; C34: 26.9 ± 8.7%, $p > 0.1$), day 6 (WT: 41.1 ± 6.2%; C34: 22.1 ± 5.2%, $p < 0.05$), day 10 (WT: 76.6 ± 4.4%; C34: 47.1 ± 8.5%, $p < 0.05$), and day 12 (see below).

(D) Results of the probe trial given on day 12. Upper panel, mean percentage of time (± SEM) spent searching in each quadrant for the wild-type (76.7 ± 6.5%) and C34 transgenic mice (48.7 ± 8.4%). Lower panel, mean number of target platform crossings performed by wild-type mice compared to the transgenic mice (WT: 5.1 ± 0.8 crossings; C34: 2.0 ± 0.6 crossings). There is a significant group difference in both measures. *$p < 0.05$ for C34 versus control group. T, target quadrant; AR, adjacent right quadrant; OP, opposite quadrant; and AL, adjacent left quadrant.

(E) The activity histogram representing the total occupancy by wild-type and transgenic mice during the last probe test. Each pixel represents 4 × 4 cm^2 space. The wild-type mice are more accurate than the transgenic mice in searching the previous platform location (black circle).

2.5%; at 3 hrs: 98.4 ± 4.2%, n = 7, ns). This suggests that CaMKIV signaling may contribute to the protein synthesis-dependence of L-LTP.

Impaired Spatial Memory in Morris Water Maze Task

To investigate whether *dnCaMKIV* transgenic mice display a deficit in hippocampus-dependent learning and memory that may correlate with the synaptic plasticity impairments, we subjected these mice to the hidden platform version of the Morris water maze (Morris et al., 1982). The C34 transgenic mice consistently showed longer escape latencies (Figure 4A), although they displayed some improvement in their performance over prolonged training. There were no differences between the two types of mice during the first two days of training, suggesting that the learning impairments of the transgenic mice were not associated with initial performance deficits such as motor impairment. However, the C34 mice showed a greater tendency than the wild-type animals to swim in the vicinity of the pool wall (Figure 4B, see below). As shown in Figures 4C and 4D, with the control mice, the preference for the target quadrant increased steadily from a random level on day 1 to over 75% on day 10 and day 12. By contrast, with C34 transgenic mice, the preference for the target quadrant remained at a random level until day 6 and then increased to a moderate level (~47%) on day 10. Two more days of training did not further improve their quadrant preference (~48% on day 12). Even when both groups reached the plateau in their performance by day 12, the spatial memory attained by C34 transgenic mice seemed to be less accurate, as indicated by a larger difference in the number of platform crossing between the two genotypes (Figure 4D). This last point is further demonstrated by the analysis of the navigational paths: while wild-type mice exhibited a high total occupancy peak at the expected location of the platform, the transgenic mice navigated more diffusely around it (Figure 4E).

We next tested the wild-type and C34 transgenic mice in the fixed location/visible platform version of the Morris water maze (McDonald and White, 1994; Morris, 1981).

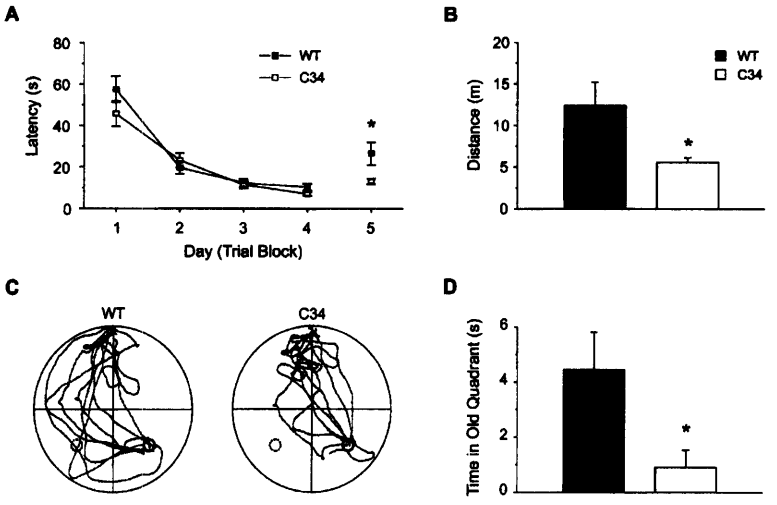

Figure 5. The Performance of *dnCaMKIV* Transgenic Mice in a Fixed Location/Visible Platform Task

(A) Mean escape latencies for each group across 4 days of acquisition trials and on a single competition test on the 5th day. The C34 transgenic mice (open squares, n = 8) are comparable to the wild-type controls (filled squares, n = 8) during the acquisition trials, but escape faster than the wild-type mice to the new platform location on the competition test (WT: 26.4 ± 5.5 s; C34: 13.0 ± 1.3 s, $p < 0.05$).

(B) Mean path lengths for each group to reach the new platform location during the competition test. The wild-type mice (black, WT: 12.4 ± 2.8 min) take longer than C34 mice (white, C34: 5.6 ± 0.5 min, $p < 0.05$) to find the platform in a different quadrant.

(C) Distribution of the swim paths of wild-type and C34 transgenic mice on the competition test. The visible platform is symbolized as a circle with solid line, and the location of the platform during the acquisition trials is shown as a circle with dotted line.

(D) Average time spent in old quadrant for wild-type (black, n = 8) and C34 transgenic (white, n = 8) mice. The C34 mice (4.46 ± 1.4 s) spent significantly longer time in old quadrant than WT mice (0.9 ± 0.6 s, $p < 0.05$). *$p < 0.05$ for C34 versus control group.

The transgenic and wild-type littermates displayed similar latency curves (Figure 5A). The average swimming speed and fractional periphery occupancy were also indistinguishable between the two groups (data not shown). However, on the 5th day when the visible platform was moved to a new location (competition test) (Devan and White, 1999), the wild-type mice exhibited significantly longer latencies than the transgenic mice (Figure 5A) and the distance they traveled to reach the new platform location was also greater than C34 transgenic mice (Figure 5B). Most of the wild-type mice (5 out of 8) swam to the area within 15 cm of the perimeter of the previous platform location, prior to directing themselves toward the visible platform which was placed in the adjacent quadrant. In contrast, 6 out of 8 transgenic mice swam directly to the new platform location (Figure 5C). The average time spent in the old quadrant (Figure 5D) also indicates that the wild-type mice preferentially employed a spatial strategy even in this visible platform version of the Morris water maze. The data suggest that the transgenic mice are impaired in the ability to use a spatial strategy and rely more on a cue-platform association strategy.

We subjected C34 transgenic mice and wild-type littermates to open-field and elevated plus maze tests. The percent dwell time in the open arms, percent number of entries into the open arms (Figure 6A), and the total number of entries into the closed and open arms (Figure 6B) were all comparable between the two groups of mice. We also found that the two types of mice were indistinguishable in both total and marginal activity in the open-field test (Figures 6C and 6D). These findings suggest that the observed higher thigmotactic tendency of C34 transgenic mice (Figure 4B) may be caused by an impairment in learning the spatial location of the platform rather than the general locomotor or emotional defects such as reduced activity or increased anxiety.

Selective Deficits in Long-Term Memory of Contextual Fear Conditioning

Because the Morris water maze task requires repeated training over several days, it is likely that the spatial memory evaluated by probe trials at day 6 and day 12 is a composite measure of acquisition and consolidation/retention of spatial memory. To assess the role of CaMKIV in different temporal phases of the mnemonic process, we turned to contextual fear conditioning in which the acquisition and consolidation phases are expected to overlap less. Thus, if CaMKIV is solely involved in the latter phase, the transgenic mice may show an enhanced decay of an initially normal freezing response over time. To address this issue, we tested mice in the same context at 24 hr and 7 days after 1 tone (CS)/shock (US) training. The *dnCaMKIV* transgenic and wild-type mice showed similar levels of freezing at 24 hr after training (Figure 7A). By contrast, transgenic mice exhibited a significant reduction (~40%) in context-dependent freezing compared to wild-type controls 7 days after training (one way ANOVA: $p < 0.05$). As Figure 7B shows, the *dnCaMKIV* mice displayed normal memory for cued conditioning at 24 hr or 7 days after training. These data suggest that *dnCaMKIV* transgenic mice have a selective deficit in the consolidation/retention phase of context-dependent fear memory.

Discussion

Importance of CaMKIV Function in CREB Phosphorylation and CRE-Dependent Gene Transcription

Using conditional transgenic mice in which the dominant-negative transgene inhibited the activation of endogenous CaMKIV only in the postnatal forebrain, we have shown that CaMKIV is crucially involved in Ca^{2+}-induced CREB phosphorylation and c-Fos expression.

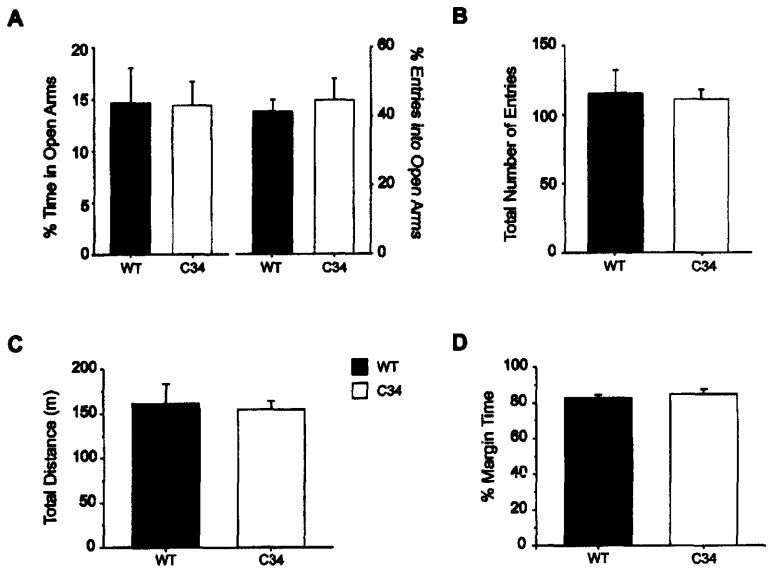

Figure 6. Normal Performance of *dnCaMKIV* Transgenic Mice in Elevated Plus Maze and Open Field Test

Mean ± SEM values are shown for the wild-type (black, n = 8) and C34 transgenic (white, n = 8) mice. There are no significant differences between groups in any of these test variables.

(A and B) Elevated plus maze. The wild-type and transgenic mice did not reveal significant difference in percent of time spent on the open arms or percent number of entries into the open arms during the 10 min testing (A). Total number of entries into the open or closed arms was also similar in wild-type and transgenic mice (B).

(C and D) Open field activity. The results show that the two groups of mice explore the activity chamber similarly. There were no group differences in activity indices such as total distance traveled (C) and percent of time spent within a margin of 1 cm from the wall (D) during the 10 min testing.

The modest yet still significant stimulation-induced increases in pCREB and c-Fos signals detected in slices from the C34 transgenic mice may be due to the incomplete inhibition of endogenous CaMKIV by dnCaMKIV (Figure 1F) and/or the involvement of other kinases in CREB/CRE signaling pathway. Ser^{133} phosphorylation of CREB has been shown to depend on multiple Ca^{2+}-activated kinases including PKA and MAPK (Impey et al., 1998; Wu et al., 2001). In fact, both PKA and MAPK signaling pathways are intact in C34 transgenic mice (Figures 2B, 2C, and 2D). A recent study suggests that the fast CaMKIV-dependent pathway and the slower MAPK-dependent pathway contribute to pCREB formation at different times after stimulation, and convey differential information to the nucleus with respect to the precise timing and stimulus amplitude, respectively (Wu et al., 2001).

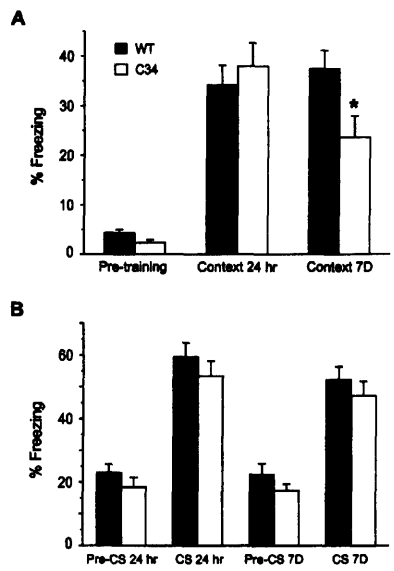

Figure 7. Fear Conditioning in *dnCaMKIV* Transgenic Mice

The transgenic mice show a selective impairment in long-term memory for contextual fear conditioning. Mean ± SEM values are plotted against the test day for the wild-type (black, n = 16) and C34 transgenic (white, n = 16) mice.

(A) Freezing responses for each group at 24 hr and 7 days after conditioning in the same context. The transgenic mice display significantly less freezing compared to wild-type mice after 7 days (WT: 37.5 ± 3.6%; C34: 22.9 ± 1.3%, $p < 0.05$) but not after 24 hr (WT: 34.3 ± 3.9%, C34: 38.0 ± 4.7%, ns). *$p < 0.05$ for C34 versus control group.

(B) Cued fear conditioning revealed no significant difference between wild-type and C34 mice at 24 hr (WT: 59.4 ± 4.4%; C34: 53.5 ± 4.6%, ns) or 7 days after conditioning (WT: 52.3 ± 3.9%; C34: 47.4 ± 4.6%, ns).

In the global CaMKIV knockout mice, the basal level of pCREB was also reduced (Ho et al., 2000; Ribar et al., 2000). In contrast, we did not observe any difference in basal levels of CREB phosphorylation or c-Fos expression in our transgenic mice (Figures 2C, 2D, and 2E). Thus, the basal level phosphorylation of CREB and activation of the *c-fos* gene seem to be achieved by the activity of CaMKIV in its basal state, which is not affected by the transgenic dnCaMKIV. A previous study also reported similarly selective action of this dominant-negative form of CaMKIV on depolarization-induced activity of CaMKIV (Impey et al., 1998). Although further work is needed to determine precise mechanisms for the dominant-negative effect of transgenic dnCaMKIV, one possibility is that the catalytically inactive form of CaMKIV with a mutation in the ATP binding site (Lys^{71}→Ala) binds to CREB and inhibits the interaction between CREB and potential CREB kinases. This mechanism, however, would not result in the specific inhibition of stimulus-induced CREB phosphorylation, which was shown in this study (Figures 2B and 2C). Moreover, our experiments showing that dnCaMKIV is without effect on PKA-mediated CREB phosphorylation do not support this possibility (Figures 2B and 2C). Another possibility is that dnCaMKIV competes with endogenous CaMKIV for the phosphorylation by CaMKK. It is known that the large increases in CaMKIV activity induced by massive depolarization require the phosphorylation of Thr^{196} by CaMKK (Tokumitsu and Soderling, 1996). The trans-

genic dnCaMKIV with Thr^{196}→Ala mutation may inhibit the stimulus-induced activation of endogenous CaMKIV by competitively blocking this critical phosphorylation event. In that case, dnCaMKIV would not interfere with the basal activity of CaMKIV but would prevent further increase of its activity mediated by CaMKK. This possibility is further supported by our experiments showing that dnCaMKIV prevents the transcriptional activation mediated by CaMKK-CaMKIV signaling in COS7 cells (Figure 2A). It should be noted that the inhibition of CaMKK function by dnCaMKIV may also hamper the function of CaM kinase I (CaMKI), which is also known to be activated by CaMKK (Sun et al., 1996). However, it is unlikely that the inhibition of CaMKI contributes to the observed effects of dnCaMKIV on CREB phosphorylation since CaMKI is not expressed in the neuronal nucleus (Picciotto et al., 1995). Regardless of the actual mechanism, the selective effects of dnCaMKIV on stimulus-induced CaMKIV activation and CREB phosphorylation allowed us to assess the consequence of these stimulus-induced events in synaptic plasticity and memory.

L-LTP Is Disrupted in *dnCaMKIV* Transgenic Mice

Activation of CREB and CRE-dependent transcription have been proposed to contribute to L-LTP but not to E-LTP (Impey et al., 1996; Silva et al., 1998). In support of these notions suggested by earlier studies, both the CREB-dependent signaling pathway in the hippocampus and the L-LTP at Schaffer collateral-CA1 synapses were impaired in our forebrain-specific *dnCaMKIV* transgenic mice. Furthermore, as shown in Figure 3D, the decay kinetics of L-LTP in C34 slices parallels that observed in anisomycin-treated wild-type slices, suggesting a specific inhibition of protein synthesis-dependent component of L-LTP by transgenic dnCaMKIV. Since CaMKIV has been shown to contribute to Ca^{2+}-induced activation of CREB (Bito et al., 1996; Finkbeiner et al., 1997; and Figures 2B and 2C), which has been in turn implicated in L-LTP, it is tempting to conclude that the L-LTP impairment observed in C34 transgenic mice is due to the dominant-negative effect of the transgene product on CREB activation. There is, however, no direct evidence for this causal relationship. For instance, the requirement of CaMKIV for L-LTP could result from the action of CaMKIV on the components of other transcriptional machinery, such as serum-response factor (SRF), and CREB binding protein CBP (Hu et al., 1999; Sun et al., 1996).

DnCaMKIV Transgenic Mice Are Impaired in the Consolidation/Retention Phase of Hippocampus-Dependent Memory

The C34 transgenic mice are clearly impaired in learning the hippocampus-dependent, hidden platform version of the Morris water maze task. Nevertheless, the transgenic mice seem to overcome the learning deficit to some extent as the training becomes more extensive. We do not know how these mice achieved this partial and/or slower learning. One explanation would be the incomplete inhibition of CaMKIV by the transgenic dnCaMKIV (Figure 1F). Another possibility would be that the requirement for CaMKIV is not absolute and other kinases are recruited as the training becomes more extensive. One can speculate that as the training is extended, kinases such as PKA (Yamamoto et al., 1988) or MAP kinase (Wu et al., 2001) known to be capable of activating CREB may be recruited to compensate for the inhibition of CaMKIV.

The idea that the observed behavioral deficits are due to the animal's inability or difficulty in adopting a spatial strategy is strongly suggested by the results of the competition test in the fixed location/visible platform version of the Morris water maze. Furthermore, these results indicate that *dnCaMKIV* transgenic mice have intact vision, escape motivation, and coordinated motor skills required for learning the water maze task. The specificity of the behavioral deficits of *dnCaMKIV* transgenic mice was further supported by the results of the open field test and the elevated plus maze, which revealed no discernable abnormalities in general locomotor or emotional aspects of behavior.

The *dnCaMKIV* transgenic mice displayed a deficit in the neural activity-dependent activation of CREB/CRE signaling pathway and a relatively specific impairment in synaptic plasticity, namely the late component of L-LTP. Since these protein synthesis-related events have been suggested as a molecular or cellular basis for memory consolidation, it was of great interest to determine whether the memory deficit displayed by these mice in the Morris water maze task was primarily in its consolidation phase rather than in the acquisition phase. Our fear conditioning study demonstrates that in C34 transgenic mice, the contextual memory is intact one day after training but is attenuated significantly 7 days after training. These data support the view that the effect of dnCaMKIV on context-dependent fear conditioning is not on the acquisition phase of the memory but on its consolidation or retention phase. The in vivo process of memory consolidation is likely to require a cascade of gene activation, protein synthesis, and protein alterations in a series of different types of synapses within a complex neural circuitry, which may take days or weeks. On the other hand, the readout of in vitro L-LTP at one particular type of synapse (e.g., Schaffer collateral-CA1 synapses) is an enhancement of synaptic transmission that can be detected within hours. Therefore, the deficit of L-LTP evident within hours may well underlie the impairment in memory consolidation detected 7 days after conditioning. Similar to our results, in AC1/AC8 double knockout mice, while hippocampal L-LTP was impaired within 1 hr after induction, the impairment of the contextual fear conditioning was detectable only after 8 days (Wong et al., 1999). It was also previously shown that rats subjected to hippocampal lesions one day after training exhibited a profound deficit in context-dependent fear conditioning, whereas those lesioned one month after training maintained the contextual fear memory. This suggests that the consolidation of hippocampus-dependent memory may occur sometime between one to 30 days after training (Anagnostaras et al., 1999; Kim and Fanselow, 1992).

Although the most robust site of the transgenic dnCaMKIV expression is the hippocampus, it is also expressed in other forebrain areas, albeit at lower levels (Figure 1C). Therefore, we cannot conclude that the consolidation-dampening effect of the transgenic dnCaMKIV

is exerted within the hippocampus. Nonetheless, it is interesting to note that such an effect was not observed in cue-dependent fear conditioning (Figure 7B), known to be independent of the integrity of the hippocampus (Phillips and LeDoux, 1992). These results can be explained either by the lower levels of dnCaMKIV expression outside of the hippocampus or by the possible differential role of CaMKIV in the consolidation of hippocampus-independent implicit memory. In either case, our data are consistent with the notion that hippocampal CaMKIV plays a crucial role in the consolidation and/or retention of hippocampus-dependent explicit memory.

Possible Links among CaMKIV and CREB Activation, L-LTP, and Memory Consolidation

We have shown that the postnatal forebrain-specific expression of a *dnCaMKIV* transgene results in deficits at multiple levels of complexity. At the molecular level, neural activity-induced activation of CaMKIV, CREB, and CRE-dependent transcription was impaired in the hippocampus. At the level of synaptic physiology, the L-LTP in hippocampal CA1 area was impaired while basic synaptic function and protein synthesis-independent E-LTP were intact. At the level of behavior, the *dnCaMKIV* transgenic mice were impaired in the consolidation and/or retention phase of hippocampus-dependent memory but not in its acquisition phase, or in any of these phases of hippocampus-independent memory. While one cannot conclude that these deficits observed at different levels of complexity are causally related from the lower to higher levels, our data are not only consistent with this notion but also add information to that in the literature and thereby strengthen the hypothesis. First, unlike the L-LTP deficits observed earlier in dnPKA (*R(AB)*) mice or adenylyl cyclase knockout mice, the LTP deficit observed in *dnCaMKIV* transgenic mice seems to be targeted to the protein synthesis-dependent component and hence correlates better with the deficit in the protein synthesis-dependent memory consolidation and/or retention (Davis and Squire, 1984). Second, in *dnCaMKIV* transgenic mouse, the perturbation at the molecular level is restricted to a neural activity-induced activation, be it of CaMKIV, CREB, or CRE-dependent transcription. Since L-LTP and memory consolidation are also neural activity-induced phenomena, the correlation of the deficits observed at the molecular level with those at the higher levels can be regarded as more stringent. Finally, unlike the global knockout mice (Ho et al., 2000; Wu et al., 2000), the *dnCaMKIV* transgenic mice, along with the *dnPKA* transgenic mice, are perturbed only in the postnatal forebrain. This certainly helps when one evaluates the relationship between deficits observed at multiple levels of complexity. For instance, we could dissociate the role of CaMKIV in the forebrain from that in many other brain areas of the adult animal as well as from its developmental function. Indeed, all tests we performed for detection of motor or emotional impairments gave negative results and we could detect no gross developmental abnormality.

How do the roles of CaMKIV in CREB/CRE-mediated signaling, L-LTP, and long-term memory relate to those of cAMP signaling pathway or MAP kinase pathway that have also been implicated in similar molecular, physiological, and behavioral processes? In view of the findings that the duration of CREB phosphorylation is a key factor in determining transcriptional initiation (Bito et al., 1996), it is conceivable that these three kinase pathways act in concert to accomplish optimal levels of sustained CREB phosphorylation and memory consolidation events. Alternatively, CaMKIV may play a dominant role in CREB phosphorylation by modulating other kinase pathways. Studies in cell culture system have demonstrated the regulatory role of CaMKIV in both MAP kinase and cAMP pathway (Enslen et al., 1996; Wayman et al., 1996). Regardless, perturbations in any one of these pathways would disrupt the balanced control of CREB-mediated gene expression and consequently result in L-LTP and long-term memory impairments.

In summary, our study demonstrates that interfering with neural activity-dependent CaMKIV signaling in the nucleus of neurons in the postnatal forebrain impairs the consolidation/retention but not the acquisition of hippocampus-dependent long-term memory. Deficits in the neural activity-dependent activation of the CREB/CRE signaling pathway and in the late component of L-LTP in the hippocampus may contribute to this memory impairment.

Experimental Procedures

Generation of Transgenic Mice and Genotyping

A cDNA encoding a dominant-negative form of murine CaMKIV has the following mutations: (1) Lys^{71} in the ATP binding site is mutated to Ala; (2) the phosphorylation site for CaMK kinase, Thr^{196}, is mutated to Ala; and (3) the autoinhibitory domain is inactivated by the triple mutation, $HMDT^{308-311}$ to DEDD. Transgenic mice were generated following the standard procedures using C57BL/6 embryos and kept in this pure genetic background. All analysis was carried out on 8- to 12-week-old mice unless specified otherwise.

Northern Blot Analysis

Approximately 15 μg of total forebrain RNA was subjected to electrophoresis through 1% agarose-formaldehyde gels and blotted onto Zeta-Probe membranes (Bio-Rad). RNA blots were then hybridized with ^{32}P-labeled DNA probes containing either SV40 poly(A) (from pMSG) or α*CaMKII* cDNA. The blots were stripped and reprobed with a human *G3PDH* cDNA (Clonetech) to confirm that each lane contained similar amounts of RNA.

In Situ Hybridization

The mouse brains were dissected and rapidly frozen in mounting medium. Cryostat sections (20 μm) were taken and post-fixed for 15 min in 4% paraformaldehyde in PBS (pH 7.3). The sections were hybridized to a SV40 poly(A) probe specific for the transgene. Hybridization was performed at 60°C overnight in a solution containing 50% formamide, 10 mM Tris-HCl (pH 8.0), 10% dextran sulfate, 1× Denhardt's, 600 mM NaCl, 0.25% SDS, 1 mM EDTA, 200 μg/ml tRNA, and [α-^{33}P]-labeled antisense probe. The hybridized sections were exposed to films, dipped in Kodak NTB3 nuclear emulsion, and developed after 12 days.

Western Blot Analysis and Kinase Assay

Fifty micrograms of forebrain homogenates were resolved by SDS-PAGE and then transferred onto PVDF membranes for immunoblotting. After a blocking reaction (5% nonfat milk in PBS [pH 7.3] and 0.05% Tween-20), the blots were incubated for 1 hr at room temperature with one of the following primary antibodies: mouse monoclonal anti-FLAG M2 antibody (Sigma), anti-CaMKIV antibody (Transduction Laboratories), anti-CaMKIIα antibody (GibcoBRL), or anti-Actin antibody (Boehringer Mannheim). After incubation with a secondary antibody (HRP-conjugated goat anti-mouse antibody), the blots

were developed using an ECL chemiluminescence procedure (Amersham).

To monitor activity-dependent changes in pCREB and c-Fos immunoreactivity, the hippocampal slices were prepared and perfused with 90 mM KCl for 10 min or with either 100 μM glutamate or 50 μM forskolin for 20 min in a submerged chamber. After certain periods of time specified in the text, the slices were lysed in RIPA buffer (50 mM Tris-HCl [pH 7.5], 150 mM NaCl, 1% NP-40, 0.5% sodium deoxycholate, Complete protease inhibitor tablet [Boehringer Mannheim], 1 mM DTT, 1 mM Na_3VO_4, and 1 mM NaF). Western Blot analysis was conducted as described above using rabbit polyclonal anti-phospho CREB antibody (NEB), anti-CREB antibody (NEB), anti-phospho MAPK antibody (NEB), anti-MAPK antibody (NEB), or anti-c-Fos (Ab-2) antibody (Oncogene Research Products). Quantification was done using NIH Image software. The mean pixel density for pCREB or c-Fos signal was measured and normalized to the background.

For kinase activity assays, hippocampal slices were stimulated with 90 mM KCl for 10 min and then immediately homogenized in RIPA buffer. The lysates were immunoprecipitated overnight with 5 μg of anti-CaMKIV antibody (Transduction Laboratories) or goat polyclonal CaMKIIβ antibody (Santa Cruz Biotechnology). The final immunoprecipitates were resuspended in 30 μl CaMK assay buffer and assayed for CaMKIV or CaMKII activity as previously described (Gringhuis et al., 1997). Peptide-γ and autocamtide-2 (Biomol) were used as peptide substrates for CaMKIV and CaMKII, respectively.

Transient Transfection and Luciferase Assay

COS7 cells were transfected when 80% confluent with LipofectAMINE (Gibco BRL) according to the manufacturer's instructions. The pRL-TK vector containing *Renilla* luciferase (Promega) was included in each transfection to normalize for protein levels and transfection efficiency. The following plasmids were transfected with the amounts indicated per 10 cm dish: caCaMKIV (0.02 μg), caCaMKK (0.4 μg), dnCaMKIV (0.2 μg), $CREB^{S133A}$ (0.2 μg), *Renilla* luciferase (0.3 μg), and 5XCRE-luciferase (0.5 μg). Empty vector was used to compensate amounts of plasmids. The caCaMKIV was generated by the triple mutation in the autoinhibitory domain of CaMKIV ($HMDT^{306-311}$ → DEDD) and has been shown to be active in the absence of Ca^{2+}/CaM (Ensien et al., 1996). The caCaMKK was a truncated form (residues 1–413) of CaMKK. Forty-eight hours after transfection, COS7 cells were lysed and luciferase levels were measured using the dual-luciferase reporter assay system (Promega).

Electrophysiology

Transverse hippocampal slices (400 μm thick) were prepared and submerged in a stream (2 ml/min) of ACSF (119 mM NaCl, 2.5 mM KCl, 1.3 mM $MgSO_4$, 2.5 mM $CaCl_2$, 1.0 mM NaH_2PO_4, 26.2 mM $NaHCO_3$, and 11.0 mM glucose) oxygenated with 95% O_2/5% CO_2. Bath temperature was maintained at 22–24°C. Extracellular fEPSPs were evoked by stimulation of the Schaffer collateral afferents at a frequency of 0.033 Hz and at a stimulus intensity that produces fEPSP slopes approximately 35% of the maximum. TBS consisted of 10 bursts of stimuli with four pulses each (100 Hz, 100 μs duration) and 200 ms interburst interval; this TBS was repeated two times with an ISI of 30 s. Tetanic stimulation was delivered at the test intensity in 1 s trains at 100 Hz, with 4 trains 5 min apart to induce late LTP (L-LTP). Anisomycin (Sigma) was added to the perfusate at a final concentration of 40 μM 30 min prior to the application of the first tetanus. We analyzed the initial slope of the fEPSP and used it as a measure of synaptic strength. Paired pulse facilitation (PPF) was tested with 50, 100, and 200 ms interpulse interval. To assess statistical significance, paired t tests, comparing the average slope size for 10 min before LTP induction to either 50–60 min or 170–180 min after LTP induction, were performed on nonnormalized data. Between group comparisons were made of percent of baseline values using unpaired t tests; p values greater than 0.05 are designated as not significant (ns). The genotype of all animals was only revealed after the experiments.

Behavioral Tests

Behavioral tests were conducted in a blind fashion during the light phase at approximately the same time each day. Data were analyzed with one-way analysis of variance (ANOVA) and Student's t test; p values greater than 0.05 are designated as not significant (ns).

The Morris water maze tests were conducted as previously described (Tsien et al., 1997). The apparatus consisted of a circular pool (160 cm diameter, 60 cm deep at the side) filled with water at 21–22°C that was completely covered with floating polypropylene beads (Hanna resin distribution). Black curtains were drawn around the pool (90 cm from the pool periphery) and contained a number of illuminated objects that served as distal cues. Using a computerized tracking system (Dragon), we analyzed the escape latency (platform search time), path length (the distance traveled to reach the platform), the time spent in the periphery (a rim of 18 cm from the wall), and swimming velocity for each trial. For the hidden platform task, the mice were trained to find the hidden platform (10 cm × 10 cm, 1.5 cm below the surface of water) that was placed in the middle of the radial quadrant. The training was carried out in blocks of 4 trials per day (intertrial interval of about 30 min) for 12 days. During each block of trials, the mice were released from four pseudorandomly assigned start locations (N, S, E, and W). If a mouse did not find the platform within 90 s, it was manually guided to the platform and allowed to rest on the platform for 15 s. A probe test was given at the end of days 1, 6, 10, and 12 in the absence of the platform. We measured the time they spent in the radial quadrant in which the platform had been located during training (quadrant occupancy) and the number of times they crossed over the exact platform location (platform crossing).

The fixed location/visible platform task was adapted from Kim et al. (2001). In this task, the location of the platform was made apparent by attachment of an orange flag to the platform, which protruded 15 cm above the surface of water. During the acquisition trials (4 days, total of 16 trials), the mice were trained to swim to the visible platform in a fixed location, NE or SW. On day 5, the visible platform was moved to the center of the adjacent quadrant (NW For NE group, SE for SW group) and the mice were released from start positions equidistant to the old and new platform location. Analysis was performed to determine whether the mice swam to within 15 cm of the perimeter of the previous platform location before escaping to the visible platform, in the adjacent quadrant.

The general activity and anxiety level of the mice was evaluated using the two tests conducted according to the previously published methods (Churchill et al., 1998; Cruz et al., 1994). Accuscan Digiscan (Columbus, OH) automated activity monitors were used to quantify total distance and margin time. Total distance traveled was quantified by measuring the consecutive breaking of adjacent photocell beams. The percent of margin time was obtained by dividing the total testing period (10 min) by the period of time the mouse spent in close proximity (within 1 cm) to the walls of the chamber. For the elevated plus maze, the mice were placed on the central platform of the maze facing one of the walled arms and were observed for 10 min, during which the number of entries into and time spent in the open or enclosed arms were measured. The digitized image of the path taken by each animal was stored and analyzed with a semiautomated analysis system (PolyTrack, San Diego Instruments, Inc.). For contextual fear conditioning, we generally followed the procedure described in previous publication (Bourtchuladze et al., 1994). On training day, mice were placed in a shocking chamber (Coulbourn instruments) and a 30 s white noise tone (CS) was presented 2 min later. A mild foot shock (0.75 mA intensity, 2 s duration) was delivered at the end of the tone and coterminated with it. Mice were left in the training chamber for another 30 s and returned to their home cage. During testing, mice were placed back in the conditioning chamber for 3 min. Live 8 bit grayscale video was digitized at 2 Hz using computerized NIH Image software (Anagnostaras et al., 2000; Miyakawa et al., 2001). Freezing was defined as immobility for a consecutive one-second period. Cued fear conditioning tests were conducted in a similar manner to contextual tests except that on test days, mice were placed in a white plexiglass chamber for a total of 5 min. Baseline freezing in the novel context (pre-CS) was monitored for 2 min prior to delivering the continuous 3 min tone.

Acknowledgments

We would like to acknowledge Frank Bujard for help with the behavioral experiments; Jason Derwin, Chanel Lovett, and Wenjiang Yu

for excellent technical assistance; and many members of the Tonegawa lab for helpful advice and discussions during the course of this study and manuscript preparation. This work was supported by NIH grant R01-NS32925 (S.T.), RO1-NS27037 (T.R.S.), and HHMI (S.T. and H.K.).

Received May 4, 2001; revised August 21, 2001.

References

Abel, T., Nguyen, P.V., Barad, M., Deuel, T.A.S., and Kandel, E.R. (1997). Genetic demonstration of a role for PKA in the late phase of LTP and in hippocampus-based long-term memory. Cell *88*, 615–626.

Anagnostaras, S.G., Maren, S., and Fanselow, M.S. (1999). Temporally graded retrograde amnesia of contextual fear after hippocampal damage in rats: within-subjects examination. J. Neurosci. *19*, 1106–1114.

Anagnostaras, S.G., Josselyn, S.A., Frankland, P.W., and Silva, A.J. (2000). Computer-assisted behavioral assessment of Pavlovian fear conditioning in mice. Learn. Mem. *7*, 58–72.

Bartsch, D., Ghirardi, M., Skehel, P.A., Karl, K.A., Herder, S.P., Chen, M., Bailey, C.H., and Kandel, E.R. (1995). *Aplysia* CREB2 represses long-term facilitation: relief of repression converts transient facilitation into long-term functional and structural change. Cell *83*, 979–992.

Bito, H., Deisseeroth, K., and Tsien, R.W. (1996). CREB phosphorylation and dephosphorylation: a Ca^{2+}- and stimulus duration-dependent switch for hippocampal gene expression. Cell *87*, 1203–1214.

Blendy, J.A., Kaestner, K.H., Schmid, W., Gass, P., and Schutz, G. (1996). Targeting of the CREB gene leads to up-regulation of a novel CREB mRNA isoform. EMBO J. *15*, 1098–1106.

Bliss, T.V.P., and Collingridge, G.L. (1993). A synaptic model of memory: long-term potentiation in the hippocampus. Nature *361*, 31–39.

Blitzer, R.D., Wong, T., Nouranifar, R., Iyengar, R., and Landau, E.M. (1995). Postsynaptic cAMP pathway gates early LTP in hippocampal CA1 region. Neuron *15*, 1403–1414.

Bourtchuladze, R., Frenguelli, B., Blendy, J., Cioffi, D., Schutz, G., and Silva, A.J. (1994). Deficient long-term memory in mice with a targeted mutation of the cAMP-responsive element-binding protein. Cell *79*, 59–68.

Chawla, S., Hardingham, G.E., Quinn, D.R., and Bading, H. (1998). CBP: a signal-regulated transcription coactivator controlled by nuclear calcium and CaM kinase IV. Science *281*, 1505–1509.

Churchill, L., Klitenick, M.A., and Kalivas, P.W. (1998). Dopamine depletion reorganizes projections from the nucleus accumbens and ventral pallidum that mediate opioid-induced motor activity. J. Neurosci. *18*, 8074–8085.

Cruz, A.P.M., Frei, F., and Graeff, F.G. (1994). Ethopharmacological analysis of rat behavior on the elevated plus maze. Pharmacol. Biochem. Behav. *49*, 171–176.

Davis, H.P., and Squire, L.R. (1984). Protein synthesis and memory: a review. Psych. Bull. *96*, 518–559.

Devan, B.D., and White, N.M. (1999). Parallel information processing in the dorsal striatum: relation to hippocampal function. J. Neurosci. *19*, 2789–2798.

Enslen, H., Tokamitsu, H., Stork, P.J.S., Davis, R.J., and Soderling, T.R. (1996). Regulation of mitogen-activated protein kinases by a calcium-calmodulation-dependent protein kinase cascade. Proc. Natl. Acad. Sci. USA *93*, 10803–10808.

Finkbeiner, S., Tavazoie, S.F., Maloratsky, A., Jacobs, K.M., Harris, K.M., and Greenberg, M.E. (1997). CREB: a major mediator of neuronal neurotrophin responses. Neuron *19*, 1031–1047.

Frey, U., Krug, M., Reymann, K.G., and Matthies, H. (1988). Anisomycin, an inhibitor of protein synthesis, blocks late phases of LTP phenomena in the hippocampal CA region in vitro. Brain Res. *452*, 57–65.

Gringhuis, S.I., deLeij, L.F., Wayman, G.A., Tokumitsu, H., and Vellenga, E. (1997). The CA2+/calmodulin-dependent kinase type IV is involved in the CD-5 mediated signaling pathway in human T lymphocytes. J. Biol. Chem. *272*, 31809–31820.

Grewal, S.S., Fass, D.M., Yao, H., Ellig, C.L., Goodman, R.H., and Stork, P.J. (2000). Calcium and cAMP signals differentially regulate cAMP-responsive element-binding protein function via a Rap1-extracellular signal-regulated kinase pathway. J. Biol. Chem. *272*, 34433–34441.

Hardingham, G.E., Chawla, S., Cruzalegui, F.H., and Bading, H. (1999). Control of recruitment and transcription-activating function of CBP determines gene regulation by NMDA receptors and L-type calcium channels. Neuron *22*, 789–798.

Ho, N., Liauw, J.A., Blaeser, F., Wei, F., Hanissian, S., Muglia, L.M., Wozniak, D.F., Nardi, A., Arvin, K.L., Holtzman, D.M., et al. (2000). Impaired synaptic plasticity and cAMP response element-binding protein activation in Ca^{2+}/calmodulin-dependent protein kinase type IV/Gr-deficient mice. J. Neurosci. *20*, 6459–6472.

Hu, S.-C., Chrivia, J., and Ghosh, A. (1999). Regulation of CBP-mediated transcription by neuronal calcium signaling. Neuron *22*, 799–808.

Impey, S., Mark, M., Villacres, E.C., Poser, S., Chavkin, C., and Storm, D.R. (1996). Induction of CRE-mediated gene expression by stimuli that generate long-lasting LTP in area CA1 of the hippocampus. Neuron *16*, 973–982.

Impey, S., Obrietan, K., Wong, S.T., Poser, S., Yano, S., Wayman, G., Deloulme, J.C., Chan, G., and Storm, D.R. (1998). Cross talk between ERK and PKA is required for Ca^{2+} stimulation of CREB-dependent transcription and ERK nuclear translocation. Neuron *21*, 869–883.

Jensen, K.F., Ohmstede, C.-A., Fisher, R.S., and Sahyoun, N. (1991). Nuclear and axonal localization of Ca^{2+}/calmodulin-dependent protein kinase type Gr in rat cerebellar cortex. Proc. Natl. Acad. Sci. USA *88*, 2850–2853.

Kim, J.J., and Fanselow, M.S. (1992). Modality specific retrograde amnesia of fear following hippocampal lesions. Science *256*, 675–677.

Kim, J.J., Lee, H.J., Han, J.S., and Packard M.G. (2001). Amygdala is critical for stress-induced modulation of hippocampal long-term potentiation and learning. J. Neurosci. *21*, 5222–5228.

Kogan, J.H., Frankland, P.W., Blendy, J.A., Coblentz, J., Marowitz, Z., Schutz, G., and Silva, A.J. (1996). Spaced training induces normal long-term memory in CREB mutant mice. Curr. Biol. *7*, 1–11.

McDonald, R., and White, N.M. (1994). Parallel information processing in the water maze: evidence for independent memory systems involving dorsal striatum and hippocampus. Behav. Neural Biol. *61*, 260–270.

Miyakawa, T., Yamada, M., Duttaroy, A., and Wess, J. (2001). Hyperactivity and intact hippocampus-dependent learning in mice lacking the M1 muscarinic acetylcholine receptor. J. Neurosci., in press.

Morris, R.G. (1981). Spatial localization does not require the presence of local cues. Learn. Motiv. *12*, 239–260.

Morris, R.G., Garrud, P., Rawlins, J.N.P., and O'Keefe, J. (1982). Place navigation impaired in rats with hippocampal lesions. Nature *297*, 681–683.

Nakamura, Y., Okuno, S., Sato, F., and Fujisawa, H. (1995). An immunohistochemical study of Ca2+/calmodulin-dependent protein kinase IV in the rat central nervous system: light and electron microscopic observations. Neuroscience *68*, 181–194.

Nguyen, P.V., Abel, T., and Kandel, E.R. (1994). Requirement of a critical period of transcription for induction of a late phase of LTP. Science *265*, 1104–1107.

Phillips, R.G., and LeDoux, J.E. (1992). Differential contribution of amygdala and hippocampus to cued and contextual fear conditioning. Behav. Neurosci. *106*, 274–285.

Picciotto, M.R., Zoli, M., Bertuzzi, G., and Nairn, A.C. (1995). Immunochemical localization of Ca^{2+}/calmodulin-dependent protein kinase I. Synapse *20*, 75–84.

Ribar, T.J., Rodriguiz, R.M., Khiroug, L., Wetsel, W.C., Augustine,

G.J., and Means, A.R. (2000). Cerebellar defects in Ca^{2+}/calmodulin kinase IV-deficient mice. J. Neurosci. *20 (RC107)*, 1–5.

Sheng, M., and Greenberg, M.E. (1990). The regulation and function of c-fos and other immediate early genes in the nervous system. Neuron *4*, 477–485.

Shieh, P.B., Hu, S.-C., Bobb, K., Timmusk, T., and Ghosh, A. (1998). Identification of a signaling pathway involved in calcium regulation of BDNF expression. Neuron *20*, 727–740.

Silva, A.J., Kogan, J.H., Frankland, P.W., and Kida, S. (1998). CREB and memory. Annu. Rev. Neurosci. *21*, 127–148.

Soderling, T.R., and Derkach, V.A. (2000). Postsynaptic protein phosphorylation and LTP. Trends Neurosci. *23*, 75–80.

Sun, P., Lou, L., and Maurer, R.A. (1996). Regulation of activating transcription factor-1 and the cAMP response element-binding protein by Ca^{2+}/calmodulin-dependent protein kinase type I, II, and IV. J. Biol. Chem. *271*, 3066–3073.

Tokumitsu, H., and Soderling, T.R. (1996). Requirements for calcium and calmodulin in the calmodulin kinase activation cascade. J. Biol. Chem. *271*, 5617–5622.

Tsien, J.Z., Huerta, P.T., and Tonegawa, S. (1997). The essentail role of hippocampal CA1 NMDA receptor-dependent synaptic plasticity in spatial memory. Cell *87*, 1327–1338.

Wayman, G.A., Wei, J., Wong, S., and Storm, D.R. (1996). Regulation of type I adenylyl cyclase by calmodulin kinase IV in vivo. Mol. Cell. Biol. *16*, 6075–6082.

Winder, D.G., Mansuy, I.M., Osman, M., Moallem, T.M., and Kandel, E.R. (1998). Genetic and pharmacological evidence for a novel, intermediate phase of long-term potentiation suppressed by calcineurin. Cell *92*, 25–37.

Wong, S.T., Athos, J., Figueroa, Z.A., Pineda, V.V., Schaefer, M.L., Chavkin, C.C., Muglia, L.J., and Storm, D.R. (1999). Calcium-stimulated adenylyl cyclase activity is critical for hippocampus-dependent long-term memory and late phase LTP. Neuron *23*, 787–798.

Wu, G.-Y., Deisseroth, K., and Tsien, R.W. (2001). Activity-dependent CREB phosphorylation: convergence of a fast, sensitive calmodulin kinase pathway and a slow, less sensitive mitogen-activated protein kinase pathway. Proc. Natl. Acad. Sci. USA *98*, 2808–2813.

Wu, J.Y., Ribar, T.J., Cummings, D.E., Burton, K.A., McKnight, G.S., and Means, A.R. (2000). Spermiogenesis and exchange of basic nuclear proteins are impaired in male germ cells lacking Camk4. Nat. Genet. *25*, 448–452.

Yamamoto, K.K., Gonzalez, G.A., Biggs, W.H., 3rd, and Montminy, M.R. (1988). Phosphorylation-induced binding and transcriptional efficacy of nuclear factor CREB. Nature *334*, 494–498.

Yin, J.C.P., Wallach, J.S., Vecchio, M.D., Wilder, E.L., Zhou, H., Quinn, W.G., and Tully, T. (1994). Induction of a dominant negative CREB transgene specifically blocks long-term memory in *Drosophila*. Cell *79*, 49–58.

Yin, J.C.P., Vecchio, M.D., Zhou, H., and Tully, T. (1995). CREB as a memory modulator: induced expression of a *dCREB2* activator isoform enhances long-term memory in *Drosophila*. Cell *81*, 107–115.

Appendix E: Collaborative Contributions to "Formation of Temporal Memory Requires NMDA Receptors within CA1 Pyramidal Neurons"

Huerta, P. T., Sun, L. D., Wilson, M. A., and Tonegawa, S. (2000). Neuron *25*, 473-480.

Abstract:

In humans the hippocampus is required for episodic memory, which extends into the spatial and temporal domains. Work on the rodent hippocampus has shown that NMDA receptor (NMDAR) -mediated plasticity is essential for spatial memory. Here, we have examined whether hippocampal NMDARs are also needed for temporal memory. We applied trace fear conditioning to knockout mice lacking NMDARs only in hippocampal CA1 pyramidal cells. This paradigm requires temporal processing because the conditional and unconditional stimuli are separated by 30 s (trace). We found that knockout mice failed to memorize this association but were indistinguishable from normal animals when the trace was removed. Thus, NMDARs in CA1 are crucial for the formation of memories that associate events across time.

My Contribution:

Because there was not a commercially available solution to implement a trace fear conditioning protocol, I built our fear conditioning apparatus from scratch and some commercially available parts. I adapted the PC DOS program AD (written by M. Wilson) written in Borland C, to control the conditioned stimuli (white noise generator) and unconditioned stimuli (Coulbourne Instruments scrambled shocker) delivered to the mice. Fear conditioning analysis for the most part has in the literature been carried out human observers

who sample mouse behavior once every 10 seconds by looking through a peephole while the mouse is subjected to different conditional and unconditional stimuli over time. Because at the outset of this study we wanted to eliminate the possibility of human error and variability, I developed a computerized automated method for objectively analyzing behavior. This method relied on video and tracker methods and resulted in 5 Hz-60Hz sampling rates which was a significant improvement over previous human sampling rates of 0.1 Hz. Movement of mice was determined by the difference of number of pixels between successive video frames, and non-movement was scored as "freezing" behavior (Figure 1B). Additionally because of our improved tracking analysis, we were able to assess freezing behavior during the trace testing period in a way never possible before. Previous studies used a single measure of percentage freezing during this period as determined by a single human observation. However, I produced high temporal and spatial resolution occupancy plots which distinctly showed that mutant mice did not freeze during the trace period as compared to the control counterparts (Figure 3A,B). This provided significant evidence that CA1-NMDA KO mice could not form associations for events occurring over time periods lasting 15 seconds or greater.

Neuron, Vol. 25, 473–480, February, 2000, Copyright ©2000 by Cell Press

Formation of Temporal Memory Requires NMDA Receptors within CA1 Pyramidal Neurons

Patricio T. Huerta,* Linus D. Sun,* Matthew A. Wilson,*† and Susumu Tonegawa*†‡
*Howard Hughes Medical Institute
Center for Learning and Memory
Department of Biology
Department of Brain and Cognitive Sciences
†RIKEN-MIT Neuroscience Research Center
Massachusetts Institute of Technology
Cambridge, Massachusetts 02139

Summary

In humans the hippocampus is required for episodic memory, which extends into the spatial and temporal domains. Work on the rodent hippocampus has shown that NMDA receptor (NMDAR) –mediated plasticity is essential for spatial memory. Here, we have examined whether hippocampal NMDARs are also needed for temporal memory. We applied trace fear conditioning to knockout mice lacking NMDARs only in hippocampal CA1 pyramidal cells. This paradigm requires temporal processing because the conditional and unconditional stimuli are separated by 30 s (trace). We found that knockout mice failed to memorize this association but were indistinguishable from normal animals when the trace was removed. Thus, NMDARs in CA1 are crucial for the formation of memories that associate events across time.

Introduction

Human studies have indicated that the hippocampus participates in the acquisition of declarative and/or episodic memory, i.e., the ability to consciously recollect events from everyday experience set in their spatiotemporal context (Cohen and Eichenbaum, 1993; Schacter and Tulving, 1994; Vargha-Khadem et al., 1997; Squire and Kandel, 1999). In rodents, O'Keefe and Nadel (1978) postulated that the hippocampus is responsible for generating spatial maps that guide the animal's navigation, an idea that has received strong support on two grounds: (1) many studies have demonstrated that hippocampal damage leads to deficits on spatial learning tasks (O'Keefe and Nadel, 1978; Morris et al., 1982, 1986; Nadel, 1991; Jarrard, 1993; O'Keefe, 1999), and (2) the existence of "place" cells—that is, hippocampal pyramidal neurons that fire when the animal is in a particular location in its environment (O'Keefe and Nadel, 1978; O'Keefe, 1999).

Is the rodent hippocampus also involved in temporal memory? It has been previously shown that rats with hippocampal lesions or treated with an NMDA receptor (NMDAR) antagonist are deficient in learning tasks that include delays of seconds to minutes between relevant events (Meck et al., 1984; Rawlins, 1985; Lyford et al., 1993; Chiba et al., 1994; Jackson et al., 1998). However, it has been argued that these studies were inconclusive as to the role of the rodent hippocampus in temporal memory because the tasks contained an inadvertent spatial component (Nadel, 1991; O'Keefe, 1999; Wood et al., 1999). More recently, McEchon et al. (1998) reported that rats with hippocampal lesions were impaired in trace fear conditioning. This Pavlovian paradigm has a very clear timing requirement because it demands the association of a conditional stimulus (CS) with an unconditional stimulus (US) across an interval known as a "trace." Learning occurs as the animal links the originally neutral CS with the US, so that later presentation of the CS alone elicits the conditional response. A neural circuit is therefore needed for establishing the CS–US association across the gap imposed by the trace. If the hippocampus participates in this circuit, as the lesion studies suggest, a major question is whether the hippocampal mechanism responsible for temporal memory is different from the one underlying spatial mapping. Conversely, both mechanisms could be part of a more general one.

We recently reported the generation and initial characterization of knockout mice lacking the gene for the NR1 subunit of NMDARs in CA1 pyramidal cells (named NR1-CA1-KO or mutant, henceforth). These mice were shown to be deficient in NMDAR-dependent synaptic plasticity (within CA1 synapses) and spatial memory formation (Tsien et al., 1996). They also displayed degraded coactivation of CA1 place cells during exploration (McHugh et al., 1996). In this study, we have subjected NR1-CA1-KOs to trace fear conditioning. Our purpose was 2-fold: (1) to confirm that hippocampal function is needed for encoding temporal memory by using a more stringent lesion method, namely a cell type–specific gene knockout, and (2) to examine whether NMDAR function within CA1 pyramidal cells is specifically required. We found that mutant mice displayed a memory impairment following trace conditioning, i.e., they were unable to memorize the association between the CS and the US across the trace interval. Conversely, mutant mice could acquire the conditional response when the trace interval was removed in a delay conditioning paradigm.

Results

NR1-CA1-KO Mice Are Slower in the Acquisition of Trace Fear Conditioning

To identify the conditional fear response, we measured the freezing behavior of mice with an automated method. First, we determined that the scores generated by this method were equivalent to the more traditional way of scoring freezing by visual inspection. In order to compare the two methods, mice (n = 6) were subjected to "contextual" fear conditioning, in which animals were placed in a conditioning chamber and after 3 min were shocked three times with an interval of 1 min between shocks. The next day, mice were tested in the conditioning chamber for 6 min. As it is well established, mice

‡ To whom correspondence should be addressed (e-mail: tonegawa@mit.edu).

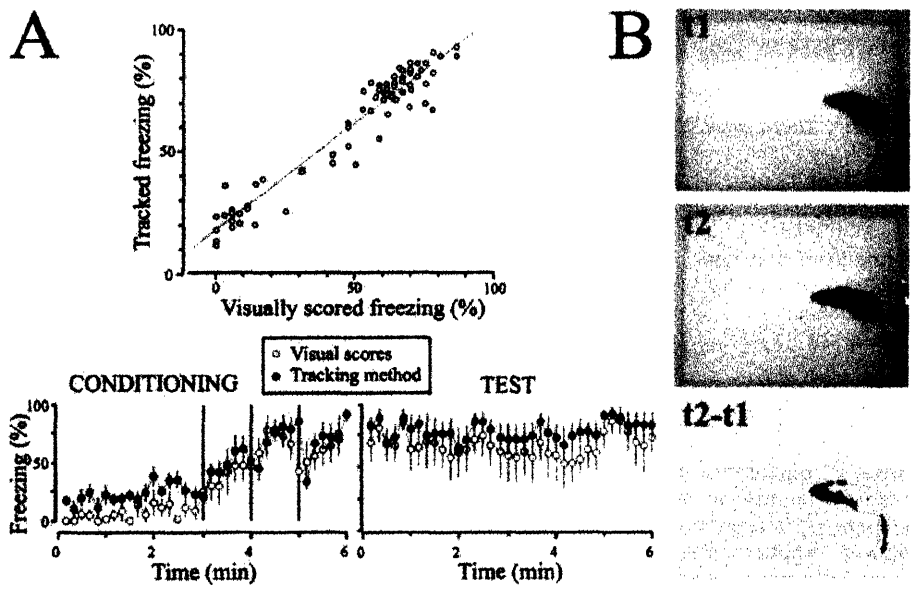

Figure 1. Calibration of the Tracking Method for Measuring Freezing

(A, top) The comparison of visually scored freezing done by blind observers (x axis) to freezing scores generated with the tracking method (y axis). The data were fitted by a linear regression with $y = 18 + 0.87x$, $r = 0.96$.

(A, bottom) The time course of the context conditioning paradigm ($n = 6$ mice) used to generate the visual (open circles) and tracked (closed circles) freezing scores. Details of the paradigm are given in the Experimental Procedures. The green bars during conditioning represent US deliveries.

(B) Sequence of video frames, at times t1 and t2 (200 ms later), showing a mouse exploring the chamber. The video method calculates the difference (t2 − t1). The leading edge of the mouse is represented by black, whereas the trailing edge is represented by yellow.

showed robust freezing during the 24 hr test. Figure 1 shows that the freezing scores generated with the automated method matched well with visually scored freezing.

For trace training, a mouse was placed in a conditioning chamber and, after 60 s, received the CS (white noise, 15 s), followed by a trace period (30 s) and the US (foot shock, 0.5 s). The sequence was repeated ten times with an intertrial interval (ITI) of 210 s. Comparison of the freezing scores revealed that mutants froze significantly less than controls after the initial trial (ITI-1, 105–315 s, mutant, 27.7% ± 2.6%, control, 41.7% ± 2.9%, $p < 0.001$, $F_{1,44} = 13.2$) and the subsequent two trials (ITI-2, 360–570 s, mutant, 41.9% ± 4.5%, control, 60.3% ± 4.6%, $p < 0.01$, $F_{1,44} = 8.1$; ITI-3, 615–825 s, mutant, 52.3% ± 5.0%, control, 68.9% ± 4.8%, $p < 0.05$, $F_{1,44} = 5.7$). However, thereafter the conditioning of mutants quickly caught up with that of controls, and by the end of the training session the scores from the two groups were not significantly different (ITI-10, 2400–2610 s, mutant, 66.6% ± 4.0%, control, 67.8% ± 4.8%, $p = 0.85$, $F_{1,44} = 0.04$). Since mice stayed in the conditioning chamber for over 40 min during the training session, it was quite feasible that habituation also contributed to the increase of immobility. To measure habituation, we placed control mice that received neither CS nor US into the conditioning chamber for 43.5 min (these mice are labeled "naive" hereafter). By the end of the session, the freezing scores of naive animals were only slightly less than those of controls and mutants (ITI-10, naive, 52.2% ± 8.7%; control versus naive, $p = 0.1$, $F_{1,28} = 2.5$; mutant versus naive, $p = 0.1$, $F_{1,28} = 2.8$). This suggests that habituation might be a significant factor contributing to the behavior of control and mutant mice as the conditioning progressed.

Additionally, a group of control mice was subjected to pseudo-conditioning (see Experimental Procedures; these mice are labeled "pseudo" hereafter). Following subsequent deliveries of the US, pseudo mice exhibited increasing levels of freezing (Figure 2C). This effect has been observed previously (Phillips and LeDoux, 1994; McEchon et al., 1998). It has been interpreted as resulting from the association of the US with the background context, i.e., the static stimuli within the conditioning chamber (Phillips and LeDoux, 1994).

NR1-CA1-KO Mice Fail to Show the Conditional Response during a Memory Test, after Trace Conditioning

The memory test for trace conditioning was conducted 24 hr after the training session. A mouse was placed in a novel chamber and, after 60 s, was exposed to the CS ten times (ITI of 210 s). Upon introduction into the chamber, mutants and controls showed elevated freezing compared to naive mice (pre-CS period, 0–60 s, mutant, 53.1% ± 3.7%, control, 56.9% ± 2.0%, naive, 24.0% ± 4.1%; mutant versus naive, $p < 0.001$, $F_{1,28} = 17.0$; control versus naive, $p < 0.0001$, $F_{1,28} = 62.0$). This effect has been described as a generalization of the fear response. That is, rodents that have undergone strong fear conditioning are found to freeze upon mere exposure to environments that were not used for conditioning. Unavoidable factors in the experimental environment, such as being manipulated by an experimenter,

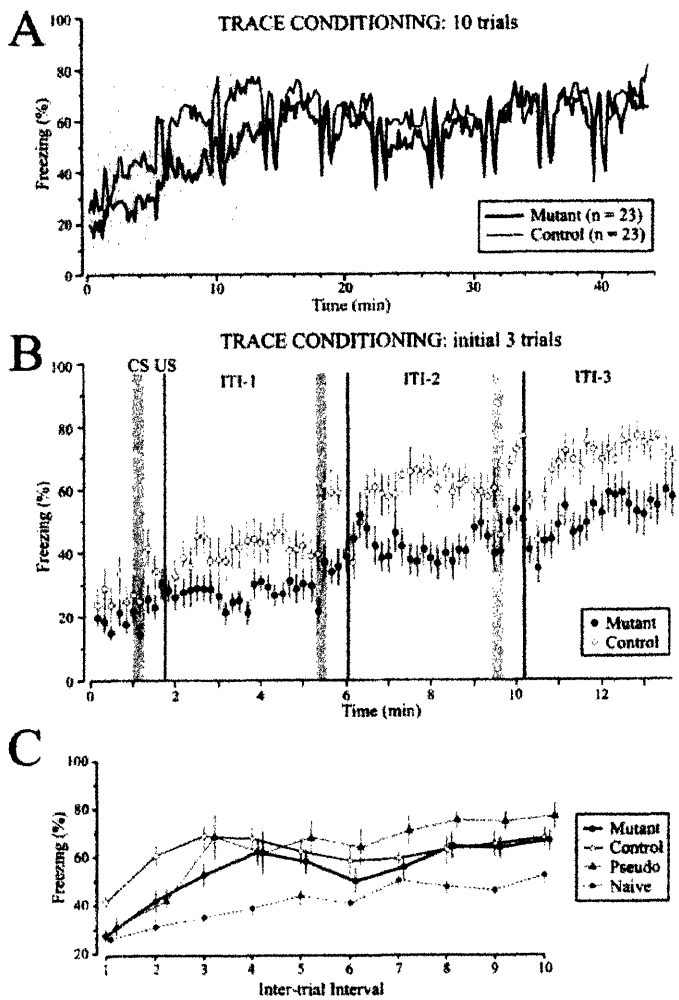

Figure 2. NR1-CA1-KO Mice Are Slower in the Acquisition of Trace Fear Conditioning

(A) Time course of the average percent freezing displayed by mutants (n = 23) and controls (n = 23) during trace conditioning. The gray box, at left, indicates the initial three trials, which are enlarged in (B).

(B) Pooled data showing the average percent freezing on the initial phase of acquisition for NR1-CA1-KOs (closed circles) and controls (open circles). Symbols represent mean freezing (± SEM) on a 10 s epoch. CS presentations are indicated by gray bars and US occurrence by green bars. It is clear that mutants show lower freezing during this initial phase.

(C) Average percent freezing during the ITIs for mutant (n = 23), control (n = 23), pseudo-conditioned (n = 12), and naive (n = 7) mice.

being placed in a box that differs from the home cage, and others, may contribute to the generalization of fear (Fanselow, 1990; Radulovic et al., 1998). During the first ITI (75–285 s), the freezing of NR1-CA1-KOs remained at the same level as that of the pre-CS period, whereas the freezing of controls was elevated to above 80% (Figure 3). The difference in freezing scores between the two groups was highly significant (ITI-1, 75–285 s, mutant, 56.3% ± 2.2%, control, 84.3% ± 2.9%, $p < 0.0001$, $F_{1,44} = 58.3$) and remained as such for the subsequent trials (ITI-2, 300–510 s, mutant, 60.5% ± 2.2%, control, 85.1% ± 2.7%, $p < 0.0001$, $F_{1,44} = 58.3$; ITI-3, 525–735 s, mutant, 62.7% ± 1.6%, control, 83.6% ± 2.3%, $p < 0.0001$, $F_{1,44} = 54.9$).

The maximal conditional response displayed by controls occurred roughly 30 s after CS delivery (Figure 3B), suggesting that the animals were expecting the shock exactly at the time that it had occurred in the training session. Thus, controls seemed to have developed a strong CS–US association across the trace interval. To demonstrate that the enhanced freezing exhibited by controls was specifically linked to the CS, we compared their behavior to that of pseudo mice. Had the CS elicited a nonspecific fear response on the 24 hr test, then pseudo mice should also respond to the CS with enhanced freezing. However, this was not the case (Figures 3A and 3C). Statistical comparison revealed that the pseudo group froze significantly less than controls (ITI-1, pseudo, 37.7% ± 10.4%, control, 84.3% ± 2.9%, $p < 0.0001$, $F_{1,33} = 65.9$; ITI-2, pseudo, 50.8% ± 6.3%, control, 85.1% ± 2.7%, $p < 0.0001$, $F_{1,33} = 65.9$; ITI-3, pseudo, 59.3% ± 8.8%, control, 83.6% ± 2.3%, $p < 0.001$, $F_{1,33} = 14.9$), implying that only controls had formed the temporal association as a consequence of trace training. Moreover, comparison of the pseudo and mutant groups showed that freezing between the two groups differed statistically after the first trial (ITI-1, mutant versus pseudo, $p < 0.01$, $F_{1,33} = 16.7$) but did not reach statistical significance for the subsequent trials (ITI-2, $p = 0.07$, $F_{1,33} = 3.5$; ITI-3, $p = 0.6$, $F_{1,33} = 0.3$).

In order to more fully characterize the differential conditional response produced by the CS on the 24 hr trace test, we computed the mean change in freezing between the interval prior to (0–60 s) and following (75–135 s) the first CS (Figure 3C). A nonparametric test (Kolmogorov-Smirnov) showed that the mutant score was significantly different from the control score ($p < 0.0001$, $d = 0.8$) but not different from the naive ($p = 0.01$, $d = 0.7$) and

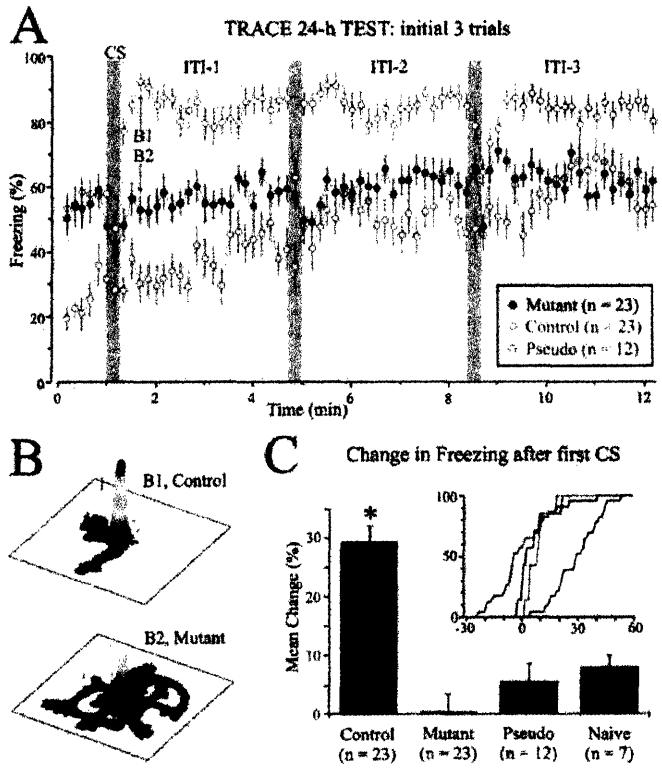

Figure 3. NR1-CA1-KO Mice Do Not Show Enhanced Freezing during the Trace Memory Test

(A) Pooled data showing the average percent freezing on the initial three trials of the 24 hr test after trace training for NR1-CA1-KOs (n = 23, closed circles) and controls (n = 23, open circles). The test was given in a novel chamber that differed from the conditioning chamber. Symbols represent mean freezing (± SEM) on a 10 s epoch. CS presentations are indicated by gray bars. For convenience, pooled data for pseudo-conditioned mice (n = 12, green circles), which received pseudo-training 24 hr earlier, are also plotted.

(B) Occupancy plots of 12 mutants and 12 controls for the 10 s epoch (105–115 s) indicated by "B1" and "B2" in (A). Plots were created by summing frame captures (200 ms in between frames) per mouse. The center of mass of the first frame was defined as the starting location of the mouse, which was then translated to the center of the plot. The x and y axes represent position (total of 300 pixels, which equals 25 cm). The vertical axis is color coded; 100% is red and equals the maximum possible occupancy for that location. High values indicate greater freezing and low values (and wider areas of occupancy) reflect exploration.

(C) Mean change in freezing elicited by the first CS in the memory test of trace fear conditioning. Change in freezing was calculated by computing the difference (F2 − F1) for each mouse, where F1 was freezing for the pre-CS period (0–60 s) and F2 was freezing for an equally long period during the ITI (75–135 s). Scores were averaged across animals, so that each column represents the mean value ± SEM for each mouse group. Asterisk indicates $p < 0.0001$ (one-way ANOVA between controls and mutants). The inset shows the mean change in freezing expressed as normalized cumulative distributions. Colors: control, red; NR1-CA1-KO, black; naive, blue; pseudo-conditioned, green.

the pseudo ($p = 0.02$, $d = 0.6$) scores. Moreover, the scores of controls were significantly higher than those of naive ($p < 0.01$, $d = 0.7$) and pseudo ($p < 0.001$, $d = 0.8$) groups.

Examination of the later segments of the 24 hr trace test (ITI-4 to ITI-10) revealed that controls maintained their high freezing until the end of the test session (data not shown). Comparison of control scores on ITI-10 (84.6% ± 3.1%) versus ITI-1 (84.3% ± 2.9%) showed no statistical difference ($p = 0.9$, $F_{1,44} = 0.006$). This implies that controls did not extinguish their enhanced conditional response even after several exposures to the CS. The freezing of NR1-CA1-KOs increased gradually as the test advanced. By the end of the test, it was only slightly below the freezing level attained by controls (ITI-10, 2100–2310 s, mutant, 75.9% ± 2.3%, control, 84.6% ± 3.1%, $p < 0.01$, $F_{1,44} = 11.6$). Since similar gradual increases in freezing were observed in the naive and the pseudo groups, we attribute these slow rises to habituation to the test chamber.

Finally, it was interesting to investigate whether the trace paradigm could be shortened. To this end we subjected NR1-CA1-KOs (n = 7), controls (n = 7), and pseudo mice (n = 10) to a training session of three CS–trace–US trials, instead of the previous ten trials. NR1-CA1-KOs froze somewhat less than controls during training (data not shown). On the 24 hr test, however, the three groups had similar scores (data not shown). A gradual increment in freezing observed in all groups was consistent with habituation. Thus, three trials of trace training did not seem sufficient for control mice to develop the temporal memory.

NR1-CA1-KO Mice Show Intact Memory in Delay Fear Conditioning

To demonstrate that the lack of enhanced freezing response displayed by the NR1-CA1-KO mice in the trace conditioning paradigm was not due to an impairment in expressing the conditional response per se, we trained a different set of mice in the delay fear conditioning paradigm (McEchon et al., 1998). In this paradigm, the CS onset preceded the US and both stimuli coterminated. The training sequence consisted of ten CS/US presentations with an ITI of 210 s. In this case, the freezing of mutants (n = 13) was only slightly less than controls (n = 15) throughout the training session, without reaching statistical significance (Figures 4A and 4B, overall scores: mutant, 60.8% ± 5.8%, control, 69.0% ± 3.2%, $p = 0.2$, $F_{1,26} = 1.6$; ITI-1, 75–285 s, mutant, 47.8% ± 8.2%, control, 49.4% ± 5.2%, $p = 0.9$, $F_{1,26} = 0.03$; ITI-2, 300–510 s, mutant, 51.4% ± 6.9%, control, 64.5% ± 5.2%, $p = 0.1$, $F_{1,26} = 2.4$; ITI-3, 525–735 s, mutant, 62.7% ± 8.0%, control, 74.1% ± 5.3%, $p = 0.2$, $F_{1,26} = 1.4$). This implies that NR1-CA1-KOs were able to freeze as efficiently as controls and were not exhibiting a generalized fear deficit during trace training.

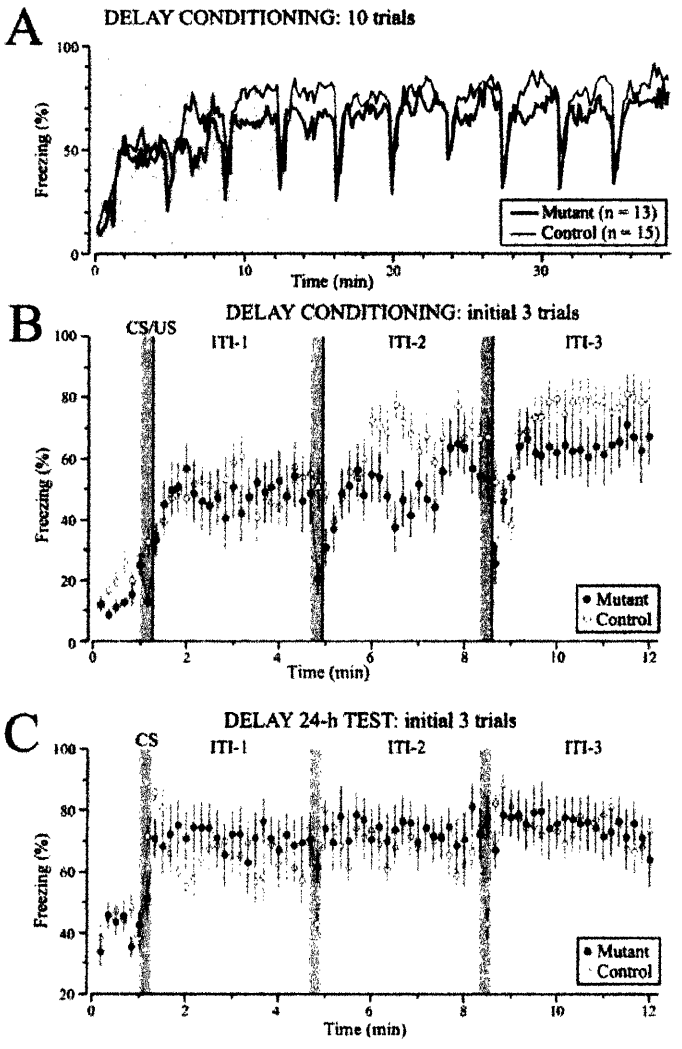

Figure 4. NR1-CA1-KO Mice Are Intact on Delay Fear Conditioning

(A) Time course of the average percent freezing displayed by mutants (n = 13) and controls (n = 15) during the acquisition of delay conditioning. The gray box, at left, indicates the initial three trials, which are enlarged in (B).

(B) Pooled data showing the average percent freezing on the initial phase of acquisition for NR1-CA1-KOs (closed circles) and controls (open circles). Symbols represent mean freezing (± SEM) on a 10 s epoch. CS presentations are indicated by gray bars and US occurrence by green bars.

(C) Pooled data showing the average percent freezing on the initial three trials of the 24 hr test after delay training for NR1-CA1-KOs (closed circles) and controls (open circles).

Additionally, we examined the behavior of delay-trained mice during a 24 hr memory test (Figure 4C). Had the lack of enhanced freezing after the CS of NR1-CA1-KOs in the trace 24 hr test been due to a sensory-motor deficiency that blocked the reaction to the CS (for instance, mutants could have a hearing deficit), it would be expected that mutants show lowered freezing during the delay 24 hr test. However, we found that the freezing responses of mutants did not differ from controls during the ITI periods (Figure 4C; ITI-1, 75–285 s, mutant, 70.8% ± 7.8%, control, 65.3% ± 5.3%, $p = 0.5$, $F_{1,26} = 0.4$; ITI-2, 300–510 s, mutant, 73.6% ± 7.1%, control, 67.7% ± 4.9%, $p = 0.5$, $F_{1,26} = 0.5$; ITI-3, 525–735 s, mutant, 74.8% ± 6.5%, control, 73.9% ± 3.9%, $p = 0.9$, $F_{1,26} = 0.02$). This implies that the white noise used as a CS was able to elicit a robust conditional response in mutants, but only when the appropriate CS–US contingency was met during training. During the presentation of the CS, control mice displayed a reduction in freezing, whereas mutants did not. This could mean that controls were able to learn that it was safe to move during the delivery of the CS, while mutants did not. However, we did not address this point further.

Our results point to a behavioral dissociation in the mutants; that is, they show impaired trace but intact delay conditioning. Since it is accepted that the neural substrate for delay fear conditioning involves the amygdala (LeDoux, 1993; Davis et al., 1994; Rogan et al., 1997; Fendt and Fanselow, 1999), it was reassuring that mutants lacking NMDARs only in CA1 cells were normal in this variant of Pavlovian learning.

Discussion

Our work provides a demonstration that NMDA receptors within CA1 pyramidal neurons are crucial for the formation of a memory based on the association of events across time. What mechanisms involving NMDARs in CA1 could bridge the temporal gap required to learn the association? In what follows we offer two potential mechanisms, the first based on the activity of single hippocampal cells and the second on hippocampal ensembles.

A fundamental assumption regarding the substrate of conditioning is that it requires temporal overlap of the

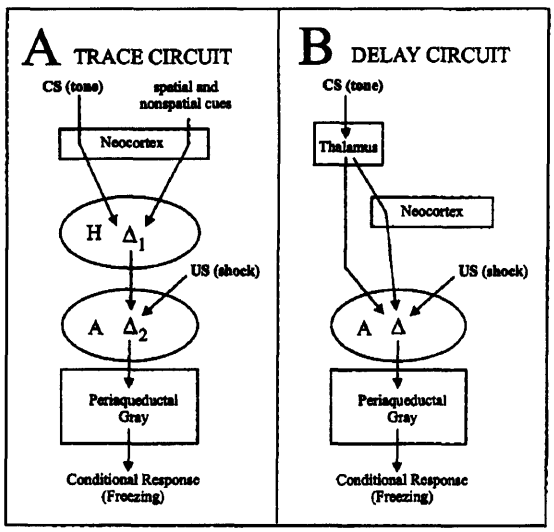

Figure 5. Putative Neural Substrate for Trace Fear Conditioning

(A) The trace circuit shows the brain regions underlying the association of the CS (tone) with the US (shock) across the trace interval. The CS, spatial, and nonspatial cues are processed in neocortex and converge into the hippocampus (H). We hypothesize that NMDAR-dependent synaptic plasticity (indicated by Δ_1) is needed to associate the spatial and nonspatial cues with the CS. This relational representation is fed into the amygdala (A), which associates it with the US via synaptic plasticity (Δ_2). The trace circuit terminates in the periaqueductal gray, which executes the conditional response (freezing).

(B) The delay circuit is simpler and requires the conjunction of the CS (tone) with the US (shock) in the amygdala. Notice that the CS representation reaches the amygdala from the auditory thalamus as well as from the auditory cortex. The delay circuit finishes in the periaqueductal gray, which executes the conditional response (freezing).

neural activities representing the CS and the US. These activities would converge and be associated within neural structures such as the amygdala for delay fear conditioning (Figure 5; LeDoux, 1993; Davis et al., 1994; Rogan et al., 1997; Fendt and Fanselow, 1999) or the cerebellum for motor conditioning (Kim and Thompson, 1997). In the case of trace fear conditioning, in which the CS and the US are temporally dissociated, a straightforward possibility is that individual CA1 cells could respond selectively to the CS and sustain their activity after CS removal, allowing for the ongoing activity to be associated with the US. Hippocampal recordings during trace eye blink conditioning, in which the trace interval is usually 1 s, have shown that certain CS-responsive cells maintain their firing for about 1 s after CS cessation (Berger et al., 1976; McEchon and Disterhoft, 1997). Thus, it is possible that on trace fear conditioning there might be CA1 cells that respond to the CS and fire for up to 30 s upon CS removal, although such activity has not yet been observed.

A different possibility stems from the observation that ensembles of CA1 cells can encode regularities present in the animal's experience, which include spatial and nonspatial cues as well as behavioral actions. In particular, it is well established that pyramidal neurons in CA1 can exhibit place cell activity; that is, they can fire in a location-specific manner (O'Keefe and Nadel, 1978; Wilson and McNaughton, 1993; O'Keefe, 1999). It is also well known that CA1 cells can fire in response to nonspatial stimuli in rodents performing tasks in which these stimuli occur in a regular fashion (Olton, 1989; Sakurai, 1996; Eichenbaum et al., 1999; Wood et al., 1999). A recent proposal that we shall call the *episodic encoding* model (Eichenbaum et al., 1999) posed that individual hippocampal cells that fire at about the same time, in response to both spatial and nonspatial features, could be organized into an ensemble that represents an event. Moreover, event ensembles could be organized along a temporal sequence, comprising an episode.

Applying these notions to trace fear conditioning, we hypothesize that ensembles of CA1 cells play an intermediary role for the association of the temporally dissociated CS and US. As a mouse is introduced into the conditioning chamber, distinct CA1 cell ensembles would be activated in a continuous manner. These ensembles would be composed of place cells as well as cells encoding nonspatial features. It follows that each US delivery will be paired with an active ensemble. The temporal overlap of CA1 ensemble activity and the US satisfies one of the requirements for conditional association. What remains is the need to incorporate CS-specific information into the activity of CA1 cell ensembles. In fact, it has been documented that sensory-related factors can strongly influence place cell activity (O'Keefe and Speakman, 1987). Also, given the regular occurrence of the CS, it is feasible that distinct CA1 cells become activated by it. We hypothesize that the CS representation is *entrained* into CA1 cell ensembles through NMDAR-dependent synaptic plasticity in CA1 (Figure 5A), possibly leading to enhanced covariance of ensemble responses, which has been shown to be NMDAR dependent (McHugh et al., 1996; Tonegawa et al., 1996). Repeated CS delivery during training would progressively pair the CS with multiple hippocampal ensembles. Subsequent US delivery would overlap with these CS-entrained ensembles, forming hippocampally dependent associations in downstream structures such as the amygdala (Figure 5A). Notice that our description can easily be phrased in terms of the episodic encoding model. Namely, CS-paired and US-paired ensembles represent events that are organized into a repetitive sequence, i.e., the conditioning episode.

Our hypothesis must also explain how the association can be recalled during the memory test in a novel environment. What is required is that, upon presentation of the CS only, the CS-entrained hippocampal ensembles (established on training) become *reactivated* and then trigger downstream circuits responsible for the conditional response. Support for this idea comes from the observation that transient cue delivery can reactivate hippocampal ensembles established through prior association with those cues (Muller and Kubie, 1987; Quirk et al., 1990). This has led to suggestions that the hippocampus is capable of carrying out pattern completion, in which subsets, or even single cues, are capable of reestablishing an original pattern of activity (Marr, 1971; McNaughton and Morris, 1987; Recce and Harris, 1996). In the present study, mice were introduced into a novel

environment during the memory test, presumably activating CA1 cell ensembles that differed from those present in the previous conditioning chamber. Upon CS delivery, ensembles related to the conditioning chamber would be strongly reactivated, driving downstream circuits to execute the freezing response. Such reactivation has not been experimentally tested but would be predicted based on our proposal.

In conclusion, our results point to a novel function of NMDARs within CA1 neurons by showing that they are essential in the formation of temporal memory. The fact that hippocampus-dependent memories in rodents extend into the spatiotemporal domain makes it feasible that they are conceptually close to the episodic memories described in humans.

Experimental Procedures

Subjects

The generation of knockout mice is detailed elsewhere (Tsien et al., 1996). NR1-CA1-KO male mice (49–78 days of age) were heterozygous for the viral *Cre* recombinase gene and homozygous for the floxed *NR1* gene. Mice in the control, pseudo-conditioned, and naive groups were male littermates, homozygous for the floxed *NR1* gene. Their age range was 49–85 days of age. Mice were handled for 5 min per day during a week before testing. They were kept in isolation only during conditioning.

Apparatus

Training occurred in chamber A (25 cm × 30 cm, height 35 cm; two adjacent walls were painted white, while the others were red and yellow). The floor was a removable foot-shocking grid (Coulbourn, Allentown, PA). Illumination was provided by seven white 1 W bulbs placed onto a transparent plexiglass ceiling. Chamber A was inside a sound-attenuating enclosure. For the 24 hr test we used chamber B (round basket; diameters: 30 cm bottom, 40 cm top, height 60 cm; bedding at the floor, gray walls) and chamber C (25 cm × 25 cm, height 60 cm; white PVC walls and floor). Chambers B and C were illuminated by three orange 25 W bulbs. A CCD camera (Phillips, LDH 351, b/w) was mounted above them. Chambers were manufactured by Mike's Machine Company (Attleboro, MA).

Conditioning

Stimuli were US (scrambled foot-shock, 0.5 s, 0.7 mA intensity) controlled by a shocker (Coulbourn) and CS (white noise, 15 s, 80 db volume) delivered through a speaker (Med Associates, St. Albans, VT) located outside the chambers. Presentations of CS and US were controlled by routines (L. D. S.) within *ad* software (M. A. W. and L. Frank) running in a DOS PC. For trace training, a mouse was placed in chamber A and, after 60 s, was subjected to ten CS–trace–US–ITI trials (trace of 30 s, ITI of 210 s). The next day, mice were exposed to the memory test (in chamber B or chamber C, located in a different room), which consisted of a 60 s introduction followed by ten CS–ITI trials (ITI of 210 s). Delay training occurred in chamber A and consisted of ten CS/US–ITI trials (CS and US coterminated). The next day, mice received the memory test (ten CS–ITI trials). Mice in the pseudo-conditioned group underwent a training session of unpaired stimuli with the CS and the US separated by 120 s. The sequence of delivery was CS–US–CS–CS–US–CS–CS–US–CS–US–CS–US–US–CS–US–CS–US–CS–US–US. The next day animals were given ten CS–ITI trials in chamber B. Mice in the naive group were placed into chamber A for 43.5 min on the first day and, 24 hr later, were given ten CS–ITI trials in chamber B.

Data Collection and Analysis

We used two independent methods for data collection. For the "tracking" method, the CCD camera provided the signal to a contrast tracker (Dragon, SA-3) with a pixel resolution of 327 horizontal by 243 vertical. Dark objects (i.e., the mouse coat) were tracked on a light background. The x/y coordinates of the tracked points stored in the tracker's cache were transmitted to PC through a 16 bit i/o card (CIO-CTR10, Computer Boards) into the *ad* software (60 Hz sampling rate; each time instance consisted of 50–150 tracked points, maximum of 253) for storage. Data was then transferred to a Linux PC and analyzed with C routines (I. H. Chan and P. T. H.). A masking filter was first applied to those cases that presented streaks of noise. Noise was common in chamber A because of the reflections of the shock bars onto the floor. Then, 12 consecutive frames were collapsed (5 Hz data binning) and the center of mass was calculated. Freezing was defined as a distance of <2 pixels between centers of mass of two consecutive frames. Freezing was summed over a 10 s epoch and expressed as a percentage (where 100% is a value of 50, given the 5 Hz binning) for each mouse. Time course plots were generated by averaging the percentage values across all mice in the group. Statistical analysis consisted of one-way analysis of variance (ANOVA) performed between subjects of two appropriate groups. The tracking method was calibrated by comparing the freezing scores to visually scored freezing done by blind observers (Figure 1). Briefly, six observers scored freezing for six mice subjected to contextual fear conditioning. Mice were placed in chamber A and after 3 min were shocked three times with an interval of 1 min between shocks. The next day, mice were placed in chamber A for 6 min. The observers scored freezing every 10 s (1 s observations on a video monitor).

For the "video" method, the CCD camera provided the video signal to a VCR (taping in SVHS-SP mode). Taped data were replayed into MATLAB (The MathWorks, Natick, MA) video acquisition software (5 Hz sampling rate) through a video card (Matrox Meteor) running in a Linux PC. Each frame was an 8 bit grayscale image (320 × 240 pixels). Routines in MATLAB (B. Fedeles and L. D. S.) first applied a filter (a bitmapped image of a mouse subtracted from the environment) and then calculated the pixel difference between frames (Figure 1B), which ranged between 0 and 2500 pixels. A difference of <50 pixels was defined as freezing. The freezing scores produced with this method confirmed the results obtained with the tracking method.

Acknowledgments

We thank Francis Bushard, Ian Chan, Bogdan Fedeles, Dennis King, and James B. Williams II for their assistance. We are also grateful to Michael Davis, Howard Eichenbaum, Michael Fanselow, Joseph LeDoux, Richard G. Morris, and Larry Squire for their insightful comments on versions of the manuscript. This work was supported by the National Institutes of Health. P. T. H. is a Pew Latin American Fellow.

Received November 4, 1999; revised February 3, 2000.

References

Berger, T.W., Alger, B.E., and Thompson, R.F. (1976). Neuronal substrates of classical conditioning in the hippocampus. Science *192*, 483–485.

Chiba, A.A., Kesner, R.P., and Reynolds, A.M. (1994). Memory for spatial location as a function of temporal lag in rats: role of hippocampus and medial prefrontal cortex. Behav. Neural Biol. *61*, 123–131.

Cohen, N.J., and Eichenbaum, H. (1993). Memory, Amnesia and the Hippocampal System (Cambridge, MA: MIT Press)

Davis, M., Rainnie, D., and Cassell, M. (1994). Neurotransmission in the rat amygdala related to fear and anxiety. Trends Neurosci. *17*, 208–214.

Eichenbaum, H., Dudchenko, P., Wood, E., Shapiro, M., and Tanila, H. (1999). The hippocampus, memory, and place cells: is it spatial memory or a memory space? Neuron *23*, 209–226.

Fanselow, M.S. (1990). Factors governing one-trial contextual conditioning. Anim. Learn. Behav. *18*, 264–270.

Fendt, M., and Fanselow, M.S. (1999). The neuroanatomical and neurochemical basis of conditioned fear. Neurosci. Biobehav. Rev. *23*, 743–760.

Jackson, P.A., Kesner, R.P., and Amann, K. (1998) Memory for duration: role of the hippocampus and medial prefrontal cortex. Neurobiol. Learn. Mem. *70*, 328–348.

Jarrard, L.E. (1993). On the role of the hippocampus in learning and memory in the rat. Behav. Neural Biol. *60*, 9–26.

Kim, J.J., and Thompson, R.F. (1997). Cerebellar circuits and synaptic mechanisms involved in classical eyeblink conditioning. Trends Neurosci. *20*, 177–181.

LeDoux, J.E. (1993). Emotional memory systems in the brain. Behav. Brain Res. *58*, 69–79.

Lyford, G.L., Gutnikov, S.A., Clark, A.M., and Rawlins, J.N.P. (1993). Determinants of non-spatial working memory deficits in rats given intraventricular infusions of the NMDA antagonist AP5. Neuropsychologia *31*, 1079–1098.

Marr, D. (1971). Simple memory: a theory for archicortex. Proc. R. Soc. Lond. B Biol. Sci. *262*, 23–81.

McEchon, M.D., and Disterhoft, J.F. (1997). Sequence of single neuron changes in CA1 hippocampus of rabbits during acquisition of trace eyeblink conditioned responses. J. Neurophysiol. *78*, 1030–1044.

McEchon, M.D., Bouwmeester, H., Tseng, W., Weiss, C., and Disterhoft, J.F. (1998). Hippocampectomy disrupts auditory trace fear conditioning and contextual fear conditioning in the rat. Hippocampus *8*, 638–646.

McHugh, T.J., Blum, K.I., Tsien, J.Z., Tonegawa, S., and Wilson, M.A. (1996). Impaired hippocampal representation of space in CA1-specific NMDAR1 knockout mice. Cell *87*, 1339–1349.

McNaughton, B.L., and Morris, R.G.M. (1987). Hippocampal synaptic enhancement and information storage within a distributed memory system. Trends Neurosci. *10*, 408–415.

Meck, W.H., Church, R.M., and Olton, D.S. (1984). Hippocampus, time, and memory. Behav. Neurosci. *98*, 3–22.

Morris, R.G.M., Garrud, P., Rawlins, J.N.P., and O'Keefe, J. (1982). Place navigation impaired in rats with hippocampal lesions. Nature *297*, 681–683.

Morris, R.G.M., Anderson, E., Lynch, G.S., and Baudry, M. (1986). Selective impairment of learning and blockade of long-term potentiation by an N-methyl-D-aspartate receptor antagonist, AP5. Nature *319*, 774–776.

Muller, R.U., and Kubie, J.L. (1987). The effects of changes in the environment on the spatial firing of hippocampal complex-spike cells. J. Neurosci. *7*, 1951–1968.

Nadel, L. (1991). The hippocampus and space revisited. Hippocampus *1*, 221–229 [accompanying debate, 230–291].

O'Keefe, J. (1999). Do hippocampal pyramidal cells signal non-spatial as well as spatial information? Hippocampus *9*, 352–364.

O'Keefe, J., and Nadel, L. (1978). The Hippocampus as a Cognitive Map (London: Oxford University Press).

O'Keefe, J., and Speakman, A. (1987). Single unit activity in the rat hippocampus during a spatial memory task. Exp. Brain Res. *68*, 1–27.

Olton, D.S. (1989). Mnemonic functions of the hippocampus: single unit analyses in rats. In The Hippocampus—New Vistas, V. Chan-Palay and C. Kohler, eds. (New York: A. R. Liss), pp. 411–424.

Phillips, R.G., and LeDoux, J.E. (1994). Lesions of the dorsal hippocampal formation interfere with background but not foreground contextual fear conditioning. Learn. Mem. *1*, 34–44.

Quirk, G.J., Muller, R.U., and Kubie, J.L. (1990). The firing of hippocampal place cells in the dark depends on the rat's recent experience. J. Neurosci. *10*, 2008–2017.

Recce, M., and Harris, K.D. (1996). Memory for places: a navigational model in support of Marr's theory of hippocampal function. Hippocampus *6*, 735–748.

Radulovic, J., Kammermeier, J., and Spiess, J. (1998). Generalization of fear responses in C57BL/6N mice subjected to one-trial foreground contextual fear conditioning. Behav. Brain Res. *95*, 179–189.

Rawlins, J.N.P. (1985). Associations across time: the hippocampus as a temporary memory store. Behav. Brain Sci. *8*, 479–496.

Rogan, M.T., Staubli, U.V., and LeDoux, J.E. (1997). Fear conditioning induces associative long-term potentiation in the amygdala. Nature *390*, 604–607.

Sakurai, Y. (1996). Hippocampal and neocortical cell assemblies encode memory processes for different types of stimuli in the rat. J. Neurosci. *16*, 2809–2818.

Schacter, D.L., and Tulving, E. (1994). Memory Systems 1994 (Cambridge, MA: MIT Press).

Squire, L.R., and Kandel, E.R. (1999) Memory: From Mind to Molecules, Scientific American Library, No. 69 (New York: Freeman and Company).

Tonegawa, S., Tsien, J.Z., McHugh, T.J., Huerta, P.T., Blum, K.I., and Wilson, M.A. (1996) Hippocampal CA1-region-restricted knockout of NMDAR1 gene disrupts synaptic plasticity, place fields, and spatial learning. Cold Spring Harbor Symp. Quant. Biol. *61*, 225–238.

Tsien, J.Z., Huerta, P.T., and Tonegawa, S. (1996) The essential role of hippocampal CA1 NMDA receptor–dependent synaptic plasticity in spatial memory. Cell *27*, 1327–1338.

Vargha-Khadem, F., Gadian, D.G., Watkins, K.E., Connelly, A., Van Paesschen, W., and Mishkin, M.F. (1997). Differential effects of early hippocampal pathology on episodic and semantic memory. Science *277*, 376–380.

Wilson, M.A., and McNaughton, B.L. (1993). Dynamics of the hippocampal ensemble code for space. Science *261*, 1055–1058.

Wood, E.R., Dudchenko, P.A., and Eichenbaum, H. (1999). The global record of memory in hippocampal neuronal activity. Nature *397*, 613–616.

Autoclave all metal non-sterile surgery equipment or soak in 100% EtOH O/N before starting. On the surgery table have ready: acrylic, silver paint, screw, shrink wrap ready to go. The last few minutes of the surgery are critical especially since the mouse becomes out from the anesthesia and can wake up at any time.

I. Anesthesia

- **Stock Solution (II):** 2.5% Tribromoethanol (Avertin) in Tert Amyl Alcohol. Make by mixing 1 Gm of Tribromoethanol powder into 630ul T-Amyl-Alcohol. Vortex and mix well O/N. Store at 4°C.
- Dilute Stock 60µl into 5ml 1xPBS (sterile), shake vigorously, then filter sterilize. Final concentration is 18mg/ml TriBrEtOH. Store at 4°C.
- Advice: The primary goal is to get your mouse down as quickly as possible w/o causing harm. It's better to have fewer injections over all rather than a little bit again and again and again.
- This is a sample of a *long lasting* surgical anesthesia protocol with a WT mouse: We used a low dosage injection into a 29.5gm mouse with 0.6cc diluted Avertin. The mouse passed out at medium speed while his breathing was still fairly fast. He was a little light at 8' so we gave him additional 0.2cc. At 25' still light so give 0.15cc additional. At 30' still light (toe pinch gave reaction). An additional 0.2cc by 35' he was dead. At 1:09' injection 0.25cc. 2:08 done exposure/suture up time. Begin to whisk.

0:00 M. Wilson Surgical Time Elapsed (LDS Current Time Elapsed)

Wipe the mouse's belly with isopropyl alcohol and let dry for a few seconds!!!

Inject Avertin with a 26 gauge needle into the interperitoneal area. Don't inject too deep, but deep enough to enter peritoneal cavity. Injecting too high near his ribcage will damage his liver, too low will damage the intestines. After inserting the hypodermic, pull back slightly on syringe to insure that no blood (red) or bile (yellow) is present indicating organ penetration. If not clear, withdraw and discard syringe and start again. DO NOT REINJECT.

Appendix G: Surgical Protocol

Wilson Lab Mouse Surgery Protocol
L.D.Sun, M.A. Wilson
Version 5.9: 8/14/2003

Pre-surgery setup required:

___ 10% Povidine-Iodine

___ 70% EtOH

___ Saline

___ Silicone Grease/Bone wax

___ Cotton Swabs

___ Sterile Field

___ Ophthalmic Anti-Biotic Ointment

___ Pipette + bulb for saline

___ 2xEREM 00d5a tweezer for suture

___ Roboz Tweezers (Micro 45° RS-5005)

___ scalpels

___ scrapers

___ scissor

___ stereotaxic setup

___ skin clip + nuts

___ Drill bit HP-1/4 Stoelting

___ Calipers (mm)

___ MICRO screwdriver

___ 12x screws (.77mm width)

___ 1x ground screw (1 screw w/glued by silver paint 3" stripped wire A-M Systems 15 .005 bare/.0065 coated)

___ shrink wrap

___ Dental acrylic + Solvent + dish

___ silver paint

___ suture [FS-2 3/8 19mm 4-0]

___ surgical gloves

___ metaphane breather

___ 3 x 1cc syringe with 1" 26 gauge needle + 0.8cc Diluted 18mg/ml Avertin.

___ 1 x 1cc syringe with 1" 27 gauge needle + 0.25cc Lidocane.

___ 1 mouse in a relaxed state.

___ Spray down area/stereotax with 70% EtOH let dry.

NOTE: Notice how quickly animal goes down, this will indicate the sensitivity of your mouse and the concentration of your anesthetic, which is necessary to have a good feeling for esp. for the second application of anesthetic.

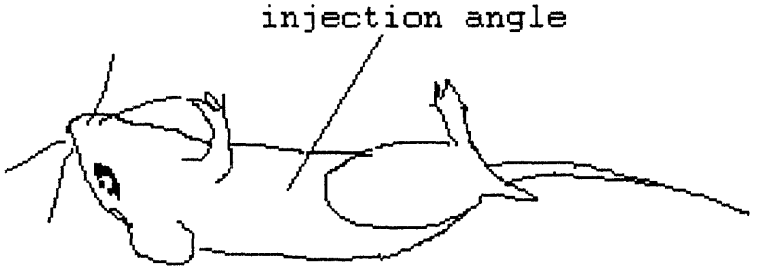

While the animal shows no movement, apply ophthalmic ointment (chloremphenicol in glycerin) to eyes of unconscious animal. Then shave its skull hair off in the area indicated and wipe it down with a fresh wet paper towel at least 3 times to get rid of extraneous hair matter which WILL get into the surgical wound!

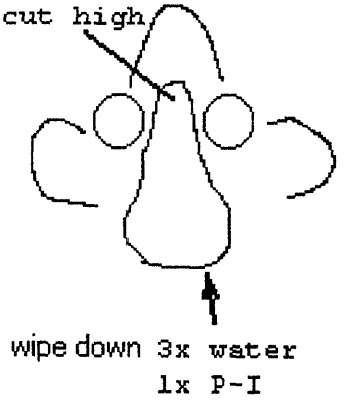

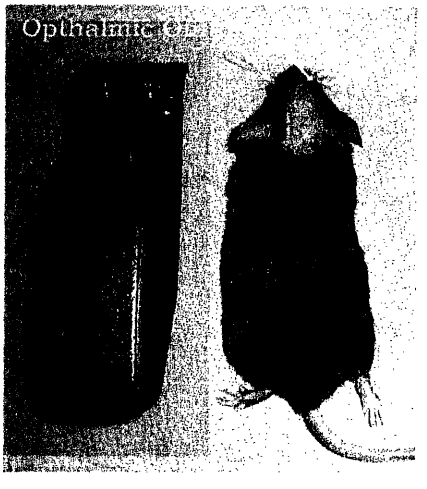

Meanwhile have the isothermic pad microwaved and ready or use electric thermal pad/blanket.

II. Stereotaxic Equipment

Tools needed:

- Stereotaxic bars
- Ophthalmic antibiotic ointment
- Add topical Otic Drops to the ears of the mouse before applying ear bars.

Find spot where the ear bars fit (only use light pressure inwards to the skull). Notice that the mouse might blink if he light on anesthesia, when both bars are in place and the mouse is suspended. Do not clamp the ear bars on too tightly but tight enough so the skull won't move when drilling! The earbars are the most difficult part of the surgery.

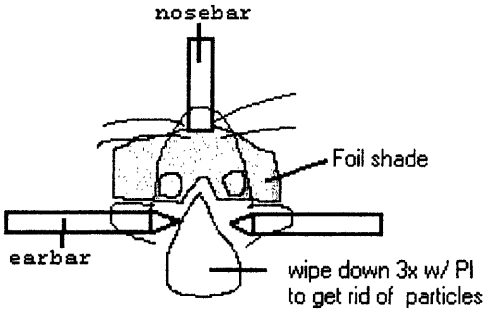

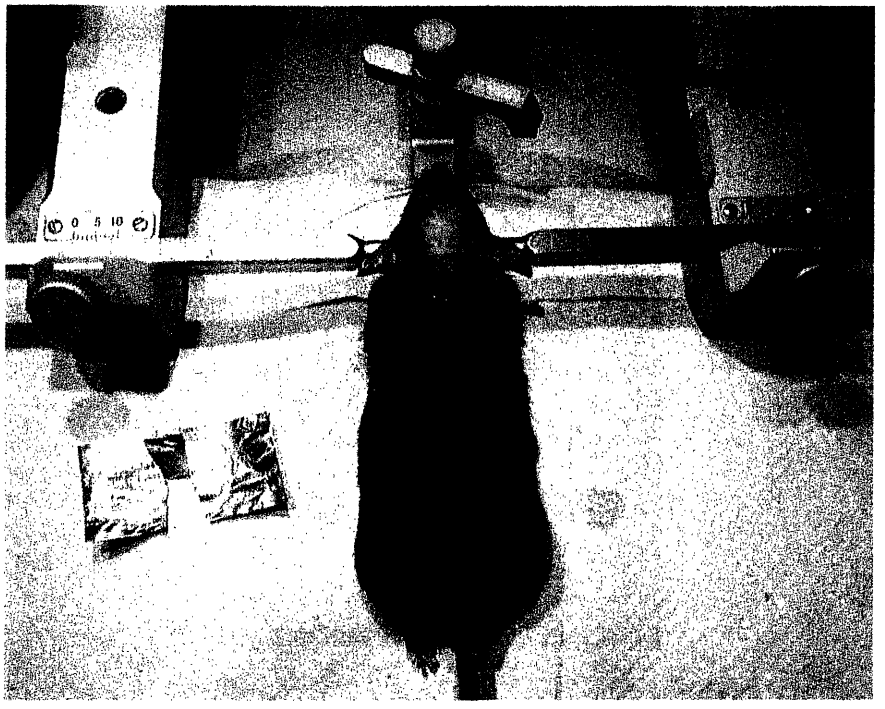

The mouse's ears will be pointing sideways after it is clamped and you can rotate it's body along the ear axis by lifting and lowering it's body from it's tail.

0:10 Ear bars done (0:22)

Appendix F: Collaborative Contributions to "Neurotrophin-3 modulates noradrenergic neuron function and opiate withdrawal"

Akbarian, S., Bates, B., Liu, R. J., Skirboll, S. L., Pejchal, T., Coppola, V., Sun, L. D., Fan, G., Kucera, J., Wilson, M. A., *et al.* (2001). Mol Psychiatry *6*, 593-604.

Abstract:

Somatic symptoms and aversion of opiate withdrawal, regulated by noradrenergic signaling, were attenuated in mice with a CNS-wide conditional ablation of neurotrophin-3. This occurred in conjunction with altered cAMP-mediated excitation and reduced upregulation of tyrosine hydroxylase in A6 (locus coeruleus) without loss of neurons. Transgene-derived NT-3 expressed by noradrenergic neurons of conditional mutants restored opiate withdrawal symptoms. Endogenous NT-3 expression, strikingly absent in noradrenergic neurons of postnatal and adult brain, is present in afferent sources of the dorsal medulla and is upregulated after chronic morphine exposure in noradrenergic projection areas of the ventral forebrain. NT-3 expressed by non-catecholaminergic neurons may modulate opiate withdrawal and noradrenergic signaling.

My Contribution:

This study claims that the opiate withdrawal response learning is modulated by NT-3 activity as manipulated by a transgene-delivered overexpression mouse model. In order to eliminate the possibility that the reduced opiate withdrawal symptoms seen in NT-3 conditional knockouts wasn't due to a generalized learning deficit, I conducted a fear conditioning

experiment utilizing my custom made automated fear conditioning analysis system which I developed previously (Huerta, Sun, Wilson, Tonegawa, 2000). I showed that there was a five fold increase in freezing behavior in both NT-3 conditional knockouts and in control mice thus eliminating the possibility that the reduced withdrawal symptoms was the result of a generalized learning deficit in the mutant NT-3 conditional knockout mice.

Here's the trick: place left ear bar on stereotax platform first, then grab the head of the mouse between your middle and thumb finger with the thumb on top of the skull and middle finger underneath the jaw, find the spot where the ear bar can fit nicely by "playing" with the head slightly onto the ear bar. Do the same for the other ear bar. Set up screw on right stereotax so you clamp down on the ear bar quickly. Lift up mouse by the tail and see if he can be suspended by the ear bars only. Next, clamp on nose bar to prevent head pitch movement.

III. Pre-exposure Anesthesia

Items needed:

- metaphane breather (metaphane on a piece of gauze in an eppendorf tube).
- 0.25cc Lidocane in 1cc syringe 27 gauge needle.
- tweezers.
- Antibiotics: ophthalmic ointment, Povidine-Iodine.

This intermediate step is very important. You must test wakefulness of the animal. Pinch the mouse's foot with your thumbnail. If there is a response, wait 5 minutes to see if the Avertin takes hold. If not, then inject with no more than 0.1cc of Avertin, at a maximum of a full dose every 45 minutes. Wait until the mouse is totally knocked out (i.e. no response). Look for lack of these responses for deep anesthesia:

➔ whisking of whiskers

➔ Leg withdrawal- Pull on leg so muscle is extended + pinch toes. If the leg stays there then the animal is out and it's reflex arcs are not responsive.

➔ breathing speed- the deeper the animal the slower the breathing.

➔ tail pinch- leads to absence of diaphragm contraction.

0:15 Lidocane Injection (0:31)

First, clean scalp with 70% EtOH swab followed by Povidine-Iodine and saline. Use cotton swab in outward spiraling wiping motion (clean from center -> out).

Spread a single dose of Lidocane (0.1-0.15mls) with sub-cutaneous injections along the incision line of the scalp.

- Technique: Lift skin with tweezers, and then apply needle to skin pocket.

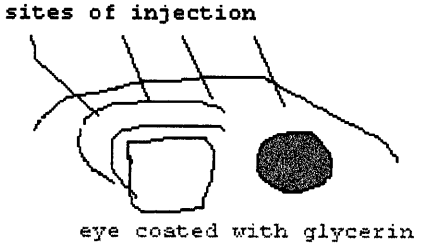

IV. First Cut

Tools needed:

- tweezers
- scalpel with fresh blade

0:17 First Cut (0:35)

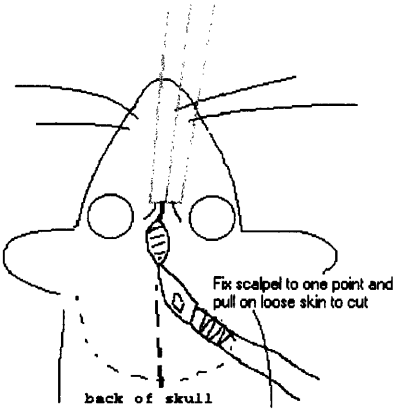

Grab skin just at the front of the orbits and make a single incision with a scalpel from the tweezers to the back of the skull. Preferred technique: Put scalpel down on skull and then drag skin across. When in doubt, cut skin further forward and further back. You will see some bleeding at back of skull which is normal.

Use a pair of micro-dissection scissors to cut fatty tissue near the back of the skull. This is necessary to expose the rear skull for bone screws.

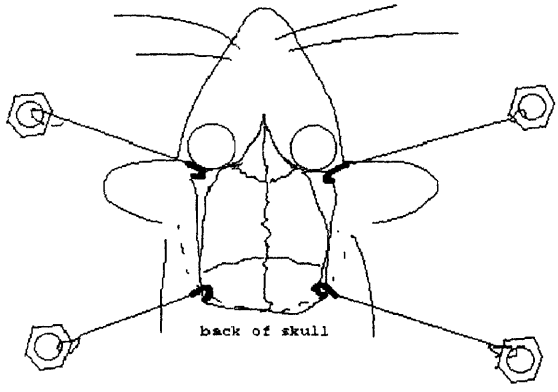

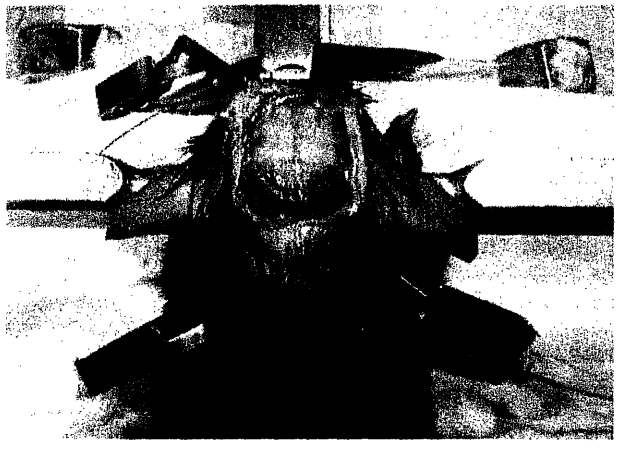

Next, use hooks and nuts to hold scalp skin open.

NOTE: If there is minor bleeding due to high vascularization of skin around the orbits, cauterize the blood with hot pen (not recommended) or plug with bone wax.

Next, scrape down periosteum with scraping tool, i.e. remove soft tissue layering. Finally wipe the scalp down with saline with sterile cotton swabs.

0:18 Finished cleaning/scraping down skull (0:43)

V. Dremel part 1: Bone Screws

Items needed:

- White Burs drill bit: (SSW)HP-¼ + working dremel.
- 6 bone screws + 1 ground screw.

The ground screw is a bone screw plus a wire attached to it. It is made the previous day by wrapping 0.005 mill wire around a skull screw + silver paint.

0:20 Drilling Time (0:45-1:00 for 3 screws!!! Shit!)

Start drilling!!! If you are right handed make seven holes as in the diagram in the ORDER SHOWN since it will make your life much easier to hold screws with your left hand while tightening with a screw driver your right hand.

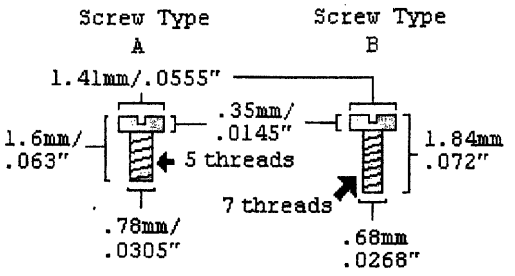

(smaller screw requires a smaller drill hole, though it works, maybe less stable)

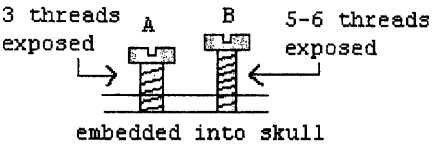

Technique: Hold drill handle with right hand and hold with left hand finger the head of the handle. Your left hand should be gently pushing upwards to support drill. Drill directly downwards, but not too deep. For HP-1/4 drills, the hole for a .78mm width screw is barely larger than the drill bit tip.

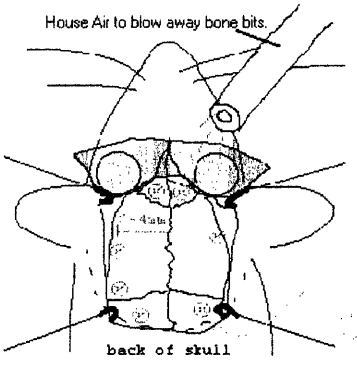

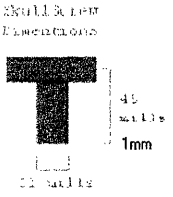

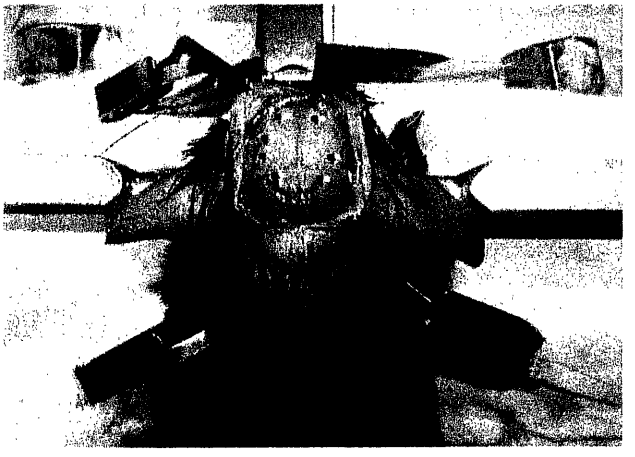

Screw down each skull screw vertically in by 1-1½ turns, until it catches and an additional ½ turn to lock it down. If you drill a hole too big, fill it with bone wax and drill another at some distance.

0:35 Exposure Drilling (Prepare secondary IP anesthetic)

VI. Dremel Part 2: Drive Entry Point

Use Capillary action of saline + cotton swab to suck off blood.

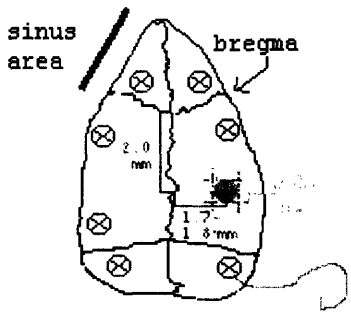

Note: Do not implant screws too close together on skull! Allow plenty of room for exposure to take place and implant screws as laterally as possible.

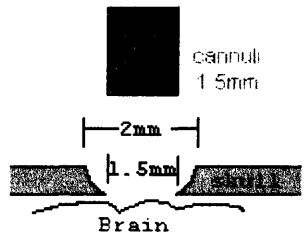

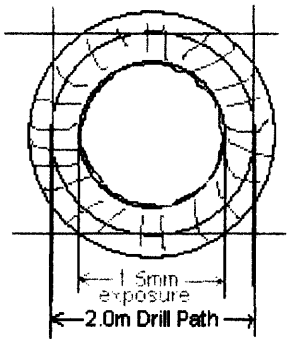

At a point 2.0-2.1 mm posterior to the bregma and 1.7-1.8 mm lateral from the midline mark off using a custom made caliper and a scalpel blade the center of your exposure hole. Also mark the boundaries for a 1.5-2mm wide exposure w/scalpel.

Note: Make an initial size of exposure 0.5-0.75mm larger than the bottom cannuli due to skull fragment underhang thus to allow sufficient clearance for tetrodes. This is due to the drill bit being cone shaped at bottom.

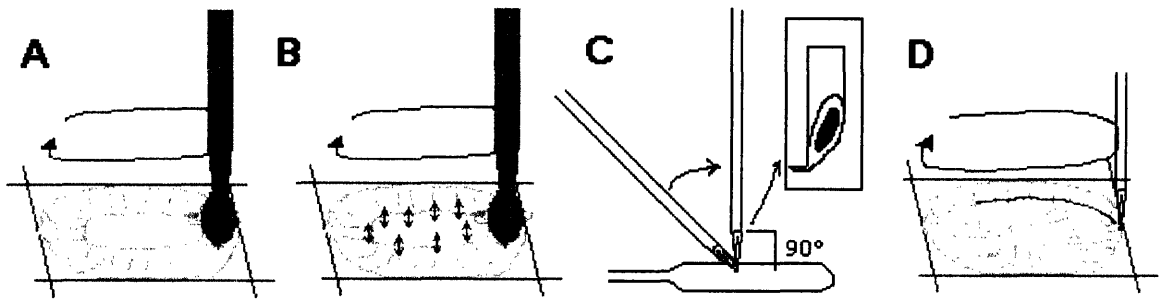

Fig A: Try and make a perfect circle and drill using medium to high (but NOT highest or lowest) speed of the drill. Slowly ever so slowly work down a perfect donut valley of thin skull fragment, but do NOT puncture the skull. Go so so slowly. Make sure to LEAVE a middle thick island of skull fragment.

Fig B: Notice that when it becomes paper thin, when you press down with your spinning drill bit, the entire think skull circle will move down ever so slightly together. There may be bleeding through skull capillaries, you can get rid of this by cotton swabs or plugging it with a wad of

bone wax. Avoid letting the brain tissue dry out by keeping it moist with saline and decreasing the air speed that is blowing away the bone fragments and also decreasing the lamp intensity.

Fig C: Create a skull cap tool. Take a 27 gauge needle and on a sterile spatula, bend the very tip backwards to create a hook ~90° in angle.

Fig D: Use the tool to cut at edge of exposure. You might see some bleeding, go slowly and carefully. If bleeding occurs continue but add some saline to prevent coagulation. Using the super fine FST Dumont 5/45 tweezers, remove the skull cap. Don't worry about duramater, the tetrodes will penetrate it.

Avoid letting the brain tissue dry out. BUT DON'T TOUCH THE BRAIN W/COTTON! Soak up some saline with a small ball of cotton and put it to the side of the exposure while keeping the exposure area moist. You must use the cotton ball retainer/gauze otherwise the saline will run off into the mouse's mouth obstructing his breathing. Meanwhile make sure that the surface of the skull is clean; wipe surface with a cotton swab.

While setting up drive in the stereotax, add 1 drop of saline to surface of the brain and a little bit of cotton. NOTE: It is probably about this time that a secondary injection of Avertin is made.

0:45 Exposure done (1:22). Glue drive on.

VII. Applying the drive to skull surface.

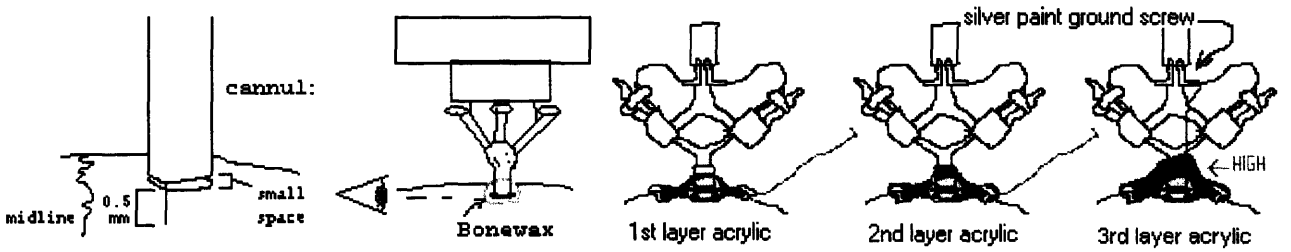

Make sure that the skull surface is clean and DRY!!!

Add 20 µl of Mineral Oil to the bottom 18ga cannuli of the microdrive to help prevent the plugging of the 30 gauge cannuli from brain CSF/serum.

Setup drive so that it is vertical to the plane of the mouse's head.

New Technique: Application of SILICONE GREASE. Arrange microdrive with stereotax so that it aims directly over the exposure. Then remove excess moisture around skull. Lower the cannuli until it sits directly on the brain (touching). With the sharpest pointed tweezers (e.g. the Dumont 5/45 skull cap tweezers) add globs of sterile silicone around cannuli sealing it (avoid clogging under cannuli if possible). Do not "mix up" the grease at all as it will reduce the viscosity and become runny. Now it is time to add dental acrylic. Warning: Avoid letting the Silicone grease touch the tetrodes, otherwise it will stick to the tips and ruin your recordings.

Old Bone Wax Protocol: With wet tweezers, seal the drive to the skull with bone wax to prevent dental acrylic from entering the opening. The cannuli should almost be touching the surface of the brain. If the skull surface is not perpendicular to the bottom of the cannuli, don't worry about it. There can be a small space on one side of the cannuli compared to the other. The real magic trick to making bone wax work is to put a small crumbly blob of wax against the side of the cannuli and skull and then with a 'scooping' action into the cannuli and down onto the skull cut, press, and shape the bone wax into place.

0:50 Setup and lower drive then Dental Acrylic app (1:35)

VII. Dental Acrylic/Grounding

Add acrylic in 3 stages total. Make it fresh for each application. The consistency should be viscous, setting, but not dry so that it will barely drip from a spatula. DONT RUSH THIS STEP! Too much acrylic will fry the little dude's brain because of setting reaction's exothermic properties.

0:53 Dental Acrylic app (1:40)

The first two applications should be done to secure the drive to the skull screws. For the last, move the rest of the ground screw against the base acrylic and add the third application to hold it in place.

0:55 Dental Acrylic app (1:45)

Before the third application, attach the skull ground to the drive's reference pin (with silver paint only. No heat is needed!)

0:60 Suture (1:55)

Remove Millmax connector from clamp (via screw) and then use saline + gauze to rehydrate skin for suturing.

VIII. Suture up!

Now you are ready to suture the animal. Use serrated tweezers to hold suture line. Only 2 sutures are necessary on each side of the drive (front/back).

Procedure for suturing a strong Double Square Knot (recommended by suture manufacturer):

1. Hold needle in right hand and pass needle once through skin folds right to left (puncture skin about 1-2mm from edge), pull needle through skin folds with left hand leaving about 1" of thread protruding to the right.
2. Put the needle again in your right hand.
3. *With needle in right hand, loop the thread clockwise (in a forward rolling motion) once over the free left hand tweezer*, leave loop in place and keep holding on to the needle with your right hand.
4. With left hand tweezer (still looped once by thread), grab the 1" thread protruding from the right side of the mouse's head. Proceed to make a knot tight but not so tight as to cut the skin.
5. Next pass the needle from your right hand to your left hand.
6. *With needle in left hand, loop the thread counter-clockwise (in a forward rolling motion) over the free right hand tweezer.* Grab the 1" thread which should be pointing to the left. Proceed to make a knot, you may pull tight for this one. One square knot has been completed!
7. Now pass the tweezer from your left hand to your right hand.
8. *With needle in right hand, loop the thread counter-clockwise (in a backwards rolling motion) once over the free left hand tweezer.* Again, make a tight knot. You have just completed two square knots!

Prepare Acetaminophen + Mouse Nutrical cocktail for little dude.

1:05 Done!!! (2:10)

IX. Calibrating tetrodes after surgery

[24 8^{th}s is equivalent to 3 full turns of a screw]

It takes about 20-40 8^{th}s on an 00-80 screw to get to the CA1 pyramidal cell layer over a two week period. Going quickly the first few days is recommended by slow careful adjusting the following week.

X. Future Planned improvements

1. A much better stereotax way to hold the drive (need to have more pins to hold the drive and a better way to release it from the stereotax).
2. A better stereotax. Micro manufacture a small ruler made with markings that will specify 1-3mm distances.
3. A better way to remove the skull cap: perhaps a sticky "pick up tool" which is designed to touch the center of the skull cap, stick to it and "pick it up".

PSD95 Knockout PCR Protocol

L.D.Sun 4/23/2001 / KA2U NAKA24WA

Purpose

To improve PCR protocol for typing PSD-95 Knockout mice (S. Grant Lab), which I had limited success.

Reagents

Primer Pair #1 giving 200 bp band:

	%GC	Melt Temp °C	bp
PSD#1a PSD Sense 986-997 5' AGG ACT CTC TTT GGT GGG CA 3'	55%	70.3°	20
PSD#1b PSD Anti-sense intron (probably) 5' AAC CAA GGC GGA TCG TGA TCC A 3'	54.5%	73.2°	22

Primer Pair #2 giving ~500bp band:

PSD#2a Neo Cassette-2*** 5' GCC GCT TTT CTG GAT TCA TCG A 3'	50%	71.3°	22
PSD#2b PSD Anti-sense 1775-95 Coding region 5' AAT CGC GGC CGT CTA TCT CAT 3'	52%	70.8°	21

PCR Machine: PE Biosystems PCR System 9700

Conditions

Sigma Taq Polymerase 0.5ul. Sigma Taq Buffer & NTP's.
1ul of each oligo at 40uM stock in 50ul reaction volume.

Perkin Elmer PCR Machine
Intro
1x 95°C 5 mins.
Then,
94°C 1 min
60°C 1 min +++
72°C 1 min
for 35 cycles, then,
72°C 5 minutes
Store
4°C forever

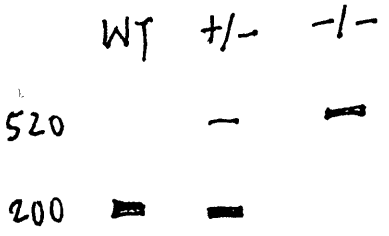

The ~520bp band may sometimes look a little fuzzy, but this procedure leads to pretty good results.

+++ A 58°C annealing temperature gave very smeary bands (barely visible) around the 500bp mark, so stick with 60°C instead. Yield of the 520bp band isn't as bright as the 200bp band, so there can still be further optimizations possible.

*** Note: A good reference in primer design is found on page 271 of Qiagen's Product Guide 2000. Below was the old primer from the protocol originally used. It was redesigned above to #2a being a little longer (22bp), a little less gc-rich (lower melt temp), ~30bp upstream, and non complementary 3' ends with PSD#1b (i.e. the 2a-bad primer competitively decreased both primer pair reactions).

	%GC	Melt Temp °C	bp
PSD#2a-bad Neo cassette (BAD) TGT GGC CGG CTG GGT GTG G	73%	76.18°	19

REFERENCES

Akbarian, S., Bates, B., Liu, R. J., Skirboll, S. L., Pejchal, T., Coppola, V., Sun, L. D., Fan, G., Kucera, J., Wilson, M. A., *et al.* (2001). Neurotrophin-3 modulates noradrenergic neuron function and opiate withdrawal. Mol Psychiatry *6*, 593-604.

Bailey, C. H., Bartsch, D., and Kandel, E. R. (1996). Toward a molecular definition of long-term memory storage. Proc Natl Acad Sci U S A *93*, 13445-13452.

Barrionuevo, G., Schottler, F., and Lynch, G. (1980). The effects of repetitive low frequency stimulation on control and "potentiated" synaptic responses in the hippocampus. Life Sci *27*, 2385-2391.

Beique, J. C., and Andrade, R. (2003). PSD-95 regulates synaptic transmission and plasticity in rat cerebral cortex. J Physiol *546*, 859-867.

Bi, G., and Poo, M. (1999). Distributed synaptic modification in neural networks induced by patterned stimulation. Nature *401*, 792-796.

Bi, G., and Poo, M. (2001). Synaptic modification by correlated activity: Hebb's postulate revisited. Annu Rev Neurosci *24*, 139-166.

Bi, G. Q., and Poo, M. M. (1998). Synaptic modifications in cultured hippocampal neurons: dependence on spike timing, synaptic strength, and postsynaptic cell type. J Neurosci *18*, 10464-10472.

Bi, H., and Sze, C. I. (2002). N-methyl-D-aspartate receptor subunit NR2A and NR2B messenger RNA levels are altered in the hippocampus and entorhinal cortex in Alzheimer's disease. J Neurol Sci *200*, 11-18.

Bliss, T. V., and Lomo, T. (1970). Plasticity in a monosynaptic cortical pathway. J Physiol *207*, 61P.

Brenman, J. E., Chao, D. S., Gee, S. H., McGee, A. W., Craven, S. E., Santillano, D. R., Wu, Z., Huang, F., Xia, H., Peters, M. F., *et al.* (1996). Interaction of nitric oxide synthase with the postsynaptic density protein PSD-95 and alpha1-syntrophin mediated by PDZ domains. Cell *84*, 757-767.

Burette, A., Zabel, U., Weinberg, R. J., Schmidt, H. H., and Valtschanoff, J. G. (2002). Synaptic localization of nitric oxide synthase and soluble guanylyl cyclase in the hippocampus. J Neurosci *22*, 8961-8970.

Buzski, G., Buhl, D. L., Harris, K. D., Csicsvari, J., Czh, B., and Morozov, A. (2003). Hippocampal network patterns of activity in the mouse. Neuroscience *116*, 201-211.

Cho, Y. H., Giese, K. P., Tanila, H., Silva, A. J., and Eichenbaum, H. (1998). Abnormal hippocampal spatial representations in alphaCaMKIIT286A and CREBalphaDelta- mice. Science *279*, 867-869.

Dracheva, S., Marras, S. A., Elhakem, S. L., Kramer, F. R., Davis, K. L., and Haroutunian, V. (2001). N-methyl-D-aspartic acid receptor expression in the dorsolateral prefrontal cortex of elderly patients with schizophrenia. Am J Psychiatry *158*, 1400-1410.

Dudek, S. M., and Bear, M. F. (1992). Homosynaptic long-term depression in area CA1 of hippocampus and effects of N-methyl-D-aspartate receptor blockade. Proc Natl Acad Sci U S A *89*, 4363-4367.

El-Husseini, A. E., Schnell, E., Chetkovich, D. M., Nicoll, R. A., and Bredt, D. S. (2000). PSD-95 involvement in maturation of excitatory synapses. Science *290*, 1364-1368.

El-Husseini Ael, D., Schnell, E., Dakoji, S., Sweeney, N., Zhou, Q., Prange, O., Gauthier-Campbell, C., Aguilera-Moreno, A., Nicoll, R. A., and Bredt, D. S. (2002). Synaptic strength regulated by palmitate cycling on PSD-95. Cell *108*, 849-863.

Evans, D. A., Funkenstein, H. H., Albert, M. S., Scherr, P. A., Cook, N. R., Chown, M. J., Hebert, L. E., Hennekens, C. H., and Taylor, J. O. (1989). Prevalence of Alzheimer's disease in a community population of older persons. Higher than previously reported. Jama *262*, 2551-2556.

Fujii, S., Saito, K., Miyakawa, H., Ito, K., and Kato, H. (1991). Reversal of long-term potentiation (depotentiation) induced by tetanus stimulation of the input to CA1 neurons of guinea pig hippocampal slices. Brain Res *555*, 112-122.

Gardoni, F., Schrama, L. H., Kamal, A., Gispen, W. H., Cattabeni, F., and Di Luca, M. (2001). Hippocampal synaptic plasticity involves competition between Ca2+/calmodulin-dependent protein kinase II and postsynaptic density 95 for binding to the NR2A subunit of the NMDA receptor. J Neurosci *21*, 1501-1509.

Gerlai, R., Henderson, J. T., Roder, J. C., and Jia, Z. (1998). Multiple behavioral anomalies in GluR2 mutant mice exhibiting enhanced LTP. Behav Brain Res *95*, 37-45.

Grant, S. G., O'Dell, T. J., Karl, K. A., Stein, P. L., Soriano, P., and Kandel, E. R. (1992). Impaired long-term potentiation, spatial learning, and hippocampal development in fyn mutant mice. Science *258*, 1903-1910.

Hayashi, Y., Shi, S. H., Esteban, J. A., Piccini, A., Poncer, J. C., and Malinow, R. (2000). Driving AMPA receptors into synapses by LTP and CaMKII: requirement for GluR1 and PDZ domain interaction. Science *287*, 2262-2267.

Hebb, D. O. (1949). The Organization of Behavior. *New York: Wiley.*

Huerta, P. T., Sun, L. D., Wilson, M. A., and Tonegawa, S. (2000). Formation of temporal memory requires NMDA receptors within CA1 pyramidal neurons. Neuron *25*, 473-480.

Imamura, F., Maeda, S., Doi, T., and Fujiyoshi, Y. (2002). Ligand binding of the second PDZ domain regulates clustering of PSD-95 with the Kv1.4 potassium channel. J Biol Chem *277*, 3640-3646.

Kang, H., Sun, L. D., Atkins, C. M., Soderling, T. R., Wilson, M. A., and Tonegawa, S. (2001). An important role of neural activity-dependent CaMKIV signaling in the consolidation of long-term memory. Cell *106*, 771-783.

Kemp, N., and Bashir, Z. I. (2001). Long-term depression: a cascade of induction and expression mechanisms. Prog Neurobiol *65*, 339-365.

Kennedy, M. B. (1998). Signal transduction molecules at the glutamatergic postsynaptic membrane. Brain Res Brain Res Rev *26*, 243-257.

Kentros, C., Hargreaves, E., Hawkins, R. D., Kandel, E. R., Shapiro, M., and Muller, R. V. (1998). Abolition of long-term stability of new hippocampal place cell maps by NMDA receptor blockade. Science *280*, 2121-2126.

Kim, E., Niethammer, M., Rothschild, A., Jan, Y. N., and Sheng, M. (1995). Clustering of Shaker-type K+ channels by interaction with a family of membrane-associated guanylate kinases. Nature *378*, 85-88.

Klocker, N., Bunn, R. C., Schnell, E., Caruana, G., Bernstein, A., Nicoll, R. A., and Bredt, D. S. (2002). Synaptic glutamate receptor clustering in mice lacking the SH3 and GK domains of SAP97. Eur J Neurosci *16*, 1517-1522.

Komiyama, N. H., Watabe, A. M., Carlisle, H. J., Porter, K., Charlesworth, P., Monti, J., Strathdee, D. J., O'Carroll, C. M., Martin, S. J., Morris, R. G., *et al.* (2002). SynGAP regulates ERK/MAPK signaling, synaptic plasticity, and learning in the complex with postsynaptic density 95 and NMDA receptor. J Neurosci *22*, 9721-9732.

Lei, G., Xue, S., Chery, N., Liu, Q., Xu, J., Kwan, C. L., Fu, Y. P., Lu, Y. M., Liu, M., Harder, K. W., and Yu, X. M. (2002). Gain control of N-methyl-D-aspartate receptor activity by receptor-like protein tyrosine phosphatase alpha. Embo J *21*, 2977-2989.

Long, J. F., Tochio, H., Wang, P., Fan, J. S., Sala, C., Niethammer, M., Sheng, M., and Zhang, M. (2003). Supramodular structure and synergistic target binding of the N-terminal tandem PDZ domains of PSD-95. J Mol Biol *327*, 203-214.

Lynch, G. S., Dunwiddie, T., and Gribkoff, V. (1977). Heterosynaptic depression: a postsynaptic correlate of long-term potentiation. Nature *266*, 737-739.

Malenka, R. C., and Nicoll, R. A. (1999). Long-term potentiation--a decade of progress? Science *285*, 1870-1874.

Malinow, R., and Malenka, R. C. (2002). AMPA receptor trafficking and synaptic plasticity. Annu Rev Neurosci *25*, 103-126.

Markram, H., Lubke, J., Frotscher, M., and Sakmann, B. (1997). Regulation of synaptic efficacy by coincidence of postsynaptic APs and EPSPs. Science *275*, 213-215.

McHugh, T. J., Blum, K. I., Tsien, J. Z., Tonegawa, S., and Wilson, M. A. (1996). Impaired hippocampal representation of space in CA1-specific NMDAR1 knockout mice. Cell *87*, 1339-1349.

McNaughton, B. L., Barnes, C. A., and O'Keefe, J. (1983). The contributions of position, direction, and velocity to single unit activity in the hippocampus of freely-moving rats. Exp Brain Res *52*, 41-49.

Mehta, M. R., Barnes, C. A., and McNaughton, B. L. (1997). Experience-dependent, asymmetric expansion of hippocampal place fields. Proc Natl Acad Sci U S A *94*, 8918-8921.

Mehta, M. R., Lee, A. K., and Wilson, M. A. (2002). Role of experience and oscillations in transforming a rate code into a temporal code. Nature *417*, 741-746.

Mehta, M. R., Quirk, M. C., and Wilson, M. A. (2000). Experience-dependent asymmetric shape of hippocampal receptive fields. Neuron *25*, 707-715.

Migaud, M., Charlesworth, P., Dempster, M., Webster, L. C., Watabe, A. M., Makhinson, M., He, Y., Ramsay, M. F., Morris, R. G., Morrison, J. H., *et al.* (1998). Enhanced long-term potentiation and impaired learning in mice with mutant postsynaptic density-95 protein. Nature *396*, 433-439.

Morris, R. G., Anderson, E., Lynch, G. S., and Baudry, M. (1986). Selective impairment of learning and blockade of long-term potentiation by an N-methyl-D-aspartate receptor antagonist, AP5. Nature *319*, 774-776.

Moser, E., Moser, M. B., and Andersen, P. (1993). Synaptic potentiation in the rat dentate gyrus during exploratory learning. Neuroreport *5*, 317-320.

Mulkey, R. M., and Malenka, R. C. (1992). Mechanisms underlying induction of homosynaptic long-term depression in area CA1 of the hippocampus. Neuron *9*, 967-975.

Nakazawa, K., Quirk, M. C., Chitwood, R. A., Watanabe, M., Yeckel, M. F., Sun, L. D., Kato, A., Carr, C. A., Johnston, D., Wilson, M. A., and Tonegawa, S. (2002). Requirement for hippocampal CA3 NMDA receptors in associative memory recall. Science *297*, 211-218.

Nakazawa, K., Sun, L. D., Quirk, M. C., Rondi-Reig, L., Wilson, M. A., and Tonegawa, S. (2003). Hippocampal CA3 NMDA receptors are crucial for memory acquisition of one-time experience. Neuron *38*, 305-315.

Nicoll, R. A., and Malenka, R. C. (1999). Expression mechanisms underlying NMDA receptor-dependent long-term potentiation. Ann N Y Acad Sci *868*, 515-525.

Niethammer, M., Kim, E., and Sheng, M. (1996). Interaction between the C terminus of NMDA receptor subunits and multiple members of the PSD-95 family of membrane-associated guanylate kinases. J Neurosci *16*, 2157-2163.

Ohnuma, T., Kato, H., Arai, H., Faull, R. L., McKenna, P. J., and Emson, P. C. (2000). Gene expression of PSD95 in prefrontal cortex and hippocampus in schizophrenia. Neuroreport *11*, 3133-3137.

Ohnuma, T., Kato, H., Arai, H., McKenna, P. J., and Emson, P. C. (2003). Expression of Fyn, a non-receptor tyrosine kinase in prefrontal cortex from patients with schizophrenia and its correlation with clinical onset. Brain Res Mol Brain Res *112*, 90-94.

O'Keefe, J., and Dostrovsky, J. (1971). The hippocampus as a spatial map. Preliminary evidence from unit activity in the freely-moving rat. Brain Res *34*, 171-175.

O'Keefe, J., and Recce, M. L. (1993). Phase relationship between hippocampal place units and the EEG theta rhythm. Hippocampus *3*, 317-330.

Pak, D. T., Yang, S., Rudolph-Correia, S., Kim, E., and Sheng, M. (2001). Regulation of dendritic spine morphology by SPAR, a PSD-95-associated RapGAP. Neuron *31*, 289-303.

Ranck, J. B., Jr. (1973). Studies on single neurons in dorsal hippocampal formation and septum in unrestrained rats. I. Behavioral correlates and firing repertoires. Exp Neurol *41*, 461-531.

Rasband, M. N., Park, E. W., Zhen, D., Arbuckle, M. I., Poliak, S., Peles, E., Grant, S. G., and Trimmer, J. S. (2002). Clustering of neuronal potassium channels is independent of their interaction with PSD-95. J Cell Biol *159*, 663-672.

Rotenberg, A., Abel, T., Hawkins, R. D., Kandel, E. R., and Muller, R. U. (2000). Parallel instabilities of long-term potentiation, place cells, and learning caused by decreased protein kinase A activity. J Neurosci *20*, 8096-8102.

Rotenberg, A., Mayford, M., Hawkins, R. D., Kandel, E. R., and Muller, R. U. (1996). Mice expressing activated CaMKII lack low frequency LTP and do not form stable place cells in the CA1 region of the hippocampus. Cell *87*, 1351-1361.

Ruiz-Canada, C., Koh, Y. H., Budnik, V., and Tejedor, F. J. (2002). DLG differentially localizes Shaker K+-channels in the central nervous system and retina of Drosophila. J Neurochem *82*, 1490-1501.

Sanes, J. R., and Lichtman, J. W. (1999). Can molecules explain long-term potentiation? Nat Neurosci *2*, 597-604.

Selkoe, D. J. (2002). Alzheimer's disease is a synaptic failure. Science *298*, 789-791.

Scoville, W. B., and Milner, B. (2000). Loss of recent memory after bilateral hippocampal lesions. 1957. J Neuropsychiatry Clin Neurosci *12*, 103-113.

Sheng, M., and Kim, M. J. (2002). Postsynaptic signaling and plasticity mechanisms. Science *298*, 776-780.

Silva, A. J. (2003). Molecular and cellular cognitive studies of the role of synaptic plasticity in memory. J Neurobiol *54*, 224-237.

Silva, A. J., Paylor, R., Wehner, J. M., and Tonegawa, S. (1992). Impaired spatial learning in alpha-calcium-calmodulin kinase II mutant mice. Science *257*, 206-211.

Silva, A. J., Wang, Y., Paylor, R., Wehner, J. M., Stevens, C. F., and Tonegawa, S. (1992). Alpha calcium/calmodulin kinase II mutant mice: deficient long-term potentiation and impaired spatial learning. Cold Spring Harb Symp Quant Biol *57*, 527-539.

Sorra, K. E., and Harris, K. M. (2000). Overview on the structure, composition, function, development, and plasticity of hippocampal dendritic spines. Hippocampus *10*, 501-511.

Squire, L. R. (1992). Memory and the hippocampus: a synthesis from findings with rats, monkeys, and humans. Psychol Rev *99*, 195-231.

Tanemoto, M., Fujita, A., Higashi, K., and Kurachi, Y. (2002). PSD-95 mediates formation of a functional homomeric Kir5.1 channel in the brain. Neuron *34*, 387-397.

Tao, H., Zhang, L. I., Bi, G., and Poo, M. (2000). Selective presynaptic propagation of long-term potentiation in defined neural networks. J Neurosci *20*, 3233-3243.

Tejedor, F. J., Bokhari, A., Rogero, O., Gorczyca, M., Zhang, J., Kim, E., Sheng, M., and Budnik, V. (1997). Essential role for dlg in synaptic clustering of Shaker K+ channels in vivo. J Neurosci *17*, 152-159.

Tezuka, T., Umemori, H., Akiyama, T., Nakanishi, S., and Yamamoto, T. (1999). PSD-95 promotes Fyn-mediated tyrosine phosphorylation of the N-methyl-D-aspartate receptor subunit NR2A. Proc Natl Acad Sci U S A *96*, 435-440.

Tonegawa, S., Nakazawa, K., and Wilson, M. A. (2003). Genetic neuroscience of mammalian learning and memory. Philos Trans R Soc Lond B Biol Sci *358*, 787-795.

Tonegawa, S., Tsien, J. Z., McHugh, T. J., Huerta, P., Blum, K. I., and Wilson, M. A. (1996). Hippocampal CA1-region-restricted knockout of NMDAR1 gene disrupts synaptic plasticity, place fields, and spatial learning. Cold Spring Harb Symp Quant Biol *61*, 225-238.

Toyooka, K., Iritani, S., Makifuchi, T., Shirakawa, O., Kitamura, N., Maeda, K., Nakamura, R., Niizato, K., Watanabe, M., Kakita, A., *et al.* (2002). Selective reduction of a PDZ protein, SAP-97, in the prefrontal cortex of patients with chronic schizophrenia. J Neurochem *83*, 797-806.

Tsien, J. Z., Chen, D. F., Gerber, D., Tom, C., Mercer, E. H., Anderson, D. J., Mayford, M., Kandel, E. R., and Tonegawa, S. (1996). Subregion- and cell type-restricted gene knockout in mouse brain. Cell *87*, 1317-1326.

Tsien, J. Z., Huerta, P. T., and Tonegawa, S. (1996). The essential role of hippocampal CA1 NMDA receptor-dependent synaptic plasticity in spatial memory. Cell *87*, 1327-1338.

Uetani, N., Kato, K., Ogura, H., Mizuno, K., Kawano, K., Mikoshiba, K., Yakura, H., Asano, M., and Iwakura, Y. (2000). Impaired learning with enhanced hippocampal long-term potentiation in PTPdelta-deficient mice. Embo J *19*, 2775-2785.

Watanabe, Y., Song, T., Sugimoto, K., Horii, M., Araki, N., Tokumitsu, H., Tezuka, T., Yamamoto, T., and Tokuda, M. (2003). Post-synaptic density-95 promotes calcium/calmodulin-dependent protein kinase II-mediated Ser847 phosphorylation of neuronal nitric oxide synthase. Biochem J *372*, 465-471.

Wilson, M. A. (2002). Hippocampal memory formation, plasticity, and the role of sleep. Neurobiol Learn Mem *78*, 565-569.

Wilson, M. A., and McNaughton, B. L. (1993). Dynamics of the hippocampal ensemble code for space. Science *261*, 1055-1058.

Wong, W., Newell, E. W., Jugloff, D. G., Jones, O. T., and Schlichter, L. C. (2002). Cell surface targeting and clustering interactions between heterologously expressed PSD-95 and the Shal voltage-gated potassium channel, Kv4.2. J Biol Chem *277*, 20423-20430.

Xia, Z., Gray, J. A., Compton-Toth, B. A., and Roth, B. L. (2003). A direct interaction of PSD-95 with 5-HT2A serotonin receptors regulates signal transduction and receptor trafficking. J Biol Chem.

Yamaguchi, Y., Aota, Y., McNaughton B.L., and Lipa P. (2002). Bimodality of theta phase precession in hippocampal place cells in freely running rats. J Neurophysiol *87*, 2629-2642.

Yan, J., Zhang, Y., Jia, Z., Taverna, F. A., McDonald, R. J., Muller, R. U., and Roder, J. C. (2002). Place-cell impairment in glutamate receptor 2 mutant mice. J Neurosci *22*, RC204.

Yu, H., Saura, C. A., Choi, S. Y., Sun, L. D., Yang, X., Handler, M., Kawarabayashi, T., Younkin, L., Fedeles, B., Wilson, M. A., Younkin S., Kandel E.R., Kirkwood A., Shen J. (2001). APP processing and synaptic plasticity in presenilin-1 conditional knockout mice. Neuron *31*, 713-726.

Zola-Morgan, S., Squire, L. R., and Amaral, D. G. (1986). Human amnesia and the medial temporal region: enduring memory impairment following a bilateral lesion limited to field CA1 of the hippocampus. J Neurosci *6*, 2950-2967.

Molecular Psychiatry (2001) 6, 593–604

www.nature.com/mp

ORIGINAL RESEARCH ARTICLE

Neurotrophin-3 modulates noradrenergic neuron function and opiate withdrawal

S Akbarian[1,2*], B Bates[1*], R-J Liu[3], SL Skirboll[4], T Pejchal[5], V Coppola[6], LD Sun[7], G Fan[1], J Kucera[8], MA Wilson[7], L Tessarollo[6], BE Kosofsky[5], JR Taylor[3], M Bothwell[4], EJ Nestler[3], GK Aghajanian[3] and R Jaenisch[1,7]

[1]*Whitehead Institute for Biomedical Research, Cambridge, MA;* [2]*Dept of Psychiatry and* [5]*Dept of Neurology, Massachusetts General Hospital, Boston, MA;* [3]*Dept of Psychiatry, Yale University, New Haven, CT;* [4]*Dept of Physiology and Biophysics, University of Washington, Seattle, WA;* [6]*National Cancer Institute, Frederick, MD;* [7]*Dept of Biology, Massachusetts Institute of Technology, Cambridge, MA;* [8]*Dept of Neurology, Boston University, MA, USA*

Keywords: locus coeruleus; morphine; addiction; norepinephrine; cre recombinase; pons; medulla

Somatic symptoms and aversion of opiate withdrawal, regulated by noradrenergic signaling, were attenuated in mice with a CNS-wide conditional ablation of neurotrophin-3. This occurred in conjunction with altered cAMP-mediated excitation and reduced upregulation of tyrosine hydroxylase in A6 (locus coeruleus) without loss of neurons. Transgene-derived NT-3 expressed by noradrenergic neurons of conditional mutants restored opiate withdrawal symptoms. Endogenous NT-3 expression, strikingly absent in noradrenergic neurons of postnatal and adult brain, is present in afferent sources of the dorsal medulla and is upregulated after chronic morphine exposure in noradrenergic projection areas of the ventral forebrain. NT-3 expressed by non-catecholaminergic neurons may modulate opiate withdrawal and noradrenergic signalling. *Molecular Psychiatry* (2001) **6,** 593–604.

Ongoing drug use in an opiate-addicted individual could be reinforced by withdrawal reactions that occur when drug use is halted abruptly.[1] Overactivity and disinhibition of brainstem noradrenergic neurons is thought to be a key mechanism for the hyperautonomic state and for many of the somatic symptoms that occur during acute withdrawal[2] and also for the acquisition of avoidance behaviors after occurrence of withdrawal reactions.[3]

Little is known about endogenous factors that regulate noradrenergic neuron function and opiate withdrawal-related behaviors. Molecules of the nerve growth factor family may influence neuronal health and plasticity both in the developing and in the adult brain, including the reward and addiction circuitry.[4] Brainstem noradrenergic neurons of the adult rodent and primate brain express the neurotrophin-3 (NT-3) high affinity receptor, TrkC,[5–7] as well as the brain derived neurotrophic factor (BDNF) and neurotrophin-4/5 (NT-4/5) receptor TrkB. In selected neuronal populations, NT-3 may promote growth and survival by binding to TrkB or TrkA, the high affinitity receptor for nerve growth factor (NGF).[8–10]

Although levels of NT-3 and TrkC mRNA are altered in several brain areas during opiate withdrawal,[5] *in vivo* evidence of a role for NT-3 in opiate withdrawal and noradrenergic neuron function is still lacking. The perinatal lethality of conventional NT-3 knock-out mice,[11,12] due to major cardiovascular malformations,[13] prevented the use of these mice to study NT-3 in the adult brain. Using a conditional knock-out strategy with Cre/loxP mediated NT-3 gene deletion that results in complete loss of NT-3 in the central nervous system in mice with normal viability, fertility and lifespan,[14] we show here for the first time that NT-3 modulates electrophysiological responses and neurochemistry of brainstem noradrenergic neurons and that NT-3 is essential both for opiate withdrawal-induced avoidance behavior and for the somatic symptoms that occur during acute withdrawal.

NT-3 modulates expression of tyrosine hydroxylase but is not essential for survival of noradrenergic neurons

We used two transgenic lines, a conditional NT3 mutant[14] and a transgenic line carrying an NT3 transgene under the control of the DBH promoter to examine the consequences of NT3 deficiency as well as NT3 overexpression in opiate withdrawal reactions and in noradrenergic neuron function *in vivo*. Expression of the recombinase cre under control of the nestin promoter results in complete deletion of NT-3 during prenatal development of the brain and spinal cord.[14] To ascertain ubiquitous nestin-cre expression, a reporter line that expressed beta-galactosidase in all tissues upon cre-mediated removal of a stop translation sequence[15] was crossed with the nestin-cre transgenic line. The results shown in Figure 1a–c indicate that cre-mediated recombination is complete throughout the brain, consistent with previous Northern blot results.[14]

In adult brain, NT-3 has been implicated in survival of noradrenergic neurons[16] and therefore neuronal numbers and expression of selected neurochemical markers were analyzed in adult mutants and controls. Coronal sections from the brainstem of 3-month-old

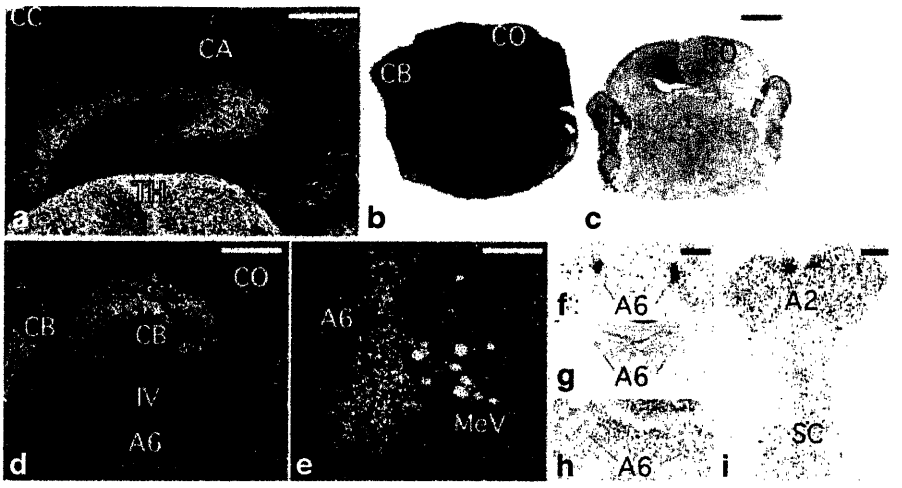

Figure 1 Regional pattern of Nestin-Cre transgene expression and of DBH-NT-3 transgene expression. (a) Representative part of forebrain and (b) rostral hindbrain of newborn animal showing ubiquitous activation of the Rosa-26 Cre/lox lacZ reporter by the Nestin-Cre transgene. (c) Control section (caudal pons/rostral hindbrain) of Rosa-26 Cre/lox lacZ +; Nestin-Cre – animal. Emulsion-dipped coronal sections of dorsal pons/rostral cerebellum from 10-week-old wild-type mouse (d) and from DBH-NT-3/wt transgenic mouse (e), hybridized with ^{35}S-labeled NT-3 cRNA. Note strong signal over cerebellar cortex but not over A6 in wild-type (d) and strong signal over A6 and MeV in DBH-NT-3 transgenic mouse (e). Film autoradiograms of sections from dorsal pons (f) and medulla (i) from 14-month-old DBH NT-3/wt transgenic mouse and dorsal pons (h) of 4-month-old wild-type mouse, hybridized with ^{33}P-labeled NT-3 cRNA, showing strong labeling bilateral over A6 and A2 in the DBH-NT-3 transgenic mouse (f, i) but not the control (h). (g) Same section as shown in (f) after counterstain with cresyl violet. Abbrevations: IV = IVth ventricle; CA = CA fields of Ammon; CB = cerebellar cortex; CC = cerebral cortex; CO = colliculi; TH = thalamus; and SC = spinal cord. Magnification bars in mm (a) 0.5; (b, c) 1; (f, g, h, i) 1; (d) 0.8; (e) 0.1.

NT-3 conditional mutant mice (Figures 2b, d, f and 4b, d) and littermate controls (Figure 4a, c) were stained for tyrosine hydroxylase (TH) immunohistochemistry and total numbers of A6 neurons in the dorsal pons (Figure 2b) and of A2 neurons in the medial solitary tract nucleus (Figure 2d, f) were counted, as outlined by Kalia *et al.*[17] TH is the rate-limiting enzyme in the biosynthesis of norepinephrine. The difference in neuronal numbers between the conditional mutants and the controls was less than 15% and not significant (Figure 3a).

Previous studies have shown that expression of TH is upregulated during chronic morphine exposure, presumably as a compensatory mechanism for increased neuronal inhibition.[18] This transcriptional regulation is mediated, in part, by cAMP-dependent transcription factors and repressors.[19] Western blot analysis of microdissected A6 from wild-type mice that received morphine (total of 500 mg over 60 h) showed increased TH immunoreactivity in comparison to drug-free animals. In contrast, the conditional NT-3 mutant mice revealed no up-regulated TH immunoreactivity within this brain region upon chronic morphine administration (Figure 3b). This difference to morphine-treated controls was consistent for 5/5 morphine-treated mutants tested (mean ± SE: controls 193.3 ± 18.3; mutants 84.8 ± 22.2).

We determined total numbers of TH+ neurons in A2 and A6 of mice which expressed an NT-3 transgene under control of the 5.8-kb fragment of the human dopamine-beta hydroxylase gene (DBH) promoter[20] (see also Methods). In these mice, NT-3 was expressed at high levels in A6 and A2 noradrenergic cell groups (Figure 1e, f, i), in the proprioceptive mesencephalic trigeminal tract nucleus, peripheral sympathetic ganglia, and the adrenal medulla by *in situ* hybridization and ELISA (data not shown). Activity of the DBH promoter in sensory neurons and other tissues was previously described for a transgenic lacZ reporter line.[20] In sections obtained from wild-type mice, no specific labeling was observed over noradrenergic cell groups including A6 (Figure 1d).

In the DBH-NT-3 transgenic mice, total numbers of TH+ cells were increased in A2 by 30% (unpaired two-tailed *t*-test (T); $P < 0.05$) but in A6 did not differ from controls (Figure 3a). It is not clear if the observed increase in TH+ cells in A2 reflects a true increase in total number of neurons or if, alternatively, more neurons express detectable levels of TH. In the DBH-NT-3 transgenic mice, TH immunoreactivity both in somata and in the neuropil of the A2 region appeared more robust (Figure 2c), in comparison to NT-3 conditional mutants (Figure 2d).

In the conditional NT-3 mutant mice, strong and ubiquitous nuclear staining for phosphorylated CREB,[21] a transcription factor known to be involved in opiate withdrawal[22,23] was preserved in A6, A2 and all other noradrenergic cell groups such as A1 in the ventral medulla (Figure 4c, d) and no significant differences were found in levels of CREB immunoreactivity in TH-positive neurons of mutants and controls (data not shown). The CREB transcription factor regulates expression of the proto-oncogene c-fos.[21] Opiate withdrawal stimulates strong c-fos expression in norad-

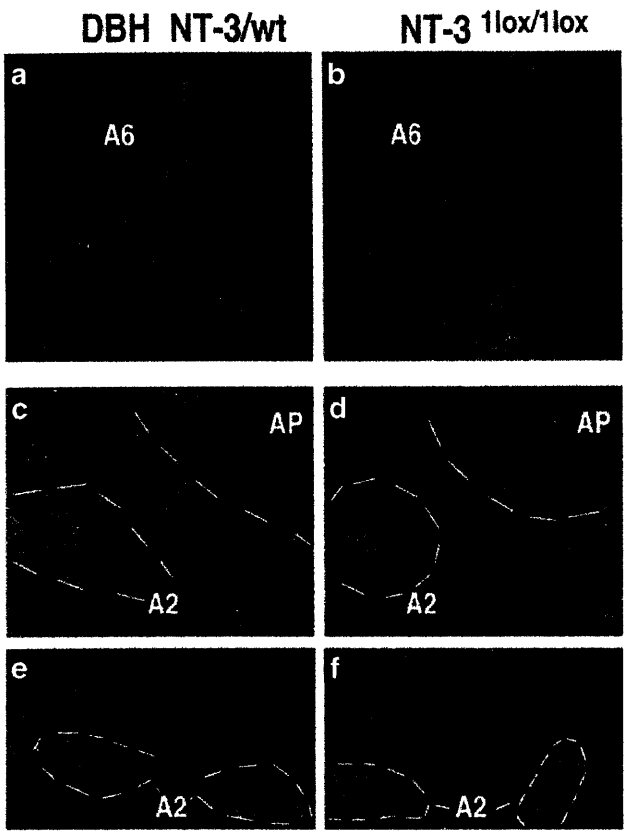

Figure 2 Immunohistochemistry of noradrenergic neurons in NT-3 mutant mice. (a, b) Representative example of Texas Red-labeled TH immunoreactive neurons of DBH-NT-3/wt transgenic mouse (a, c, e) and of NT-3 conditional mutant mouse (b, d, f). The A6 cell group is shown in (a, b), the A2 cell group at the level of area postrema (AP) shown in (c, d) and caudal parts of A2 at the level of the obex are shown in (e, f). Area of the A2, as outlined by Kalia *et al*[17] marked by dotted line. Notice subtle increase in TH immunoreactivity in (c, e) in comparison to (d, f). (a–f) Images taken at 10 × 10 magnification.

renergic neurons.[24] The expression of c-fos was up-regulated in the wild-type mice of the present study after morphine withdrawal (Figure 4a), which was induced with the μ-(opioid) receptor antagonist naloxone. This up-regulation was found to be unperturbed in the conditional null mutant (Figure 4b). Ligand binding autoradiography with nisoxetine, a ligand for noradrenergic re-uptake transporters selectively expressed by noradrenergic neurons, showed a labelling pattern in the fore- and hindbrain that was indistinguishable between conditional mutant and control (data not shown). Taken together these findings suggest that NT-3 modulates TH expression in noradrenergic neurons during chronic opiate exposure but this neurotrophin is not essential for neuronal survival and noradrenergic innervation.

NT-3 deficiency causes abnormal cAMP-mediated signal transduction in A6 neurons

In order to clarify if loss of NT-3 alters the functional state of brainstem noradrenergic neurons we conducted electrophysiological recordings in A6. The focus of these experiments was on standard measures for the cAMP signal transduction pathway that activates Ca^{2+} and Na^{+} channels, causing depolarization and excitation. In wild-type animals, the activity of this intracellular signal transduction pathway is upregulated under conditions of increased neuronal inhibition, including chronic opiate exposure.[25] This mechanism is thought to compensate for drug-induced neuronal hypoactivity. When drug use is halted abruptly, these and other neurochemical adaptations[26] result in overexcitation of noradrenergic neurons by intrinsic mechanisms and by increased excitatory afferent input,[4] causing the withdrawal syndrome.

Coronal slices containing the A6 were obtained from 10–16-week-old conditional NT-3 mutant and control mice treated with saline or morphine. Using extracellular recordings from single A6 neurons, the effects on firing rate of substances applied in the perfusate were measured. Neurons recorded from 10-week-old mice did not differ from those recorded in 16-week-old mice. Examples of recordings are shown in Figure 5.

The cAMP pathway mediates neuronal excitation in noradrenergic neurons and was examined in conditional mutants and controls treated with saline or chronic morphine. Forskolin stimulates adenylyl cyclases and when it was added to the slice perfusate, neuronal firing in saline-treated wild-type A6 neurons was increased (Figure 5a, e). This forskolin-mediated increase in neuronal firing was significantly reduced in saline-treated conditional mutants (Figure 5b, e).

After 60 h of a progressive treatment schedule for morphine (total dose = 500 mg kg^{-1}), forskolin caused a robust increase in neuronal firing in wild-type mice which was, on average, stronger than the forskolin-induced neuronal firing in saline-treated control mice (Figure 5c, e). This apparent upregulation of the cAMP pathway after chronic opiate exposure is consistent with previous results.[23] Interestingly, morphine-treated conditional mutants showed at baseline a significant elevation in neuronal firing, in comparison to morphine-treated controls (Figure 5d, e). However, addition of forskolin to the perfusate caused a further increase in neuronal firing in the conditional mutants (Figure 5d) and was similar to the firing rate of forskolin-treated controls (Figure 5e).

We conclude that cAMP mediated signal transduction in A6 neurons is altered in NT-3 deficient mice both under drug-free conditions and after chronic morphine exposure. In saline-treated mutant mice, the cAMP pathway is hypoactive because the forskolin-induced increase in neuronal firing was reduced. In morphine-treated mutants, cAMP-mediated signaling is dysregulated because the baseline firing rate was abnormally elevated, which made further elevation of

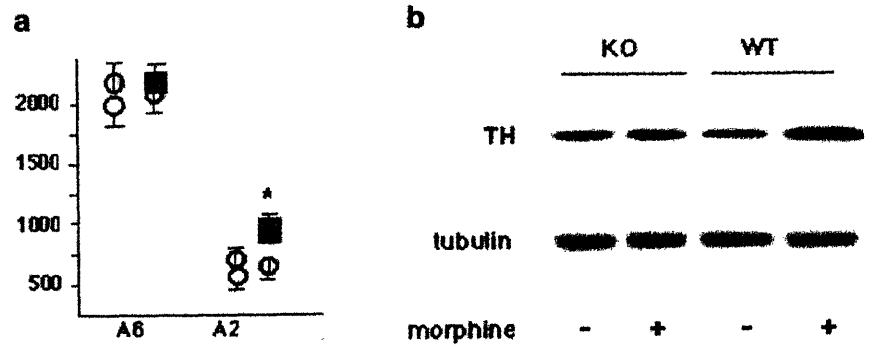

Figure 3 Regulation of TH expression in noradrenergic cell groups of NT-3 mutants. (a) total numbers of TH+ neurons (*y*-axis) in bilateral A6 and A2 noradrenergic cell groups. (■) = DBH-NT-3/wt transgenic mice; (○) = NT-3 conditional mutant mice; (Φ) = controls. NT-3 deficient mice have no loss of neurons. Data collected in pairwise fashion (mutant and wild-type control) and therefore two sets of controls are used. Data expressed as mean ± SE. $^*P < 0.05$. (b) Representative example of Western blots for TH of A6 region in drug-free (– morphine) and drug-treated (+ morphine) conditional mutant (KO) and wild-type (wt) mice, with loading control (tubulin). Notice that KO mice maintain at baseline TH levels similar to control but fail to upregulate TH after drug-treatment.

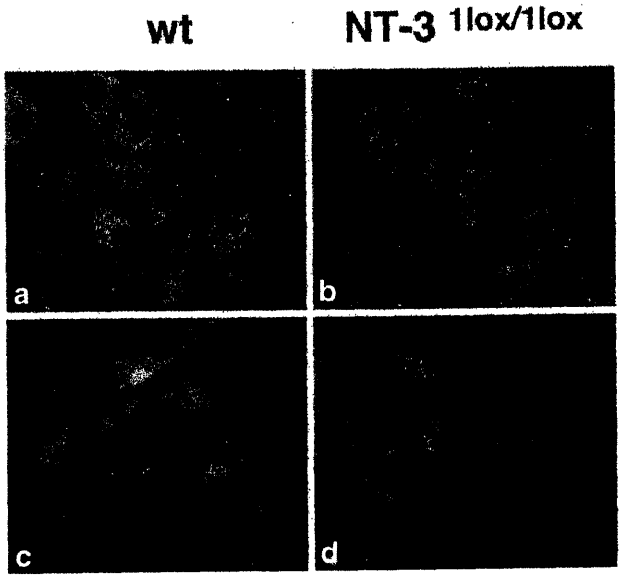

Figure 4 Regulation of c-fos and CREB expression in NT-3 conditional mutants. Sections double stained for Texas Red-labeled TH immunoreactivty and FITC-labeled c-fos immunoreactivity of A6 (a) control and (b) NT-3 conditional mutant mouse 110 min (a, b) after naloxone-induced morphine-withdrawal, showing robust c-fos expression TH neuron nuclei. (c, d) Sections from ventral medulla double stained for Texas-Red labeled TH immunoreactivity and FITC-labeled CREB immunoreactivity in A1 neurons of (c) control and (d) NT-3 conditional mutant mouse after chronic opiate exposure. Note robust expression of c-fos and CREB in nuclei of mutant and control. (a–d) Images taken at 40 × 10 magnification.

neuronal firing by activation of the cAMP pathway less effective.

G-protein coupled inhibitory receptors are intact in mutant noradrenergic neurons

Hyperpolarization and functional inhibition of noradrenergic neurons is, in part, mediated through G-protein coupled opioid- and α2-adrenoreceptors. Brief exposure to enkephalin (100 μM), an endogenous opioid receptor agonist, caused total neuronal inhibition lasting approximately 2 min in all neurons recorded from A6 of controls (Figure 5a, c) and conditional mutants (Figure 5 b, d). In addition, the suppression of neuronal firing by successively increased concentrations of the synthetic μ-(opioid) receptor-agonist DAMGO was evaluated in 10-week and 16-week-old mice, and no differences were found between mutants and controls (Figure 5f). The IC_{50} was very similar in both groups of mice (mutants: 46.9 nM; controls: 47.9 nM). Also, all mutants and controls showed robust α2-adrenoreceptor mediated inhibition (data not shown). Therefore, the mechanisms of cellular inhibition appear to be fully preserved in A6 neurons of NT-3 conditional mutants.

NT-3 deficiency attenuates opiate withdrawal and withdrawal-induced aversion

We next tested whether the observed abnormalities in opiate-induced neurochemical and physiological adaptations of noradrenergic neurons in the conditional mutants resulted in altered opiate withdrawal behavior. A withdrawal reaction was induced in 12-week-old mice after 60 h of a progressive treatment of morphine (total dose 500 mg kg^{-1}) with an s.c. injection of naloxone (1 mg kg^{-1}). Wild-type mice showed symptoms characteristic of opiate withdrawal, including signs of autonomic hyperactivity, wet dog shakes, tremors and digging. As shown in Figure 6a, b, the NT-3 conditional mutant mice scored, in comparison to wild-type mice, 35% lower on ratings for autonomic hyperactivity (ANOVA $F = 15.4$, $P < 0.01$, Fisher's PLSD –1.1, $P < 0.01$) and also had a significant attenuation in various behavioral symptoms, including wet dog shakes (ANOVA $F = 3.36$, $P < 0.05$; Fisher's PLSD –3.28; $P = 0.018$). The total withdrawal score for this

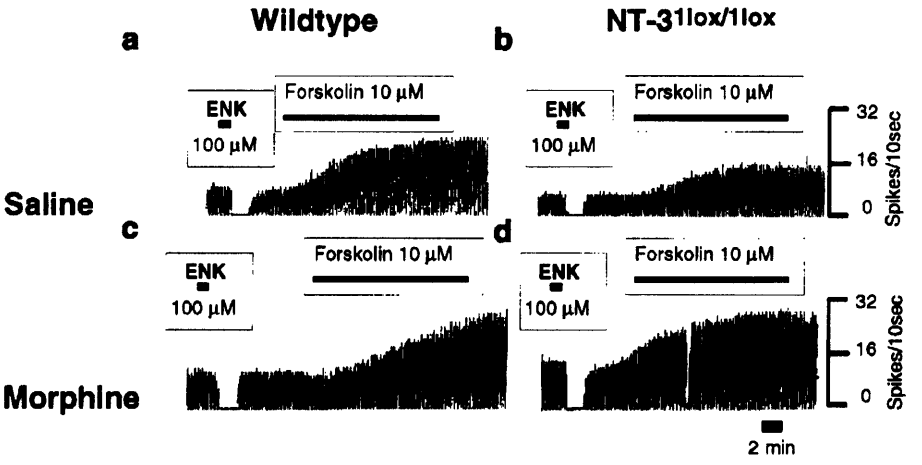

e

A6 neuron firing rate (spikes/10sec)
mean ± SE

recording condition		wildtype	NT-3 1lox/1lox	% difference
saline	baseline	7.8 ± 0.6	7.5 ± 0.5	- 4 % (N.S.)
	forskolin	20.7 ± 1.3	15.7 ± 1.6	- 25 % ($p < 0.05$)
morphine	baseline	9.6 ± 1.1	14.8 ± 1.3	+ 50% ($p < 0.05$)
	forskolin	26.9 ± 2.7	27.0 ± 2.2	0

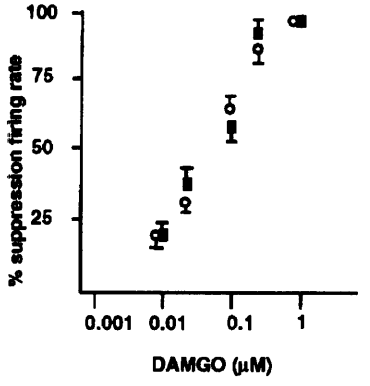

Figure 5 Activity of A6 neurons in NT-3 conditional mutant and control mice at baseline, after stimulation of the cAMP pathway and G protein-coupled receptors. (a–d) Representative traces of single unit recordings of A6 neurons in 15-week-old wild-type animal (a, c) and 15-week-old NT-3 conditional mutant mouse (b, d) treated with saline (a, b) or chronic morphine (c, d). *y*-axis shows firing rate (spikes per 10 s), horizontal axis represents running time, bold bars represent running time period of perfusate application (calibration bar = 2 min). Notice reduced neuronal firing in drug-free conditional mutant after application of forskolin (b) in comparison to wild-type (a) and increased neuronal firing at baseline prior to application of forskolin in morphine-treated conditional mutant (d) in comparison to wild-type (c). Table (e) summarizes recording data and % differences for the four cohorts of saline- and morphine-treated conditional mutants. (f) Dose-response curve for μ-receptor agonist DAMGO, measured as % suppression of baseline firing rate (*y*-axis) after successive increase in DAMGO concentration in perfusate (*x*-axis) in 10-week-old mutant (O) and control (■) mice. Note similar dose-response curves in mutant and control. Data shown as mean ± SE. Significance of differences between mutants and controls was calculated by an unpaired two-tailed *t*-test.

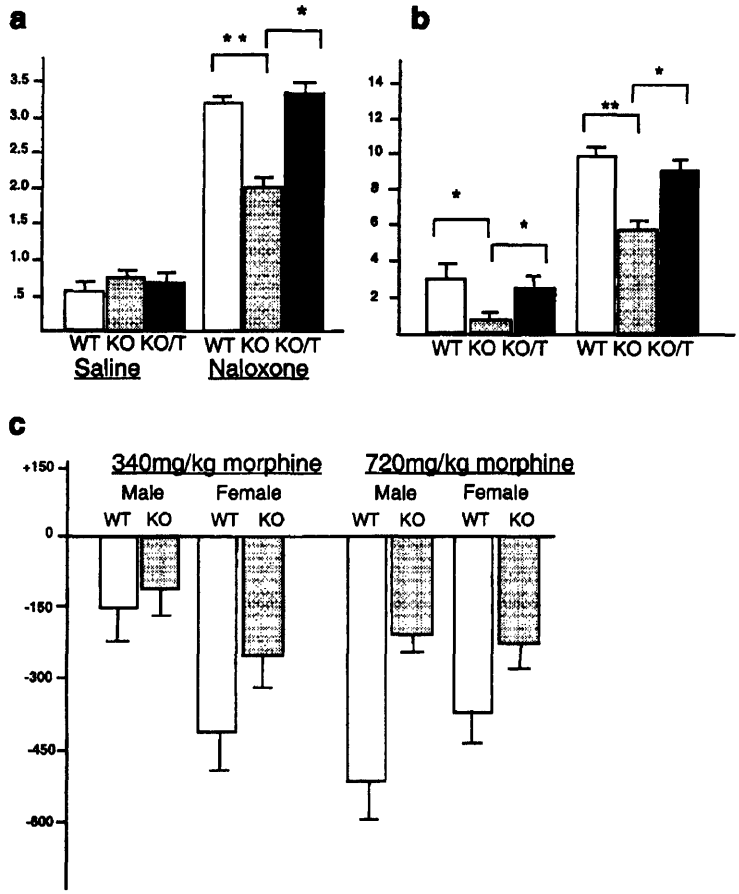

Figure 6 Opiate withdrawal reactions and withdrawal-induced aversion in NT-3 mutant mice. (a, b) Summarize observer-based ratings of naloxone-precipitated withdrawal in the NT-3 conditional mutant mice (gray bars), in comparison to conditional mutants that carried the DBH-NT-3 transgene (black bars) and wild-type controls (white bars). (a) Total number of checked signs (diarrhea, rhinorhea, lacrimation, abnormal posture, irritability, ptosis) in saline-treated animals (left-sided bars) and after chronic morphine administration (500 mg kg^{-1} total dose per 60 h) (right-sided bars). White bar (WT) = wild-type mice, gray bar (KO) = NT-3 conditional mutant mice, black bar (KO/T) = conditional mutant mice carrying the DBH-NT-3 transgene. (b) Total number of wet dog shakes (left-sided bars) and total overall withdrawal score (right-sided bars) in morphine-treated animals. Bar codes as in (a). $*P < 0.05$; $**P < 0.01$. (c) Avoidance (*y*-axis, in seconds) of aversive chamber 24 h after morphine withdrawal in male and female conditional NT-3 mutants and controls. Data are expressed as mean ± SE.

group of mutant mice also was 30% lower in comparison to age-matched controls (total score mutant 6.1 ± 0.47 (mean ± SE); controls 8.9 ± 0.97; (ANOVA) F = 9.69, $P < 0.01$).

To confirm if this behavioral difference was a primary effect of NT-3 on noradrenergic neurons, we tested the opiate withdrawal response of NT-3 conditional mutants that also carried one copy of the DBH-NT-3 transgene. We found that the response was indistinguishable from wild-type animals (Figure 6a, b). This result provides strong genetic evidence for a role of NT-3 in normal opiate withdrawal and suggests that the attenuated withdrawal reaction in NT-3 deficient mice is, at least in part, due to dysfunction of noradrenergic neurons.

Withdrawal acts as a negatively reinforcing stimulus, which is thought to be a component for the development or maintenance of the addicted state.[1] Aversive conditioning to opiate withdrawal was measured by the conditioned place aversion paradigm. In a pre-conditioning test, all animals with a strong side preference at baseline were removed from further testing. Then, mice were placed on a progressive treatment schedule for morphine. One group of mutants and controls received 340 mg kg^{-1} per 60 h, another group received 720 mg kg^{-1} per 72 h. Twenty-four hours after the animals underwent a naloxone-induced withdrawal reaction in one particular chamber, wild-type mice spent less time in that aversive chamber, in comparison to NT-3 conditional mutants (Figure 6c). This difference was significant (mixed factor ANOVA: genotype–F = 4.20, $P < 0.05$; sex–F = 1.22, $P = 0.28$; dose–F = 1.34, $P = 0.26$). After collapsing the data for sex and dose, pairwise comparisons using the Newmans–Keuls test revealed a significant difference between null and wild-type mice ($P < 0.05$).

A simple fear conditioning paradigm was applied, in order to rule out a generalized learning deficit in the

conditional mutant. After repeated exposure to electrical footshocks in a conditioning chamber, both controls and conditional mutant mice developed, within minutes, an approximately five-fold increase in freezing behavior, as quantified by computerized video-monitoring. When returned to the aversive chamber 24 h after receiving shocks, this increase in freezing time was retained in the first 5 min both in mutants (ratio freezing/non-freezing time 0.57 ± 0.08; baseline 0.11 ± 0.02) and controls (0.48 ± 0.07; baseline 0.08 ± 0.01).

Regional distribution pattern of NT-3 expression suggests target-derived modulation of noradrenergic neuron function

It is not known whether NT-3 expression is dynamically regulated in adult mouse brain. Differential expression of NT-3 after opiate exposure may imply a role for NT-3 in drug-induced neuronal and behavioral adaptations. In order to learn more about the regional distribution and transcriptional regulation of NT-3 in opiate-exposed mice, we studied transgenic mice with a lacZ reporter coding sequence integrated into the endogenous NT-3 locus.[27] In the forebrain and midbrain, the regional distribution pattern of lacZ expressing cells in morphine-treated animals (500 mg kg^{-1} per 60 h) appeared qualitatively normal and similar to the distribution pattern described previously for drug-free animals.[27] However, morphine-treated animals consistently showed much stronger lacZ reporter activity for the lateral septum and the CA2 region and the dentate gyrus of the hippocampus, in comparison to drug-free littermate controls (Figure 7a–d). The bed nucleus of the stria terminalis (BNST) contained, in areas of immediate vicinity to the lateral septum, a few scattered lacZ+ neurons in morphine-treated animals while drug-free animals had no lacZ reporter activity in that brain region (Figure 7e, f). Noteably, the BNST, the lateral septum and other NT-3 expressing areas such as the cingulate and entorhinal cortex are comparatively rich in noradrenergic fibers.[28]

The expression pattern of NT-3 in the hindbrain did not show qualitative or quantitative differences between morphine-treated and drug-free animals: only few areas of the hindbrain contained significant numbers of lacZ+ neurons. A subgroup of neurons of the nucleus prepositus hypoglossi (NPH) and adjacent vestibular nuclei were among the most heavily stained neurons in any brain region (Figure 7i). The cerebellar cortex, the dorsal cochlear nucleus, and the lateral and rostral portions of the solitary tract nucleus (NTS) were also labeled (Figure 7j). The paragigantocellular nucleus, which together with the NPH and the NTS comprises a major afferent input source to brainstem noradrenergic neurons, contained no NT-3 expressing cells.

Sections from the midbrain that were processed for TH immunoreactivity and lacZ reporter activity contained numerous double-stained sections in the substantia nigra and ventral tegmental area (Figure 7g), as described.[27] However, NT-3 reporter gene expression was, both in newborn and adult brain, strikingly absent in catecholaminergic neurons of the entire hindbrain and pons, including A6 and A2 (Figure 7h). These results are consistent with data obtained from emulsion-dipped sections from wild-type pons hybridized with radiolabeled NT-3 antisense cRNA, showing no specific labeling over noradrenergic cells (Figure 1d).

Discussion

We report genetic evidence for a role of NT-3 in opiate withdrawal and noradrenergic neuron function. Mice with a CNS-wide deletion of NT-3 had attenuated withdrawal reactions which was restored by transgene-derived overexpression of NT-3 in noradrenergic neurons. Noradrenergic neurons of adult conditional NT-3 mutants had alterations in electrical activity both under drug-free conditions and after chronic opiate exposure. The upregulation of TH after chronic opiate exposure was reduced. The NT-3 deficient mice maintained normal numbers of noradrenergic neurons, therefore NT-3 is not essential for noradrenergic neuron survival. These results suggest that loss of NT-3 affects the function of noradrenergic neurons, including the capacity for opiate-induced neurochemical and functional adaptations.

Reduced opiate withdrawal in conditional mutants is accompanied by noradrenergic neuron dysfunction

Brainstem noradrenergic neurons play a key role in the neurobiology of the withdrawal reaction.[2] NT-3 may interfere with the biological effects of opiates by direct effects on noradrenergic neurons: NT-3 opposes, *in vitro*, the observed decline in embryonic A6 neuron numbers after chronic morphine exposure.[29] Furthermore, opiate exposure alters the expression of neurotrophic factors, including NT-3. In rat A6 neurons, NT-3 expression was increased after chronic morphine exposure but fell below baseline levels after acute withdrawal.[5] The high affinity receptor for NT-3, trkC, also shows dynamic changes in expression during chronic opiate exposure and withdrawal.[5] These studies suggested indirectly that NT-3, by affecting noradrenergic neuronal function, modulates opiate addiction and withdrawal behaviors. This hypothesis is supported by the observation that overexpression of NT-3 by noradrenergic neurons restored the withdrawal reaction in the NT-3 conditional mutants.

Upregulation of TH after chronic morphine exposure was present in wild-type noradrenergic neurons, consistent with previous observations in rats and transgenic mice expressing a lacZ reporter under control of the TH promoter.[18,23] While the functional significance of TH upregulation is not clear, the fact that it is diminished in NT-3 deficient mice suggests impaired capacity to adapt to chronic opiate exposure. Alterations in neuronal activity, including a hypoactive cAMP signaling cascade under drug-free conditions, an

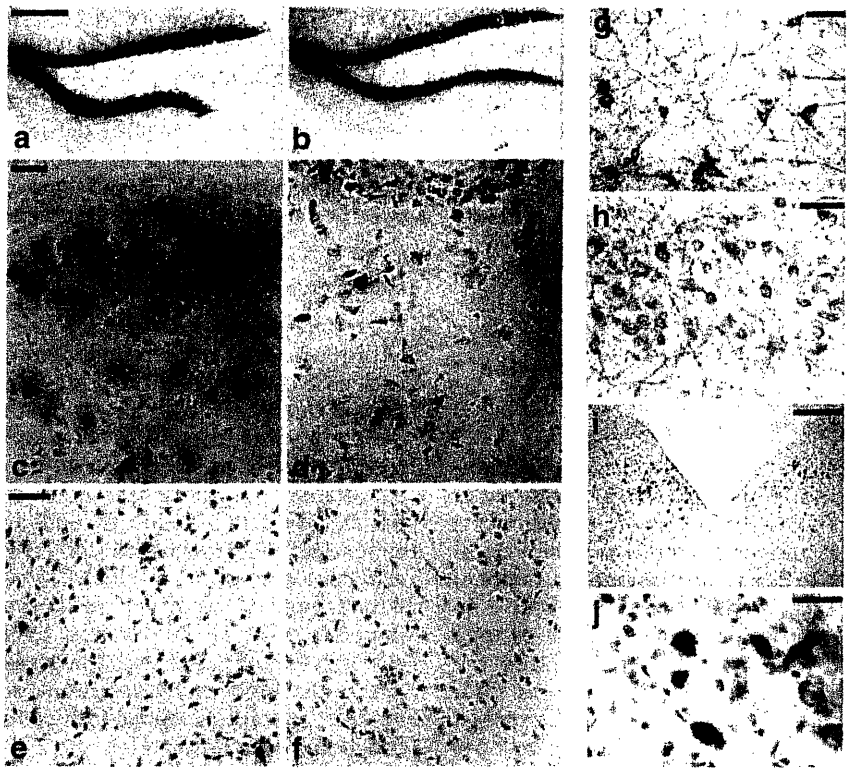

Figure 7 Transcriptional regulation of NT-3 expression. (a–j) Show X-gal stained coronal sections of mice carrying a lacZ reporter knock-in in the endogenous NT-3 locus.[27] (a, b) Show representative examples of labeling in the dorsal dentate gyrus, (c, d) the lateral septum and (e, f) the adjacent bed nucleus of the stria terminalis (BNST) after chronic morphine administration (a, c, e) in comparison to saline-treated littermate (b, d, f). Note increased labeling in morphine-treated animals. (g, h) Sections stained for TH and for lacZ, showing (g) double-labeled dopaminergic neurons in midbrain but (h) no double-labeled neurons in A6 of the same animal. (i) Coronal section of medulla, showing labeled neurons bilateral in area corresponding to the nucleus prepositus hypoglossi (NPH). (j) Medulla section double stained for TH and lacZ, showing co-localizaton of TH+ and lacZ+ neurons in rostral area of the solitary tract nucleus (NTS). Magnification bars in mm: (a, b) 0.5; (c, d) 0.04; (e, f) 0.15; (g) 0.05; (h) 0.05; (i) 0.25; (j) 0.02.

abnormal elevation in baseline firing rate after chronic morphine exposure, provide additional evidence that noradrenergic neurons are dysfunctional in NT-3 conditional mutants. Because total numbers of TH expressing noradrenergic neurons were maintained in adult conditional mutants, NT-3 is not required for neuronal survival and maintenance. Normal numbers of noradrenergic neurons in the mutant brain also argue that the observed alterations in noradrenergic neuron function and opiate withdrawal are due to a physiological role of NT-3 rather than due to a defect in brain development.

Noradrenergic neurons are organized in multiple clusters in the pons and medulla, which may explain the observation that lesions of individual clusters and fiber pathways do not abolish opiate withdrawal reactions.[3,30,31] Pharmacological inhibition of the entire noradrenergic system, on the other hand, is a very effective treatment for opiate withdrawal.[2] Whereas recent evidence points to an important role of the noradrenergic cell groups in the medulla at least for withdrawal-induced aversion,[3] traditionally the A6, which is the largest noradrenergic cell cluster in the brain, has served as a model system for the pharmacology and cellular basis of opiate tolerance and withdrawal.[4] Application of electrical recording and other analytical techniques to noradrenergic cell groups other than the A6 is extremely difficult in the mouse and thus it remains unclear if morphine-induced alterations in A6 neuron electrophysiology and neurochemistry are representative of alterations occurring in other noradrenergic cell groups. However, we found, by TH immunohistochemistry, subtle changes in medullary (A2) noradrenergic neurons in transgenic mice that overexpress NT-3 in these neurons. Therefore, NT-3 may modulate the neurochemistry of several or all noradrenergic populations in the brainstem.

Noradrenergic neurons do not express NT-3

We found no evidence for NT-3 expression in wild-type noradrenergic neurons in postnatal and adult mouse brain. This is in contrast to previous studies in the rat localizing NT-3 mRNA to A6,[5,32] suggesting that related species may differ in regional patterns of neurotrophin gene expression. Because neurotrophins are

subject to retrograde[33] and anterograde transport,[34,35] other NT-3 expressing neuronal populations in adult brain[27,36,37] may supply noradrenergic cells with target-derived NT-3. Furthermore, the observed alterations in electrical activity of A6 neurons and the failure to upregulate TH after chronic opiate exposure in the conditional mutants may be explained by lack of target-derived NT-3. Alternatively, these changes in mutant A6 neurons could be secondary, with the primary defect being in other neuronal populations that depend on autocrine or paracrine NT-3[38] and that are interconnected with the noradrenergic system.

We found that NT-3 expressing neurons are present in two brainstem nuclei that are interconnected with the noradrenergic system and that provide a major afferent input. These were the nucleus prepositus hypoglossi (Figure 7i) and the rostral portions of the nucleus of the solitary tract (Figure 7j).[39,40] NT-3 expressed in these nuclei may be subject to anterograde axonal transport and may be released from presynaptic terminals to postsynaptic noradrenergic neurons.[35] Alternatively, TrkC or TrkB receptors on axon terminals of noradrenergic neurons may take up NT-3 and transport ligand and receptor in a retrograde direction. In this regard, it is of interest that chronic opiate exposure upregulates endogenous NT-3 gene expression in selected forebrain areas, including the lateral septum (LS), parts of the neighboring bed nucleus of the stria terminalis (BNST) and the dorsal hippocampus (DH). These areas compose part of a circuit mediating avoidance and aversion behavior[41,42] and noradrenergic fibers innervating this particular circuitry are thought to be essential for opiate withdrawal-induced aversion.[3] Therefore, NT-3 produced in these forebrain regions could be important for opiate-induced adaptations of noradrenergic neurons and may explain why withdrawal-induced aversion was reduced in the NT-3 deficient mice of our study. Target-derived NT-3, by modulating noradrenergic neuron function, may affect complex, long-term behavioral sequelae of opiate dependence and withdrawal. This is of particular interest from a clinical point of view. In patients addicted to opiates, the experience of opiate withdrawal may act as strong negative reinforcement, thus maintaining the addicted state.[1] Previous studies suggested that target-derived NT-3 plays an essential role during the developmental period, by modulating neuronal survival in the peripheral nervous system, including proprioceptive and sympathetic neurons.[11,43–45] Our findings suggest, indirectly, that in adult brain, selected neuronal populations, including the noradrenergic system, require target-derived NT-3 for proper function but not necessarily for neuronal maintenance and survival. Future experiments, using genetically engineered mice with a tagged NT-3 coding sequence[46] should clarify if modulation of opiate withdrawal by NT-3 is due to target-derived modulation of noradrenergic signalling and/or additional effects on other neuronal populations of the circuitry that mediates opiate withdrawal and withdrawal-related aversion.

Methods

Genetic engineering

For characterization of the NT-3 conditional knock-out allele and of the Nestin-Cre transgene, see Bates *et al*[14] and Trumpp *et al.*[47] The DBH-NT-3 transgenic mice were generated by pronuclear injection of a plasmid containing sequentially a 5.8-kb fragment of the human dopamine-beta hydroxylase gene promoter as described by Mercer *et al*,[20] a 0.15-kb fragment comprising intron A of the human insulin gene, a 0.96-kb fragment containing the complete translated sequence of a human neurotrophin-3 cDNA, and a 0.27-kb fragment of a mouse protamine I cDNA 3′ UTR, containing the polyadenylation sequence. The line employed for these studies contained 5–10 tandemly integrated copies of the transgene. The genetic background of all mutant and control mice was mixed, but predominantly *129* and *C57/Black6*. Breeding strategies were chosen to obtain wild-type littermates as controls for the NT-3 mutants, in order to minimize the variability in genetic background.

Morphine injection protocol

Procedures were similar to Taylor *et al*[48] and Punch *et al.*[49] Opiate dependence was induced by a progressive treatment schedule of morphine sulfate i.p. spaced every 6–10 h (day 1: 20–40–60 mg kg^{-1}, day 2: 80–100–100 mg kg^{-1}, day 3: 100 mg kg^{-1}). Thus, the total cumulative morphine dose was for each animal 500 mg kg^{-1} per 60 h. These protocols was used for the Western blot analysis, the histological studies, the electrophysiological recordings, the analgesia experiments and the observer-based ratings for somatic withdrawal. For the conditioned place aversion experiments, 50% of animals were subject to a 'low dose morphine' progressive treatment schedule (340 mg kg^{-1} total over 60 h) and 50% of animals were subject to a 'high dose morphine' progressive treatment schedule (720 mg kg^{-1} total over 72 h) schedule. For the rating and conditioning experiments, withdrawal was precipitated 2 h after the last morphine injection with naloxone.HCl s.c. 1 mg kg^{-1}).

In situ hybridization

Brains were perfusion-fixed with phosphate-buffered 4% paraformaldehyde, postfixed overnight in the same fixative, cryoprotected in 30% phosphate-buffered sucrose, frozen and cut on a cryostat in series of 20-μm thick coronal sections which were stored in above fixative for another 2 h, then mounted on Vectabond (Vector, Burlingame, CA, USA) coated slides and air-dried. Sections were washed twice in 0.1 M phosphate-buffered glycine and once in phosphate buffer (pH 7.4), then digested with proteinase K (1 μg ml^{-1} in 0.1 M Tris pH 8.0, 50 mM EDTA) for 30 min at 37°C, then washed for 10 min at RT in 0.25% acetic anhydride in 0.1 M TEA (pH 8.0), then washed twice in 2 × SSC (15 min, RT). They were then dehydrated, defatted in 100% chloroform for 10 min, rehydrated and airdried, then incubated in a humidified chamber for 24 h at 60°C in hybrization buffer (10% dextrane, 50× dionized

formamide, 50× Denhardts, 300 μg ml^{-1} herring sperm DNA, 0.15 mg ml^{-1} yeast t-RNA, 20 mM DTT) containing 10000 cpm μl^{-1} of a P^{33} or S^{35}-labeled NT-3 full length cRNA or a 250-bp fragment of protamine cRNA. Sections were washed in 4 × SSC (twice for 30 min at 60°C), then digested with RNAse A (20 μg ml^{-1}) in RNAse buffer (0.5 M NaCl, 10 mM Tris pH 8.0/1 mM EDTA), then washed twice in 2 × SSC, twice in 0.5 × SSC, once at 0.1 × SSC (30 min each, 60°C), dipped in water, airdried and either exposed to beta max hyperfilm (Amersham, Piscataway, NJ, USA) for 10 days or dipped in Kodak (Rochester, NY, USA) NTB2 emulsion and developed after 28 days, then counterstained and coverslipped.

Western blot analysis

Brains of 10 control mice and 10 conditional mutants (5 per group were untreated, 5 per group received chronic morphine; 500 mg per 60 h) were rapidly removed after decapitation, and A6 was excised using a 15-gauge syringe as previously described for the mouse.[18] Samples were homogenized in 2% SDS and aliquots of A6 containing 20 μg of protein were loaded on 7.5% SDS polyacrylamide gels, electrophoresed and transferred to nitrocellulose (Schleicher and Schuell, Keene, NH, USA). Blots were immunolabeleled for TH exactly as described.[23] Equal loading and transfer was controlled by immunolabeling for tubulin. Differences between mutants and controls were quantified using optical densitometry of film autoradiograms and NIH imaging software.

Immunohistochemistry

For immunohistochemical experiments, drug-naive mice were compared with mice exposed to chronic morphine (see above). c-fos immunoreactivity in noradrenergic neurons was examined in drug-naive mice and in mice that were exposed to chronic morphine and that received naloxone.HCl s.c. 1 mg kg^{-1} after the last morphine injection. Withdrawal reactions (as described above) were verified by a trained observer, and 110 min after the naloxone injection, the animals were killed. All mutant and control brains were perfusion-fixed with phosphate-buffered 4% paraformaldehyde, postfixed in the same fixative for 2 h, cryoprotected in 30% phosphate-buffered sucrose, frozen and cut in series of 20-μm thick coronal sections on a cryostat (Reichert-Jung, Vienna, Austria). Sections were incubated free floating at room temperature for 20 h with a monoclonal antibody for tyrosine hydroxylase (1:1000) (Incstar, Stillwater, MN, USA), and for double-labeling, an antiserum for the 43-kDa phosphorylated form of CREB (1:500),[21] Upstate Biotech (Lake Placid, NY, USA), or an antiserum recognizing c-fos (1:500) (Oncogene, Boston, MA, USA) in phosphate-buffered 0.3% Triton X-100 with 4% horse or goat serum. After washing, sections were incubated either in biotinylated secondary antibodies processed for DAB staining (Vectastain, Burlingame, CA, USA), according to the manufacturer's instruction or incubated in FITC or Texas Red conjugated secondary antibodies (1:200, Vector) for 60 min. For all immunohistochemical experiments, thionine-stained parallel sections were used for cytoarchitectonic studies and anatomical localization. A separate set of sections, obtained from mice carrying a lacZ reporter in the endogenous NT-3 locus[27] were first stained free floating for beta-galactosidase activity: sections were rinsed twice (5 min and 20 min, RT) in buffer A (0.1 M phosphate buffer (pH 7.4), 2 mM $MgCl_2$, 5 mM EGTA), then rinsed twice (5 min each) in buffer B (0.1 M phosphate buffer pH 7.4, 2 mM $MgCl_2$, 0.01% sodium deoxycholate, 0.02% NP-40) and then transferred into the staining solution (buffer B, 5 mM $K_3Fe(CN)_6$, 5 mM $K_4Fe(CN)_6$, 1 mg ml^{-1} X-gal), incubated for 16 h at 37°C, then washed in phosphate buffer and then were either processed for TH immunohistochemistry as above or mounted on gelatin/chrom alum coated slides, counterstained with Neutralred, dehydrated and coverslipped.

Cell counting studies

Drug-naive mutant and control animals were used for cell counting studies. Total numbers of bilateral A6 and A2 neurons were determined in series of 20-μm thick sections that were processed for DAB-stained TH immunoreactivity and then counterstained with cresyl violet. Every second section was used for counting. Because both A6 and A2 showed in all mutants and controls considerable variability in neuronal distribution and density along the rostrocaudal axis, optical dissector and volume-based cell counting methods that rely on constant cell densities in a given volume were inaccurate for the present study. Instead, TH immunoreactive neurons (defined by brown cytoplasm in DAB-stained material) cut through the level of the nucleus were counted in each section and total neuronal numbers were calculated by adding counts of single sections. The noradrenergic cell group A2 was localized using the detailed cytoarchitectonic descriptions of Kalia *et al*.[17] Three-month-old NT-3 conditional knockout mice and littermate controls and DBH NT-3 transgenic mice and littermate controls of the same age groups were used, with a minimum of five animals for each age group and genotype. Data from the two age groups were taken together and differences between genotypes expressed as means ± SE.

Electrophysiology

Electrophysiological recordings from A6 neurons were performed on a series of 3-week, 10- and 15–16-week-old mutant mice and controls, as previously described.[23] Briefly, brain slices containing the A6 were transferred onto the stage of a gas–liquid interface brain slice chamber under a constant flow of humidified 95% O_2:5% CO_2 and physiological buffer. The A6 were visually identified and single-unit extracellular potentials were recorded with glass microelectrodes filled with 2 M NaCl. Consecutive cells were sampled by multiple electrode tracts randomly positioned within the A6 and recorded for a minimum of 3–5 min to ensure that the firing rates were stable. Recordings were conducted on drug-naive untreated animals and

on mice exposed to chronic morphine. Recordings began not earlier than 90 min after setting up the slice preparation. This waiting period ensured complete wash-out of morphine in the drug-treated animals, as described.[25] Transient electrical silencing after brief application of short-lived enkephalin was used to confirm that recording was done from LC neurons. Firing rates of A6 neurons were recorded after bath application (for at least 10 min) of forskolin (10 μmol). At this concentration, maximal electrophysiological responses from A6 neurons are elicited. In addition, μ (opioid) receptor inhibition was examined by dose-response curves with the synthetic agonist DAMGO. For statistical analysis, the firing rates of neurons (typically 10–14 from a single A6) were averaged and considered as a single data point. A minimum of 12 animals was used for each genotype and treatment.

Somatic withdrawal

Behavioral ratings were calculated over a 15-min period by a trained observer blind to experimental treatment and genotype. Three different groups of mice were tested (minimum 10 animals per group): (1) 3-month-old NT-3 conditional mutant mice; (2) 3-month-old conditional NT-3 mutant mice carrying the DBH NT-3 transgene; (3) wild-type controls. Additional experiments were conducted with NT-3 conditional mutants and controls that were ≥4 months of age. The overall withdrawal score was determined by the total number of checked signs (diarrhea, rhinorhea, lacrimation, abnormal posture, irritability, ptosis) and the frequency of each counted sign (wet dog shakes, freezing, grooming, rear, dig, jumping, tremor) as described.[48] Analgesic effects of morphine were evaluated by the warm-water tail-flick test. Conditional mutants, in comparison to controls, did not show significant differences in tail flick latencies after receiving a single dose of 20 mg kg^{-1} morphine (mutants: 11.3 ± 6.4 ms; controls 10.4 ± 3.4 ms) or at the 100 mg kg^{-1} endpoint of the progressive morphine treatment regimen (mutants 9.5 ± 6.3 ms; controls 11.8 ± 7.0 ms), suggesting that analgesic effects and development of tolerance is preserved in the mutant.

Conditioned place aversion

A total of 20 mutant and 20 age- and gender-matched control mice (age range 10–16 weeks) were utilized, under blind conditions, for the conditioned place aversion (CPA) test. Animals were housed individually in a temperature and humidity-controlled room on a 12/12 h light-dark cycle with food and water *ad libitum*. Conditioning and testing occurred in custom built mouse CPA chambers (MED Associates, Ludlow, VT, USA). During pre- and post-conditioning (day 1 and day 6, respectively), animals explored the two chambers and the middle compartment freely for 900 s. Subjects spending more than 540 s in either chamber or preferring the middle compartment during pre-conditioning were discarded. A progressive treatment schedule of 'low dose morphine' (340 mg kg^{-1} total over 60 h) and 'high dose morphine' (720 mg kg^{-1} over 72 h) was administered. On the last day of conditioning (day 5) animals underwent pairing of one side of the chamber with saline, the other with naloxone (1 mg kg^{-1}). Test performance was defined as the difference in the time spent in each compartment before *vs* after conditioning. Simple conditioning with electric foot shocks was performed as described,[50] including analysis by MATLAB software (see also http://web.mit.edu/linus/www/meteor/).

Data analysis

In order to examine significance of differences between mutants and controls, unpaired two-tailed *t*-tests were conducted for cell counting, histology, electrophysiology data and the simple conditioning (footshock) experiments. ANOVA and Fisher's PLSD for post hoc comparison was used for the ratings of somatic withdrawal. The data of the conditioned place aversion experiments were first subjected to a mixed factor ANOVA to evaluate the effect of genotype, sex and morphine dose regimen and then pairwise comparisons were performed with the Neuman–Keuls test.

Acknowledgements

The authors thank Ruth Curry, Valyphone Phantharagnsy, Cathy Steffen, Victoria Stewart and Jeannie Reis for technical assistance, Drs Maribel Rios, Christine Konradi and William Carlezon Jr for experimental advice. This work was supported by NARSAD (National Alliance for Research on Schizophrenia and Depression), by the National Institute of Drug Abuse (NIDA) grant 1-K08-DA00479 to SA, by NCI/NIH grant 5-R35-CA44339 to RJ and by the Fidelity Foundation.

References

1 Koob GF, Le Moal M. Drug abuse: hedonic homeostatic dysregulation. *Science* 1997; **278**: 52–58.
2 Maldonado R. Participation of noradrenergic pathways in the expression of opiate withdrawal: biochemical and pharmacological evidence. *Neurosci Biobehav Rev* 1997; **21**: 91–104.
3 Delfs JM, Zhu Y, Druhan JP, Aston-Jones G. Noradrenaline in the ventral forebrain is critical for opiate withdrawal-induced aversion. *Nature* 2000; **403**: 430–434.
4 Nestler EJ, Aghajanian GK. Molecular and cellular basis of addiction. *Science* 1997; **278**: 58–63.
5 Numan S, Lane-Lad SB, Zhang L, Lundgren KH, Russell DS, Seroog KB *et al*. Differential regulation of neurotrophin and trk receptor mRNA in catecholaminergic nuclei during chronic opiate treatment and withdrawal. *J Neurosci* 1998; **18**: 10700–10708.
6 Sandell JH, Baker LS Jr, Davidov T. The distribution of neurotrophin receptor trkC like immunoreactive fibers and varicosities in the rhesus moneky brain. *Neuroscience* 1998; **86**: 1181–1194.
7 King VR, Michael GJ, Joshi RK, Priestley JV. trkA, trkB and trkC messenger RNA expression by bulbospinal cells of the rat. *Neuroscience* 1999; **92**: 935–944.
8 Davies AM, Minichiello L, Klein R. Developmental changes in NT-3 signalling via TrkA and TrkB in embryonic neurons. *EMBO J* 1995; **14**: 4482–4489.
9 Tessarollo L, Tsoulfas P, Donovan MJ, Palko ME, Blair-Flynn J, Hempstead BL *et al*. Targeted deletion of all isoforms of the trkC gene suggests the use of alternate receptors by its ligand neurotrophin-3 in neuronal development and implicates trkC in normal cardiogenesis. *Proc Natl Acad Sci USA* 1997; **94**: 14776–14781.
10 Huang EJ, Wilkinson GA, Farinas I, Backus C, Zang K, Wongl SL *et*

al. Expression of Trk receptors in the developing mouse trigeminal ganglion: *in vivo* evidence for NT-3 activation of trk A and trkB in addition to trkC. *Development* 1999; **126**: 2191–21203.
11 Farinas I, Jones KR, Backus C, Wang XY, Reichardt LF. Severe sensory and sympathetic deficits in mice lacking neurotrophin-3. *Nature* 1994; **369**: 658–661.
12 Ernfors P, Lee K-F, Kucera J, Jaenisch R. Lack of neurotrophin-3 leads to deficiencies in the peripheral nervous system and loss of limb proprioceptive afferents. *Cell* 1994; **77**: 503–512.
13 Donovan MJ, Hahn R, Tessarollo L, Hempstead BL. Identification of an essential non-neuronal function of Neurotrophin-3 in mammalian cardiac development. *Nat Genet* 1996; **14**: 210–213.
14 Bates B, Rios M, Trumpp A, Chen C, Fan G, Bishop JM *et al*. Neurotrophin-3 is required for proper cerebellar development. *Nat Neurosci* 1999; **2**: 115–117.
15 Soriano P. Generalized lacZ expression with the ROSA26 Cre reporter strain. *Nat Genet* 1999; **21**: 70–71.
16 Arenas E, Persson H. Neurotrophin-3 prevents the death of adult central noradrenergic neurons in vivo. *Nature* 1994; **376**: 368–371.
17 Kalia M, Fuxe K, Goldstein M. Rat medulla oblongata. II. Dopaminergic, noradrenergic (A1 and A2) and adrenergic neurons, nerve fibers, and presumptive terminal processes. *J Comp Neurol* 1985; **233**: 308–332.
18 Boundy VA, Gould SJ, Messer CJ, Chen J, Son JH, Joh TH *et al*. Regulation of tyrosine hydroxylase promoter activity by chronic morphine in TH9.0-LacZ transgenic mice. *J Neurosci* 1998; **18**: 9989–9995.
19 Tinti C, Conti B, Cubells JF, Kim KS, Baker H, Joh TH. Inducible cAMP early repressor can modulate tyrosine hydroxylase gene expression after stimulation of camp synthesis. *J Biol Chem* 1996; **271**: 25375–25381.
20 Mercer EH, Hoyle GW, Kapur RP, Brinster RL, Palmiter RD. The dopamine beta hydroxylase gene promoter directs expression of *E. coli* lacZ to sympathetic and other neurons in adult transgenic mice. *Neuron* 1991; **7**: 703–716.
21 Ginty DD, Bonni A, Greenberg ME. Nerve growth factor activates a Ras-dependent protein kinase that stimulates c-fos transcription via phosphorylation of CREB. *Cell* 1994; **77**: 713–725.
22 Maldonado R, Blendy JA, Tzavara E, Gass P, Roques BP, Hanoune J *et al*. Reduction of morphine abstinence in mice with a mutation in the gene encoding CREB. *Science* 1996; **273**: 657–659.
23 Lane-Ladd SB, Pineda J, Boundy V, Pfeuffer T, Krupinski J, Aghajanian GK *et al*. CREB in the locus coeruleus: biochemical, physiological, and behavioral evidence for a role in opiate dependence. *J Neurosci* 1997; **17**: 7890–7901.
24 Hayward MD, Duman RS, Nestler EJ. Induction of the c-fos proto oncogene during opiate withdrawal in the locus coeruleus and other regions of rat brain. *Brain Res* 1990; **525**: 256–266.
25 Kogan JH, Nestler EJ, Aghajanian GK. Elevated basal firing rates and enhanced responses to 8-Br-cAMP in locus coeruleus neurons in brain slices from opiate-dependent rats. *Eur J Pharmacol* 1992; **211**: 47–53.
26 Zhang J, Ferguson SS, Barak LS, Boddulir SR, Laporte SA, Law PY *et al*. Role for G protein-coupled receptor kinase in agonist-specific regulation of responsiveness. *Proc Natl Acad Sci USA* 1998; **95**: 7157–7162.
27 Vigers AJ, Baquet ZC, Jones KR. Expression of neurotrophin-3 in the mouse forebrain: insight from a targeted lacZ reporter. *J Comp Neurol* 2000; **416**: 398–415.
28 Gehlert DR, Schober DA, Gackenheimer SL. Comparison of (R)–[3H] tomoxetine and (R/S)–[3H] nisoxetine binding in rat brain. *J Neurochem* 1995; **64**: 2792–2800.
29 Sklair-Tavron L, Nestler EJ. Opposing effects of morphine and the neurotrophins, NT-3, NT-4 and BDNF, on locus coeruleus neurons *in vitro*. *Brain Res* 1995; **702**: 117–125.
30 Christie MJ, Williams JT, Osborne PB, Bellchambers CE. Where is the locus in opioid withdrawal? *Trends Pharmacol Sci* 1997; **18**: 134–140.
31 Caille S, Espejo EF, Reneric JP, Cador M, Koob GF, Stinus L. Total neurochemical lesion of noradrenergic neurons of the locus coeruleus does not alter either naloxone-precipitated or spontaneous opiate withdrawal nor does it influence ability of clonidine to reverse opiate withdrawal. *J Pharmacol Exp Ther* 1999; **290**: 881–892.
32 Smith MA, Makino S, Altemus M, Michelson D, Hong SK, Kvetnansky R *et al*. Stress and antidepressants differentially regulate neurotrophin 3 mRNA expression in the locus coeruleus. *Proc Natl Acad Sci USA* 1995; **92**: 8788–8792.
33 DiStefano PS, Friedman B, Radziejewski C, Alexander C, Boland P, Schick CM *et al*. The neurotrophins BDNF, NT-3 and NGF display distinct patterns of retrograde axonal transport in peripheral and central neurons. *Neuron* 1992; **8**: 983–993.
34 Altar CA, DiStefano PS. Neurotrophin trafficking by anterograde transport. *Trends Neurosci* 1998; **21**: 433–437.
35 Conner JM, Lauterborn JC, Gall CM. Anterograde transport of neurotrophin proteins in the CNS—a reassessment of the neurotrophic hypothesis. *Rev Neurosci* 1998; **9**: 91–103.
36 Maisonpierre PC, Belluscio L, Friedman B, Alderson RF, Wiegand SJ, Furth ME *et al*. NT-3, BDNF, and NGF in the developing rat nervous system: parallel as well as reciprocal patterns of expression. *Neuron* 1990; **5**: 501–509.
37 Lauterborn JC, Isackson PJ, Gall CM. Cellular localization of NGF and NT-3 mRNAs in postnatal rat forebrain. *Mol Cell Neurosci* 1994; **5**: 46–62.
38 Acheson A, Lindsay RM. Non-target derived roles of the neurotrophins. *Philos Trans R Soc Lond Biol Sci* 1996; **351**: 417–422.
39 Drolet G, Van Bockstaele EJ, Aston-Jones G. Robust enkephalin innervation of the locus coeruleus from the rostral medulla. *J Neurosci* 1992; **12**: 3162–3174.
40 Van Bockstaele EJ, Peoples J, Telegan P. Efferent projections of the nucleus of the solitary tract to peri-locus coeruleus dendrites in rat brain: evidence for a monosynaptic pathway. *J Comp Neurol* 1999; **412**: 410–428.
41 Duncan GE, Knapp DJ, Breese GR. Neuroanatomical characterization of Fos induction in rat behavioral models of anxiety. *Brain Res* 1996; **713**: 79–81.
42 Desmedt A, Garcia R, Jaffard R. Vasopressin in the lateral septum promotes elemental conditoning to the detriment of contextual fear conditioning in mice. *Eur J Neurosci* 1999; **11**: 3913–3921.
43 DiCicco-Bloom E, Friedman WJ, Black IB. NT-3 stimulates sympathetic neuroblast proliferation by promoting precursor survival. *Neuron* 1993; **11**: 1101–1111.
44 Albers KM, Perrone TM, Goodness TP, Jones ME, Green MA, Davis BM. Cutaneous overexpression of NT-3 increases sensory and sympathetic neuron number and enhances touch dome and hair follicle innervation. *J Cell Biol* 1996; **134**: 487–497.
45 Francis N, Farinas I, Brennan C, Rivas-Plata K, Backus C, Reichardt L *et al*. NT-3, like NGF, is required for survival of sympathetic neurons, but not their precursors. *Dev Biol* 1999; **210**: 411–427.
46 Moller JC, Kruttgen A, Heymach JV Jr, Ghori N, Shooter EM. Subcellular localization of epitope-tagged neurotrophins in neuroendocrine cells. *J Neurosci Res* 1998; **51**: 463–472.
47 Trumpp A, Depew MJ, Rubenstein JL, Bishop JM, Martin GR. Cre-mediated gene inactivation demonstrates that FGF8 is required for cell survival and patterning of the first branchial arch. *Genes Dev* 1999; **13**: 3136–3148.
48 Taylor JR, Elsworth JD, Garcia EJ, Grant SJ, Roth RH, Redmond DE Jr. Clonidine infusions into the locus coeruleus attenuate behavioral and neurochemical changes associated with naloxone-precipitated withdrawal. *Psychopharmacology* 1988; **96**: 121–134.
49 Punch LJ, Self DW, Nestler EJ, Taylor JR. Opposite modulation of opiate withdrawal behaviors on microinfusion of a protein kinase A inhibitor versus activator into the locus coeruleus or periaqueductal gray. *J Neurosci* 1997; **17**: 8520–8527.
50 Huerta PT, Sun LD, Wilson MA, Tonegawa ST. Formation of temporal memory requires NMDA receptors within CAI pyramidal neurons. *Neuron* 2000; **25**: 473–480.

Correspondence: R Jaenisch, Professor of Biology, Whitehead Institute, 9 Cambridge Center, Cambridge, MA 02142, USA. E-mail: jaenisch@wi.mit.edu
*SA and BB contributed equally to this work.
Current affiliation of BB: Genetics Institute, Cambridge, MA. SS: Division of Neurosurgery, University of New Mexico, Albuquerque, NM. EJN: Dept of Psychiatry, UT Southwestern, Dallas, TX.
Received 8 December 2000; revised and accepted 2 February 2001